Durham University

Durham E-Theses

Surface aspects of the natural and artificial aging of some aromatic polymers as studied by means of ESCA

Hugh Semple Munro

How to cite:

Munro, Hugh Semple (1982) Surface aspects of the natural and artificial aging of some aromatic polymers as studied by means of ESCA. Doctoral thesis, Durham University.

Use policy

The full-text may be used and/or reproduced, and given to third parties in any format or medium, without prior permission or charge, for personal research or study, educational, or not-for-profit purposes provided that:

- a full bibliographic reference is made to the original source
- a https://etheses.durham.ac.uk/id/eprint/7511/ is made to the metadata record in Durham E-Theses
- the full-text is not changed in any way

The full-text must not be sold in any format or medium without the formal permission of the copyright holders.

Please consult the full Durham E-Theses policy for further details.

Academic Support Office, The Palatine Centre, Durham University, Stockton Road, Durham, DH1 3LE
e-mail: e-theses.admin@durham.ac.uk Tel: +44 0191 334 6107
https://etheses.durham.ac.uk

The copyright of this thesis rests with the author.
No quotation from it should be published without
his prior written consent and information derived
from it should be acknowledged.

A thesis entitled

SURFACE ASPECTS OF THE NATURAL AND ARTIFICIAL AGING OF SOME AROMATIC POLYMERS AS STUDIED BY MEANS OF ESCA

submitted by

HUGH SEMPLE MUNRO, B.Sc.

A candidate for the Degree of Doctor of Philosophy

Graduate Society,
University of Durham

July 1982

DURHAM UNIVERSITY
23 SEP 1982
SCIENCE LIBRARY

To Helen and my parents

ACKNOWLEDGEMENTS

I am indebted to my supervisor, Professor D.T. Clark for his help, encouragement and enthusiasm towards the work of this thesis, and my sincere gratitude is due to him. I would also like to thank Dr. A. Davis (P.E.R.M.E. Waltham Abbey) and Professor J. Peeling (University of Petroleum and Minerals, Dhahran, Saudi Arabia) for helpful discussions as well as provision of samples.

Gratitude is also expressed to my colleagues, Bill Brennan, Andy Fowler, Dick Hutton, Rosemary Wilson, Mohammed Abu-Shbak and Steve Johnson for their friendship and also the Science and Engineering Research Council and the Ministry of Defence for the provision of an S.E.R.C./CASE studentship.

Finally I would like to thank Mrs. Elizabeth Nevins for her help in the preparation of some of the figures and Mrs. Marion Wilson for her great patience and secretarial skill in typing this manuscript.

H. S. MUNRO

DURHAM 1982

ABSTRACT

X-ray photoelectron spectroscopy, (ESCA), has been used to investigate the changes in surface chemistry of some aromatic polymers during natural and artificial weathering.

Particular emphasis has been placed on the photodegradation (λ>290nm) of Bisphenol A polycarbonate. Model studies to investigate the changes in surface chemistry as functions of irradiation time, photon flux, temperature and the partial pressures of oxygen and water at the solid/gas interface have been carried out in conjunction with natural exposures. The results show that photooxidation (involving the gem dimethyl and phenyl groups) and not a photo-Fries type rearrangement is the predominant process in the surface regions. Calculations at the non- and semi-empirical levels on model polycarbonate systems suggest that the first excited singlet state of polycarbonate arises from a $\Pi \rightarrow \Pi^*$ transition. The changes in surface chemistry of polycarbonate exposed to reactive oxygen species have been studied and indicate that singlet oxygen does not react with this polymer.

The photoaging studies for polycarbonate have been extended to polystyrene, Bisphenol A polysulphone, polyethersulphone, polyphenylene oxide phenoxy resin and polyetherketone and similar trends to those observed for polycarbonate are shown to occur in these systems, i.e. extensive oxygen uptake in the surface regions with the mechanism involving the aromatic groups of the various systems.

MEMORANDUM

The work described in this thesis was carried out at the University of Durham between October 1979 and July 1982. It has not been submitted for any other degree and is the original work of the author except where acknowledged by reference.

Work in this thesis has formed the whole, or part of the following publications:

1. An MNDO SCF MO Investigation of the Electronic Structures and Conformational Preferences of Model Polycarbonate Systems, D.T. Clark and H.S. Munro, Polym.Degrad. and Stab., 4 83 (1982).
2. An STO-3G Investigation of Barriers to Rotation in Model Systems for Aromatic Polycarbonates, D.T. Clark and H.S. Munro, Polym.Degrad. and Stab., in press (1982).
3. Surface Aspects of the Photodegradation of Bisphenol A Polycarbonate in Oxygen and Nitrogen atmospheres as revealed by ESCA, D.T. Clark and H.S. Munro, Polym.Degrad. and Stab., in press (1982).
4. Surface Aspects of the Photodegradation of Bisphenol A Polycarbonate, in Oxygen and Air as a Function of Relative Humidity as Revealed by ESCA, D.T. Clark and H.S. Munro, Polym.Degrad. and Stab., submitted (1982).

CONTENTS

Page No.

Page No.

Page No.

Page No.

CHAPTER ONE

THE PHOTODEGRADATION AND PHOTOOXIDATION OF POLYMERS

DURHAM UNIVERSITY
23 SEP 1982
SCIENCE LIBRARY

1.1 Introduction

Since the beginning of recorded history, man has recognised that water, sunlight and fresh air are the most bountiful gifts of Nature. Yet more than a hundred years ago it was recognised that these same agents were the cause of the degradation observed in natural rubbers.[1] It was found that Indian telegraph wire coatings made from natural rubber gradually lost their advantageous properties thereby causing substantial financial loss. On investigation of this phenomena it was concluded that oxidation (from exposure to air and accelerated by light) was responsible for the deterioration of the rubber. The problem that was encountered then is not too different from the present day in the degradation of synthetic polymers.

Although the resistance of polymers to photodegradation varies widely, continual exposure to solar radiation will eventually deteriorate almost every polymer.

Outside the atmosphere and from the direction of the sun, the earth is seen to reflect diffusely a fraction of the incident radiation.[2] This fraction is ~40%. The emission is reflected from the clouds, the earth's surface and the sea and in part scattered in the atmosphere. Of the remaining inward flux about 45% reaches the surface to be absorbed and about 15% is absorbed in the atmosphere. This 60% of the incident power is re-radiated into space at infra-red wavelengths differing in spectral distribution from the original solar spectrum. The region of sunlight reaching the earth's surface that is of primary importance in the degradation of

polymers is that of the ultraviolet (the so-called solar ultraviolet). The atmosphere filters out practically all the radiation below 295 nm. The exact wavelength limit of atmospheric transmission has been investigated by many workers over the years and has been found to be dependent on the elevation of the observing site, the ozone content and the turbidity of the atmosphere.[2] The solar ultraviolet represents only about 5% of the total radiation of the sun reaching the surface but is the most damaging to polymers.[3]

1.2 General Principles of Photochemistry

1.2.1 The Absorption of Light

All electromagnetic radiation may be described in terms of either the wavelength λ, the frequency ν, the wavenumber $\bar{\nu}$ or the energy, E, of a quantum of radiation in the ultraviolet-visible region of the electromagnetic spectrum that is of interest. The wavelengths in this region extend from 200 to 800 nm. Table 1.1 compares this wavelength scale with the same scale in cm^{-1}, kcal $mole^{-1}$ and eV.

Table 1.1 Comparative energy scales

nm	$cm^{-1} \times 10^3$	kcal $mole^{-1}$	eV
200	50	142.93	6.2
300	33	94.33	4.13
400	25	71.46	3.1
500	20	57.17	2.48
600	16.67	47.65	2.07
700	14.29	40.85	1.77
800	12.5	35.73	1.55

A necessary condition for a photochemical reaction to take place is the excitation of a molecule due to the absorption of light quanta of sufficient energy by some component of the system. This is the first law of photochemistry called the Grotthus-Draper Principle. The second law of photochemistry, the Stark-Einstein Principle, states that a molecule can only absorb one quantum of radiation. The resultant excited molecule may then follow one or more paths, photophysical processes, before a photochemical reaction can take place. A photochemical process has been defined as a "physical process (i.e. one which does not involve a chemical change) resulting from the excitation of a molecule by non-ionizing electromagnetic radiation".[6] A primary photochemical process arises when decomposition or dissociation of the molecule occurs as a direct consequence of the absorption of radiation. The absorption of light by molecules only occurs if the difference between two energy levels is exactly the same as the energy of a quantum:

$$E = h\nu = E_2 - E_1$$

where E_2 and E_1 are the energies of a molecule in the final (higher level) and initial (lower level) states respectively. The absorption occurs in accordance with the well known Beer-Lambert Law. The Beer Law states that the amount of light absorbed is proportional to the concentration of absorbing species, whereas the Lambert Law states that the fraction of incident light absorbed is independent of the intensity of the light and that each successive layer of the medium absorbs an equal fraction of the incident light. When combined these laws give the expression for absorption in solution:

$$\log_{10} Io/I_t = \Sigma cl$$

where Io and I_t are the intensities of the incident and transmitted light, respectively, c is the concentration ($mol.dm^{-3}$) of the absorbing species, l is the path length (mm) and Σ is a proportionality constant, referred to as the molar decadic extinction coefficient ($m^2.mol^{-1}$). The quantity Σcl is called the absorbance or optical density. It follows from the Beer-Lambert Law that the absorption coefficient is independent of the concentration, layer thickness and radiation intensity but varies with the wavelength of radiation.

Many experiments in the field of polymer photochemistry are carried out with films (as were the experiments carried out in this thesis) and Figure 1.1 represents a schematic for light crossing through the film layer.

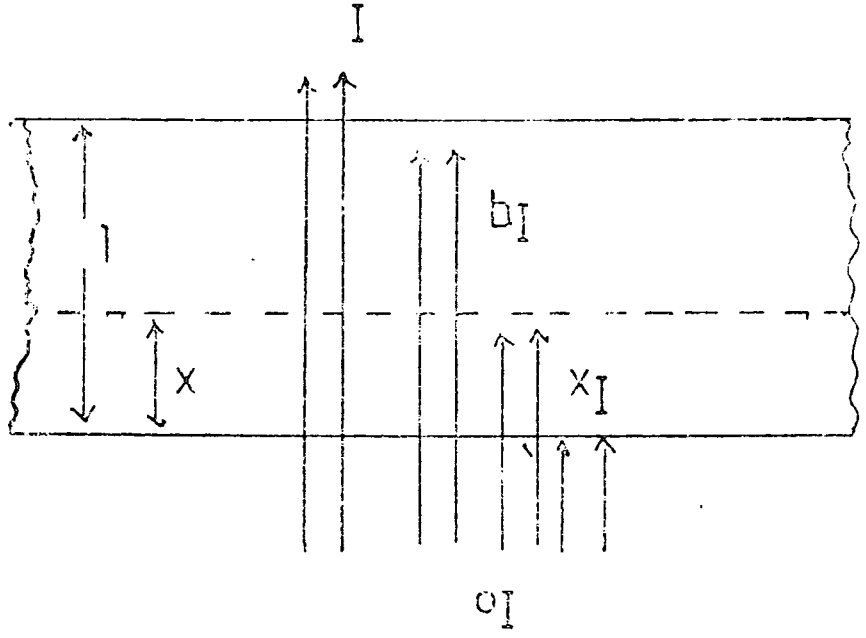

Figure 1.1 Schematic diagram of film exposed to light irradiation.

In a layer of thickness l of the film the absorbed light, Ia, is given by

$$Ia = Io\ (1 - e^{-\Sigma l})$$

The number of quanta absorbed per unit area of thickness clx may be written as

$$d\frac{(Io-It)}{dx} = -\frac{dI_t}{dx} = Io\Sigma l^{-\Sigma x}$$

1.2.2 Electronically Excited States

All photochemical reactions occur as a result of electronically excited states which have a definite energy, structure and lifteime.

The total energy (E) of a particular energy state of a molecule is the sum of the electronic excitation energy (Ee), the vibrational energy (Ev) and the rotational energy (Er):

$$E = Ee + Ev + Er$$

$$Ee > Ev >> Er$$

There are two types of excited states to be considered, singlet and triplet. In a singlet state the spins of the electrons are paired; this is almost always the case for the ground state for which the notation So is used. (A notable exception is the triplet ground state of molecular oxygen for which the spins are unpaired).

The main photochemical reactions occur from the lowest excited singlet state (S_1). The very fast rate of internal conversion from the upper excited singlet states (S_2, S_3 ----) to the lowest excited singlet state makes photo-

chemical reaction from the upper states unlikely. The lowest excited triplet state (T_1) is formed mainly by radiationless transition intersystem crossing from the lowest excited singlet state (S_1). The formation of a triplet state by direct absorption of a photon is a forbidden transition. Higher triplet states (T_2, T_3 ---) may be formed when a molecule in its lowest triplet state (T1) absorbs a new photon.[7] Each electronic level is split into a series of vibrational levels and each vibrational level is itself split into a series of rotational levels.[8] A modified Jablonsky diagram[9] which represents the structure of electronically excited states and the most important processes in which they are involved is shown in Figure 1.2.

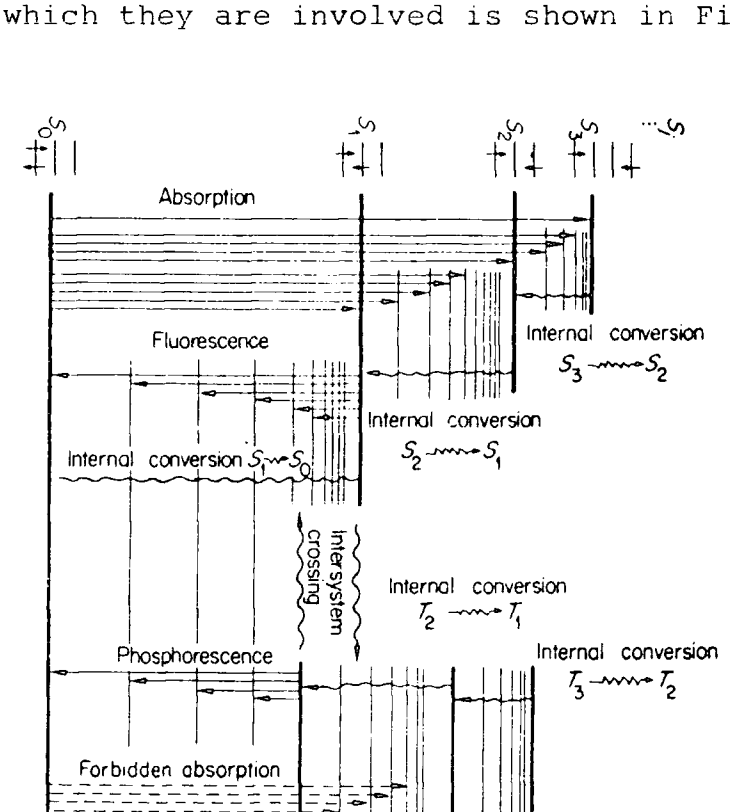

Figure 1.2 Modified Jablonsky diagram for the most important processes involving electronically excited states.

The dissipation of the excitation energy of a molecule in its excited state may occur by the following processes:

(i) Radiative processes: luminescence (fluorescence and phosphcrescence);

(ii) Radiationless processes;

(iii) Bimolecular deactivation processes;

(iv) Dissociation processes.

Luminescence arises from the emission of radiation as the electronically excited molecule loses its energy. There are two main kinds of emission:

(a) Fluorescence; this is an emission process occurring from the lowest excited singlet (S_1), to the ground state (So);

(b) Phosphorescence; this is an emission from the lowest triplet state (T_1) to the ground state.

A radiationless process converts one electronic state to another without the absorption of light. This can arise as a result of Internal conversion and/or Intersystem crossing.

Internal conversion is a process between two different electronic states of the same multiplicity, i.e. singlet-singlet (S_2 ⇝ S_1, S_1 ⇝ So) or triplet-triplet processes (T_2 ⇝ T_1). The rate of Internal conversion from the excited singlet (S_1) to the ground state (So) is of the order 10^6-10^{12} sec.$^{-1}$.[10] Intersystem crossing involves processes between singlet and triplet states (S_1 ⇝ T_1) or triplet and ground state (T_1 ⇝ So) occurring with spin inversion followed by vibrational relaxation. The rate of intersystem crossing for S_1 ⇝ T_1 is of the order 10^4-10^{12} sec.$^{-1}$ and for T_1 ⇝ So 10^{-1}-10^{-5} sec.$^{-1}$.[10]

1.2.3 Absorption of Light in Polymers

Somersall and Guillet[11] have classified polymers into two main types depending on their absorption and emission properties. The first, termed type A, absorb and emit light through isolated impurity chromophores situated as in chain or end chain groups. The second, termed type B, absorb and emit light through chromophores present in the repeat unit (or units) that form the backbone structure of the polymer.

There are many commercial polymers of type A which should theoretically only absorb light at wavelengths below 290 nm.[10,12] As previously mentioned the lower wavelength limit for sunlight reaching the earth's surface is ~290 nm and consequently type A polymers should theoretically not photodegrade under natural conditions. It is now generally believed that impurities, introduced during polymerization and/or processing are responsible for absorption of light above 290 nm.[10,12]. Examples of polymers belonging to this group are polyethylene, nylon and polystyrene. The absorption spectra for these systems are displayed in Figure 1.3 where for comparison some group B polymers are also included.

It can be seen that for polyethylene, nylon and polystyrene that little light is absorbed above 290 nm. However, it should be noted that the actual absorption spectra of these polymers is complicated since they all exhibit weak absorption in the near ultraviolet. As an example, in polyethylene, which is more crystalline, the absorption spectrum is not a true representation of the 'pure' molecule since light is scattered by the crystallites, particularly at shorter wavelengths.[13,14] All the polymers mentioned above are susceptible

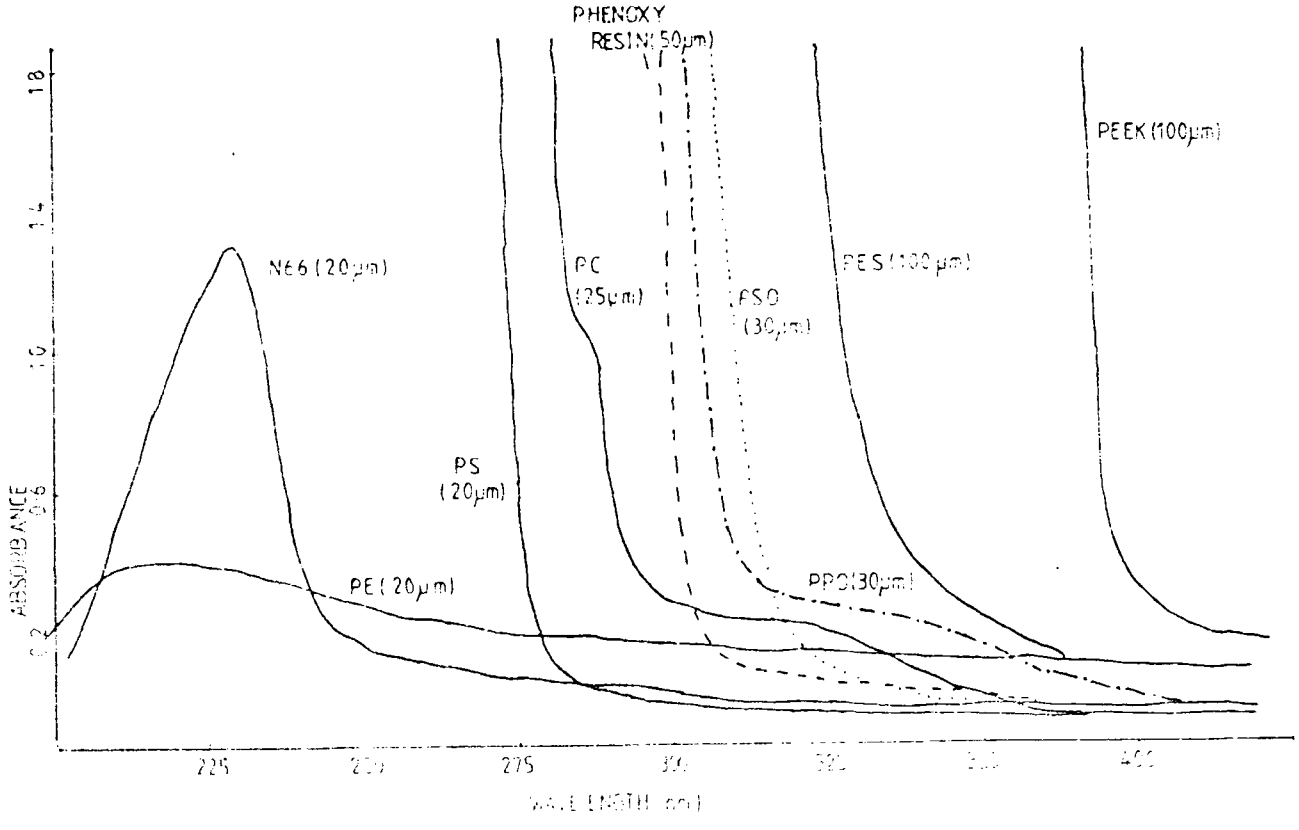

Figure 1.3 Ultraviolet absorption spectra of polyethylene (PE), nylon 66(N66), polystyrene (PS), polysulphone (PSO), polycarbonate (PC), phenoxy resin, polyphenylene oxide (PPO), polyether sulphone(PES) and polyether-ketone (PEEK) films.

to thermal degradation and oxidation to varying degrees during their manufacture and in particular processing and fabrication. The formation of chromophones (e.g. extended unsaturation and carbonyl groups)[10,12,15] extending the capacity of the polymer to absorb in the near ultraviolet may occur. Hydroperoxides groups may also be formed, but due to their low molar extinction coefficient will only make a small contribution.[10,12]

There are numerous commercial synthetic polymers which absorb sunlight through chromophoric groups that form part of the backbone structure of the system (i.e. type B). With the exception of polystyrene, all the polymers for which

the surface aspects of photoaging are discussed in later chapters belong to this group. Figure 1.3 displays the absorption spectra for polysulphone, polycarbonate, phenoxy resin, polyphenylene oxide, polyether sulphone and poly-etherketone. It can be clearly seen that they absorb strongly in the region 290-400 nm.

1.3 The Mechanism of Polymer Photooxidation

The mechanism of polymer photooxidation is very similar to that of thermal oxidation. At present, the theories of the oxidation of polymers have been based on the mechanism proposed by Bolland and Gee.[16,17,18]

General Mechanism of Oxidation

1.3.1 The initiation Reaction

A necessary condition for the rapid process of polymer oxidation is the formation of polymer radicals:

$$PH \longrightarrow P\cdot + H\cdot \qquad (1)$$

where PH is the polymer and P· the polymer radical. The initiation reaction may be induced by

(i) Physical factors such as UV radiation, ionizing radiation, temperature, ultrasonics and mechanical treatment,

(ii) Chemical factors such as catalysts, direct activity of oxygen, singlet oxygen or ozone.

(a) Physical factors

The chemical structure of the polymer will greatly influence the type of macro-radicals formed. The dissociation energies of particular bonds between the atoms of the polymer will dictate the type of fragmentation that occurs in relation

to the amount of energy being input to the system. Thus it is not surprising that most commercial polymers are susceptible to degradation in sunlight as there is no shortage of available energy in the near ultraviolet. In fact the quantum energy in this region is sufficient to cleave most polymer chemical bonds. The relationship between bond energy and the energy available from light is shown in Figure 1.4

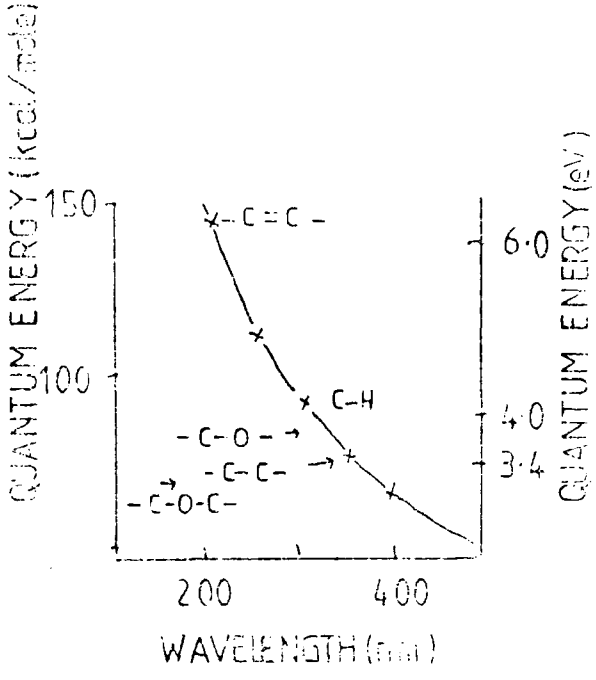

Figure 1.4 Bond strength in relation to light energy

(b) Chemical agents

(i) Initiation induced by molecular oxygen

The electronic configuration of the oxygen molecule may be written as follows:[19]

$$KK(\sigma g2S)^2(\sigma u2S)^2(\sigma g2P)^2(\pi u2P)^4(\pi g2P)^2$$

There are two unpaired electrons with each one in orbits having the orbital angular momentum equal to unity on the molecular axis but revolving in different directions. The total orbital angular momentum is zero. This configuration is denoted by the symbol $^3\Sigma$. The two elec trons are located predominantly with one electron on each of the two nuclei. Molecular oxygen has a biradical nature and can rapidly combine with radicals by addition to form peroxy radicals.

$$R\cdot + O_2 \longrightarrow ROO\cdot \qquad (2)$$

The direct reaction of molecular oxygen with a polymer is improbable due to the endothermic nature of the reaction (30-45 kcal $mole^{-1}$).[20]

(ii) Initiation by external initiators

Impurities in the form of catalysts, peroxides, hydroperoxides, inhibitors, solvents and other materials used in the synthesis of polymers may catalyse or sensitise photo-oxidation. Even the purest polymer will contain trace amounts of impurities. The initiation process is induced by the decomposition of the external initiator into free radicals which are then able to react with the polymer.

(iii) Initiation induced by singlet and atomic oxygen and by ozone

The reactions resulting from the initiation due to these species are receiving greater attention and are disucssed in further detail in Chapter Six.

1.3.2 The propagation reaction

Macro-radicals produced by the initiation reactions react with molecular oxygen to form peroxy radicals.

The addition of oxygen to a radical has been shown to depend strongly on the structure of the latter and hence stability (the more stable the less reactive). Electron spin resonance (esr) studies have detected polymer peroxy radicals.[21,22]

Reaction of a peroxy radical with another polymer molecule via hydrogen abstraction results in the formation of a hydroperoxide.

$$PH + POO\cdot \longrightarrow POOH + P\cdot \qquad (3)$$

In general peroxy radicals are selective electrophilic species and abstract tertiary bonded hydrogen in preference to secondary and primary bonded.[10]

1.3.3 Decomposition of Polymer hydroperoxides

Irradiation of polymer hydroperoxides with light above 300 nm is sufficient to cleave the PH-OH and P-OOH bonds but not the POO-H bond. The respective dissociation energies are 42, 70 and 90 kcal $mole^{-1}$.[23] On exposure to natural sunlight, the large separation in bond dissociation energy between PH-OH and P-OOH means that reaction (5) will predominate

$$POOH \xrightarrow{h\nu} P\cdot + \cdot OOH \qquad (4)$$

$$POOH \xrightarrow{h\nu} PO\cdot + \cdot OH \qquad (5)$$

Elevated temperatures[24-27] and metal catalysts[28,29] can also induce and promote hydroperoxide decomposition.

1.3.4 Formation of hydroxyl groups

The formation of hydroxyl groups results from the reaction between alkoxy polymer radicals and other polymer molecules

$$PH\cdot + PH \longrightarrow POH + P\cdot \qquad (6)$$

These groups may be formed along the polymer chain or on its end groups although the latter is relatively rare.[10,30]

1.3.5 Formation of carbonyl groups[10,30]

Carbonyl groups may be formed in different ways

(i) β-Scission of alkoxy radicals[31,32]

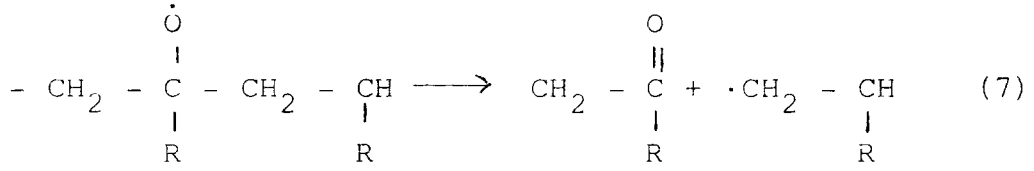

(7)

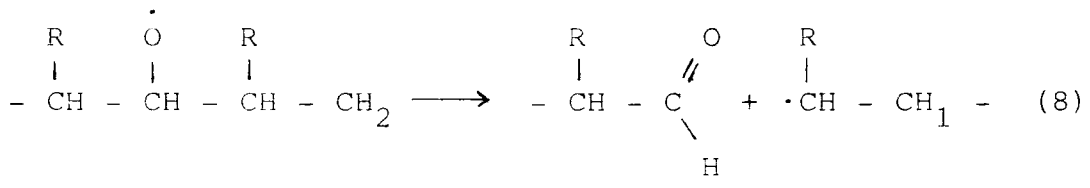

(8)

These reactions play an important role in the backbone scission of chains and in alkyl radical formation at chain ends.

(ii) A highly reactive hydroxyl radical resulting from the decomposition of a hydroperoxide may via a cage effect abstract a labile hydrogen atom, e.g. tertiary bonded hydrogen at the carbon atom. An intermediate biradical is formed which subsequently gives a carbonyl group.

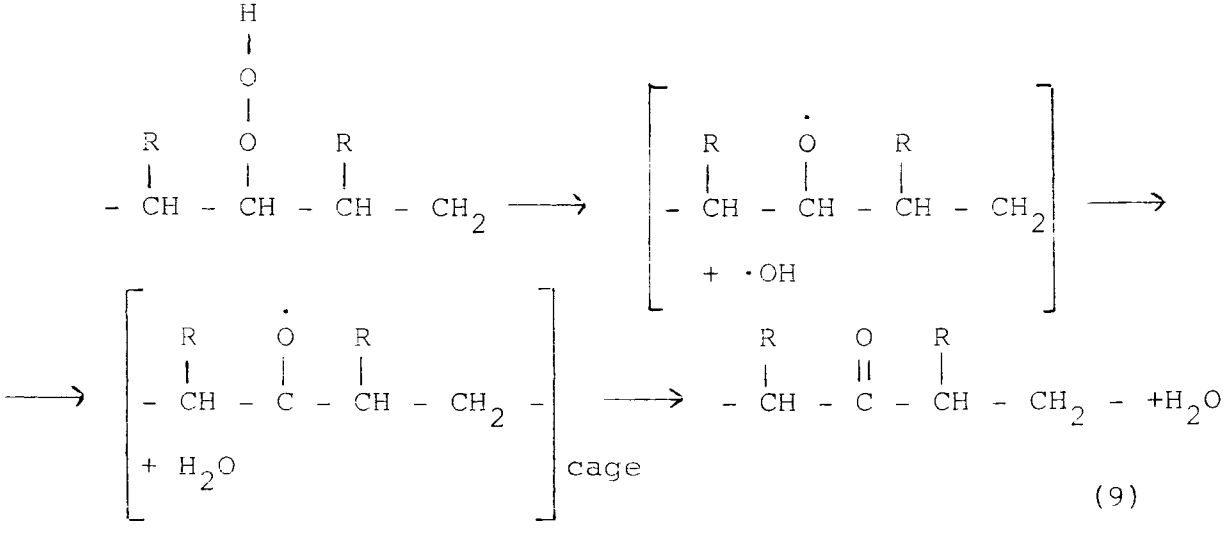

(9)

(iii) The decomposition of a hydroperoxide produces a biradical, water and the immediate formation of a ketonic group.

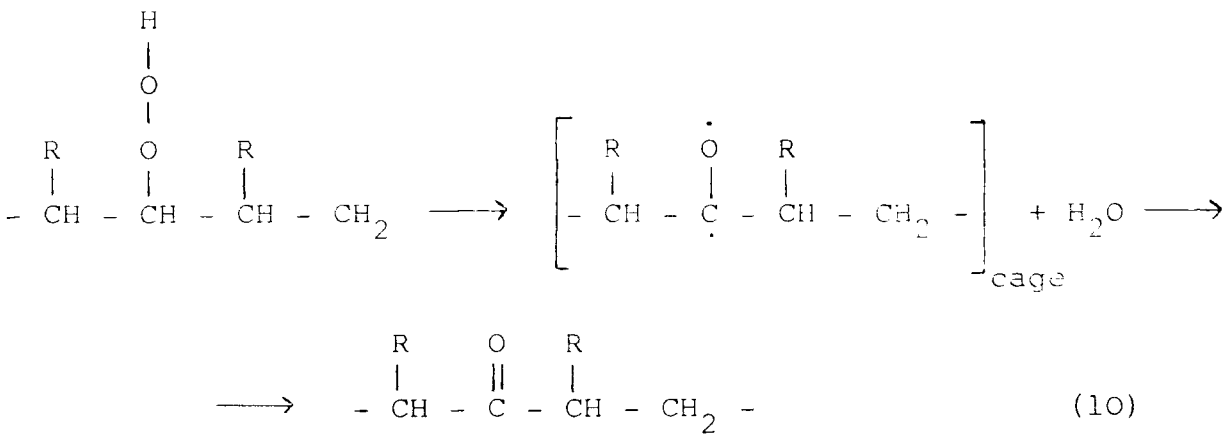

(10)

(iv) Reaction between two polymer alkoxy radicals producing simultaneously a carbonyl and hydroxyl group by disproportionation.

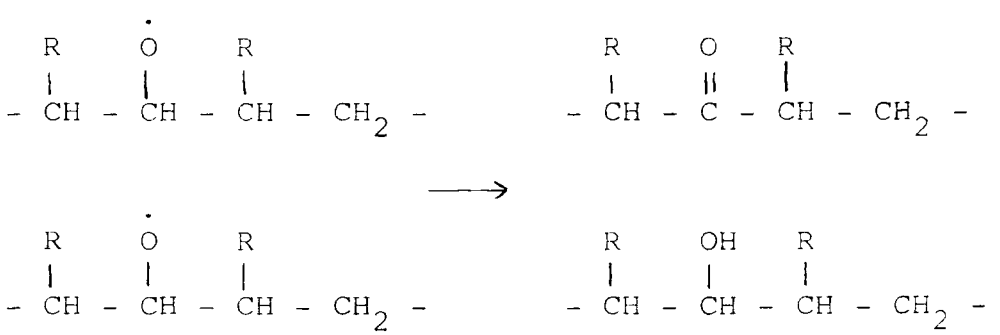

(11)

1.3.6 The Termination reaction[10,12,30]

Combination via the reactions of free radicals with each other terminate the radical chain to form inactive products.

$$\left.\begin{array}{ll} POO\cdot + POO\cdot & \\ POO\cdot + P\cdot & \text{inactive products} \\ P\cdot + P\cdot & \\ \text{etc.} & \end{array}\right\} \quad \begin{array}{l} (12) \\ (13) \\ (14) \end{array}$$

At high partial pressures of oxygen the termination reaction is predominantly equation (12).

1.3.7 Photochemical reactions of the carbonyl group

The ketonic products from the photo-oxidative processes and those found in trace amounts in pure polymers play important roles in the early stages of photo-oxidative degradation as well as in the continuation of an established reaction. The ketones may contribute to free radical processes, chain scission and energy transfer.

The carbonyl group shows absorption maxima in the range 270-330 nm.[4,8,33-35] The $n \rightarrow \pi^*$ transition involving the C = O group probably lowers the dipole moment of the ground state and reduces the negative charge on the oxygen atom or in its vicinity. The triplet state, formed by the inter-system crossing from the excited state $^1(n,\pi^*) \rightarrow {}^3(n,\pi^*)$ corresponds to the primary photochemically reactive state of carbonyl groups.[4,33-35]

The reactions involving the excited states of the carbonyl group are classified as Norrish reactions of Types I, II and III.[4,10,12,30]

(i) Type I: In the primary process, the bond between the carbonyl group and an adjacent α-carbon is homolytically cleaved. There are two possible primary reactions

$$\begin{aligned} & \qquad\qquad RCO\cdot + \cdot R^1 \longrightarrow R\cdot + CO + \cdot R^1 \\ RCOR^1 \xrightarrow{h\nu} & \qquad\qquad\qquad\qquad (15) \\ & \qquad\qquad R\cdot + R^1CO\cdot \longrightarrow R\cdot + CO + \cdot R^1 \end{aligned}$$

These reactions are responsible for the generation of free radicals and also cause chain scission

(ii) Type II: This is a non radical, intramolecular which proceeds via the formation of a six-membered cyclic intermediate. A hydrogen abstraction reaction from the γ-carbon

results in the subsequent decomposition into an olefin and an alcohol or an aldehyde:

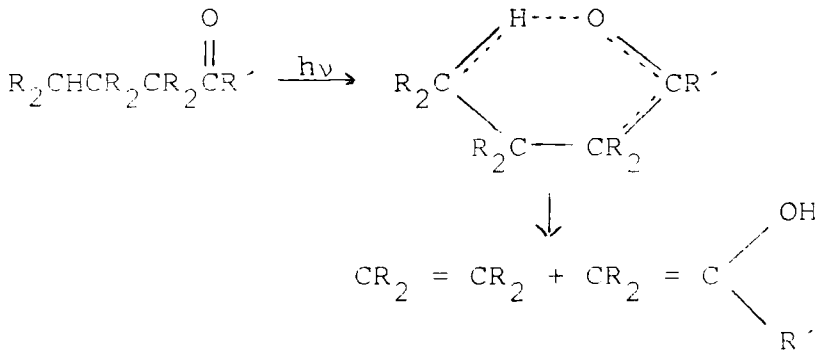

(16)

(iii) Type III: This is a non radical intramolecular process which involves transfer of a ß-hydrogen atom. This results in the formation of an aldehyde and an olefin through scission of the C-C bond adjacent to the carbonyl.

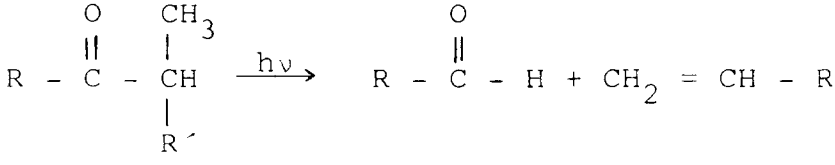

(17)

1.3.8 General mechanism of crosslinking

The process of polymer degradation is nearly always accompanied by a parallel competitive process of cross-linking which results in the formation of microgel.[30] Cross-linking may be described as the formation of new intermolecular bonds resulting in the binding of macromolecules together. It may result as a consequence of a secondary photochemical process or of subsequent thermal reactions. The overall effect is that the molecular weight increases until an insoluble gel is formed. The insoluble fraction then increases with dose while the average molecular weight of the soluble fraction decreases since the probability for the largest molecules to become crosslinked and part of the insoluble network is higher.[36]

In an oxygen free atmosphere, or in the presence of low concentrations of oxygen, the crosslinking of macroradicals follows the reaction:[37,38]

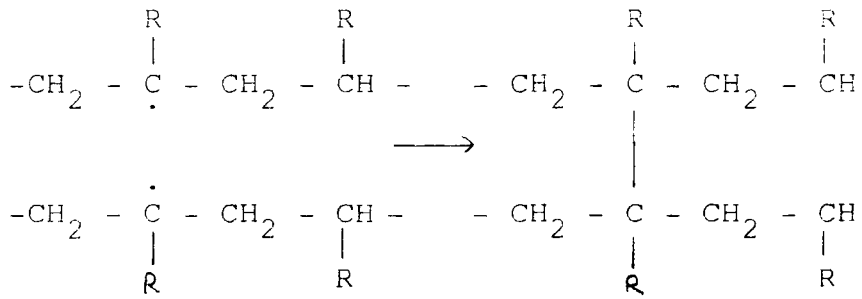

(18)

In the presence of oxygen and oxy-radicals produced, the crosslinking may involve ether and/or peroxy bridges

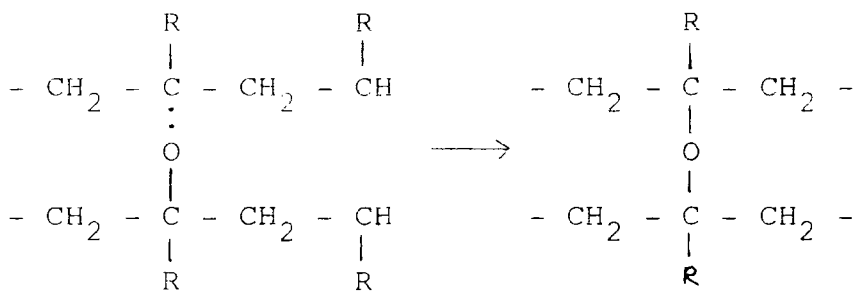

(19)

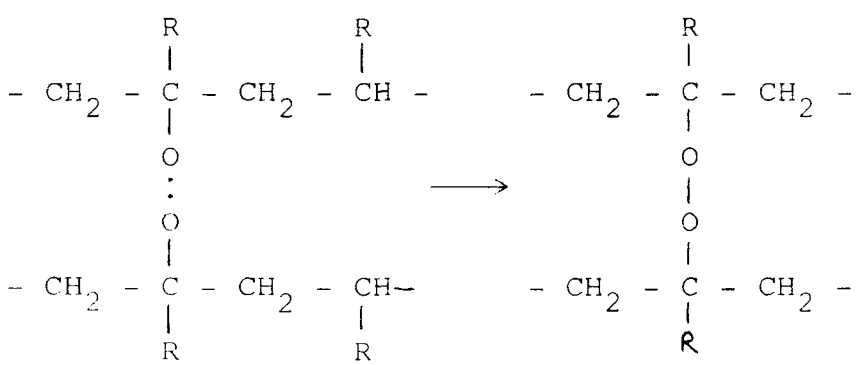

(20)

1.4 Experimental Methods

The principle behind any investigation concerned with the photodegradation of polymers is to expose the sample to light and to follow the changes in some selected property of the material. In general, commercial samples are tested in natural conditions or artifically weathered such that the environment such as light intensity, relative humidity and

temperature duplicate, as closely as possible, outdoor weathering. Purified and well characterised samples are on the other hand studied to obtain information of fundamental significance. In these cases, simple and well defined experimental conditions are used such that the influence of each variable may be studied. Both methods are complementary, since a sound knowledge of basic principles is required in order to interpret the mechanisms involved in the natural environment.

1.4.1 Evaluation of the light stability of polymers

The most practical and valuable test of polymer stability is undoubtedly that of natural weathering. However, outdoor exposures are not reproducible due to the variation of the climate, which is also dependent on location and season. Moreover, the tests are invariably slow and longer and longer exposure periods are required for the evaluation of new polymers with improved stability. As such these tests are best conducted in areas of high light intensity and/or relative humidity.

The gradual increase in exposure times and requirement for standardisation has led to the development of more powerful light sources.

1.4.2 Light Sources

The principal sources of ultraviolet radiation are carbon arcs, xenon arcs, mercury arcs and derived fluorescent lamps. A comparison of the spectral outputs of these sources with sunlight are displayed in Figure 1.5.

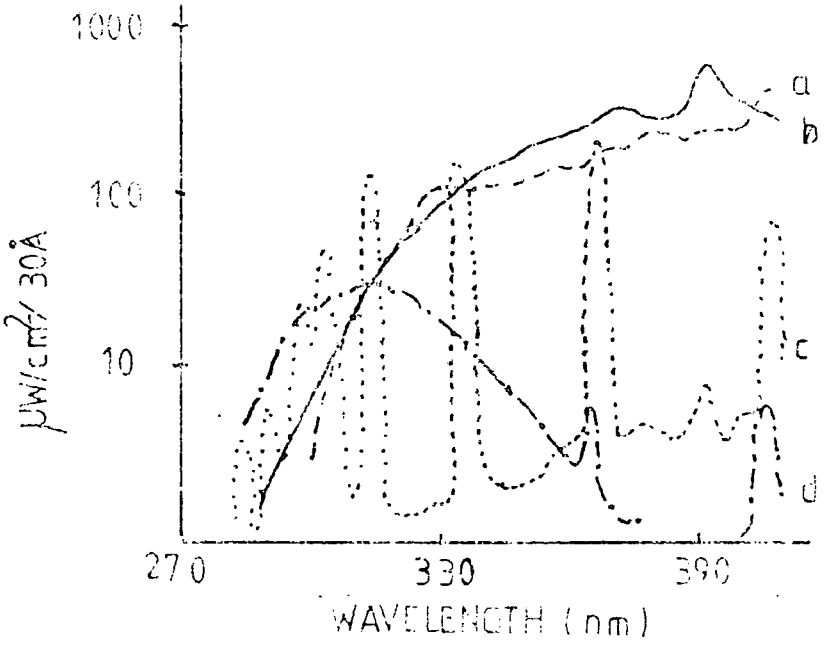

Figure 1.5 Energy distribution of various ultraviolet sources: (a) Sunlight, (b) Xenon arc, (c) Mercury lamp, (d) fluorescent lamp.

(a) Carbon arcs

Enclosed arcs have their major emission between 350 and 390 nm. The output below 350 nm is relatively weak and as this region is most damaging to clear plastics, the use of these sources for accelerating photodegradation must be treated with care. Open flame arcs employing Corex D filters give a better simulation of sunlight in the ultraviolet region.

(b) Xenon arcs[10,12,36]

These lamps are generally recognised to approximate the spectrum of sunlight better than any other commercially available equipment when appropriately filtered.

(c) Mercury arcs[4,10,12,36]

These are available in three forms, low, medium and high pressure lamps. They do not produce accurately the solar spectrum, with the energy output concentrated in the mercury emission lines. The medium pressure mercury arc lamp displays a profusion of lines of high intensity and with appropriate filtering for $\lambda > 290$nm, provides one of the cheapest sources of uv radiation of high intensity for photo-degradation studies.

(d) Fluorescent lamps[10,12,36]

In these lamps, the ultraviolet energy from the discharge through a low pressure mercury vapour is absorbed by a phosphor, applied as a coating on the inside wall of the tube, and irradiated as longer wavelength energy. Two commercially available lamps have been developed that emit in the regions around 320 nm (fluorescent sunlamp) and 360 nm (black lamp). These lamps show little individual resemblance to sunlight although a combination of both types gives a better approximation. It is of interest to note that the black lamp appears to be the only artificial ultraviolet source which induces changes in the bulk and surface chemistry of Bisphenol A polycarbonate comparable to those in natural weathering (c.f. Chapter Five).

1.4.3 Measurement of Light Intensity

Ideally all studies on the photodegradation and photo-oxidation of polymers, albeit natural or artificial weathering, will include information on the incident photon flux. Chemical actinometers such as the potassium ferrioxalate and uranyl oxalate actinometers[10,12] have been widely

employed but while they require little capital outlay and provide absolute measurements, they are time consuming and require a high degree of technical skill.

Over the years many workers have pursued the use of polymer films as disometers. Melchore[39] has shown that the growth of carbonyl groups in polyethylene films may follow the seasonal variation in solar uv. This technique is limited to high dosages due to the lack of sensitivity of polyethylene films. It also suffers from the serious limitation that the rate of photo-oxidation is dependent on temperature. Comparison of results obtained from different batches of films may be difficult due to varying degrees of surface oxidation incurred during processing.[10,12]

Davis *et al* have shown that the use of polyphenylene oxide[40] and polysulphone[41,42] films are suitable for monitoring the uv component of solar radiation. Chromophonic groups within the repeat units of these polymers are responsible for the absorption of light. The increases in optical density at 340 and 330 nm respectively are used to reflect the photon flux. Polyphenylene oxide is affected by wavelengths below 380 nm, polysulphone is only sensitive to radiation below 320 nm. The latter has been extensively used throughout this thesis. The advantages of using polymer films as dosimeters is that they may be placed in exactly the same configuration as the sample under investigation.

1.4.4 Measurement of chemical effects

The chemical changes induced by ultraviolet light have been the subject of investigation by a variety of techniques: infrared, ultraviolet and electron spin resonance

spectroscopy, vapour phase chromatography, mass spectrometry, molecular weight and gel fraction determination, luminescence measurements, etc. These techniques have been discussed in well documented reviews, on their application to polymer photo-degradation, by Searle[43] and to polymer chemistry in general by Rabek.[44]

These techniques are, in general, involved with the investigation of bulk changes. As all solids communicate with their environment via their surfaces, a knowledge of the changes in surface chemistry on exposure of polymer films to ultraviolet light is essential for a comprehensive understanding of the way in which solid polymers interact with the natural environment. The use of multiple attenuated total reflectance infrared spectroscopy (MATR-IR)[45] in part brings some understanding of surface changes but with a sampling depth of $\sim 1000\text{Å}$ it still does not necessarily reflect the changes at the gas/solid interface. Over the recent years, a surface sensitive technique, Electron Spectroscopy for Chemical Applications (ESCA), has been shown by Clark and co-workers[46-52] to be the singularily most powerful tool for the study of the degradation of polymer surfaces. With the exception of some preliminary photo-oxidation studies,[49-51] involving a broad band of incident uv radiation, ($\lambda > 230$ nm) and natural weathering investigation for extended exposure,[52] the photo-induced surface degradation of polymers has been relatively ignored in the literature. This is somewhat surprising when it is generally acknowledged that photodegradation and photo-oxidation of solid polymers is initiated in the surface.

The aim of this thesis has been to conduct a systematic

study of the model surface photoaging (λ>290 nm) of a number of aromatic polymers and to compare the results with those obtained for natural weathering.

CHAPTER TWO

ELECTRON SPECTROSCOPY FOR CHEMICAL APPLICATIONS (ESCA)

2.1 Introduction

The ESCA experiment involves the measurement of binding energies of electrons ejected by interactions of a molecule with a mono-energetic beam of soft X-rays. As with most other spectroscopic techniques, X-ray photoelectron spectroscopy was originally developed by physicists and is now extensively utilised by both organic and inorganic chemists as a tool to provide valuable information on structure, bonding and reactivity.[53]

The first experiments that observed the photoelectric effect were conducted by Hertz in 1886 and 1887.[54] It was discovered that an electric discharge between two electrodes occurred more readily when ultraviolet light falls on one of the electrodes. Lenard,[55] in 1900, showed that the absorption of light by the metal is followed by emission of electrons from the metal.

The experiments on the photoelectric effect show that the energy of photoelectrons is independent of the intensity but proportional to the frequency of the incident radiation, ν, and the number of photoelectrons emitted per second is proportional to the intensity of the incident radiation. This phenomena cannot be explained by the classical wave theory of light. But in 1905 Einstein,[56] who first realised the light quantum concept, introduced by Planck in 1900, was able to explain the photoelectric effect. He suggested that light was more like a stream of particles, photons, each possessing energy $h\nu$, where h is the Planck constant. In the photoelectric effect each of these photons gives up its energy to

an electron in the metal. Part of the photon energy is used in just removing the electron from the metal surface and the remainder appears as the kinetic energy (KE) of the photo-electron, given by the equation:

$$h\upsilon = KE + W \qquad (1)$$

where W is the 'work function', the minimum energy needed to remove the electron from the metal's surface.

The emission of electrons from various elements by the X-ray irradiation of thin foils was studied by Robinson[57] and de Broglie.[58] The distribution of electron energies for the transmitted photoelectrons was recorded photographically and analysed using a homogeneous magnetic field. Since the radiation source consisted of a continuous spectrum (bremsstrahlung) with the characteristic line spectrum of the anode material superimposed, the electron distributions obtained were characterised by long tails with distinct edges at the high energy end. Measurement of these edge positions gave a determination of the energy levels of the different atomic levels and with a knowledge of the exciting X-ray line, binding energies were calculated.

With the exception of a few isolated attempts to extend the work of Robinson and de Broglie,[59-61] X-ray photoelectron spectroscopy went into recession. It was not until the early 1950s, when Siegbahn and co-workers[62] at the Institute of Physics, Uppsala University, Sweden, developed an iron-free magnetic double focussing electron analyser for the high resolution studies of β-ray energies, that the technique was further extended. Early attempts to record high resolution photoelectron spectra excited by X-rays and the observation

of a sharp line which could be resolved from each electron veil changed the course of further developments of the technique. The photoelectrons to which this line corresponds had the important property that they did not suffer energy losses and, therefore possessed the binding energy of the atomic level from which they came and could be measured to a precision of a few tenths of an electron volt.

Much of the early work of Siegbahn and co-workers was extensively documented in 1968 in 'ESCA. Atomic, Molecular and Solid State structure studied by Means of Electron Spectroscopy'.[63] Later work was summarised in 1969 in 'ESCA Applied to Free Molecules'.[64]

The technique of ESCA is also known as:

(1) X-ray Photoelectron Spectroscopy (XPS)

(2) High Energy Photoelectron Spectroscopy (HEPS)

(3) Induced Electron Emission Spectroscopy (IEES)

(4) Photoelectron Spectroscopy of the Inner Shell (PESIS).

There are many approaches available by which electrons, characteristic of the material from which they originate, may be generated. In each of these distinct techniques, the energies of the electrons are analysed following the collision between an impacting particle or photon and an atom, molecule or solid and may be classified under the generic term 'electron spectroscopy'. Table 2.1 lists various types of electron spectroscopy and for detailed descriptions of the various techniques the reader is referred to recent reviews by Baker and Brundle[65] and Rhodin and Gadzuk[66] and references therein.

TABLE 2.1 Types of Electron Spectroscopy

Name of Technique	Basis of Technique
Photoelectron spectroscopy UPS or (Ultraviolet excitation) PES	Electrons ejected from materials by monoenergetic ultraviolet photons are energy analysed.
Photoelectron spectroscopy ESCA or (X-ray excitation) XPS	Electrons ejected from materials by monoenergetic X-ray photons are energy analysed.
Auger electron spectroscopy AES	Auger electrons ejected from materials following initial ionisation by electrons or photons (not necessarily monoenergetic) are energy analysed.
Ion neutralisation spectroscopy INS	Auger electrons ejected from surfaces following impact of a noble gas ion are energy analysed.
Penning ionisation spectroscopy PIS	Metastable atoms are used to eject electrons from materials. The electrons are energy analysed.
Autoionisation electron spectroscopy	Similar to Auger electron spectroscopy. Electrons ejected in an autoionising decay of super-excited states are measured. Electron or photon impact can be used to produce the super-excited states.
Resonance electron capture electron transmission spectroscopy	The elastic scattering cross-section for electrons is measured as a function of the energy of the electron beam and scattering angle.

2.2 Processes Involved in ESCA

2.2.1 Photoionisation

Irradiation of a molecule with X-rays causes electrons with binding energies less than that of the exciting radiation to be photoejected.[63] The X-ray sources in common use today are $MgK_{\alpha_{1,2}}$ and $AlK_{\alpha_{1,2}}$ with photon energies of 1253.7 eV and 1486.6 eV respectively. The ejected electrons may be either core or valence electrons (Figure 2.1) though the latter are usually studied using ultraviolet photoelectron spectroscopy (UPS)[67] with He(I) (21.22eV) or He(II) (40.8eV) radiation.

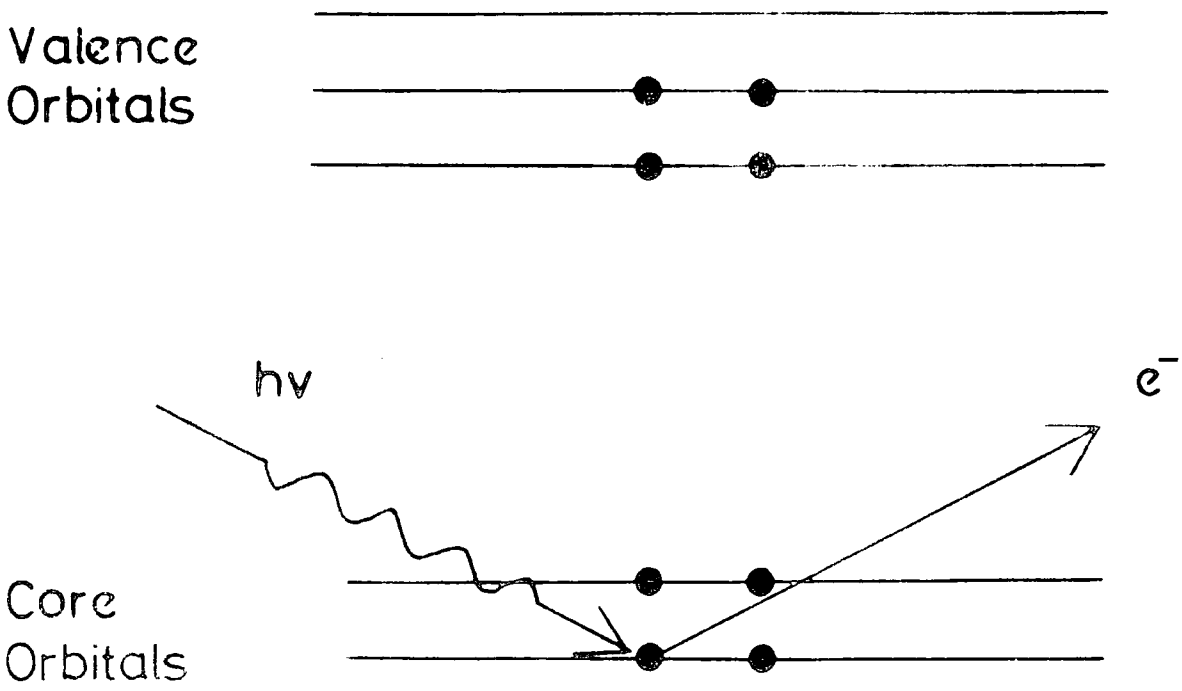

Figure 2.1 The photoionisation of a core level electron

It has been shown that the relative intensities of various peaks in the valence electron spectrum vary with differences in the incident excitation energy, not only between X-ray and uv, but between X-ray photons of different energies.[69] These effects are attributed to differences in photoionisation cross-sections involved in the various electron states in the valence band region. (The cross-section for photoionisation for a particular level is a measure of the probability of the level being ionised when irradiated by a photon of known energy).

Typically, the photoemission processes are complete in 10^{-17} secs.[70] This emphasises the extremely short time scale involved in ESCA compared with most other spectroscopic techniques.

The total kinetic energy of an emitted photoelectron (K.E., which may include the contributions from the vibrational, rotational and translational motions, as well as electronic) is given by equation (2)

$$K.E. = h\nu - B.E. - Er \qquad (2)$$

where $h\nu$ is the energy of the incident photon, h is Planck's constant and ν is the frequency of the X-ray radiation. B.E. is the binding energy of the emitted electron which is defined as the positive energy required to remove an electron to infinity with zero kinetic energy and Er is the recoil energy of the atom. Siegbahn and co-workers[63] have shown that the recoil energy is usually negligible for light atoms when using typical X-ray sources, for example $MgK_{\alpha_{1,2}}$ and $AlK_{\alpha_{1,2}}$. This is not the case however where high energy X-rays (e.g. AgKα(22000ev)) are employed, and recoil energies for light elements must be

taken into account. Recent studies by Cederbaum and Domcke[71] show that these effects can lead to modifications of the vibrational band envelopes of light atoms and hence Er is significant and must be taken into account. With the present resolution of typical ESCA spectra the excitations from the translational, vibrational and rotational motions are seldom observed to contribute to the final K.E. Therefore equation (2) for free molecules reduces to:

$$K.E. = h\nu - B.E. \qquad (3)$$

It is important to understand the relationship that exists between the binding energies observed experimentally by ESCA for solids versus free molecules when compared with the values calculated theoretically by '*ab initio*' and semi-empirical LCAO-MO-SCF treatments.

The most convenient reference level for a conducting sample is the Fermi level.[72] In a metal this level, sometimes referred to as the 'electron chemical potential', is defined as the highest occupied level at absolute zero.

The work function, ϕs, for a solid is defined as the energy gap between the free electron vacuum) level and the Fermi level in the solid, and is represented diagrammatically in Figure 2.2. The vacuum levels for the solid sample and the spectrometer may however be different and the electron will experience either a retarding or accelerating potential equal to $\phi_s - \phi_{spec.}$ where $\phi_{spec.}$ is the work function of the spectrometer.[63] In the ESCA experiment it is the kinetic energy of the electron when it enters the analyser that is measured, and taking zero binding energy to be the Fermi level of the sample the following equation results:

$$B.E. = h\nu - K.E. - \phi_{spec.} \qquad (4)$$

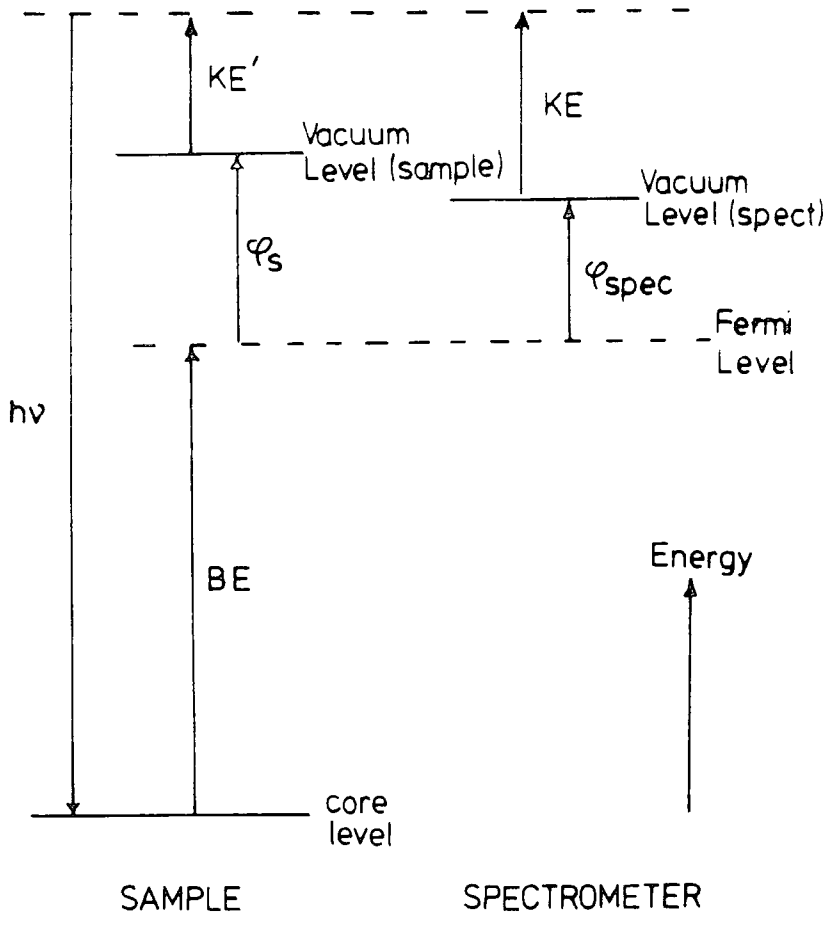

Figure 2.2 Relationship between vacuum level and Fermi level for a sample isolated from the spectrometer

The binding energy referred to the Fermi level does not depend on the work function of the sample but on that of the spectrometer and this represents a constant correction to all binding energies. Energy referencing and sample charging effects are considered in Section 2.5.

2.2.2 Processes Accompanying Photoionisation

Several processes may accompany photoionisation and these may be divided into two main categories depending upon whether they are slow compared to the original photo-ionisation or occur within a similar time span. Electronic relaxation, shake-up and shake-off occur within a similar time span and result in modification of the kinetic energy of the

photoelectrons. Auger emission and X-ray fluorescence however are comparatively slow processes and cause little effect on the kinetic energy of the photoelectron.

2.2.3 Electronic relaxation

Accompanying the photoionisation process, which is complete within a time scale of approximately 10^{-17} secs., there is a substantial electronic relaxation of the valence electrons.[73-75] Theoretical and experimental studies have shown that for a given core level the magnitude of relaxation energy (RE) is a sensitive function of the electronic environment of a molecule.[76-80] It is of considerable importance in determining not only the absolute binding energy of a core electron but also in determining the line shapes of observed peaks by means of vibrational fine structure. Relaxation energies associated with core ionisations of first row elements have been found to be considerable[80,81] and are caused by the reorganisation of the valence electrons in response to the decreased shielding of the nuclear charge. This reorganisation changes the spatial distribution of the remaining electrons. The differences in RE for closely related molecules are small and therefore cause only small changes in binding energies.

The theory of chemical shift in core electron binding energies has received much attention.[69,75,82] Whereas the ionisation energies of core electrons in small molecules can be calculated by '*ab initio*' methods, this procedure is unrealistic when dealing with polyatomic molecules. It is then necessary to resort to semi-empirical methods. The use of Koopmans' Theorem[83] in the calculation of binding energies does not account for electronic relaxation, whereas self-consistent

field (ΔSCF) calculations do take account of RE. This provides a method by which relaxation energies may be investigated.

$$R.E. = B.E.\ (Koopmans) - B.E.\ (\Delta SCF) \qquad (5)$$

2.2.4 Shake-up and Shake-off Phenomena

Although core electrons are essentially localised in the proximity of the nucleus, and do not take any part in bonding, the major contribution to the total energy of an atom or molecule arises from the core electron, which closely monitor valence electron distributions. As well as the relaxation processes described in the previous section, the sudden perturbation of the valence electron cloud accompanying core ionization gives rise to a finite probability for photoionisation to be accompanied by simultaneous emission of a valence electron from an occupied orbital to a virtual orbital (shake-up) or ionisation of a valence electron (shake-off) as illustrated in Figure 2.3.

These relaxation processes result in excited states of the core ionised species, and give rise to satellite peaks on the low kinetic energy side of the direct photoionisation peak. Therefore, a revision of equation (3) is needed to account for these multi-electron processes:

$$K.E. = h\ - B.E. + \bar{E} \qquad (6)$$

where $\bar{E}$ is the energy of the multi-electron process.

In the sudden approximation, transition intensities are directly related to the sums of one centre overlap terms involving the occupied orbitals of the initial system and the unoccupied (relaxed orbitals) of the final state.[84] It may be shown that excitation of states within the limits of the approximation obey monopole selection rules:

$$(\Delta J = \Delta L = \Delta S = \Delta M_J = \Delta M_L = \Delta M_S = 0) \qquad (7)$$

and in some ways may be viewed as an analogue of ultraviolet spectroscopy in ESCA.

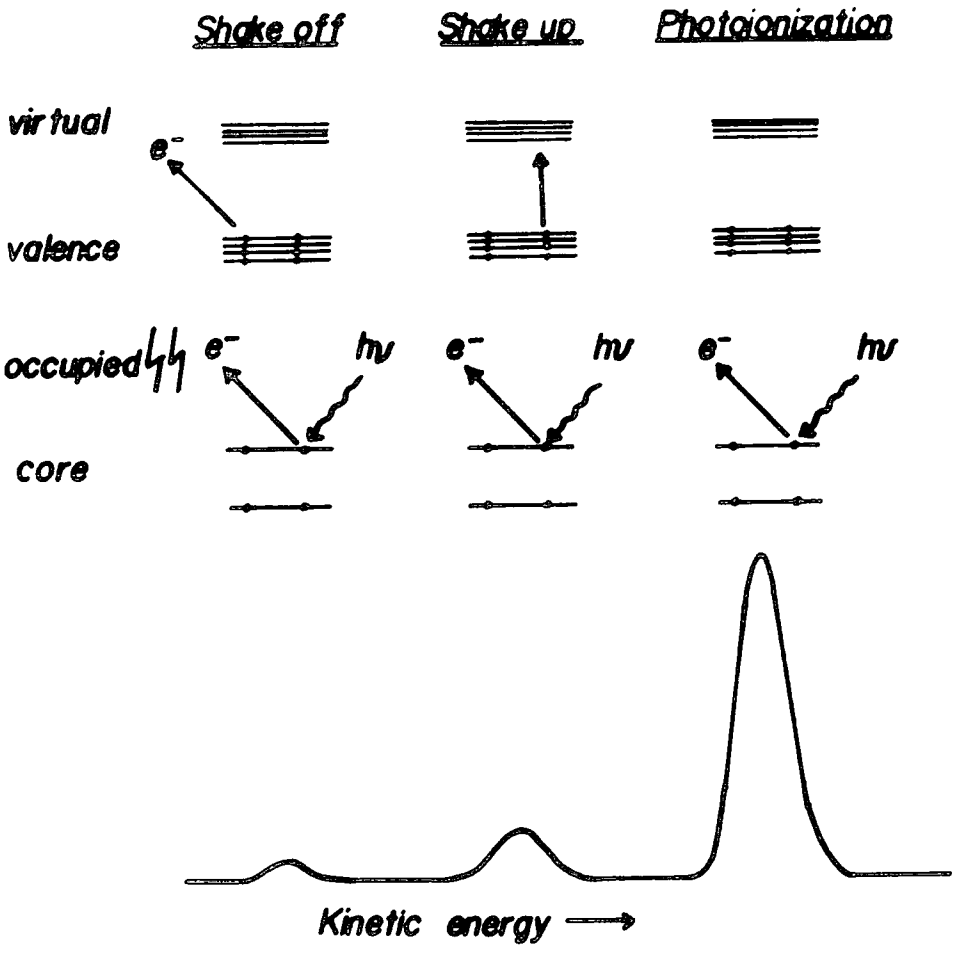

Figure 2.3 Photoionisation, shake-up and shake-off

The probability of exciting an electron from the orbital denoted by nlj of the neutral atom to the orbital n´lj of the ion, is given by:

$$P_{n'lj \longleftarrow nlj} = N\left|\int \Psi^*_{nlj} \Psi_{n'lj}\, d\tau\right|^2 \qquad (8)$$

where N is the number of electrons in orbital nlj and Ψ_{nlj}, $\Psi'_{n'lj}$ are the wavefunction of orbital nlj, n´lj in the atom and ion respectively.

Considering excitations involving a core hole state in the doublet manifold, as shown in Figure 2.4, it is apparent

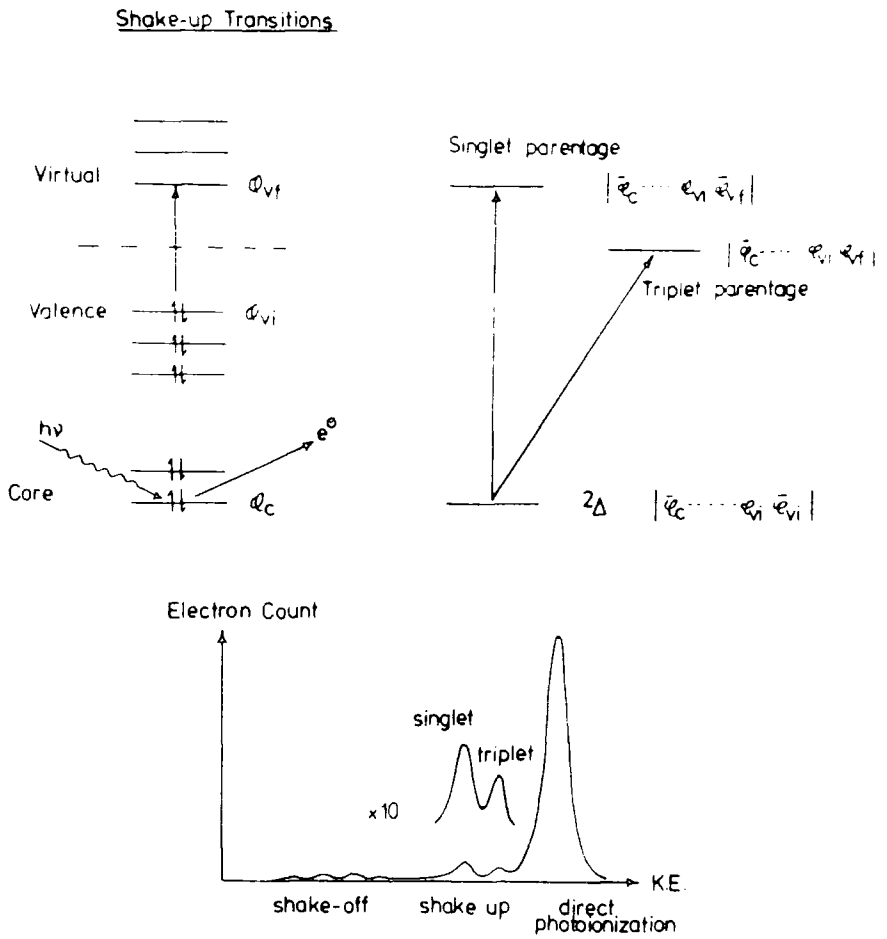

Figure 2.4 Schematic illustration of Singlet-Triplet shake-up

that within a simple orbital model, there are two possible states that can be generated. Either unpaired electron in the valence orbital and that excited to the virtual orbital will have opposite spins ("singlet origin"), or they both have the same spin, whilst the remaining core electron has the opposite spin ("triplet origin"). The triplet state is lower in energy than that of singlet origin, however since both represent doublet states, transitions from the ground state of the core hole may be viewed as both being allowed. In

principle, therefore, it should be possible to experimentally observe the energy separations and intensities for the components of the shake-up states of a given excitation configuration.

The theoretical relationship between shake-up, shake-off and electronic relaxation energies has been discussed by Manne and Åberg.[85] They showed that the weighted mean of the direct photoionisation, shake-up and shake-off peaks corresponds to the binding energy of the unrelaxed system (given by Koopmans' Theorem), and this is schematically shown in Figure 2.5.

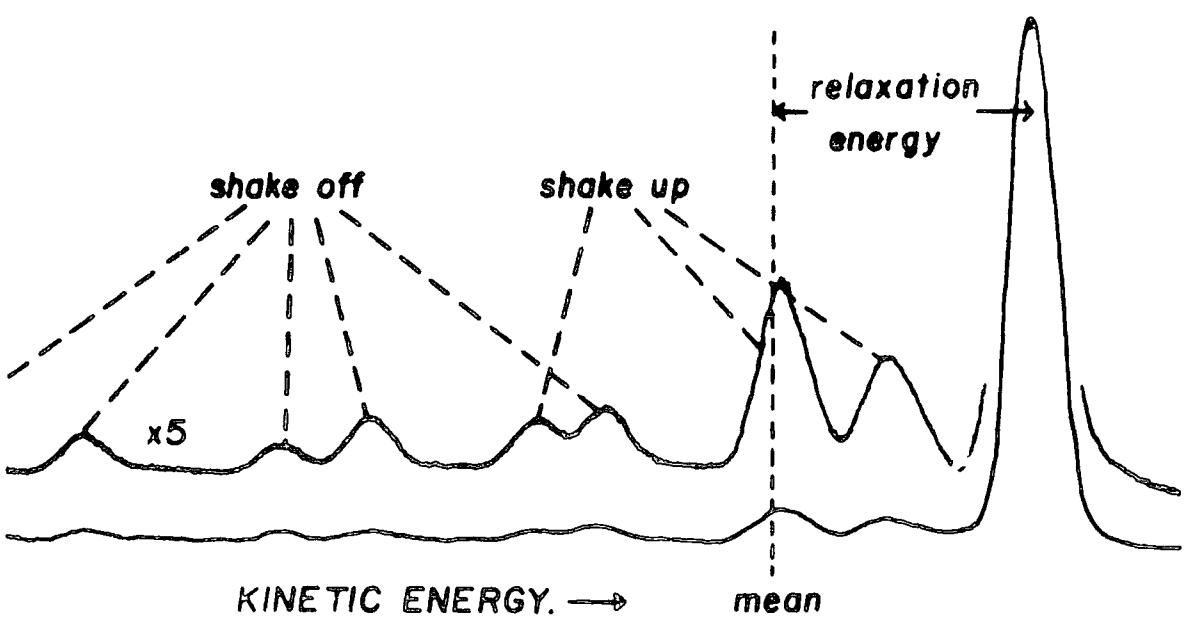

Figure 2.5 Relationship between relaxation energy, Koopmans' Theorem (mean) and the relative intensities of direct photoionisation, shake-up and shake-off.

The transition probabilities for high energy shake-off processes are relatively small compared to shake-up processes, and the transitions of highest probability fall reasonably close to the weighted mean. In principle, the relaxation energy should be available from experimental data of direct photoionisation, shake-up and shake-off, but in practice this is not feasible. This problem arises from the general 'inelastic tail' which is due to the direct photoionisation, followed by energy loss by a variety of ineleastic processes. This produces a broad energy band which peaks (for organic systems) at approximately 20 eV below the direct photoionisation peak.

Shake-up and shake-off structure has been studied in organic and inorganic materials with particular attention to the transition elements. The phenomenon of shake-up has proved to be of use in elucidating fine details of structure and bonding, in polymer systems which are not directly attainable from the primary information levels in ESCA.[86-88]

2.2.5 Auger Emission and X-ray Fluorescence

There are two principal processes through which de-excitation of the hole produced in a core sub-shell normally decays, namely Auger electron emission and X-ray fluorescence.[89] Both these processes, which are shown schematically in Figure 2.6, are comparatively slow compared to photoionisation and so they have little effect on the kinetic energy of the original photoelectron.

The probability for each process is a function of the atomic number of the atom as shown in Figure 2.7, Auger emission predominantly for lighter atoms[90] while X-ray fluorescence is

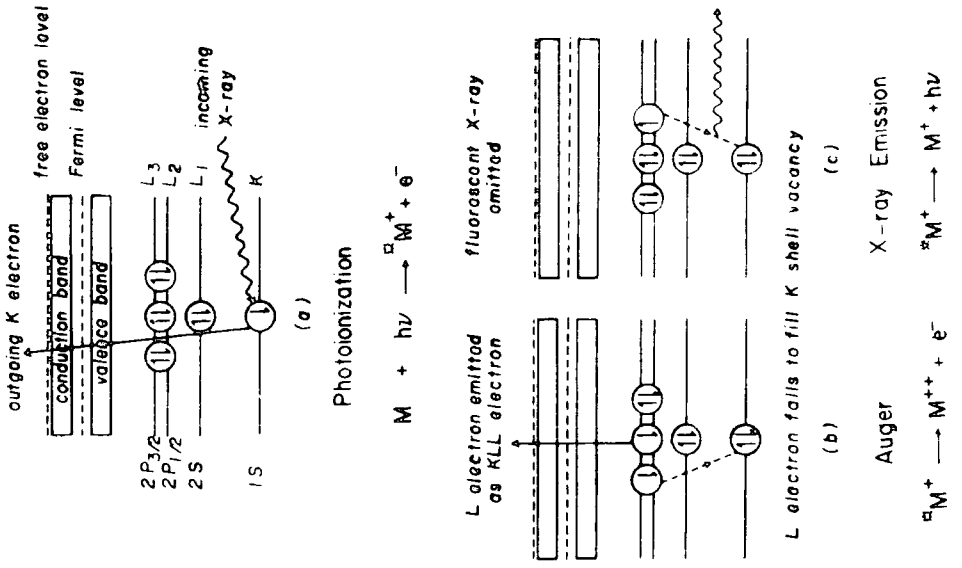

Figure 2.6 Photoionisation, Auger emission and X-ray Fluorescence

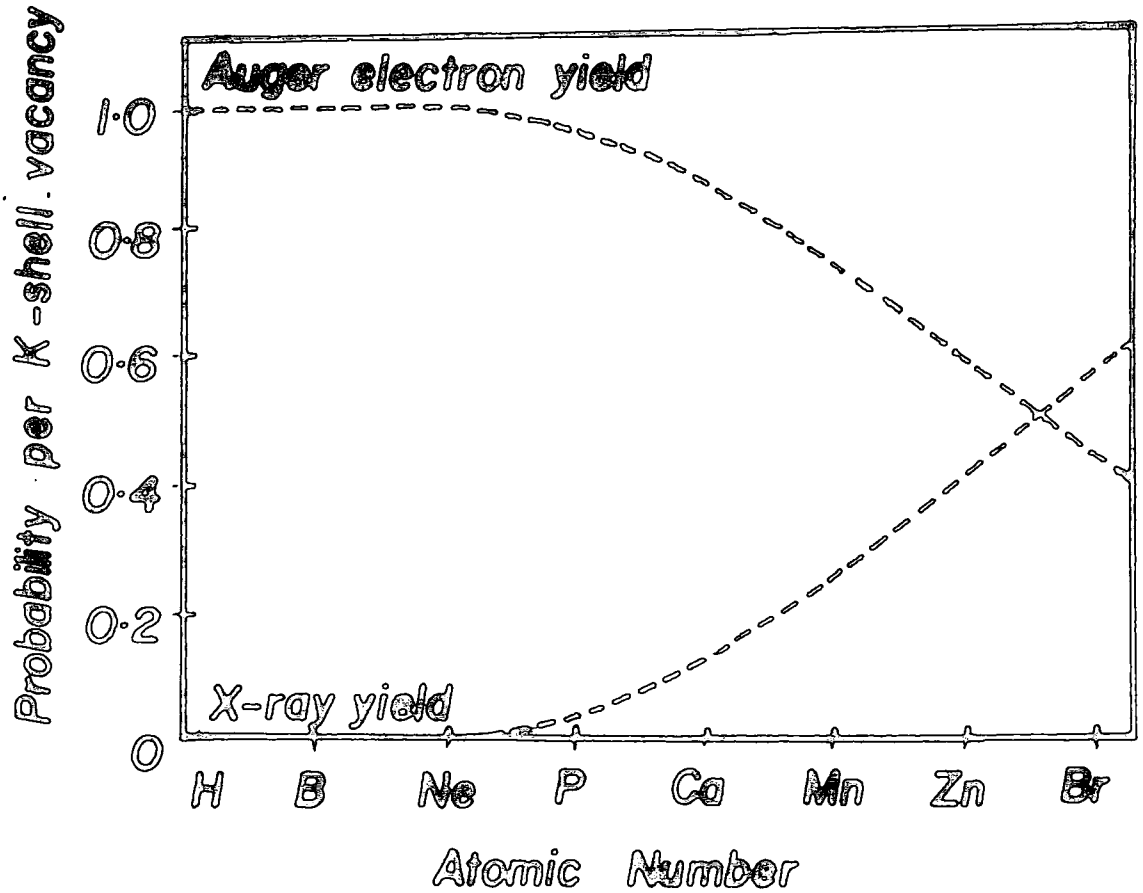

Figure 2.7 Efficiency of Auger and X-ray Fluoroescence processes as a function of atomic number

more important for heavier elements.

Auger emission may be viewed as a two-step process in which the ejection of an electron from an inner shell by a photon is followed by an electron dropping down from a higher level to the vacancy in the inner shell with simultaneous emission of a second electron.[91-96] When the electron drops from a valence orbital, the Auger spectrum is related to the energies of both the valence and core orbitals. When the electron drops from an inner orbital, a Coster-Kronig transition,[95] the Auger spectrum is related to the inner orbital transition. Such spectra are often very well resolved but unfortunately lead to broadening of the ESCA spectrum due to the very short lifetime of the process. For a Coster-Kronig process to occur, the difference in binding energies of the two inner shells must be sufficiently large to eject an electron from an orbital in the higher shell. These processes only occur in elements of atomic number <40.[97]

Auger emission spectroscopy (AES) is itself an important analytical technique and has found particular application to the study of the surfaces of metals and semi-conductors. Commercial Auger spectrometers use an electron beam as the source of excitation radiation. The flux dosage of the incident electron beam is approximately three orders of magnitude larger than typical ESCA photon beams and radiation damage to organic materials is therefore a severe problem.[98,99]

The complexity of the Auger electron signal does not allow such a straightforward extraction of chemical information as in ESCA. However, in the case of metal oxides, for example, the Auger chemical shift is much larger than the photoelectron chemical shift because of polarisation screening effects, the

direc tion of the shift being such that the kinetic energy of Auger electrons from more polarisable salts is increased more than is the energy of the photoelectrons.

From the work of Shirley, Kowalczyk, Ley, McFreely and Pollak[100-103] involving studies of Cu, Zn, Li and Na systems and the independent investigations by Wagner[104] and co-worker Bilden,[105] a relationship between shifts in Auger energy and the shifts in photoionisation was derived.[103]

The concept of the Auger Parameter has since been developed by Wagner.[106] This is taken as the kinetic energy of the sharpest and most intense Auger line minus that of the most intense photoelectron peak and is of considerable value to analytical chemists because it is a quantity independent of sample charging effects. Chemical state scatter plots[107,108] on which photoelectron and Auger data are represented for a given element are likely to be of considerable importance in the use of ESCA for identification of chemical states.

2.3 Chemical Shifts

The core electrons of an atom are essentially localised and do not take part in bonding. Their energies are characteristic of the particular element and are sensitive to the electronic environment of the atom. While the absolute binding energy of a given core level on a given atom will be characteristic of the element (Table 2.2), differences in electronic environment of a given atom in a molecule give rise to a small range of binding energies, 'chemical shifts', often representative of a given structural feature. Figure 2.8 displays the C_{1s} spectrum of ethyl trifluoroacetate, a classical illustration of chemical shifts. Shifts in core levels

TABLE 2.2 Approximate core binding energies (eV)

	Li	Be	B	C	N	O	F	Ne
1s	55	111	188	284	399	532	686	867
	Na	Mg	Al	Si	P	S	Cl	Ar
1s	1072	1305	1560	1839	2149	2472	2823	3203
2s	53	89	118	149	189	229	270	320
$2p_{1/2}$	31	52	74	100	136	165	202	247
$2p_{3/2}$	31	52	73	99	135	164	200	245

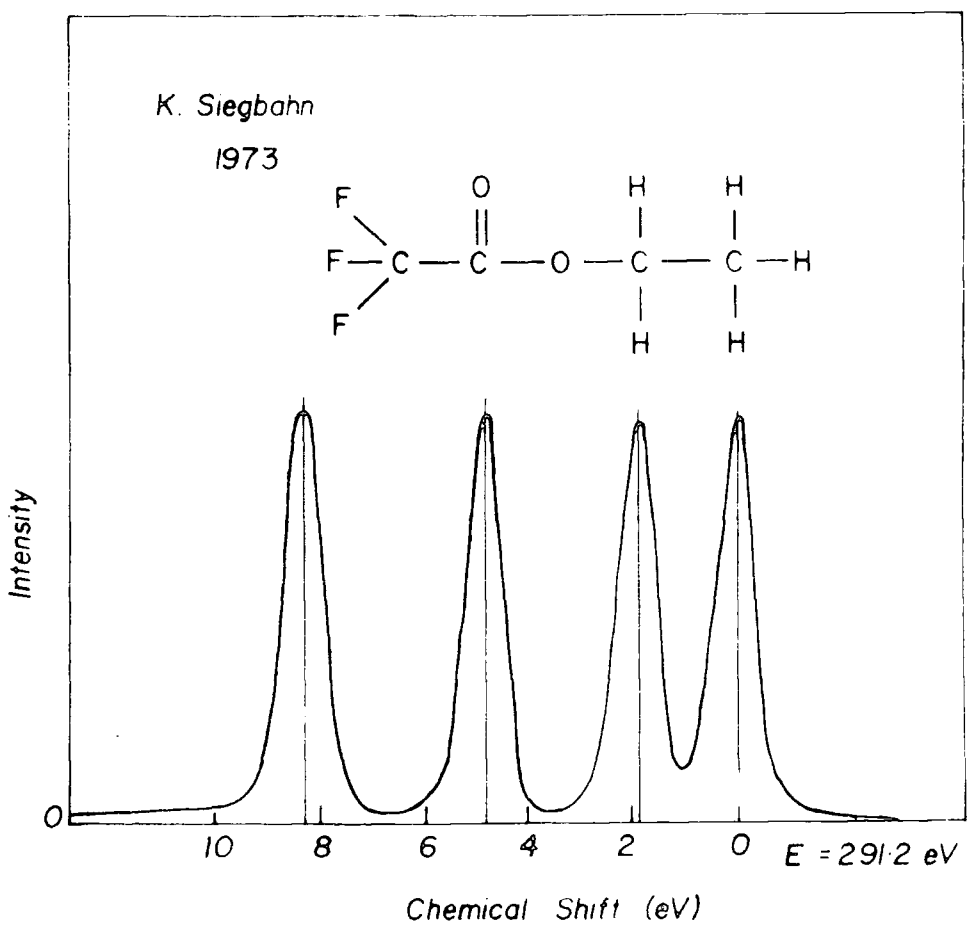

Figure 2.8 $^{C}1s$ spectrum of trifluoroacetate

as a function of substituent for a wide range of polymers which have been investigated experimentally are shown in Table 2.3

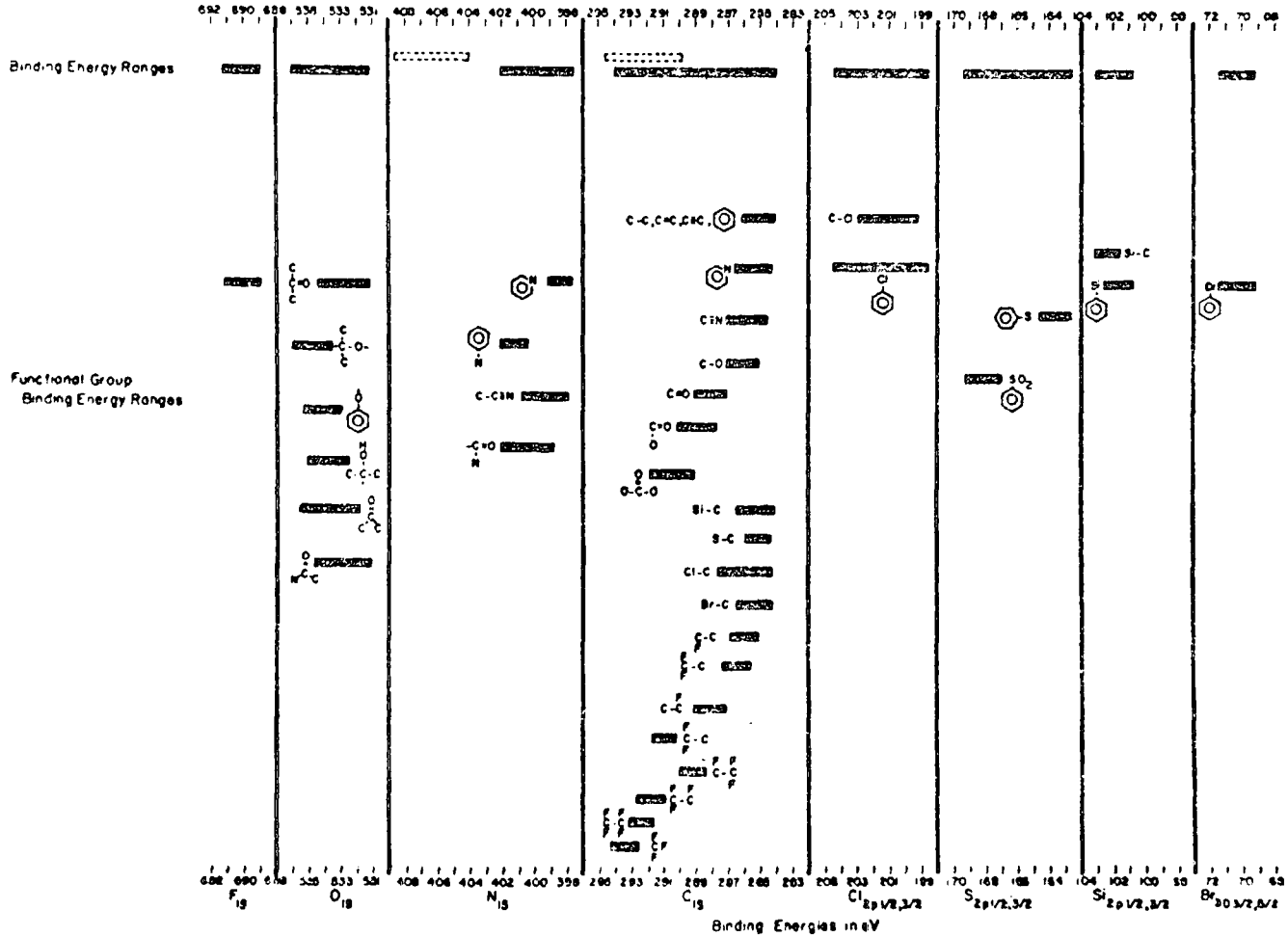

TABLE 2.3 Characteristic core level binding energies for various structural features in polymers

and similar information exists for other core levels.[107] Such data taken in conjunction with relative cross-sections for photoionisation from the relative core levels forms the basis for quantitative analysis by ESCA.

Much attention has been paid to the theoretical interpretation of the chemical shift phenomenon observed experimentally. The following distinct but interrelated approaches have been used:

(i) Koopmans' Theorem[83]

(ii) Core hole calculations[109,110] - linear combination of atomic orbitals - molecular orbital - self-consistent field method (LCAO-MO-SCF)

(iii) Equivalent cores model[111]

(iv) Charge potential model[64]

(v) Quantum Mechanical Potential model[112-114]

(vi) Many bodied formalism.

An account of the physical processes involved in electron photoemission and their effects for a theoretical standpoint has been given by Fadley.[115]

2.4 Fine Structure

2.4.1 Multiplet splitting

Multiplet splitting occurs in paramagnetic systems and is the result of interactions between unpaired electrons present in the system and the unpaired core orbital electrons remaining after photoionisation. Examples can be found in the core level spectra of transition element compounds.[116,117] The theoretical interpretation of multiplet effects is relatively straightforward only for S-hole states and is based on Van Vlecks' vector coupling model.[118] The magnitude of

splitting provides information concerning the localisation or delocalisation of unpaired electrons in a compound, since the greater the localisation and spin densities on an atom the greater will be the observed splitting. Multiplet splittings in photoelectron spectroscopy have been reviewed in some detail by Fadley.[119]

2.4.2 Spin Orbit splitting

When photoionisation occurs from an orbital for a filled shell which has an orbital quantum number (l) greater than 1, i.e. from a p,d or f orbital, then coupling can occur between the spin (S) and orbital angular momentum (L) to yield a total momentum (J):

$$J = S + L \qquad (9)$$

A doublet, which is usually well-resolved, is then observed in the spectrum instead of single peak.[63] The relative intensities of the component peaks of the doublet are proportional to the ratio of the degeneracies of the states which is quantum mechanically defined as 2J + 1. The relative intensities of the J states for s,p,d and f orbitals are shown in Table 2.4 and illustrated in Figure 2.9.

TABLE 2.4 J States for s,p,d and f orbitals

Orbital	Orbital Quantum No.	Total Quantum No.	Intensity ratio
	l	J = (l±s)	(2J+1) : (2J´+1)
s	0	1/2	singlet
p	1	1/2, 3/2	1 : 2
d	2	3/2, 5/2	2 : 3
f	3	5/2, 7/2	3 : 4

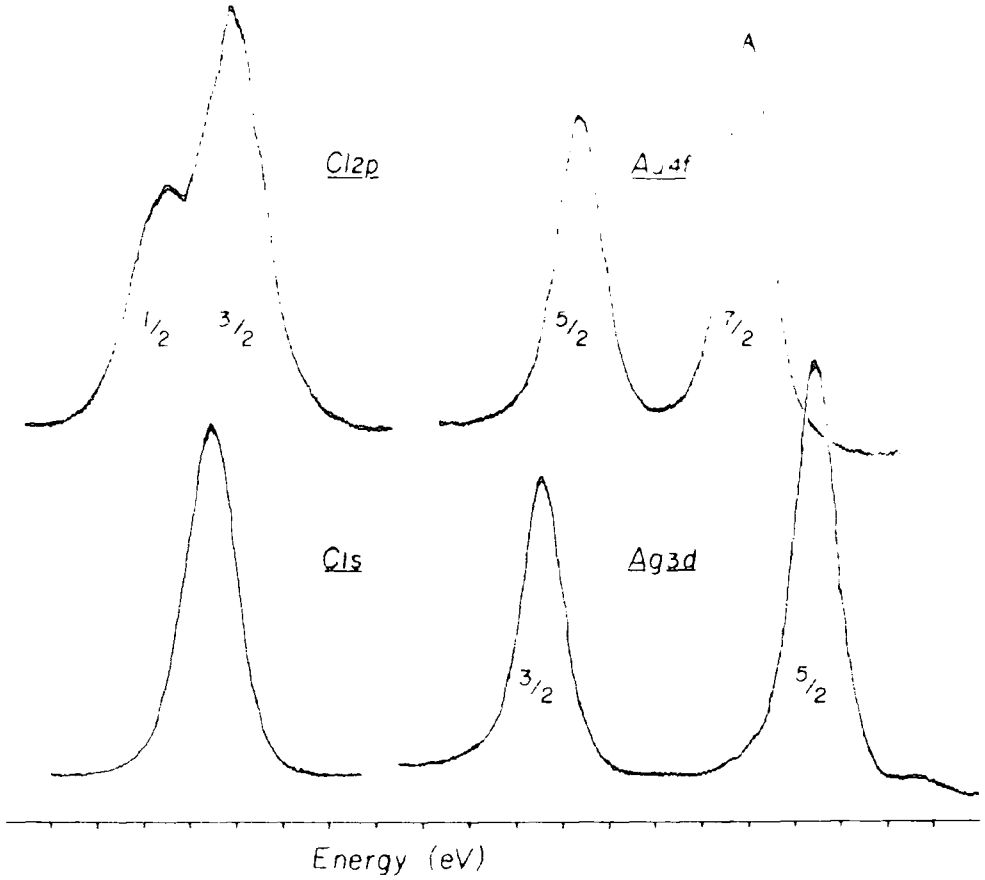

Figure 2.9 Spin-orbit splittings in C_{1s}, Cl_{2p}, Ag_{3d} and Au_{4f} core levels

2.4.3 Electrostatic splitting[120-122]

This is caused by the differential interaction between the external electrostatic field and the spin states of the core level being investigated. It has been observed for a number of systems, for example, the $5p_{3/2}$ levels of uranium and thorium and in some compounds of gold.[123,124] Correlation has been observed between electrostatic splitting and the quadrupole splittings obtained from Mössbauer spectroscopy,[125] which arise from the interaction of the nuclear quadrupole moment with an inhomogeneous electric field.

A summary of the type of splitting encountered in ESCA is shown in Figure 2.10.

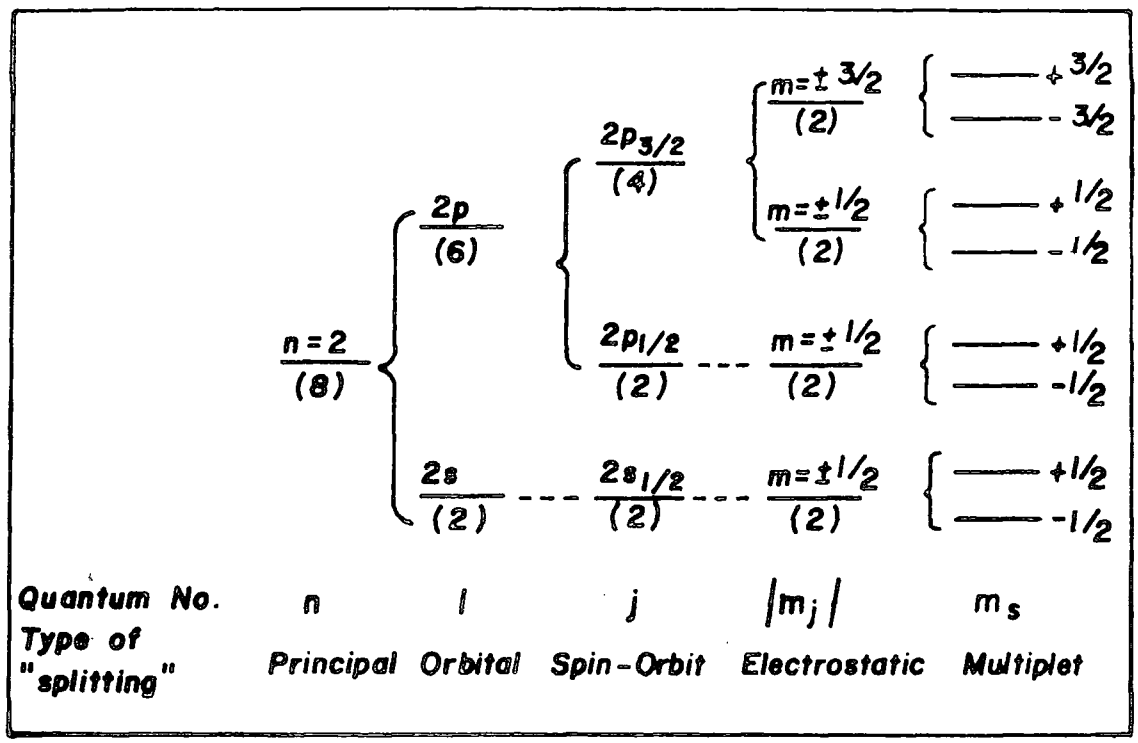

Figure 2.10 Schematic of the types of splitting encountered in ESCA

2.5 Sample Charging and Energy Referencing

As discussed previously, for conducting samples in electrical contact with the spectrometer, the Fermi level serves as a convenient level for energy referencing. However for insulating samples, such as polymers, the Fermi level is not well defined analytically, but lies somewhere between the valence (occupied) and bottom of the conduction (unoccupied) energy levels. Consequently some calibration procedure must be adopted in order to correct for this phenomenon.

Several investigations have shown that the photoelectrons (primary photoelectrons) are rapidly slowed down by the inter-

action with matter and can generate intense currents of slow 'secondary' electron clouds at the surface of the sample.[126-128] These secondary electrons play an important role in establishing the electrical equilibrium at the surface and have been found to be ~20% of the photoelectron flux in a conducting sample and ~99% of the flux in an insulating sample. Phcto-emitted electrons from the surface experience a net retardation and therefore larger binding energies are measured. All photo-electrons are affected by the same retardation voltage and shifted in energy by the same amount.

For a sample with a uniformly distributed positive surface charge, the energy equation for a solid becomes:

$$K.E. = h\nu - B.E. - \phi s - \Delta \qquad (10)$$

where Δ is the energy shift due to the positive sample charge.

A non-uniform distribution or non-equivalent positive potential (differential sample charging) over the surface of the sample will lead to a broadening of the primary photo-electron peak. This is because the electrons from core levels of atoms of different charge will experience different retard-ation potentials at the surface.

One method by which charging may be detected is to vary the incident electron flux by means of an electron 'flood gun'.[129] Additional low energy electrons are released into the sample region such that if sample charging is present the photoelectron peaks will move to lower apparent binding energy. The use of flood guns have found application in the study of the complex charging effects arising from conducting and insulating catalyst sites in industrial catalysts.[130]

When thick insulating samples are studied in spectrometers employing monochromatic X-ray sources, large sample charging

effects are observed and provide the primary motivation for the use of electron flood guns. The monochromator removes the bremsstrahlung as a supply of secondary electrons which can lead to shifts in kinetic energy of several hundred electron volts and can be compensated by flooding the sample with low energy electrons. However, the sample may become negatively charged and the method needs great care to achieve an accuracy comparable with that of other methods.

An alternative source of low energy electrons is to illuminate the sample region with uv radiation from a low pressure mercury arc lamp via a quartz viewing port. Sufficient secondary electrons are generated from photoemission, from the metal surfaces of the sample analysis chamber, that the sample charging may be reduced to a low level.[131]

In practice the problem of extracting absolute binding energies can be overcome by the use of reference standards for calibration on the binding energy scale. A correction factor calculated from the observed kinetic energy of the photoelectrons corresponding to the reference peak is then used to find the binding energies of the other peaks. The two most commonly employed calibration lines are the C_{1s} peak arising from $(\underline{C}H_2)_n$ environments at a binding energy of 285.0 eV, either inherent in the sample or arising from hydrocarbon contamination within the spectrometer, and the $Au_{4f_{7/2}}$ level at 84.0 eV if the sample has been deposited on a gold substrate. The use of the so-called 'gold decoration'[132] technique is not recommended for organic and polymeric materials. Firstly, nucleation may occur via an 'islanding' process which will almost certainly lead to differential charging, and secondly, since the gold is normally evaporated from a filament the possibility of surface damage,

and other effects cannot be discounted.

Although sample charging has been regarded as somewhat of a nuisance which must be circumvented, recent work has shown[133,134] that sample charging is an interesting phenomena in its own right and in appropriate cases provides an important addition to the hierarchy of available information levels.

2.6 Signal Intensities

Figure 2.11 shows a schematic of the general geometry of the ESCA experiment employing a fixed arrangement of analyser and X-ray source. $h\nu$ represents the incident X-rays and e^- the fraction of the photoelectrons entering the analyser. ϕ is the angle between the X-ray source and the analyser entrance slit and θ describes the angle of the sample in relation to the analyser. If the photoelectrons are emitted from a depth, d, of the sample, their true path length will be d´ where

$$d = d' \operatorname{cosec} \theta \qquad (11)$$

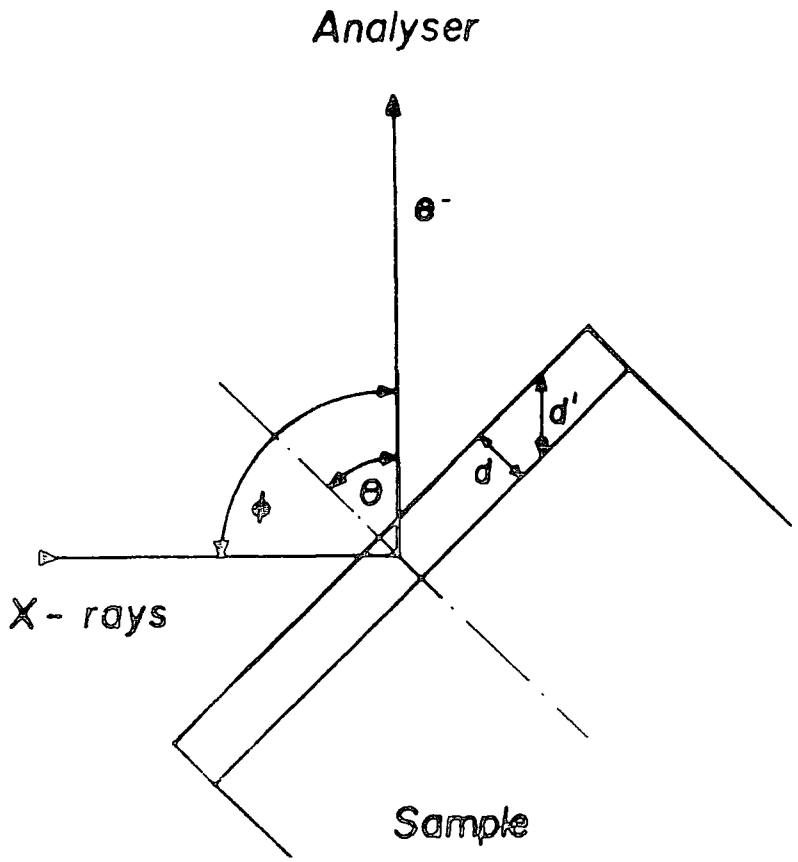

Figure 2.11 Schematic of the sample geometry relative to the X-ray gun and analyser

Due to the short mean free paths of electrons (for K.E. > 50 eV) in solids it is possible to enhance surface features with respect to bulk and subsurface by conducting experiments involving the grazing exit of the photoemitted electrons which are analysed, that is with θ approaching 90°. Angular dependence studies are only feasible on uniform flat surfaces (e.g. films or coatings) and is not applicable to samples with rough surface topographies, as in the case of powders.

For an infinitely thick homogeneous sample the intensity (I) of the elastic (no energy loss) photoionisation peak, corresponding to photoionisation from a core level i, may be expressed as:

$$dI_i = F\alpha_i N_i k_i e^{-x/\lambda_i} \, dx \qquad (12)$$

where I_i is the intensity arising from core level i,

F is the exciting photon flux,

di is the number of atoms per unit volume on which the core level i is localised,

k_i is the spectrometer factor,

λ_i is the electron mean free path.

Integration of this equation gives:

$$I_i - \int_0^{\infty} F\alpha_i N_i k_i e^{-x/\lambda_i} \, dx \qquad (13)$$

$$I_i = F\alpha_i N_i k_i \lambda_i \qquad (14)$$

The various factors and parameters affecting the intensity of a given signal in ESCA arediscussed more fully below.

The <u>X-ray flux</u>, F, is primarily dependent on the power applied to and the efficiency of the X-ray run. However, the

angle of incidence ϕ of the X-rays and the analyser and θ do have an effect on the intensity of the photoionisation peak.

The cross-section for photoionisation of core level i, α_i is a parameter which describes the probability of the core level being ionised when irradiated by a photon of known energy[135] and includes only the fraction of the total number of electrons photoemitted within the angle of acceptance of the analyser focussing lens. α_i is a function of the core level to which it relates and the energy of the incident photon. Values of α_i may be calculated from the fundamental properties of the atom[136] or determined experimentally from gas phase ESCA experiments.[64] The geometry of the X-ray source with respect to the analyser entrance slit affects α_i values, but for a particular spectrometer and using the same X-ray source and with a fixed value of ϕ then α_i is normally constant. With $MgK_{\alpha_{1,2}}$ and $AlK_{\alpha_{1,2}}$ the cross-sections for photoionisation for core levels of most elements of the periodic table are within two orders of magnitude of that for the C_{1s} levels, therefore ESCA has a convenient sensitivity range for all elements. The cross-sections for core levels are normally considerably higher than those for valence levels.

The spectrometer factor, k_i, includes contributions due to detector efficiencies, analyser transmission characteristics which are both dependent on the kinetic of the core electrons being analysed, and geometric factors such as the solid angle of acceptance of the analyser.

The Electron Mean Free path of photoemitted electrons (sometimes referred to as the escape depth) λ_i, is defined as the distance in the solid through which the electrons will travel before $^1/_e$ of them have not suffered energy loss through

inelastic collisons. Both experimental[137,138] and theoretical calculations[139] of λ_i have been undertaken. λ_i is a function of the kinetic of the photoelectrons and ranges from $\sim$4Å for electrons of about 80 eV K.E. to $\sim$30Å for electrons of about 1500 eV.

The sampling depth, which is sometimes confused with the electron mean free path, is defined as the depth from which 95% of the signal, arising from a given core level, derives and is related to λ by:

$$\text{Sampling depth} = -\lambda \ln 0.05 \tag{15}$$

$$= 3\lambda \tag{16}$$

As an example, for the carbon 1S levels studied by a $MgK_{\alpha 1,2}$ X-ray source the kinetic energy of the photoelectrons is $\sim$960 eV and the mean free path of the electrons is $\sim$15Å. 50% of the signal seen by ESCA derives from the outermost 10Å and 95% from the top 45Å. This illustrates the high surface sensitivity of ESCA.

Although the number density, Ni, is not directly related to the density of the sample, it is generally the case that for similar materials the ESCA signal for a given core level will be more intense for the higher density material.[140] The most important consequence of Ni is that the relative signal intensities for core levels in a homogeneous sample are directly related to the overall stoichiometries of the atoms sampled. Thus for two core levels i and j:

$$\frac{I_i}{I_j} = \frac{F_{\alpha_i} N_i k_i \lambda_i}{F_{\alpha j} N_j k_j \lambda_j} \tag{17}$$

If i and j correspond to the same core level in differing chemical environments, then

$$k_i \alpha_i \lambda_i = k_j \alpha_j \lambda_j \text{ and } \frac{N_i}{N_j} = \frac{I_i}{I_j}$$

If however i and j are different core levels then $k_i \alpha_i \lambda_i \neq k_j \alpha_j \lambda_j$ and

$$\frac{N_i}{N_j} = \frac{I_i k_j \alpha_j \lambda_j}{I_j k_i \alpha_i \lambda_j} \qquad \text{the ratio} \quad \frac{k_j \alpha_j \lambda_j}{k_i \alpha_i \lambda_i}$$

may be determined experimentally from standard samples of known stoichiometry containing i and j. This ratio is usually referred to as the instrumentally sensitivity ratio of the given levels.

2.7 Line widths

The natural line width, the so-called "Full width at half the maximum height" (FWHM) of the core level under investigation, ΔE_{cl}, and that of the incident radiation, ΔE_x, (unless monochromatisation is used) depend on the Uncertainty Principle.[141]

$$\Delta E . \Delta t = h/2 \qquad (18)$$

where Δt is the lifetime of the state and h is Planck's constant. From this equation a line width of $\sim$1eV corresponds to a lifetime of approximately 6.6×10^{-16} secs.[147] Table 2.5 displays some natural line widths of core levels derived from X-ray spectroscopic studies. The data displayed emphasise the fact that there is no particular virtue in studying more tightly bound core levels; for Cu, for example, the FWHM of 54eV for the 1s level would swamp any chemical shift.

TABLE 2.5 Full Width at Half Maximum of Natural line width for some core levels (eV)

Level	S	Ar	Ti	Mn	Cu	Mo	Ag	Au
1S	0.35	0.5	0.8	1.05	1.5	5.0	7.5	54
$2p_{3/2}$	0.10	-	0.25	0.35	0.5	1.7	2.2	4.4

2.8 Line Shape Analysis

The need for line shape analysis (deconvolution) arises when the chemical shift of a level is smaller than the line-width of that level. The measured linewidths of component peaks for a core level may be expressed as

$$(\Delta E_m)^2 = (\Delta E_x)^2 + (\Delta E_s)^2 + (\Delta E_l)^2 + (\Delta E_{ss})^2 \qquad (19)$$

where ΔE_m is the FWHM,

ΔE_x is the FWHM of the X-ray photon source,

ΔE_s is the contribution due to spectrometer abberations and is dependent on the emission energy and the choice of analyser slits,

ΔE_{ss} is the contribution due to the solid state effects in the sample,

ΔE_l is the natural width of the core level under investigation.

The contributions to ΔE_m from ΔE_x for the commonly used photon sources (i.e. Mg and Al) are essentially Lorentzian line shapes. The characteristics for the energy distribution in MgK radiation are essentially comprised of four major component lines, α_1, α_2, α_3 and α_4, the relative positions to the α_1 line are -0.33, + 8.4 and 10.2 eV, with relative intensities 100, 50, 12.8 and 6.9.[143] The α_3 and α_4 lines are significantly removed from the α_1 and α_2 lines and manifest themselves as satellite peaks to the high kinetic energy side of the intense primary photoionisation signal in the ESCA spectrum. A similar situation is true for AlK_α radiation.[143]

The contribution to ΔE_m from ΔE_s is considered to be Gaussian, whereas El is Lorentzian. The convolution of these

line shapes produces a hybrid shape with a Gaussian distribution dominating the overall line shape and with Lorentzian character in the tails. The use of pure Gaussian shapes introduces only small errors in line shape analysis.[64]

Deconvolution procedures may be grouped into two main categories:

(1) Deconvolution by mathematical methods which have been reviewed by Carley and Joyner.[144]

(2) Curve fitting by simulation, either in analogue or digital fashion.

The second category requires close control over a number of variables, for example, binding energy, line width and peak height. These parameters are most conveniently controlled in the analogue mode, and the work in this thesis predominantly used this method (on a DuPont 310 curve resolver). The basic approach to curve simulation is outlined in Table 2.6.

When using either form of deconvolution method a certain amount of caution is required, as it is often possible to obtain more than one solution. When dealing with complex line shapes a detailed knowledge of prototype systems is very important, such that the solution is one based on chemical uniqueness.

2.9 ESCA Instrumentation

A schematic of the essential components of an ESCA spectrometer is shown in Figure 2.12 and is largely self explanatory, including:

1. X-ray source,
2. Sample Chamber
3. Electron energy analyser,
4. Electron detection.

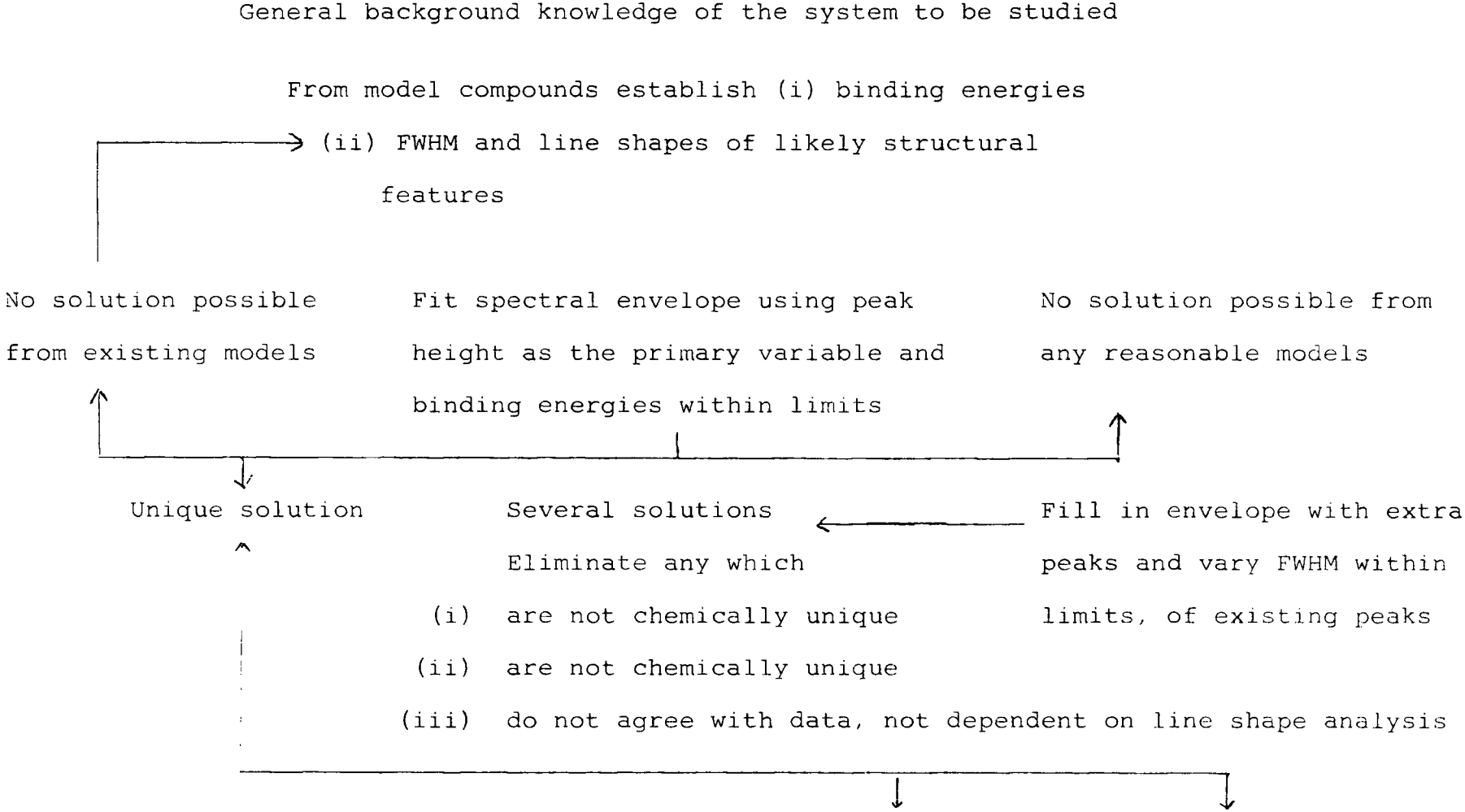

Table 2.6 Line shape analysis by curve fitting; schematic of logic procedure

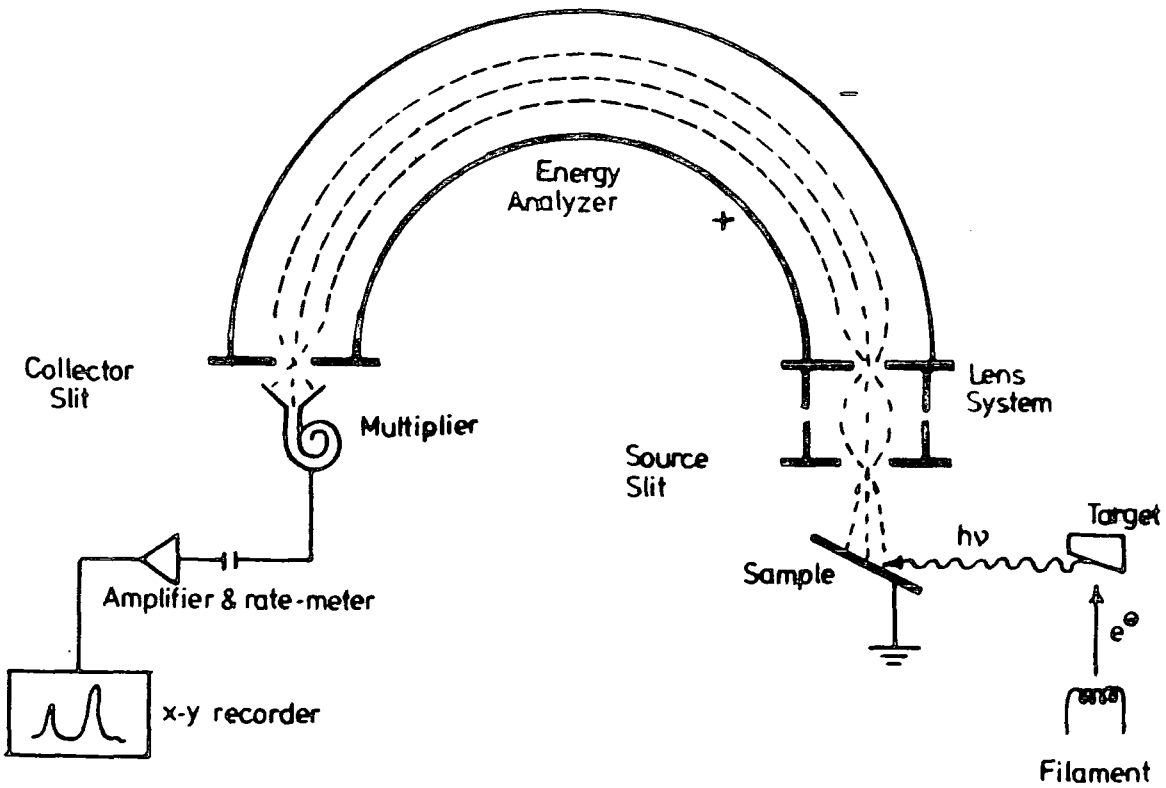

Figure 2.12 Schematic of the ESCA instrumentation

The majority of the work in this thesis was carried out using an A.E.I. ES200B spectrometer; a custom-designed Kratos ES300 spectrometer was also used.

2.9.1 X-ray Source

The X-ray beam is produced by the bombardment of a target (anode) with high energy electrons. A typical, non-monochromatic X-ray spectrum is shown in Figure 2.13, which illustrates the appearance of emission lines, characteristic of the anode material superimposed on a continuous spectrum (Bremsstrahlung).[145] The continuum's shape depends only on the energy of the incident electrons on the anode, and not on the nature of the anode material.

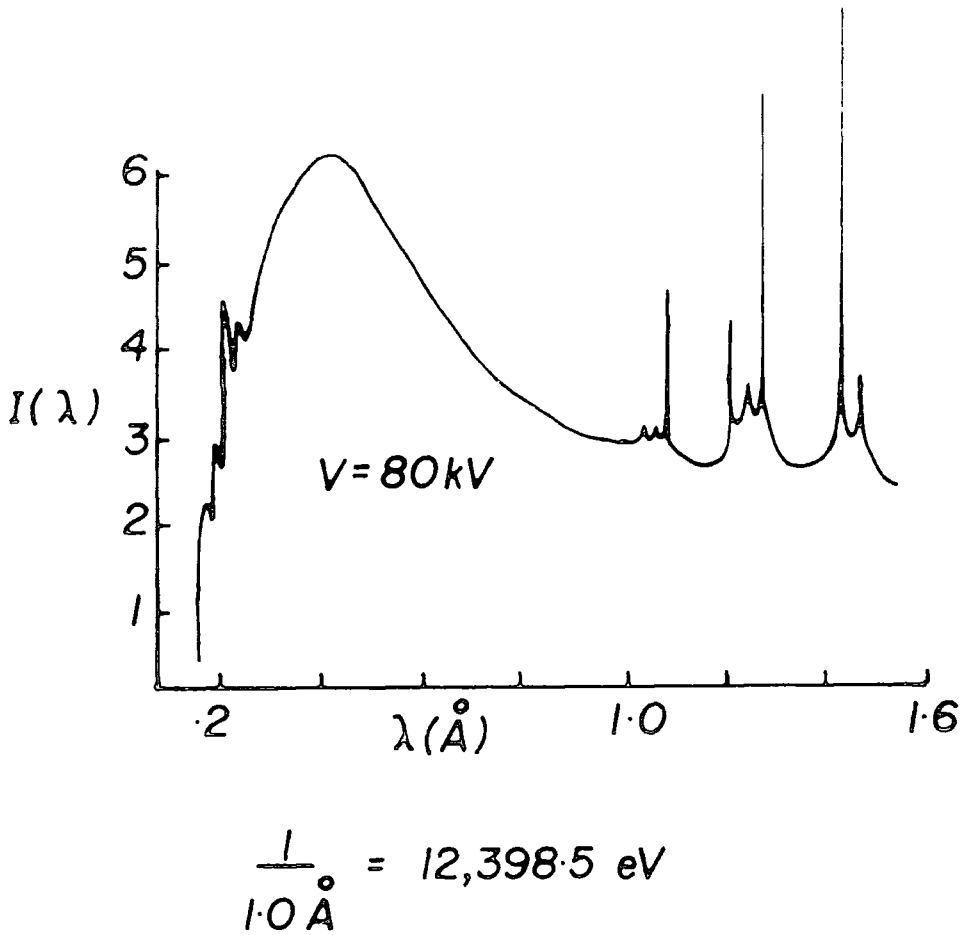

Figure 2.13 X-ray Spectrum of a tungsten anode

Soft X-ray sources are most commonly employed in ESCA. for example the MgK_α ($h\nu$ = 1253.7 eV) and AlK_α ($h\nu$ = 1486.6 eV) lines; only very occasional use being made of harder X-rays such as CuK_{α_1} ($h\nu$ = 8048 eV) and CrK_{α_1} ($h\nu$ = 5415 eV). An intermediate energy source, TiK_α (4510 eV) has also been used. It is likely that these harder X-ray sources will be employed in future Auger work.[146,147]

The ES200B spectrometer has a Marconi Elliot 9 x 5 high voltage supply unit with integrally variable voltage, 0-60 kV and current, 0-80mA. The X-ray source consists of an unmonochromatised magnesium anode of the Henke hidden filament design;[148]

this reduces risk of contamination of the target by evaporated tungsten from the electron gun filament. Normal operating conditions produce an X-ray flux of the order of 0.1 millirads^{-1},[149] which causes little or no radiation damage to the majority of systems. A thin aluminium window isolates the target from the sample to prevent interference due to electrons from the filament. The risk of scattered electrons exciting X-ray radiation from the aluminium window is reduced by operating the filament at near ground potential (+10V) and the anode at high positive voltage.

The ES300 spectrometer is equipped with a dual-anode,[150] with magnesium and titanium targets and a monochromatised $AlK_{\alpha_{1,2}}$ X-ray source. The monochromator for the $AlK_{\alpha_{1,2}}$ uses slit filtering and diffraction from the (100) plane of quartz[64] at the Bragg angle of 78.3^{o}. Other monochromators may use dispersion compensation or fine focussing systems.[151]

2.9.2 Sample Analysis Chamber

Figure 2.14 displays a schematic drawing of the ES200B spectrometer equipped with monochromator and reveals the relative positions of the sample, X-ray sources and analyser.

There are various access ports for sample introduction and treatments. Rapid sample entry is achieved by means of fast-entry insertion locks. Purpose-built reaction chambers may be attached to the source chamber via an insertion lock and this provides facilities for '*in situ*' treatment of samples.

The ES200B has a typical base pressure of 5 x 10^{-8} torr achieved using cold-trapped diffusion pumps backed by rotary pumps.

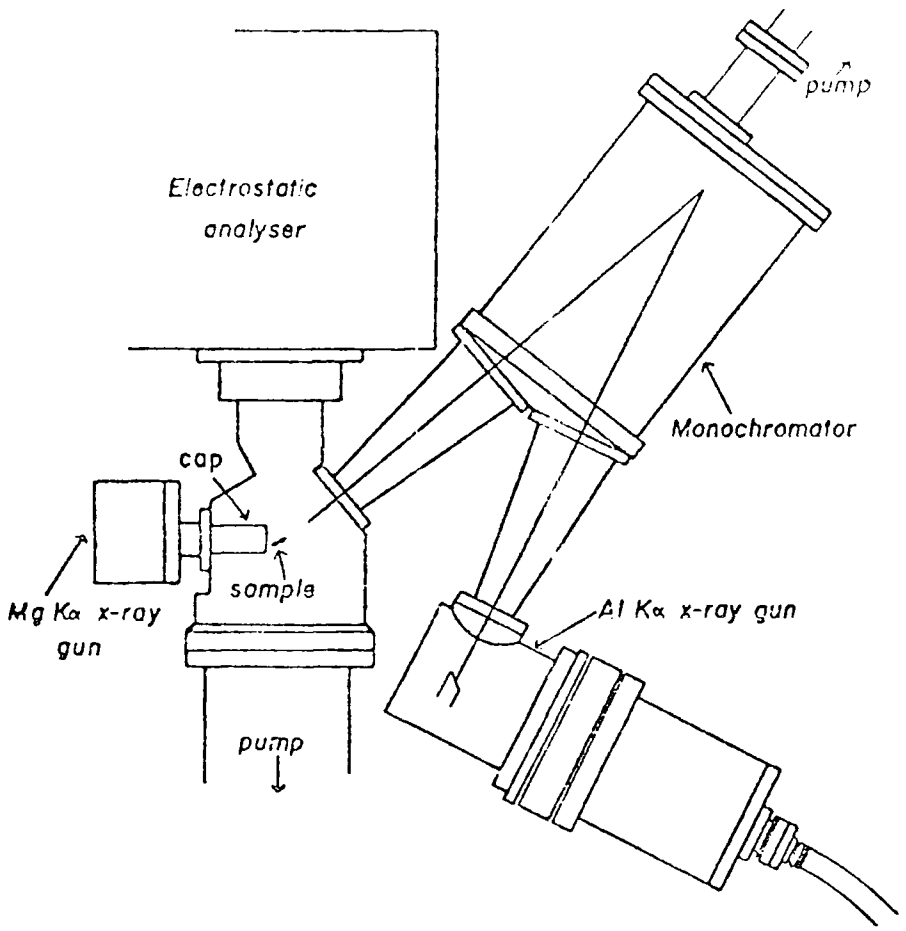

Figure 2.14 General layout of the AEI ES200B spectrometer

The ES300 has a permanently mounted preparation chamber attached to the source chamber, pumped by a diffusion pump, catering for the needs of the research interests of the laboratory. The source and analyser regions are independently pumped by means of an Alcatel 350 ls^{-1} electric turbomolecular pump. The base pressure is typically of the order 5 x 10^{-9} torr.

2.9.3 Electron Energy Analyser

The electron energy analyser on the ES200B is a hemispherical double focussing analyser based on the principle described by Purcell[152] which is screened from external magnetic interference by means of Mu-metal shields. The analyser

should have a resolution of 1 in 10^4 in order to carry out ESCA studies. The resolution of the analyser is given by:

$$\Delta E/E = R/W \qquad (20)$$

where E is the energy of the electron,

R is the mean radius of the hemisphere,

W is the combined width of entrance and exit slits.

The resolution may be improved by:

(1) Reducing the slit width, which reduces the signal intensity;

(2) Increasing the radius of the hemisphere, thereby increasing engineering costs and pumping requirements;

(3) Retarding the electrons before entry into the analyser.

In practice a compromise is made on the slit widths to obtain sufficient signal intensity and on the size of the hemisphere so as to prevent mechanical distortion and keeps costs down. A retarding lens is also employed to slow the electrons down before entry into the analyser and cuts down on the resolution requirements of the analyser. Also, the lens system allows the analyser[153] to be located at a convenient distance physically from the source chamber which permits a maximum flexibility in sample handling.

Electrons entering the analyser with the required kinetic energy may be focussed at the detector slit by one of two methods:

(1) Scanning the retarding potential applied to the lens and keeping a constant potential between the hemispheres, or

(2) Scanning the retarding potential and the potential between the analyser hemisphere simultaneously maintaining a constant ratio between the two.

The first method of fixed analyser transmission (FAT) has greater sensitivity at low kinetic energies (<500eV) and the second, fixed retardation ratio (FRR) has a greater sensitivity at higher

electron kinetic energies. The FRR mode is employed in this work.

2.9.4 Electron detection and data acquisition

Electrons of pre-selected energy pass from the analyser into an electron multiplier via the collector slit. The output from the multiplier undergoes amplification and is fed into a data handling system. Spectra may be generated by one of two methods:

(1) The continuous scan, where the electrostatic field is increased from the starting kinetic energy continuously, a ratemeter monitoring the signal from the amplifier. In this way a graph of electron count versus kinetic energy of the electrons may be recorded on an X-Y plotter.

(2) The step scan, where the field is increased by preset increments (e.g. 0.1eV) and at each increment (a) counts may be measured for a fixed length of time or (b) a fixed number of counts may be timed. The data so obtained is stored in a multichannel analyser or by the use of a mini computer or floppy disc. Many scans can be accumulated to average random fluctuations in background thereby enhancing signal to noise ratios.

In both these methods where the data acquisition is a relatively long process (of the order of an hour) care must be taken to avoid long term sample changes. Phenomena such as time dependent sample charging and hydrocarbon contamination (which may alter peak ratios) may produce erroneous results.

2.10 Sample Handling

2.10.1 Solid Samples

By the use of double sided adhesive insulating tape solids may be directly mounted onto the spectrometer probe tip.

Sample charging effects will occur under these conditions and a more satisfactory technique involves depositing a thin layer of the sample onto a gold substrate (e.g. from a suitable solvent or via sublimation). Small strips or wires may be held in a chuck and powdered samples may be mounted by pressing into a metal gauge or piece of soft metal foil such as lead or indium.

A typical probe, on the AEI ES200B and Kratos ES300 spectrometers, has the facility for heating or cooling the sample. In the former case (i.e. heating) this is achieved by means of conduction from a thermostatically controlled resistance heater. Cooling is carried out by pumping liquid nitrogen through the probe, thus enabling samples which are slightly volatile to be studied. More volatile solids are usually sublimed from a capillary tube, which may be heated, onto a cooled probe tip.

2.10.2 Liquids

Although ESCA may be applied to the analysis of solids, liquids and gases, the development of liquid studies is still in its infancy.[154] The only technique that is at present viable on commercially available instruments involves the injection of the liquid into a heatable (25 to 150^{o}C) evacuated reservoir shaft followed by diffusion of the vapour through a metrosil leak and subsequent condensation onto a cooled gold plate. The sample surface is continually renewed and contamination and radiation damage effects are thereby reduced.

Two techniques for studying liquids and solutions have been developed by Siegbahn where samples are studied as submillimeter beams[155] or as a film on a wire passing through the X-ray beam parallel to the analyser entrance slit.[156]

2.10.3 Gases

Gases may be studied either in the condensed phase using a cooled probe or in the gaseous phase for which purpose gas cells have been developed. Studies using molecules in the gas phase have the following advantages.[76]

(1) No inherent broadening of the levels due to solid state effects,

(2) Sample charging problems are removed,

(3) Increased signal to noise ratio,

(4) Radiation damage, if it occurs, is of no importance unless the sample is recirculated,

(5) By mixing with standard gases, peaks may be readily calibrated,

(6) Inelastic losses and shake-up and shake-off processes may be distinguished by varying the sample pressure,

(7) Direct comparison with theoretical calculations is simplified.

2.11 General Aspects of ESCA

ESCA is an extremely powerful tool with wide ranging applicability. The principal advantages of the technique may be summarised as follows:

(1) The sample may be solid, liquid or gas and sample sizes are small, e.g. in solids, 10^{-3}g, 0.1µl liquid and 0.5cm^3 of a gas at STP.

(2) The technique is essentially non-destructive since the X-ray flux is small (0.1 millirad sec.$^{-1}$).

(3) The technique is independent of the spin properties of the nucleus and can be used to study any element of the periodic table with the exception of hydrogen and helium. These are the only elements for which the core levels are also the valence levels.

(4) Materials may be studied '*in situ*' with a minimum of preparation.

(5) The technique provides a large number of information levels from a single experiment as displayed in Table 2.7.

(6) ESCA has a higher sensitivity than many other analytical techniques as shown in Table 2.8.

(7) The data is often complementary to that obtained by other techniques.

(8) For solids, ESCA has the capability of differentiating the surface from subsurface and bulk phenomena, allowing analytical depth profiling.

(9) The information relates directly to bonding and molecular structure and applies to both inner and valence orbitals of the molecule. This allows a thorough analysis of electronic structure of the system to be made.

(10) The information levels are such that '*ab initio*' investigations are possible and the theoretical basis is well understood.

The disadvantages of ESCA are surprisingly few:

(1) The overall costs are quite high;

(2) While the technique has superior depth resolution, $\sim$200Å, the spatial resolution is poor and an area of $0.3cm^2$ is normally sampled.

(3) If the surface differs from the bulk, then it is not possible to say anything about the bulk structure by means of ESCA without sectioning the sample.

TABLE 2.7 The Hierarchy of Information levels available in ESCA

(1) Absolute binding energies, relative peak intensities, shifts in binding energies. Elemental mapping of solids, analytical depth profiling, identification of structural features, etc. Short-range effects, longer-range effects indirectly.

(2) Shake-up/shake-off satellites. Monopole excited states; energy separation with respect to direct photoionisation and relative intensities of components of 'singlet and triplet' origin. Short and longer range effects directly. (Analogue of uv).

(3) Multiplet effects. For paramagnetic systems, spin state, distribution of unpaired electrons.

(4) Valence energy levels, longer range effects directly.

(5) Angular dependent studies. For solids with fixed arrangement of analyser and X-ray source, varying take off angle between sample and analyser provides means of distinguishing surface from subsurface and bulk effects. For gases with variable angle between analyser and X-ray source, angular dependence of cross-sections, asymmetry parameter β,[157] symmetries of levels.

TABLE 2.8 Sensitivities of Various Analytical Techniques

Bulk Techniques	Minimum Detectable Quantity (g)
Infrared absorption	10^{-6}
Atomic absorption	10^{-9} - 10^{-2}
Vapour phase chromatography	10^{-3} - 10^{-7}
High pressure liquid chromotography	10^{-6} - 10^{-9}
Mass spectroscopy	10^{-9} - 10^{-15}
Surface Techniques	
ESCA	10^{-10}
Neutron activation analysis	10^{-12}
X-ray fluorescence	10^{-7}
Ion scattering spectrometry	10^{-15}
Auger emission spectroscopy	10^{-14}
Secondary ion mass spectrometry	10^{-13}

CHAPTER THREE

THE PHOTOAGING OF BISPHENOL A POLYCARBONATE - PART I - AN MNDO SCF MO AND AN STO-3G INVESTIGATION OF CONFORMATIONAL PREFERENCES AND THE ELECTRONIC STRUCTURES OF MODEL POLYCARBONATE SYSTEMS

3.1 Introduction

Despite the scientific and technological importance of polycarbonates based on Bisphenol A and the numerous investigations which have been conducted in a wide variety of areas, such as wide line NMR studies of molecular motion[158] and photophysics of uv degradation,[159-161] the fact remains that there are a number of fundamental questions which remain concerning conformational preferences.

Most investigations have utilised the results of Flory and Williams'[162] analysis of random configuration in polycarbonates which concluded that in solution the trans-trans configuration about a given carbonate group was energetically preferred and that an orthogonal configuration of the phenyl groups was likely to be strongly favoured although no estimate was provided of the likely barriers to rotation of the phenyl groups. On the basis of solution phase data the trans-trans configuration was estimated to be $\sim$1.3k cal mole^{-1} lower in energy than the cis-trans configuration. X-ray studies however have been interpreted in favour of an energetic preference for the cis-trans configuration in the solid state.[163]

Both nmr. and ir[164] studies indicate the delicate balance of factors determining conformational preferences and with simple aliphatic carbonates the equilibrium between trans-trans and cis-trans confirmations indicates a relatively small energetic preference for one or other, depending on the substituents. The interest in chain statistics[162,165] has given rise to investigations of the conformational preferences arising from rotation of the phenyl group with respect to the gem dimethyl moiety in Bisphenol A based polycarbonates. Whilst studies

of this nature are important in interpreting mechanical and thermal properties, the more important aspect of conformational preference as far as photochemistry is concerned is the stereochemical relationship between the phenyl and carbonate groups.

Detailed photophysics studies of the photochemical transformations of polycarbonates, both in solid state and in solution,[159-161] have alluded to the question of conformational preferences in both the ground and excited state of Bisphenol A carbonate residues. It is clear that there is a need for a more quantitative description of the conformational preferences and electronic structures for this system, particularly since the assignment of the first excited singlet state to an $n\rightarrow\Pi^*$ transition seems to be incompatible with the considerable body of experimental and theoretical data which is available in the literature on simple model systems.[5,166,167]

This chapter is therefore concerned with presenting a theoretical investigation of simple model systems which goes in some way to resolving difficulties in the interpretation of data which have arisen in the literature. The complexity of even the simplest model for conformational preference in the polycarbonate system rules out the extensive use of a non-empirical quantum chemical study and thus the calculations presented here have mainly utilised the highest level of semi-empirical SCF MO treatment which has been specifically parametrised for the semi-quantitative description of heats of formation, conformational preferences and geometries, namely the MNDO SCF MO described by Dewar and Thiel.[168,169]

The work in this chapter involves an MNDO SCF MO investigation of the relative heats of formation, conformational pre-

ferences and excitation energies for simple model systems which encompass carbonyl, carboxy ester and carbonate structural features. The calculations have been extended to the non-empirical level (STO-3G)[170] to investigate in some detail the problems of flexible versus rigid rotation.

3.2 Theoretical

3.2.1 MNDO SCF MO

In the model chosen for the polycarbonate system - diphenyl carbonate - the number of independent geometric variables dictated that computations of conformational preference be carried out initially on a model system based on standard bond lengths and angles (i.e. rigid rotation). This initial study indicated a rather strong energetic preference for the orthogonal cis-trans configuration and also provided very large barriers for rotation of the phenyl groups. It became clear from this data that the assumption of fixed geometries and rigid rotation was giving rise to artefacts and a new approach was therefore indicated. This consisted of complete geometry optimisations for trans-trans and cis-trans configurations of dimethyl carbonate. (The cis-cis configuration was not investigated since the comparable configuration, even in orthogonal form, for diphenyl carbonate is very much higher in energy than the other conformation and hence need not be considered). The derived carbonate group geometries were then employed as starting points for geometry optimisations for the diphenyl carbonate orthogonal trans-trans configuration. The number of independent variables dictated that the phenyl group geometry was fixed but optimisation included the phenyl-carbonate group bonds and the carbonate group itself. These

optimisations indicated that the bond lengths were essentially invariant in replacing methyl by phenyl substituents in going from dimethyl to diphenyl carbonate other than the anticipated change in bond length involving the substituent and the carbonate group itself. Computations involving the planar trans-trans and orthogonal and planar cis-trans configurations were therefore restricted to energy minimisation with respect to bond angles involving the carbonate group.

The potential surfaces for torsion angles θ and ϕ were then investigated for both con- and disrotation of the phenyl groups in both trans-trans and cis-trans conformers, the relevant geometric parameters being linearly extrapolated from those determined by optimisation at the (0,0,90,90,360,360, 270,270) points. Geometry optimisations at these points took $\sim$30 minutes of cpu time each. To extend the range of the energy hypersurface investigated, further computations have been carried out on cis-trans and trans-trans configurations in which one phenyl group has been locked in a planar - and the other in an orthogonal - arrangement. The interconversion of orthogonal cis-trans and trans-trans configurations has also been investigated at 30^{o} intervals in the relevant rotation angle.

Dewar and Thiel[168,169] have shown, in a series of papers, that MNDO SCF computations provide a semi-quantitative description of structure and conformational preference in organic systems, and representative computations - including complete geometry optimisations - showed that for acetaldehyde as a prototype system, conformational preference (H eclipsing O), relative energy ($\sim$0.5 kcal mol^{-1}) and geometry are in good agreement with available experimental data.[171]

In order to provide a comparison of conformational preference in the ground state and relative energies of excited states model systems encompassing carbonyl and carboxy ester functionalities have also been investigated and Table 3.1 lists the molecules studied and the computations that have been made.

TABLE 3.1 List of molecules for which MNDO SCF MO computations have been made

Molecule	Ground State	Excited State	Conformational preference	Rotational barrier
Diphenyl carbonate	x		x	x
Acetone	x	x		
Methyl acetate	x	x		
Dimethyl carbonate	x	x		

The relevant energies of the lowest excited singlet and triplet states for some of the model systems have also been computed to provide theoretical data for comparison with that available from experiment and to provide a basis for comparison of the nature of the excited states of 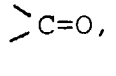 , 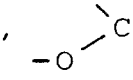 and  functionalities.

STO-3G

Consideration of the computational cost and storage that would be involved in an '*ab initio*' study of diphenyl carbonate dictates the use of a somewhat smaller model for Bisphenol A polycarbonate, namely phenyl carbonic acid, in order to investigate in greater detail the problems of flexible versus rigid rotation. MNDO SCF MO calculations on this system have also been carried out for comparison.

The computation at the STO-3G level were performed using the ATMOL 3[172] suite of programmes.

The geometry of phenyl carbonic acid as displayed in Figure 3.6, was based on the bond lengths and angles published by Flory and Williams[162] in their study of Bisphenol A polycarbonate. The potential energy surface for the torsion angle ϕ was examined by rotation of the phenyl group from the orthogonal configuration (ϕ=0) in 45^{o} increments. The computation time for each point was $\sim$25 minutes and $\sim$90 seconds of cpu time at the STO-3G and MNDO SCF MO levels respectively.

3.3 Results and Discussion

In considering the results for the various computations it is convenient to discuss those obtained for diphenyl carbonate, acetone, methyl acetate and dimethyl carbonate at the MNDO SCF MO level first.

3.3.1 The ground state of diphenyl carbonate

As it has been already noted, there appears to have been no previously published study which has considered in detail the question of conformational preference in models appropriate to Bisphenol A polycarbonates with particular reference to the discussion of photochemical transformations. In principle there are six extremes in conformation in an energy contour map for the ground state of the diphenyl carbonate system corresponding to planar and perpendicular (orthogonal) (defined in respect of the planes of the carbonate group and aromatic residues) conformations of trans-trans, cis-trans (trans-cis) and cis-cis configurations. Scale models - and indeed the MNDO SCF MO computations themselves - show that the cis-cis configurations are sterically impossible and attention has

therefore been focussed on the cis-trans and trans-trans configurations. Studies have, therefore, been made as a function of torsion angles θ and ϕ as defined in Figure 3.1.

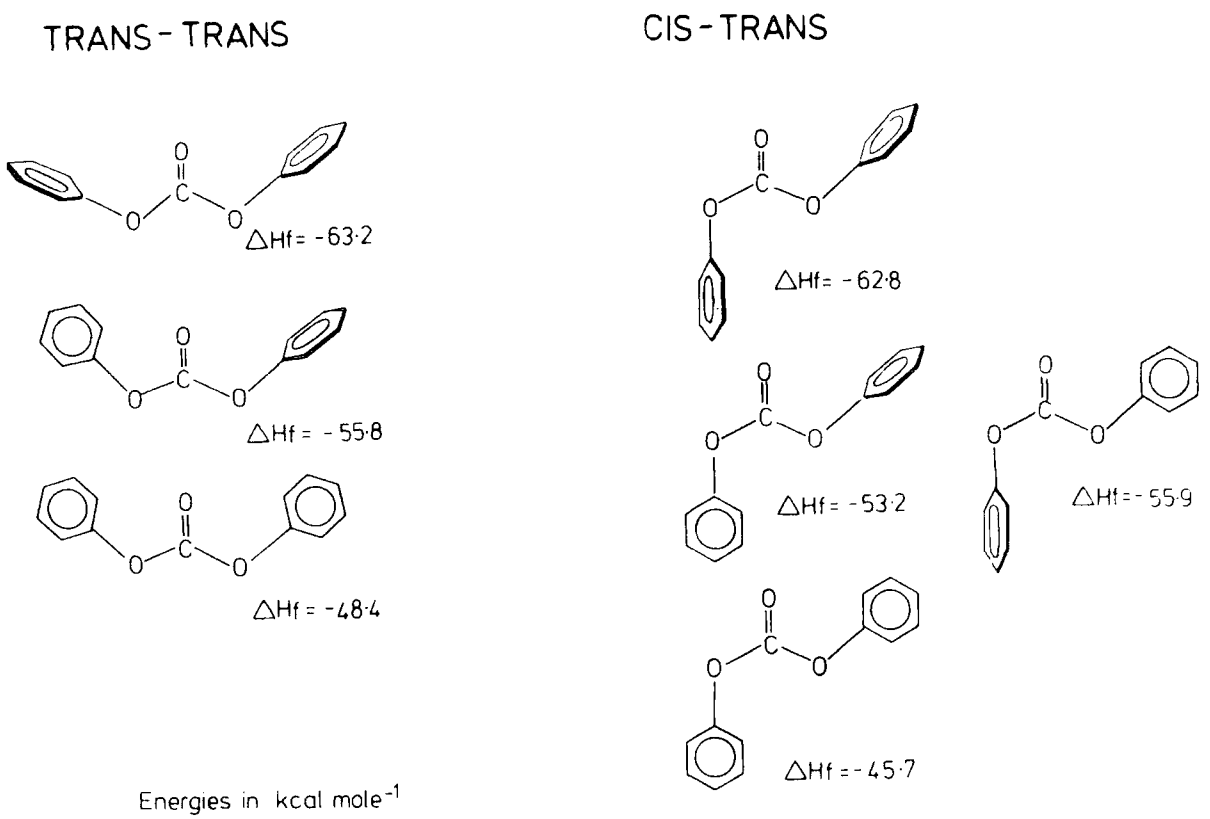

Figure 3.1 Computed heats of formation (k cal mole^{-1}) for planar and orthogonal configurations of the cis-trans and trans-trans conformers of diphenyl carbonate

Computations have been carried out corresponding to intervals in rotation in either a conrotatory or disrotatory manner in 30^{o} degree increments. For the most stable configurations of the trans-trans and cis-trans forms, studies have also been made of the barrier to their interconversion - a total of 35 computations were required for these particular aspects of the present study.

The computed heats of formation for the trans-trans and cis-trans conformations as a function of θ and ϕ (for the planar and orthogonal configurations) are also shown in Figure 3.1. The most stable configurations for both conformers have orthogonal phenyl groups and the computations indicate a small (0.4 k cal $mole^{-1}$) energetic preference for the trans-trans form.

The planar trans-trans configuration is stabilised by $\sim$2.7 k cal $mole^{-1}$ with respect to the corresponding cis-trans and both are located at substantially higher energy ($\sim$15 and 17 k cal mol^{-1}, respectively) than the corresponding orthogonal conformers. It is interesting to note that assumption of standard bond lengths and angles in a rigid rotation approximation provides estimates of the relative energetic preference of orthogonal - compared with planar-configurations nearly an order of magnitude larger than those for flexible rotation discussed here.

The data in Figure 3.2 indicate the small energetic involved in proceeding from orthogonal to planar forms for a given configuration (either trans-trans or cis-trans) for either conrotatory or disrotatory processes. The data in Figure 3.2 relate to a concerted transformation of an orthogonal to a planar to an orthogonal configuration. This can also be considered in terms of a stepwise process whereby the phenyl groups are rotated sequentially rather than simultaneously. For the orthogonal trans-trans configuration, for example, the data in Figure 3.1 show that the energy barrier for rotation of a given phenyl group to the planar configuration is 7.4 k cal $mole^{-1}$.

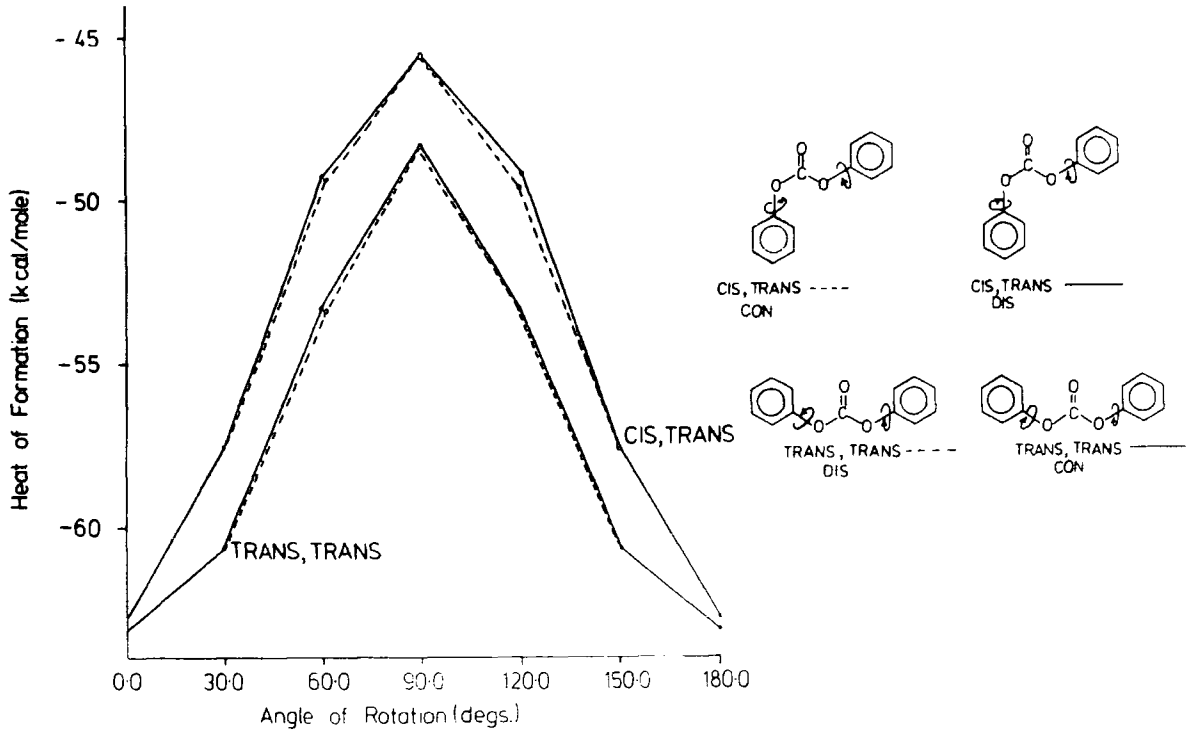

Figure 3.2 Cross-sections through the potential energy surfaces relating planar and orthogonal configurations of cis-trans and trans-trans conformers of diphenyl carbonate.

For the cis-trans configuration there is a significant energetic preference for rotation of the trans phenyl group as opposed to the cis (6.9 versus 9.6 k cal $mole^{-1}$). The rotation of the orthogonal trans phenyl group in the cis planar cis-trans configuration corresponds in energy terms roughly with the energy barrier for rotation of the phenyl groups in the trans-trans configuration. These data suggest, therefore, that there will be a significant energetic preference for a sequential rotation sequence to interconvert orthogonal or planar configurations.

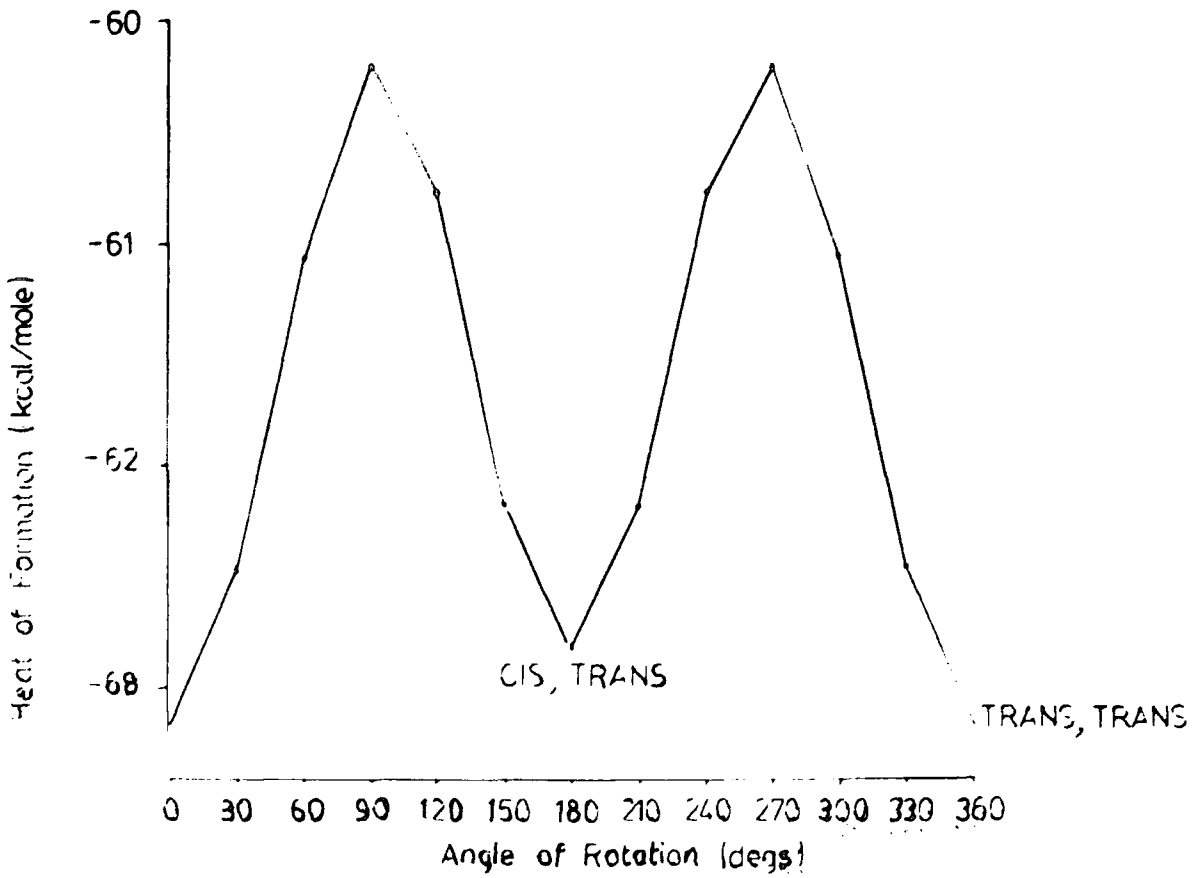

Figure 3.3 Cross-section through the potential energy surface relating the most stable (orthogonal) configurations of the cis-trans and trans-trans conformers of diphenyl carbonate.

Figure 3.3 presents a cross-section through the potential energy surface relating the most stable (orthogonal) configurations of the trans-trans and cis-trans conformers. The computed barrier height of 3 k cal mole^{-1} is comparable with that involved in ethane,[173] indicating the effective free rotation involved at normal temperatures. It is interesting to note that the barrier computed for rigid rotation is only a factor of $\sim$2 different (5.9 k cal mole^{-1}) and hence is less

sensitive to geometry optimisations than that involved in relating planar and orthogonal conformations. Analysis of the geometric parameters shows that the dominant change in going from the orthogonal to planar conformers for either the trans-trans or the cis-trans configurations is a substantial increase ($\sim 10^{o}$) in the $C\text{-}\hat{O}\text{-}C_1(C_1')$ internal angles, those for the cis-trans changing somewhat more than for the trans-trans configuration.

In summary, therefore, the computations indicate that:

(i) The trans-trans and cis-trans configurations are of comparable energy as a function of given values of θ and ϕ but there is a significant energetic preference for orthogonal forms.

(ii) The energy barrier involved in interconversion of cis-trans and trans-trans orthogonal forms is small, at least as far as diphenyl carbonate is concerned.

3.3.2 Excited States

There have been extensive studies both of the chemistry and photophysics of the uv irradiation of Bisphenol A polycarbonates both in solution and in the solid state.[159-161]

The interpretation of experimental data has generally started from an assumed trans-trans configuration for the repeat unit and some discussion has been presented of the likely nature of the excited state for the intramolecular photo-Fries rearrangement which is considered to play an important role in the overall process. From a consideration of fluorescence lifetimes Gupta *et al*[160] concluded that the important excited state was the lowest singlet state and that this was of $n\rightarrow\Pi^*$ character.

Detailed examination of experimental data for simple model systems[5,166] sheds some doubt on this assignment and, as will become apparent from the theoretical studies described in this work, the real situation must be considerably more complex than was originally envisaged.

Before considering the theoretical data in any detail it is worthwhile discussing the $n \rightarrow \pi^*$ states of simple carbonyl, carboxy ester and carbonate systems. This raises certain doubts over the assignment of the nature of the excited states of polycarbonates as has been previously presented in the literature.[160]

The $\pi \rightarrow \pi^*$ transitions for simple alkyl substituted ketones, carboxy esters and carbonates, occur at wavelengths <200 nm[5,166] and thus are not of direct interest in the uv/visible photo-Chemistry of such functionalities.

The longest wavelength transition for simple ketones and carboxy esters arises from $n \rightarrow \pi^*$ excitation and the effect of replacing a simple alkyl substituent by an alkoxy group in going from a ketone to an ester is to shift the $n \rightarrow \pi^*$ transition to shorter wavelength. This arises predominantly from the lowering in energy of the lone pair (n) level of the carbonyl group. Indeed, inspection of the relevant eigenvalues (Figure 3.4(a)) reveals that in the series acetone, methyl acetate and dimethyl carbonate there is a progressive stabilisation of the n-orbital with a concomitant increase in energy of the highest occupied π-orbital; the lowest unoccupied orbital in each case being predominantly of >C=O π^* character. In the particular case of dimethyl carbonate the n and π-orbitals are essentially degenerate and the possibility exists, therefore, that the lowest

excited state of the carbonate group is $\pi \rightarrow \pi^*$ in character. Indeed, the UPS data[174] on dimethyl carbonate, as opposed to simple carbonyl compounds and carboxy esters, show this trend in energies of the highest occupied orbitals rather graphically and the computed orbital energies of $\sim$11.4 eV compare well with the centroid of the experimentally determined ionisation potentials of $\sim$11.1 eV (cf. Figure 3.4(a)). It may be inferred, therefore, that in an orthogonal configuration of diphenyl carbonate the ordering of the n,π and π^* carbonate group orbitals would be analogous to those for an alkyl carbonate. Extensive studies have been made of the lowest excited states of substituted benzenes[5,166] and in addition, UPS studies[175] have also been made of the lowest ionisation potentials. The inevitable conclusions which arise from the detailed examination of these data are as follows:

(i) The highest occupied orbitals of π symmetry (a_{2_π}, b_{1_π}) in monosubstituted benzenes (local C_{2v} symmetry) are expected to be $\sim$1.5eV to higher energy (lower ionisation potential) compared with an n-type orbital in a carbonate group.

(ii) The lowest unoccupied orbitals in a monosubstituted benzene are significantly lower in energy than that for the lowest π^*-orbital in a carbonate group.

(iii) The first $\pi \rightarrow \pi^*$ singlet state for a Ph-O-R system is at substantially longer wavelengths ($\sim$280nm), than the longest wavelength transition for simple carbonates.

(iv) Following points (i) to (iii), little $n \rightarrow \pi^*$ (O-$\overset{\overset{O}{\|}}{C}$-O) character would be anticipated for the lowest excited state of diphenyl carbonate - and hence for Bisphenol A polycarbonates - and this is in contrast to discussions which have been presented in the literature.[159,160]

To substantiate this simple analysis, essentially based on available experimental data, computations have been carried out on the lowest excited singlet and triplet states of simple model systems encompassing the carbonyl, carboxy ester and carbonate structural features. The relevant data are shown in Figure 3.4(b). Considering this first acetone, the small energy splitting between the triplet and singlet states reveals the n→Π* nature of the lowest excited state and this is confirmed by inspection of the relevant orbital coefficients.

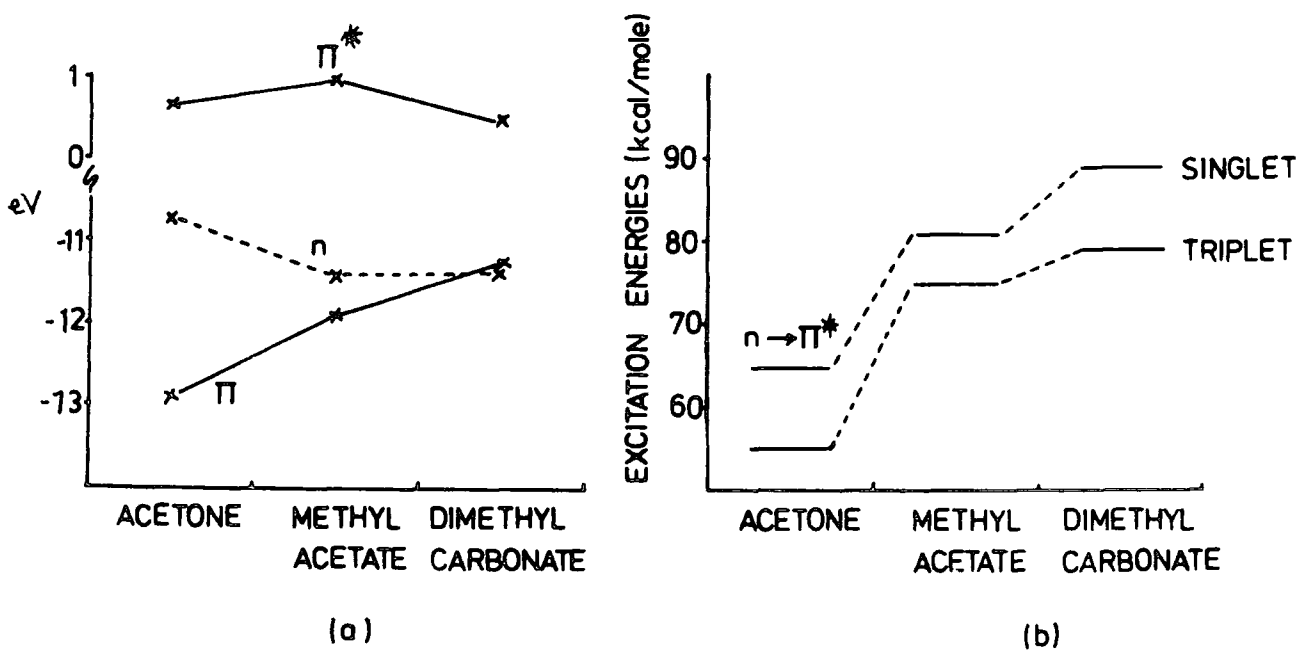

Figure 3.4 HOMOs and LUMOs for model systems; acetone, methyl acetate and dimethyl carbonate (a) and computed energies for n→Π* singlet and triplet (b).

In absolute terms the calculated transition energies are in tolerable agreement with experiment. Thus, for acetone, the singlet state is computed to be ∿80 k cal $mole^{-1}$ above the ground state, the singlet triplet separation being ∿9 k cal $mole^{-1}$.[5,166] The progressive shift on going from acetone to methyl acetate to dimethyl carbonate for the n→Π* transitions is well reproduced by the calculations. The limited facilities for configuration interaction (CI), which is so important for a realistic description of the lowest excited states of benzenoid systems, precluded any realistic theoretical discussion of the diphenyl carbonate system within the MNDO SCF formalism and the CI calculations which were attempted failed to converge: however, inspection of the eigenvalues for both the HOMOs and LUMOs for configurations of diphenyl carbonate and for the model systems shown in Figure 3.4 are highly revealing.

Even for the energetically unfavourable planar cis-trans and trans-trans configurations of diphenyl carbonate, the LUMO is predominantly composed of ring Π* orbitals with only a small percentage >C=O Π* character. Although the HOMO is ring Π-type, the in-plane interaction between the n-type, the in-plane interaction between the n-type orbital and ring σ orbitals of the trans phenyl groups leads to a destabilising influence for the n-orbital such that it is close in energy to the ring Π-orbital. For the orthogonal configurations, however, the effect of twisting the phenyl groups is to stabilise the n-type orbital and the HOMOs, by a wide energy margin, are ring Π-type character. The orthogonality of the carbonate group and phenyl ring systems leads to LUMOs from which the >C=O Π* character has all but disappeared. To summarise, therefore, the theoretical data and the available experimental data point strongly to

a description of the lowest excited state as being ring $\Pi \rightarrow \Pi^*$ in character for Bisphenol A polycarbonates. This is in direct contrast to discussions which have appeared in the literature and in particular there appears to be little justification for the claim[159,160] that in the orthogonal trans-trans configuration the $\Pi \rightarrow \Pi^*$ state would probably be at higher energy than for the $n \rightarrow \Pi^*$ state. The experimental data on simple modely systems, coupled with the theoretical analysis, points strongly to $\Pi \rightarrow \Pi^*$ excited states of ring character. This is not incompatible with the intramolecular rearrangement pathway proposed in the literature,[159-161] which from scale models, looks to be more facile from the non-planar configurations. As a further point of interest it may be noted that for the planar trans-trans configuration whilst the HOMO is strongly C(phenyl)-O anti-bonding, the LUMO involves an essentially non-bonding interaction across the C(phenyl)-O bonds and has significant >C=O Π^* character. This suggests that the excited state may well have less of an energetic preference for an orthogonal configuration and indeed the fluorescence yield and lifetime measurements would be consistent with a strong change in geometry on going from the ground to the excited state. A possible cross-section through the energy hypersurface is outlined schematically in Figure 3.5.

3.3.3 Conformational processes in Phenyl Carbonic Acid

The initial studies on diphenyl carbonate at the MNDO SCF level revealed that barriers to rotation in this system were considerably overestimated if the computations assumed rigid as opposed to flexible rotation. It is, therefore, of interest to investigate the problems of flexible versus rigid

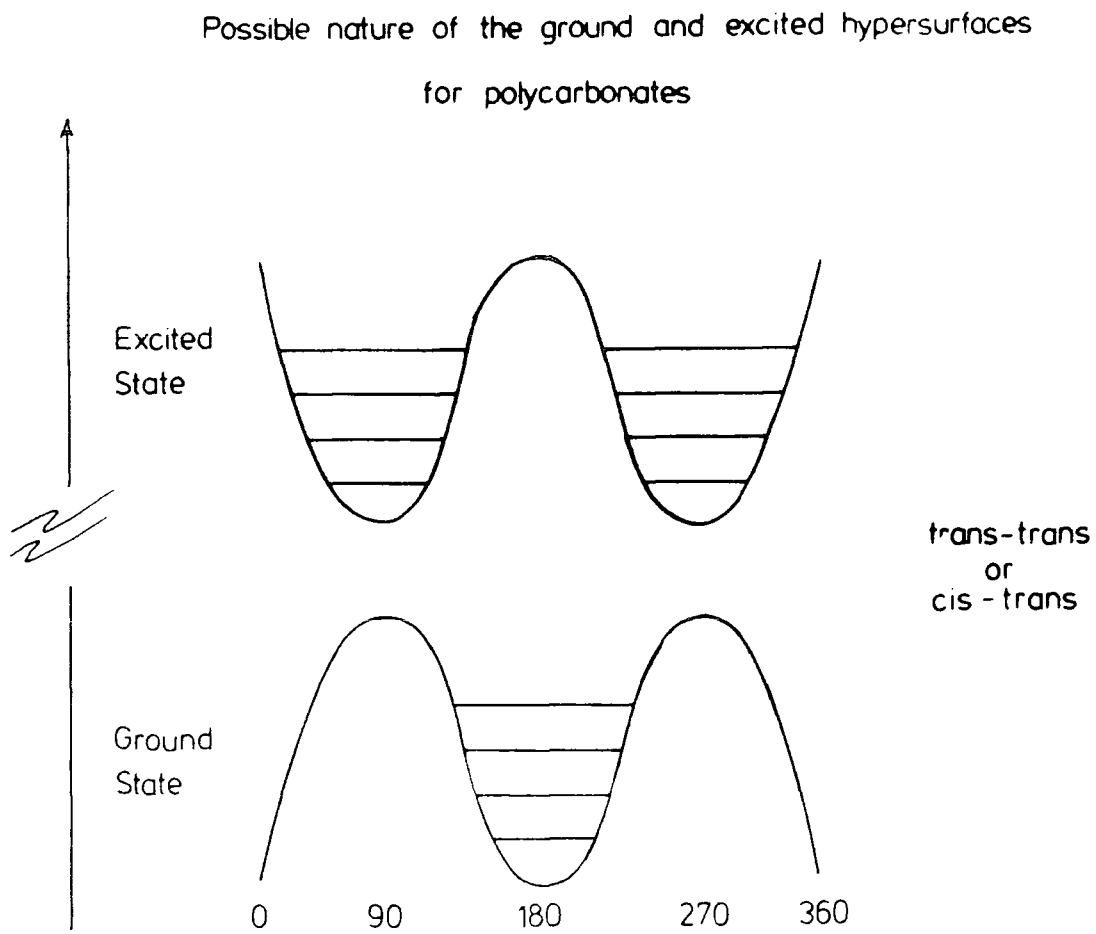

Figure 3.5 Possible nature of the ground and excited state of diphenyl carbonate indicating a preferred orthogonal configuration for the ground state and a planar configuration for the excited state.

rotation in somewhat more detail. As previously discussed, an '*ab initio*' study of diphenyl carbonate would not be feasible from the considerations of both storage and computation time, therefore, phenyl carbonic acid was utilised as the model for the investigation of rigid rotation at the STO-3G and MNDO SCF levels.

The energies as a function of rotation angle ϕ computed for the trans-trans configuration of phenyl carbonic acid at the non-empirical STO-3G and MNDO SCF levels within the rigid rotation approximation are displayed in Figure 3.6. It is clear

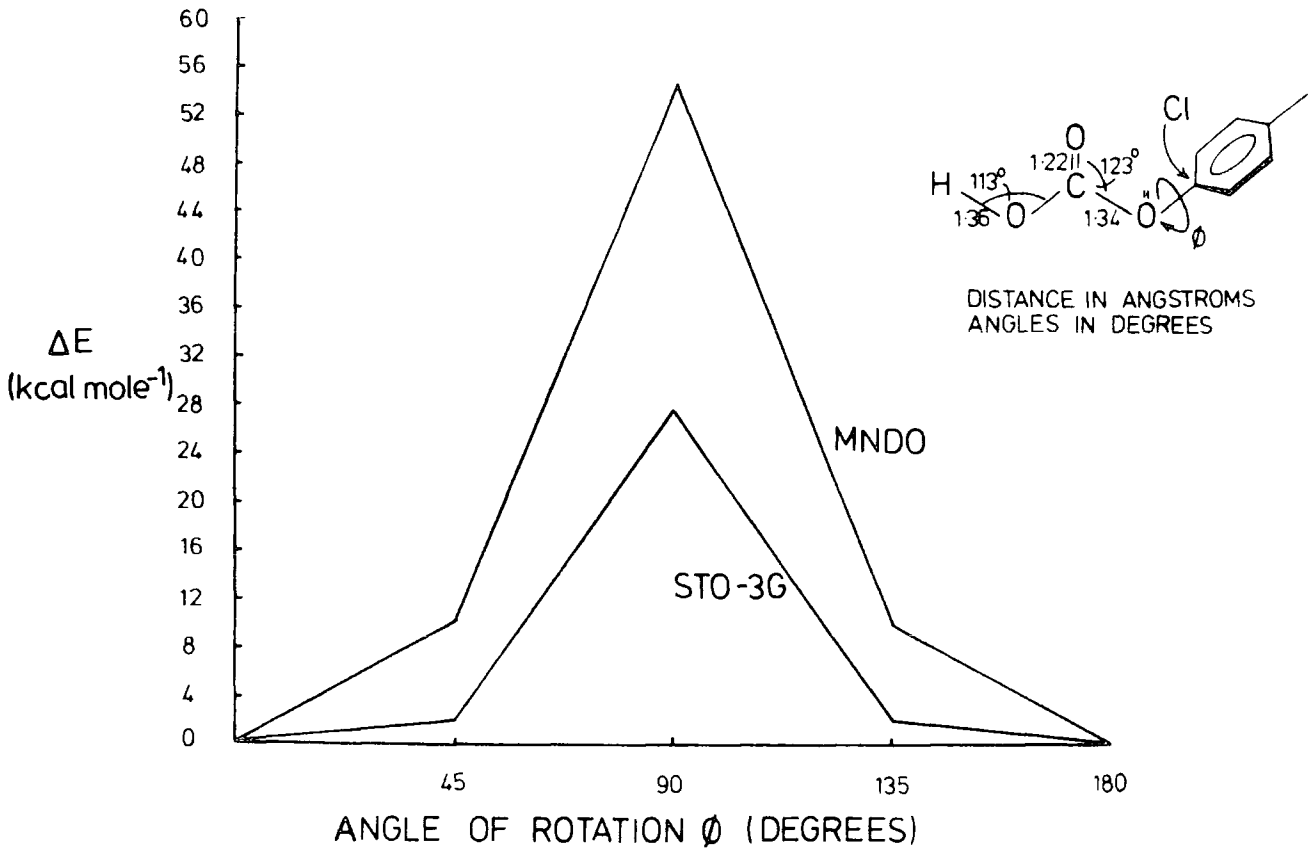

Figure 3.6 Changes in energy on rotation of the phenyl group in phenyl carbonic acid as predicted by computations at the STO-3G and MNDO SCF levels (Also shown is the geometry used in the calculations.

from this that the orthogonal conformation is strongly stabilised, however, the MNDO treatment suggests a barrier to rotation a factor of ∿2 higher than for the '*ab initio*' computation. Com parison with the computations on diphenyl carbonate, also assuming rigid rotation, shows the barriers to be roughly independent of the substituent at the other oxygen (viz. the barrier to rotation of a given phenyl substituent is roughly independent of whether there is a hydrogen or phenyl functionality at the other oxygen).

The computed flexible barrier to rotation for diphenyl carbonate may be used as a basis for estimating the flexible barrier to rotation in phenyl carbonic acid and a comparison of this with the rigid barrier to rotation (viz. ∿9 k cal $mole^{-1}$ versus ∿55 k cal $mole^{-1}$) shows the great danger of assuming rigid rotation. Comparison with the '*ab initio*' results does, however, show that the MNDO computations may well in any case overestimate the barriers by a factor of ∿2. If this is the case then an '*ab initio*' study of the barrier to flexible rotation in diphenyl carbonate might well produce a barrier to rotation for each phenyl group of ∿5 k cal $mole^{-1}$. It would seem likely that for such systems '*ab initio*' studies even at the minimal STO-3G level may not be realistic in terms of computational expense and storage requirements. A combination of flexible rotation studied at the MNDO SCF level and rigid rotation at the non-empirical level may therefore be the only realistic way of gaining information on the nature of ground state potential surfaces as an alternative to the heavily parametrised molecular force field type of investigation.[164]

3.3.4 Orbital Energies

The discussion on acetone, methyl acetate and dimethyl carbonate in Section 3.3.2 pointed to the fact that the >C=O Π orbital is progressively destablised and the n-orbital stabilised in going from a ketone to a carboxy ester and thence to a carbonate. The '*ab initio*' study reveals this rather well and Table 3.2 shows a comparison of the orbital assignments produced by the non-empirical and semi-empirical treatments for the planar configuration. The lowest virtual orbital is ring Π* with essentially non-bonding C_1-O" character.

TABLE 3.2 Non-empirical (STO-3G) orbital energies for the highest occupied orbitals of phenyl carbonic acid. Also shown for comparison are the data from the MNDO SCF study.

Orbital Energy (eV)		Dominant Composition	C_1-O" bonding characteristic
STO-3G	MNDO		
8.5	9.2	Ring $b_{1\pi}$, O"	antibonding
9.2	9.4	Ring $a_{2\pi}$	-
9.3	10.3	n	-
10.9	12.5	>C=O π	-

The lowest excited state is therefore $\pi \rightarrow \pi^*$ and the removal of the antibonding C_1-O" interaction is likely to cause a strong change in geometry on excitation. The main difference between the STO-3G and MNDO SCF treatments arises in the computed energy gap between the ring π orbitals and the n and π-orbitals of the carbonyl subset of the carbonate group.

Although strict σ-π separability does not obtain for the 45° and 90° conformers it is still possible to analyse the orbitals roughly in terms of local symmetry as being ring π, carbonate π and n type orbitals. On this basis the main change in orbital energy sequence in going from the planar to orthogonal configurations is a small progressive stabilisation of the ring π and n type orbitals and destabilisation of the carbonate π-orbital. The lowest excited states in terms of local symmetry are still, however, ring $\pi \rightarrow \pi^*$ in nature.

The '*ab initio*' computations also allow a comparison to be drawn with the measured C_{1s} levels for appropriate models with the proviso that relaxation energy changes will be slightly different for different sites within the molecule. Assuming

Koopmans' Theorem,[83] the computed shifts in going from the ring C-H carbons to the carbon singly bonded to oxygen and that of the carbonate group are 0 to 2.2 to 5.7 eV which compares very favourably to the observed shifts for C_{1s} levels in Bisphenol A polycarbonates of 0 to 1.6 eV to 6.0 eV as previously noted.[176,177]

3.3.5 Conclusions

The MNDO SCF computations show that for diphenyl carbonate the most stable configuration corresponds to an orthogonal trans-trans conformation although the corresponding cis-trans configuration is only slightly higher in energy.

Analysis of the eigenvalues for simple models containing carbonyl, carboxy ester and carbonate structural features shows the progressive stabilisation of the n-type and destabilisation of the highest Π-type orbital across the series. Experimental UPS studies confirm this trend experimentally and calculations of the excited states also reproduce the experimental finding that the enrgy of the n→Π* transition moves to shorter wavelengths across the series in going from >C=O to -O-C(=O)-O- structural features. The analysis shows that for diphenyl carbonate as a model for Bisphenol A polycarbonates the first excited state for orthogonal configurations corresponds to Π→Π* excitation (Ar-O-) for the n→Π* states are at higher energy. Whilst the ground state hypersurface exhibits double minima as a function of the rotation angles θ and φ (cf. Figure 3.2) the barriers to interconversion of orthogonal via planar configurations are not excessive and it could well be that the planar configurations are energetically preferred for the lowest excited state (Figure 3.5). The consequent Franck Condon factors would then provide an explanation for the key aspects

of the photophysics data -

(i) the low quantum yield for fluorescence, and

(ii) the low rate of intersystem crossing.

The *'ab initio'* computations on phenyl carbonic acid have highlighted the danger of assuming a rigid rotation formalism at the semi-empirical level where the barriers to rotation are overestimated by a factor of $\sim$2.

CHAPTER FOUR

THE PHOTOAGING OF BISPHENOL A POLYCARBONATE - PART II

SURFACE ASPECTS OF THE PHOTODEGRADATION OF BISPHENOL A POLYCARBONATE IN OXYGEN AND NITROGEN ATMOSPHERES AS REVEALED BY ESCA

4.1 Introduction

The environmental modification of polymeric materials is of considerable industrial and technological importance, however, the detailed investigation of the processes occurring have for the most part not been subject to detailed scrutiny at the molecular level. Since all solids communicate with the rest of the world primarily by means of their surfaces, the surface is of paramount importance in environmental modification. It might, therefore, be anticipated that reactions occurring at such an interface may be different than for the bulk. From the schematic outline in Figure 4.1 it should be evident that the partial pressure of oxygen and of trace reactive gases (e.g. NO_2, SO_2, O_3 denoted by R) in the atmosphere will be highest at the interface whilst the greatest flux of radiation will also be at the surface. (It is worthwhile noting that the electromagnetic spectrum is essentially unattenuated over the first few tens of angstroms of a polymer sample. For the bulk the attenuation coefficients at different wavelengths may lead to considerable inhomogeneities in the sample).

In systems containing additives (P) which might well enhance or retard photodegradation, their surface concentrations may be different from the bulk and this again might lead to differences in reaction. It is conceivable, however, that in specific cases rapid surface reactions leading to low molecular weight molecules which can readily desorb from the surface could dominate the overall degradation of the sample particularly if this had a high surface area to volume ratio (e.g. a film).

Photochemical Degradation of Polymers

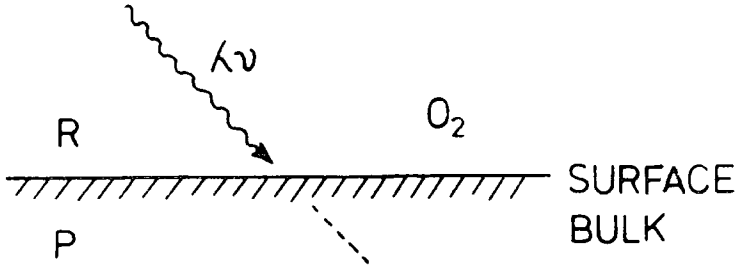

a) MODEL STUDIES
Wavelength, photon flux, partial pressure of oxygen

b) Natural weathering

Figure 4.1 The photochemical degradation of polymers; the importance of surfaces.

Studies of photodegradation of polymer systems reported to date have primarily involved monitoring bulk chemistry,[10,12] however, Clark and co-workers[49-51] have shown how ESCA may be applied to the study of such reactions including weathering at polymer surfaces.[52] In the previous chapter some theoretical aspects of the nature of the excited state involved in the photodegradation of Bisphenol A polycarbonate were considered and this chapter complements these studies by an experimental investigation of the surface reactions involved in the photochemical degradation of polycarbonate films in oxygen and nitrogen atmospheres at wavelengths >290 nm.

The majority of the investigations reported in the literature on the photochemical degradation of polycarbonates have involved solution phase studies[160,161] at wavelengths <290 nm and are thus not strictly relevant to the solid state photodegradation in sunlight. The main features of the major routes for the photochemical degradation of polycarbonate which have been described in the literature together with a summary of the available data on the nature of the excited state involved in set out in Figure 4.2. Evidence has been presented for the dominant role of photo-Fries rearrangements by both inter- and intra-molecular processes and the classic text by

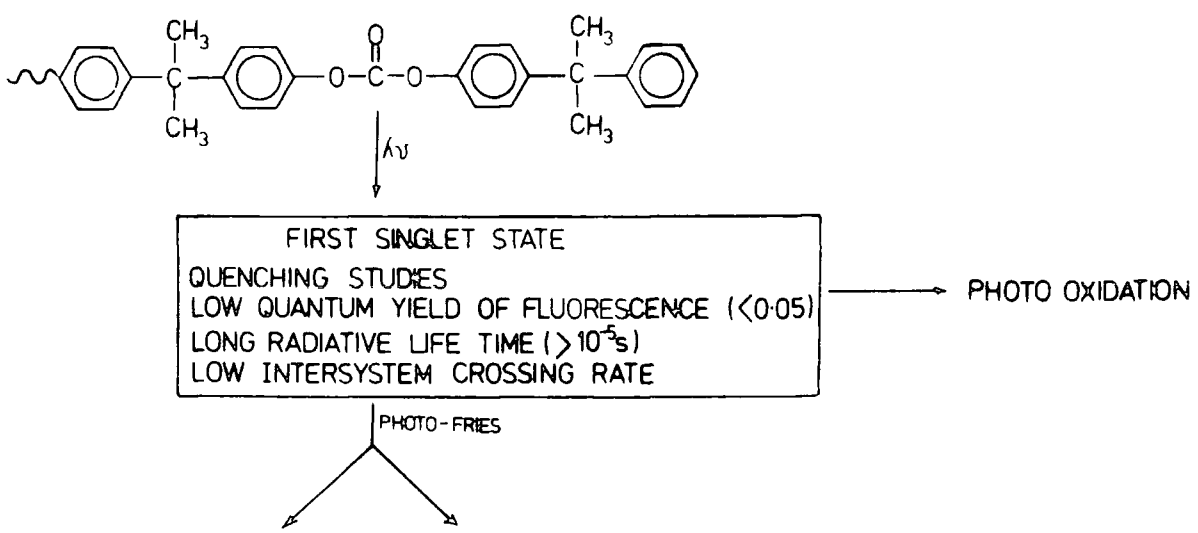

Figure 4.2 Data on the nature of the excited states involved in the photodegradation of Bisphenol A polycarbonate

Ranby and Rabek[10] also emphasises the importance of photo-Fries rearrangements. However, the detailed studies recently reported by Factor and Chu[178] suggest that photooxidative pathways involving the gem-dimethyl and phenyl groups are of greater importance in the photodegradation of polycarbonate in the solid state in oxygen rich atmospheres and at wavelengths corresponding somewhat more closely to sunlight than in previous studies. In this somewhat confused situation it is clear that a detailed investigation of the surface aspects of the photo-degradation of polycarbonate would be particularly apposite at this time.

4.2 Experimental

The main emphasis of this chapter has been to investigate reactions at the gas solid interface of Bisphenol A polycarbonate films (∿25 μm) induced by irradiation with ultraviolet light at wavelengths greater than 290 nm in oxygen and nitrogen atmospheres. To facilitate these studies, a special stainless steel reactor has been constructed (Figure 4.3), enabling polymer films to be irradiated in a controlled environment whilst mounted on an ESCA probe by means of double sided Scotch tape, so that the samples may be directly studied after exposure.

Samples were irradiated with the output of a Hanovia 500W medium pressure Hg arc lamp, filtered via a pyrex window (λ>290nm), the appropriate gas is allowed to flow continuously through the reactor during exposure (10.C.C.min.$^{-1}$) preventing the build up of any desorbed low molecular weight species from enhancing or retarding the reaction. This non static environment would perhaps provide a closer analogue of natural weathering conditions (e.g. the effect of wind) than a totally closed

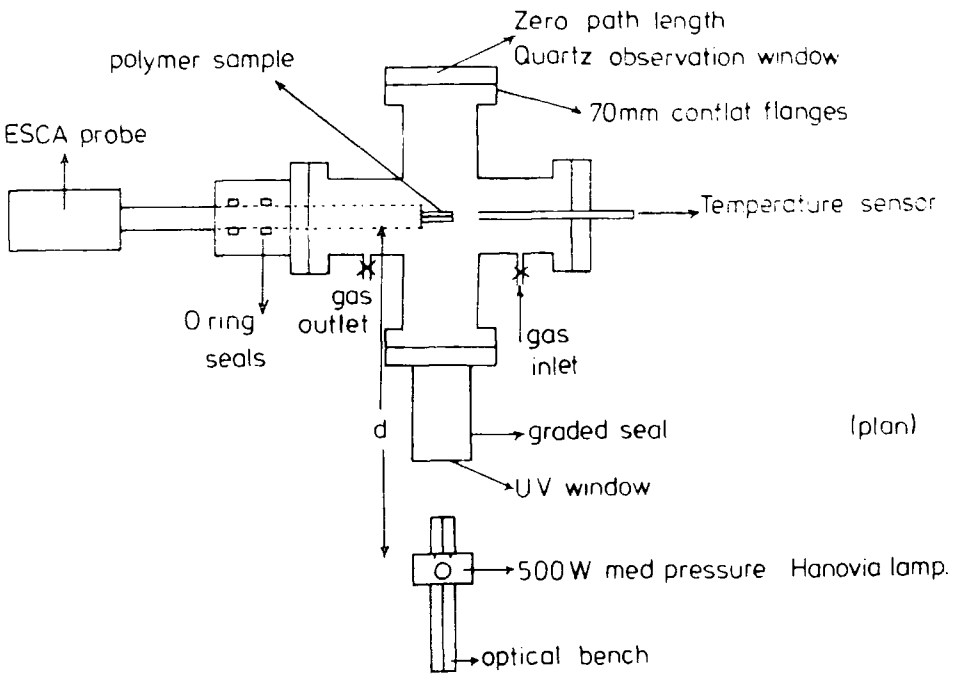

Figure 4.3 Schematic of reaction chamber used for model oxidation studies of polymers.

irradiation system. The temperature may be elevated to $\sim 100^{o}C$ by means of heating tape enclosing the reactor. The incident light intensity may be varied by altering the distance between the sample and the lamp.

The typical procedure for exposure consisted of placing the sample just beyond the second O'ring in the reactor and flushing the whole system with oxygen or nitrogen for 20 minutes. The lamp was allowed to warm up for 15 minutes prior to placing the sample directly in the path of the incident radiation. Control experiments have shown that no observable changes can be detected in the ESCA spectra during the preparatory stage.

A fresh sample was used for each exposure. The dosage of the incident radiation was determined by monitoring the changes in absorbance at 330nm of Bisphenol A polysulphone films as has been previously described by Davis *et al.*[40-42] Typical photon fluxes employed in these studies are displayed in Figure 4.4

Lamp intensities > 290 nm

(monitored at 330 nm by polysulphone)

		$whm^{-2}h^{-1}$	Equivalent times
Hanovia 500 Med pressure Lamp	50cms	5·7	15mins ≈ 90mins PERME, 54mins JTTRE
	18cms	52·5	
		$whm^{-2}\ d^{-1}$	
PERME (June)		9	
JTTRE (Australia) (October)		15	15mins at 18cms gave same charge at 330nm as 2 days in Dhahram, Saudi Arabia (September)

Figure 4.4 Photon flux data for lamp configurations employed in the model photooxidation studies. For comparison purposes, photon fluxes for natural weathering are also included.

For comparison, data are also included for photon fluxes in the environment; it is worthwhile noting at this stage that there is a cyclic phenomena involved in the intensity of solar radiation and also the distribution of wavelengths is somewhat

different for that of a mercury lamp (cf. Chapter One). The main effect of this is that the intensity of shorter wavelengths (ca. 310nm) are lower in the environment.

It is not possible from the C_{1s} and O_{1s} profiles to directly delineate the importance of hydroperoxides. To facilitate the study of their formation, it is possible to convert these groups to sulphates by the direct reaction with SO_2 [179] and monitoring the S_{2p} core level at a binding energy of ∿169.2 eV to obtain some degree of evaluation. Irradiated samples were placed, immediately after exposure, into a purex vessel which was then evacuated to $\sim 10^{-3}$ torr. The vessel was then let up to an atmospheric pressure of SO_2 (B.D.H. Chemicals) and left for 20 minutes before analysis.

ESCA spectra were recorded on AEI ES200B and Kratos ES300 spectrometers using $Mg_{K\alpha}$ and $Ti_{K\alpha}$ radiation respectively. Under the experimental conditions employed in these studies, the respective full width at half maximums (for $Mg_{K\alpha}$ radiation) for the $Au_{4f7/2}$ level at 84.0eV, used for calibration were 1.2 and 1.1 eV. Spectra were deconvoluted and integrated using a DuPont 310 curve resolver. Binding energies were referenced to the hydrocarbon component at 285.0eV.

4.3 Results and Discussion

DURHAM UNIVERSITY
23 SEP 1982
SCIENCE LIBRARY

4.3.1 Introduction

The main emphasis of this chapter has been to investigate the reactions at the gas/solid interface at wavelengths >290nm. The results in this and subsequent sections employed the stainless steel reactor described in Section 4.2. The investigations involved irradiations in both oxygen and nitrogen atmospheres with the surface chemistry being monitored

by ESCA as functions of light intensity and exposure time and temperature. It is convenient in discussing the results to consider the irradiations in oxygen and nitrogen atmospheres separately and then to draw comparisons between them.

4.3.2 Reactions in Oxygen

(a) Studies as a function of light intensity and irradiation time

As a starting point for the investigation of changes in surface chemistry it is convenient to consider firstly the irradiation of polycarbonate films in an oxygen atmosphere for varying periods of time at the lowest photon flux employed (i.e. 5.7 $Whm^{-2}h^{-1}$). The ESCA data shown in Figure 4.5 are

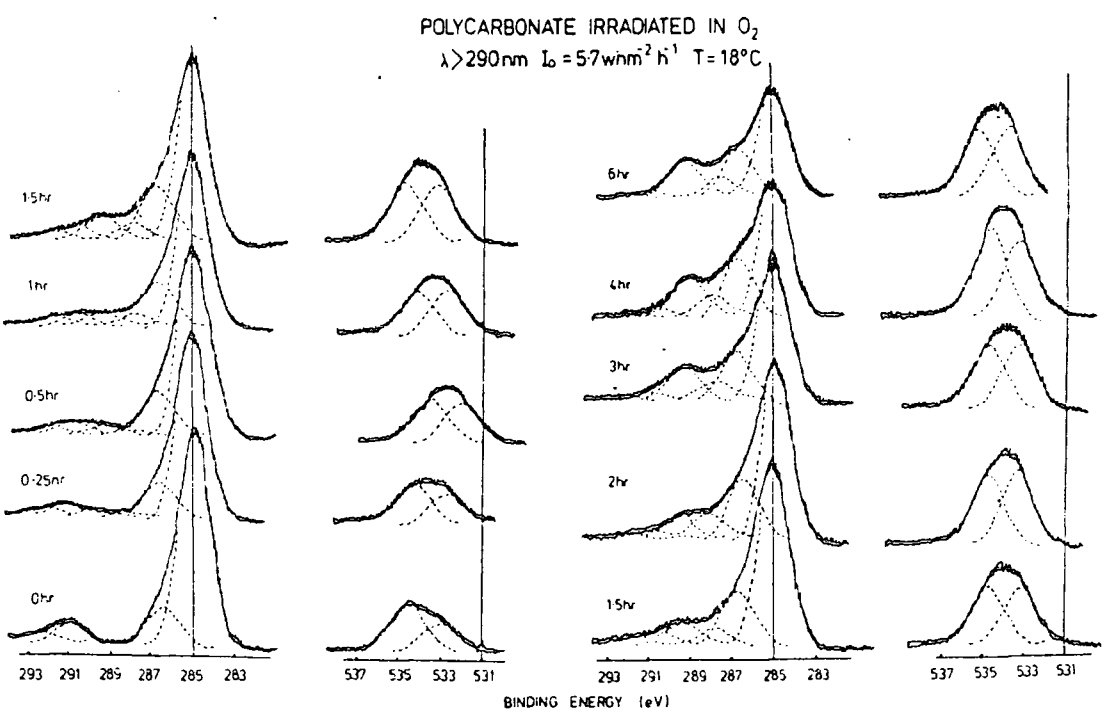

Figure 4.5 C_{1s}/O_{1s} ($Mg_{K\alpha_{1,2}}$) as a function of irradiation time for polycarbonate samples irradiated in an oxygen atmosphere (Io=5.7Whm^{-2}h-1)

distinctive and reveal the extensive changes in surface chemistry under these experimental conditions. Starting from a C_{1s} profile showing four components corresponding in increasing energy to C-H, C-O, O-C(=O)-O and $\Pi \rightarrow \Pi^*$ shake-up components (at 285.0, ∿286.5, ∿290.8 and ∿292 eV respectively), the C_{1s} profile rapidly increases in complexity with extra components originating from C=O and O-C=O functionalities. The O_{1s} signal starting from a 2:1 doublet, corresponding to the two types of oxygen environment involving the carbonate group, increases in relative intensity and after a period of 6 hours irradiation the two components are of comparable intensity. The data illustrates the great surface sensitivity of ESCA and reveal that extensive oxidative functionalisation has occurred. This is more readily apparent from a comparison of the O_{1s} and C_{1s} intensity ratios and from a consideration of the relative proportion of the C_{1s} signal arising from carbons representing oxidative functionalities and this is shown in Figure 4.6. It is clear from this that the photo-Fries rearrangement cannot represent the main contribution to the photodegradative process. At an electron take off angle of 30^{o}, 95% of the C_{1s} signal intensity displayed in Figure 4.5 originates from the outermost ∿45Å. By employing a variable take-off angle and more particularly by going to a harder X-ray source (e.g. $Ti_{k\alpha}$) sampling depth ∿120A,[180] it may be shown that the oxidative reactions extend well into the subsurface. This is apparent from the substantial changes in O_{1s} and C_{1s} core levels taken with a $Ti_{k\alpha}$ X-ray source as is evident from Figure 4.7. The distinctive 1:2 doublet of the unexposed C_{1s} spectrum is lost after 16 hours' exposure where the C_{1s} level has a broad

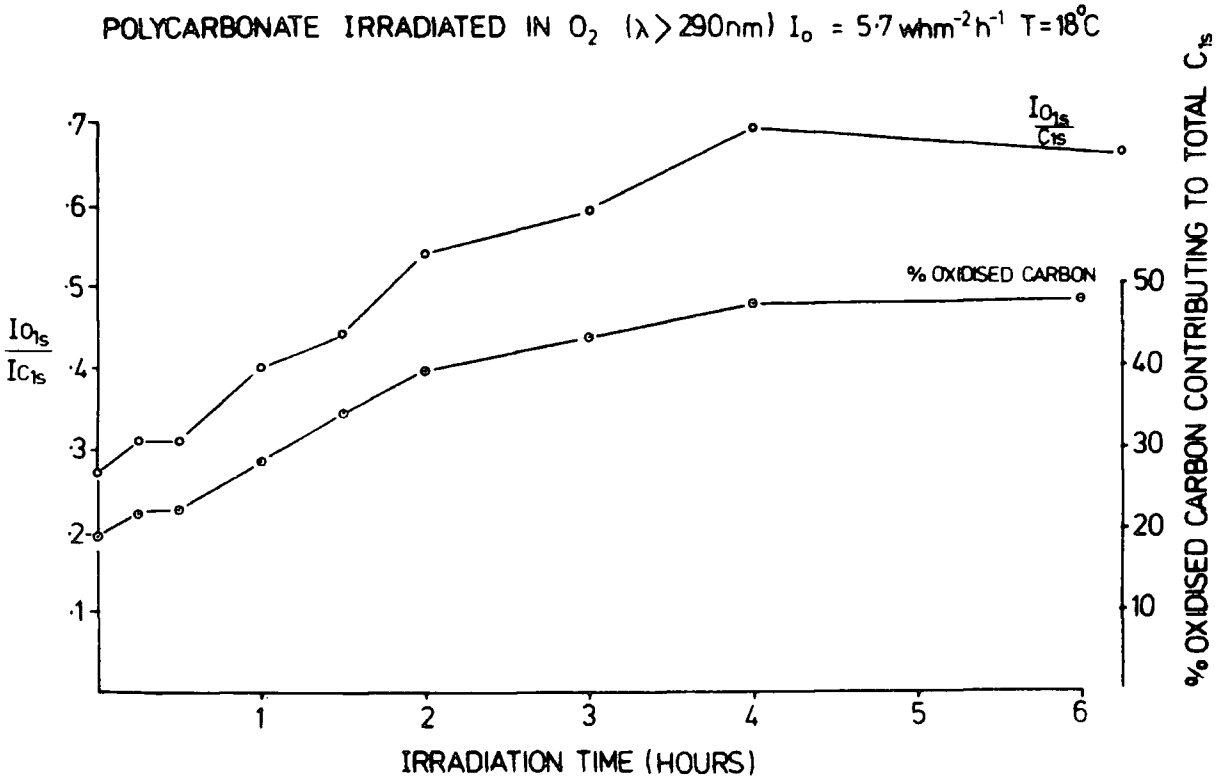

Figure 4.6 O_{1s}/C_{1s} intensity ratios and percentage oxygenated features defined from C_{1s} levels for photooxidised polycarbonate samples.

flattened appearance. This can only arise if extensive oxidative functionalisation has occurred. It is interesting to draw a comparison berween the relative O_{1s}/C_{1s} intensity ratios for the spectra obtained with $Mg_{K\alpha}$ and $Ti_{K\alpha}$ radiation. This data is shown in Table 4.1 for the % oxygen uptake after 0, 2 and 16 hours irradiation at a photon flux of 5.7Whm^{-2}h^{-1}. it is readily apparent that the reactions occurring at the surface ($\sim$45Å) are more rapid than those in the subsurface

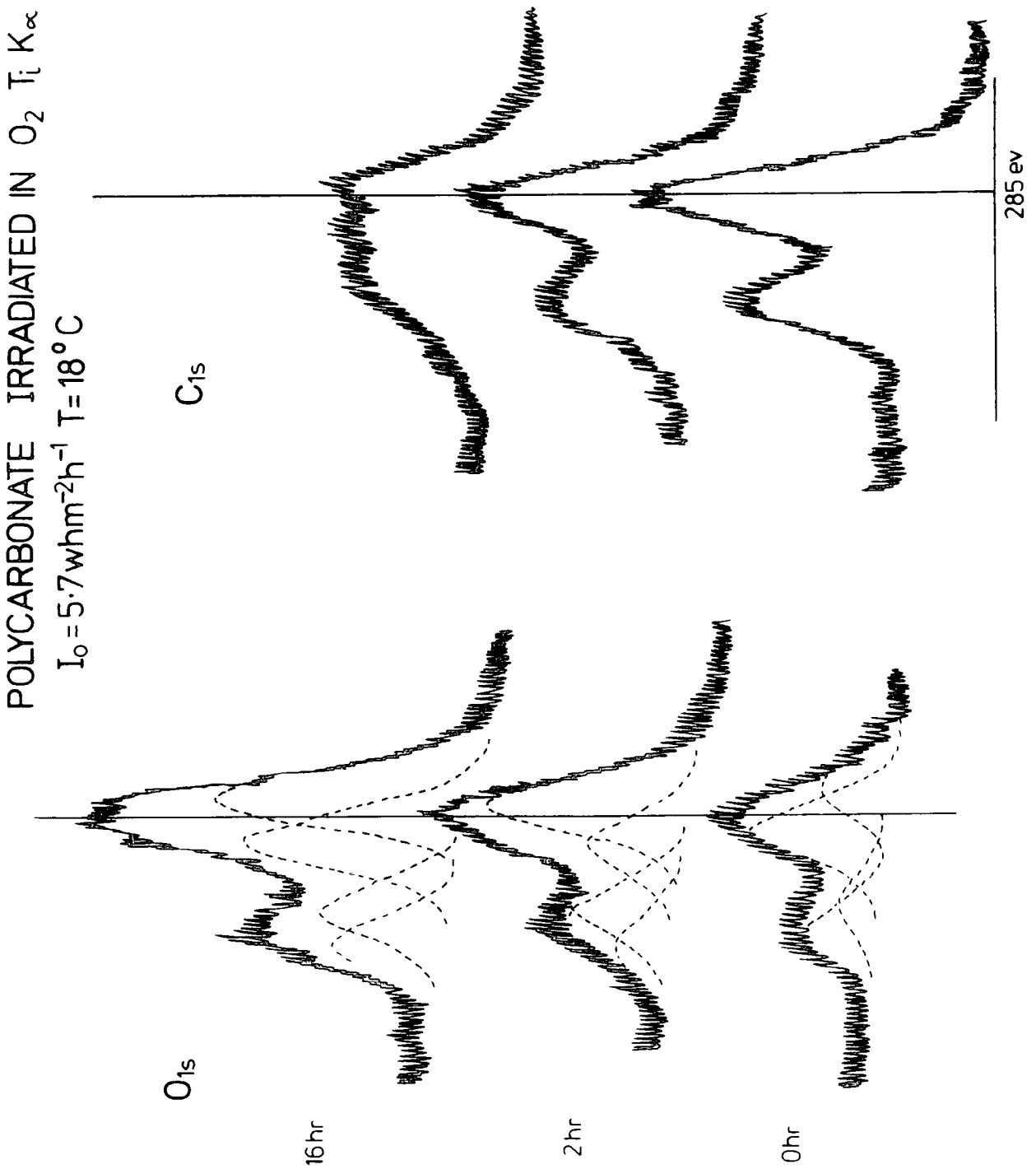

Figure 4.7 C_{1s} and O_{1s} levels (Ti_{K_α}) for polycarbonate and polycarbonate irradiated in an oxygen atmosphere ($Io = 5.7 Whm^{-2}h^{-1}$)

(∿120A) although the extent of both is similar after 16 hours exposure.

TABLE 4.1 Comparison of the % oxygen uptake as determined from the O_{1s}/C_{1s} intensity ratios for Ti_{K_α} and Mg_{K_α} spectra

Irradiation time (hours)	% oxygen uptake	
	Ti_{K_α}	Mg_{K_α}
0	0	0
2	48	110
16	200	212

It has been shown that oxygen substituent effects on the C_{1s} core hole state spectra can be treated in terms of an additive model.[186,187] The extensive background data allows a chemically unique analysis of complex C_{1s} (and O_{1s}) line profiles and this reveals the component contributions indicated in Figure 4.8

The nature of the oxidative functionalisation becomes clear from the component analysis for the spectra in Figure 4.5 displayed in Figure 4.8. The C-H component (phenyl group other than carbon directly attached to oxygen and gem-dimethyl group) decreases in intensity as a function of the irradiation time whilst the C-O, C=O and O-C=O functionalities increase in intensity. The $\pi \rightarrow \pi^*$ component intensity decreases and this is consistent with loss of aromaticity. The data therefore suggest oxidation of both the aromatic ring system and the gem-dimethyl noiety. The carbonate structural feature decreases in intensity but stabilizes at a low percentage contribution to the overall structure. This in fact appears to be a general feature of the photo-oxidation and indeed plasma oxidation[181,182] of aromatic polymers.

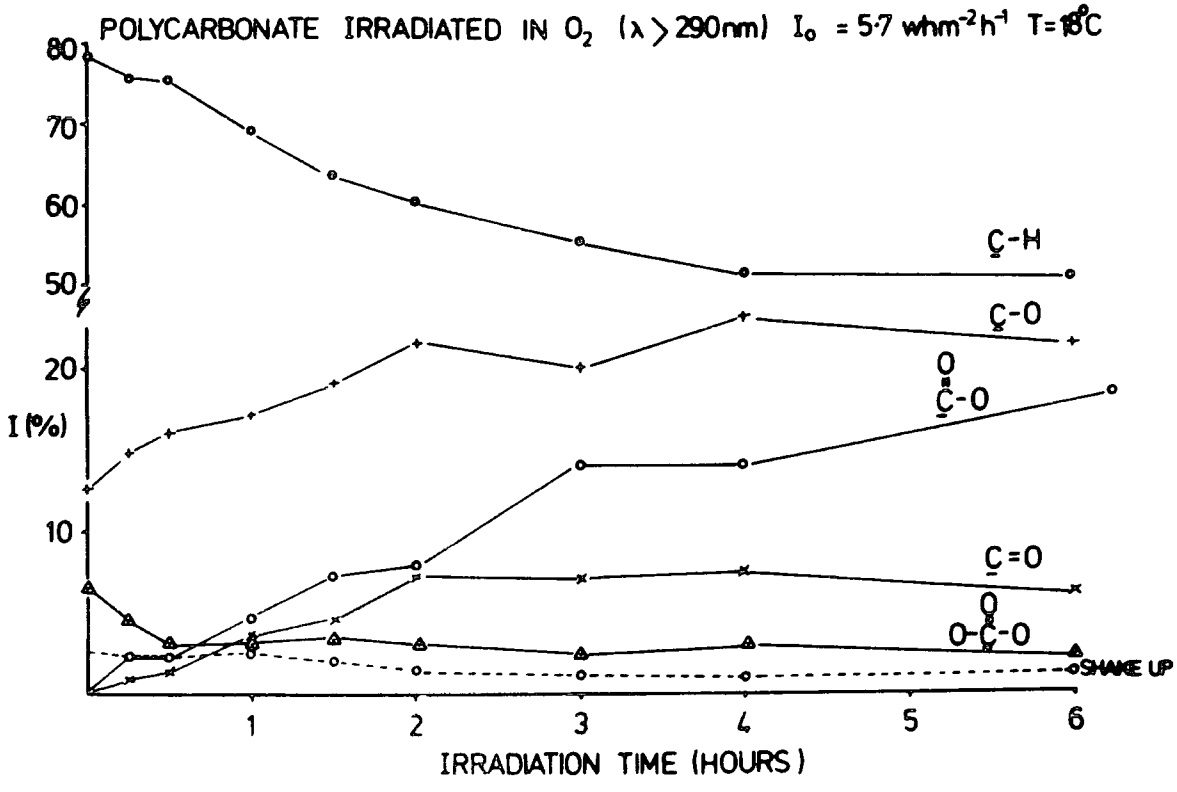

Figure 4.8 Component contributions to C_{1s} line profile for the core level spectra displayed in Figure 4.5 for photooxidised polycarbonate.

For comparison purposes Figure 4.9 shows the core level spectra for polycarbonate films irradiated for varying times at a higher photon flux of 52.5 Whm^{-2}h^{-1}. A casual perusal of the data reveals the significantly greater extent of oxidation for a given irradiation time compared to the lower photon flux.

The component analysis shown in Figure 4.10 reveals the same trend with a much higher build up of C-O and O-C=O structural features at an earlier stage than for the lower lamp intensity. It is interesting to note that an equilibrium surface structure

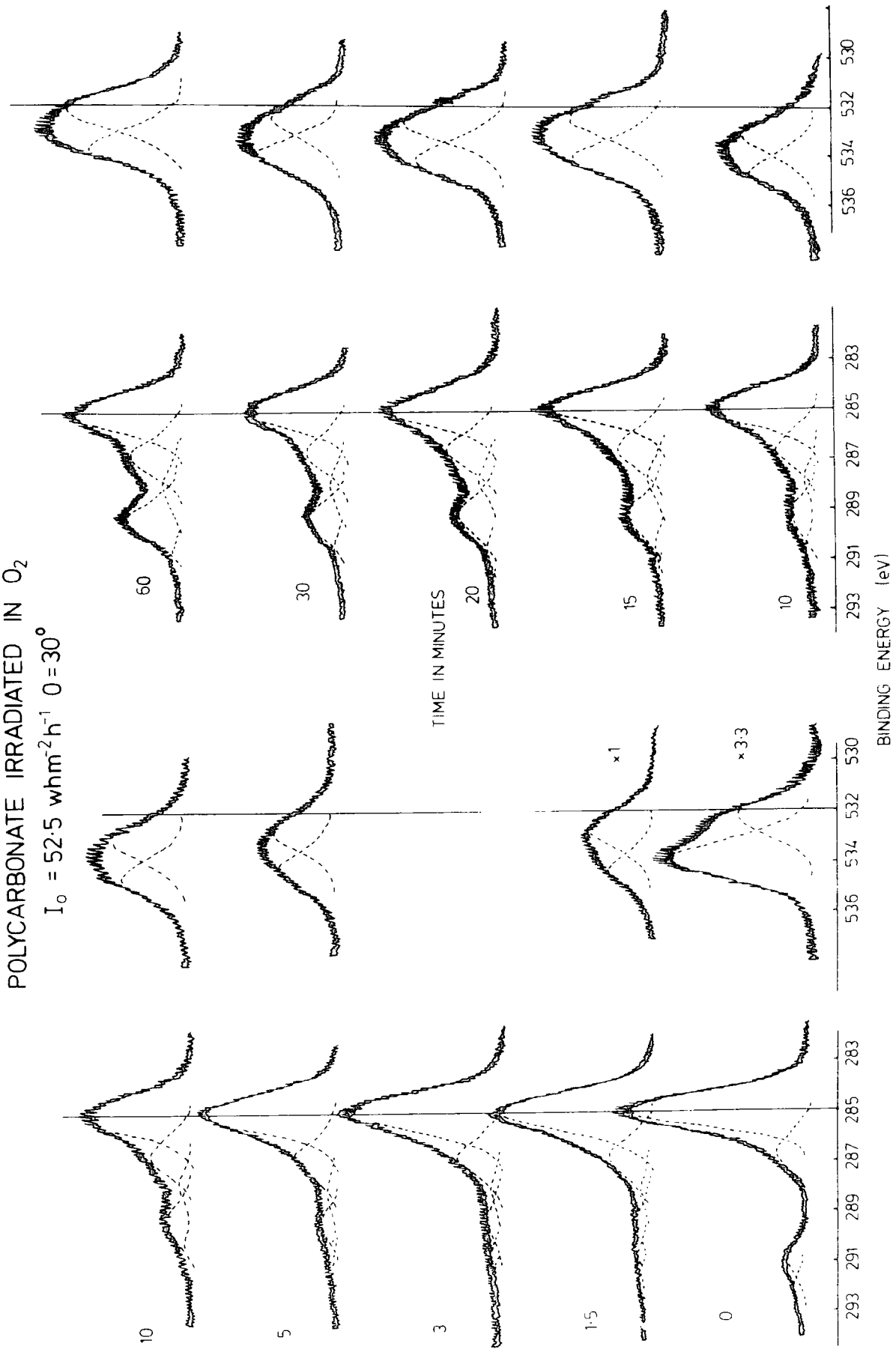

Figure 4.9 C_{1s} and O_{1s} levels ($Mg_{K\alpha_{1,2}}$) for polycarbonate films irradiated in an oxygen atmosphere (I_o = 52.5 Whm^{-2}h^{-1})

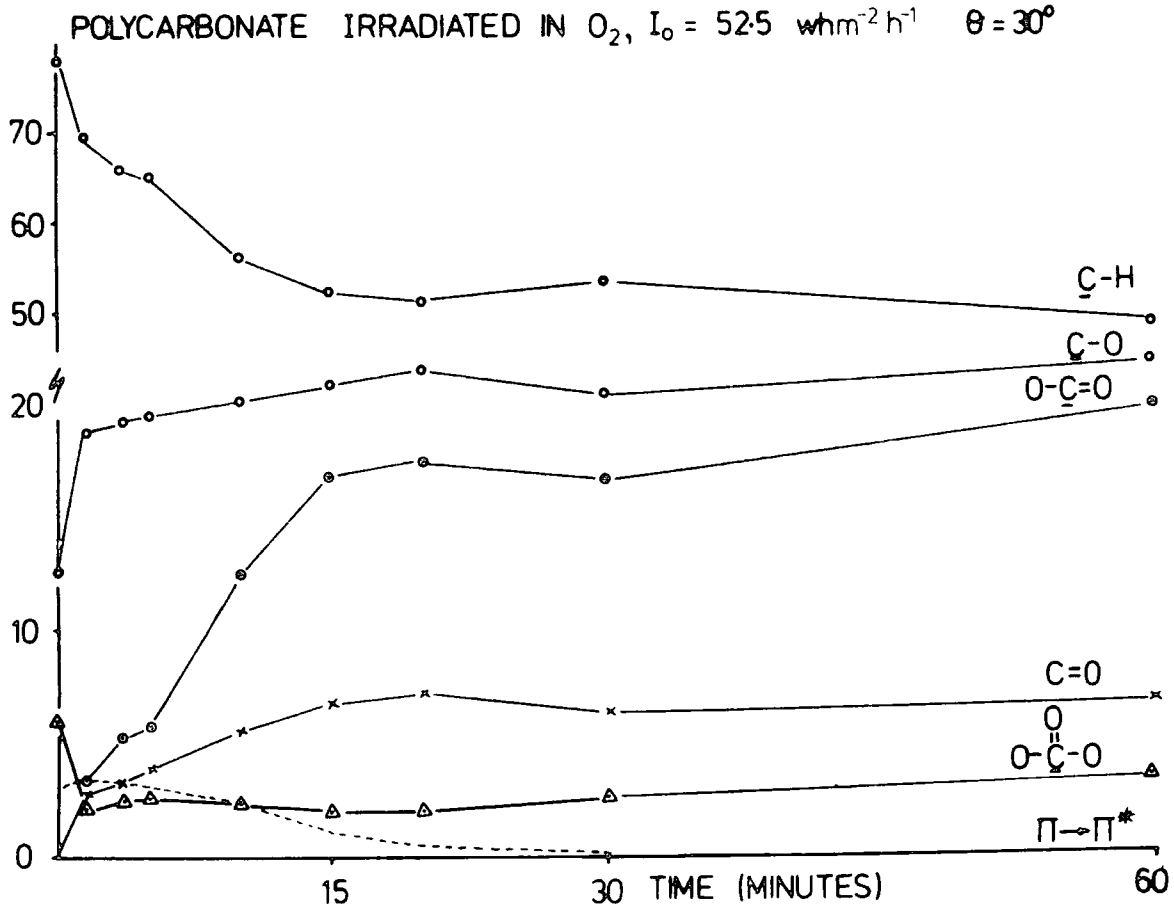

Figure 4.10 Component contributions to C_{1s} line profiles for the core level spectra displayed in Figure 4.9

seems to be established after ∿1 hour of irradiation at 52.5 $Whm^{-2}h^{-1}$ whereas oxidative functionalisation is still in the process of being built up at the lower photon flux (5.7 $Whm^{-2}h^{-1}$) over the same period. From a C:O stoichiometry for the initial polymer film of 1:0.19 after 1 hour's irradiation the oxygen content has risen by ∿30% in the case of the lower light intensity but by a factor of ∿300% for the higher intensity.

It is of interest to draw a comparison in terms of component functionality distribution and oxygen uptake for comparable total fluxes received for samples irradiated at the higher and lower lamp intensities and this is shown in Table 4.2

TABLE 4.2 Comparison of C_{1s} components and oxygen uptake for comparable total fluxes received by polycarbonate films irradiated at high and low photon fluxes

Lamp Intensity ($Whm^{-2}h^{-1}$)	Total C_{1s}	C-H	C-O	C=O	O-C=O	O-C(=O)-O	$\Pi\rightarrow\Pi^*$	O_{1s}/C_{1s}
52.5 (20 minutes)	100	51	22	7	17	2	1	0.85
5.7 (3 hours)	100	56	20	7	14	2	1	0.59

The distribution is remarkably similar, the main difference being in the level of carboxylate functionality and hence total oxygen signal. This is understandable in terms of transformations involving initially formed hydroperoxides as will become clear in the next section.

(b) Surface Hydroperoxide formation

It is not possible to directly interrogate the C_{1s} and O_{1s}

line profiles alone to delineate the importance of hydroperoxide (R-OOH) structural features. This can, however, be accomplished by selective chemical transformation to sulphate groups by direction with SO_2,[179] and this is schematically shown in Figure 4.11. With a knowledge of instrumentally dependent response factors and the distinctive binding energies for the sulphate group in the S_{2p} core level photoemission it is possible to monitor the level of hydroperoxide formation. Previous attempts at quantification of hydroperoxide structural features in Bisphenol A polycarbonate by use of this technique employing ir. spectroscopy have notably failed[178] and the success here is attributable to two main reasons:

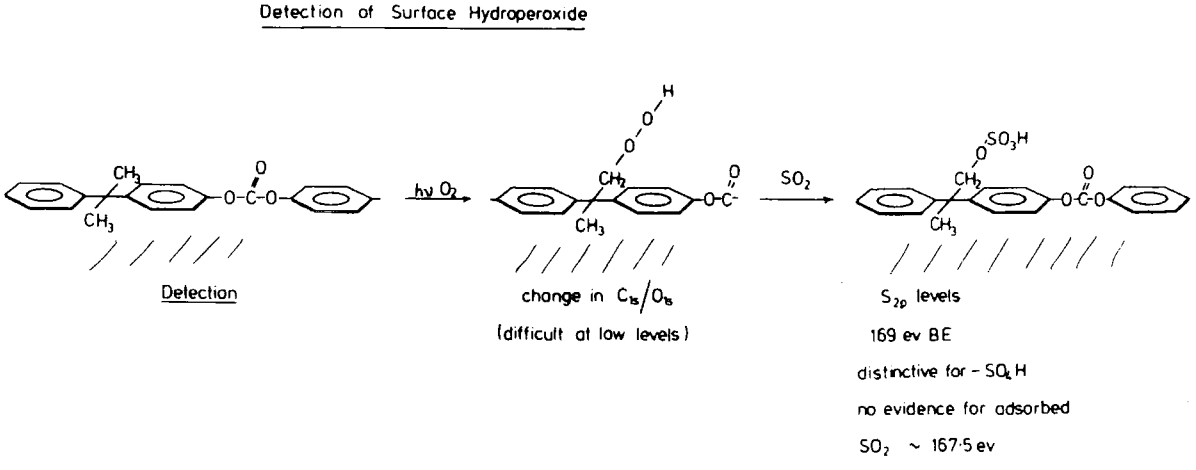

Figure 4.11 Scheme for the detection of surface hydroperoxides by conversion to sulphate groups.

(i) The inherent surface sensitivity of the ESCA technique.

(ii) The fact that the ESCA experiment involves studying samples under high vacuum conditions obviates any confusion which might arise from straightforward physisorption of SO_2. This has been independently checked by exposure of unoxidised polycarbonate films to the same treatment. This gives rise to a low level of functionalisation as is evident from the S_{2p} core level spectra in Figure 4.12 and the data in Figure 4.13.

The spectra in Figure 4.12 reveal two chemical environments centred at binding energies of ∿169·2 and 168.0 eV indicative of sulphate and sulphone groups. The presence of sulphone functionalities may at first appear to be surprising but, on consideration of the number of long lived radical sites likely to be present in the polymer after exposure to uv radiation, the uptake of SO_2 by these sites to form sulphones is not unfeasible. The technique is of necessity of a semi-quantitative nature since it takes no account of any dark reaction. This is the first time that hydroperoxide formation in the surfaces of polymers have been studied by ESCA and the technique, first applied to the study of polycarbonate photooxidation has been extended to polystyrene and polyphenylene oxide photooxidation (see Chapters Seven and Nine).

The direct monitoring of -O-O-H structural features by direct derivatization by reaction with SO_2 is very revealing and Figure 4.13 shows data for films exposed over given periods of time as a function of two different lamp intensities. Considering firstly the lower photon flux (Figure 14.3(a)) the

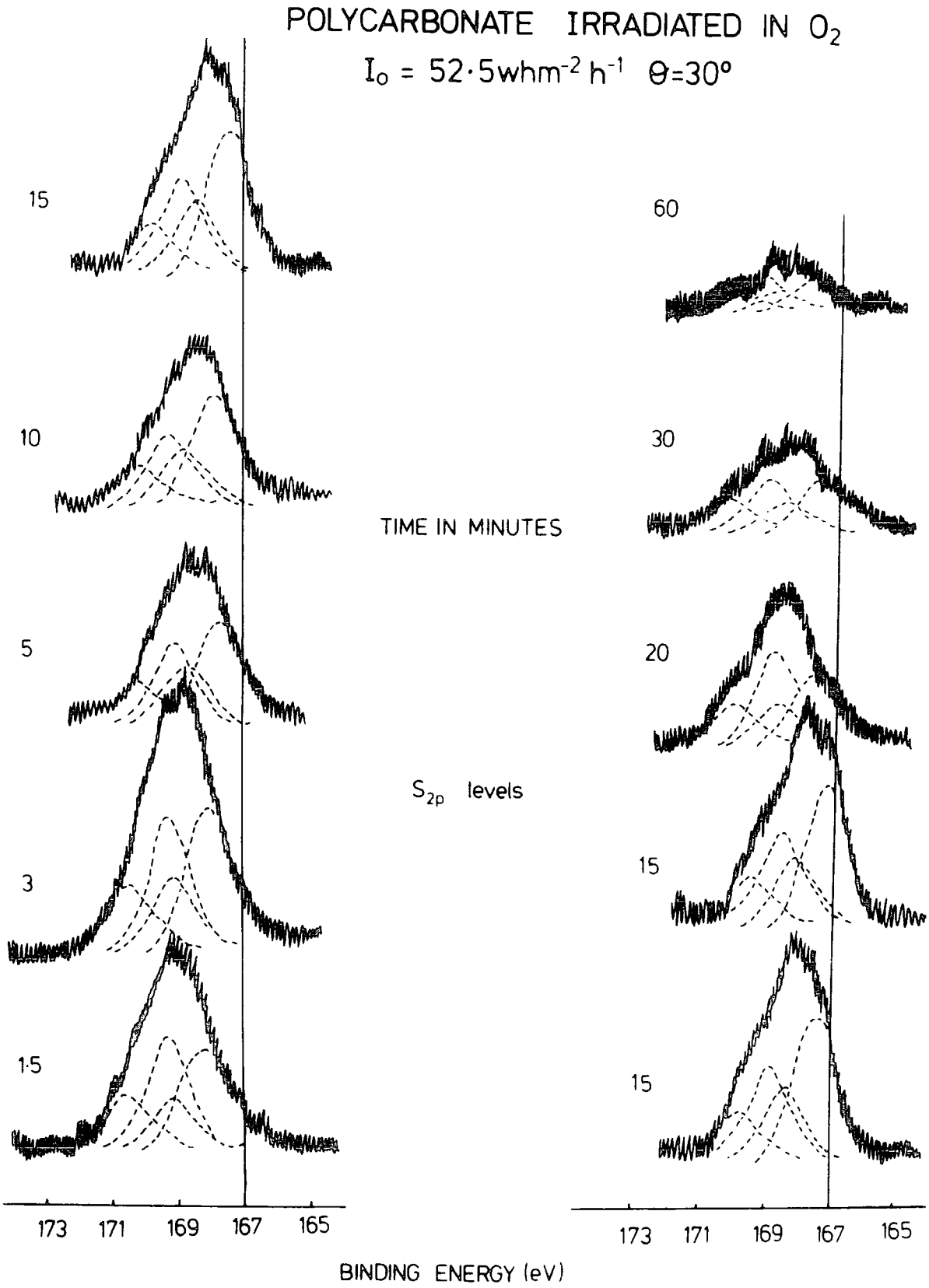

Figure 4.12 S_{2p} core levels for photooxidised polycarbonate films exposed to SO_2.

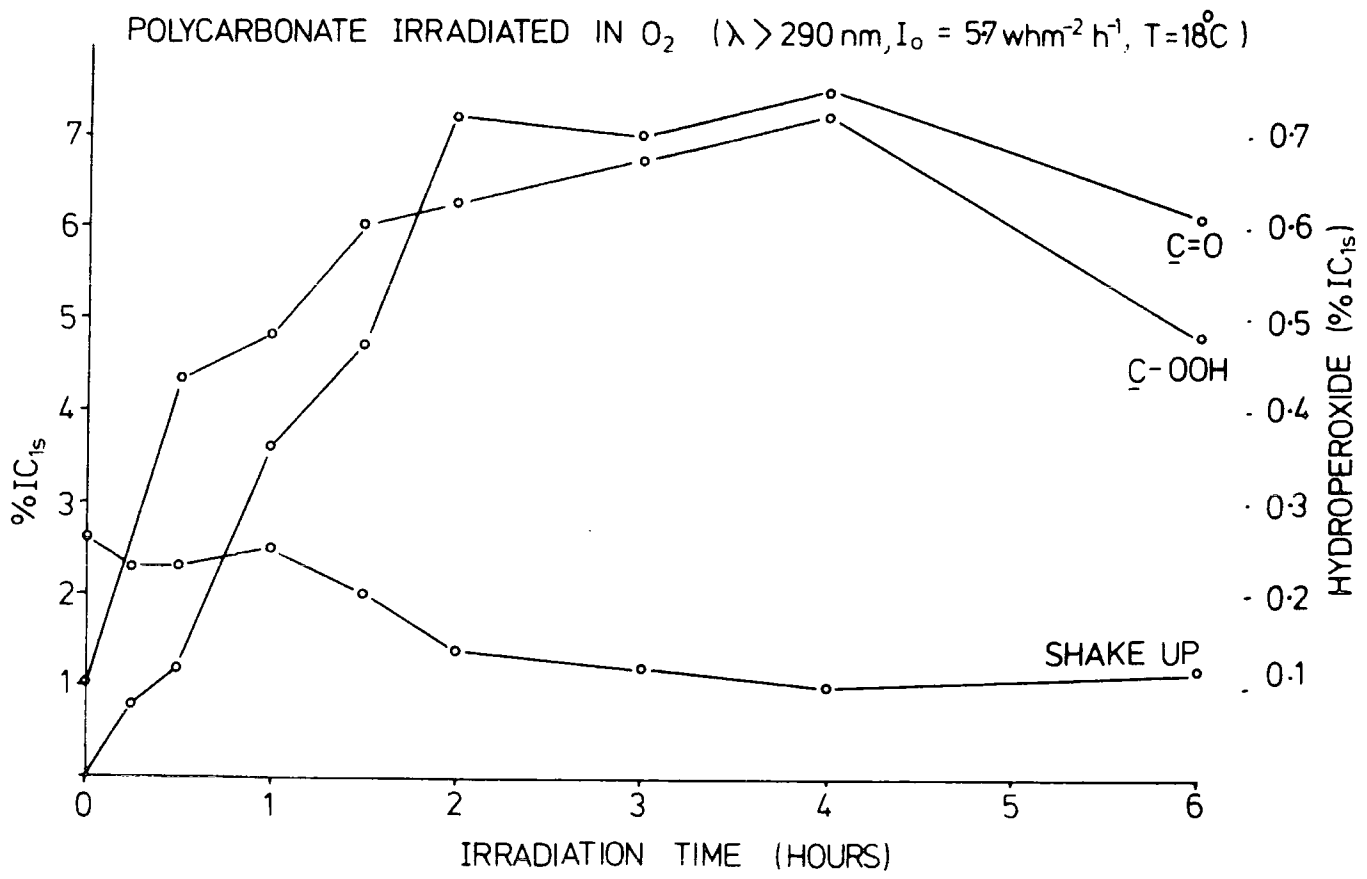

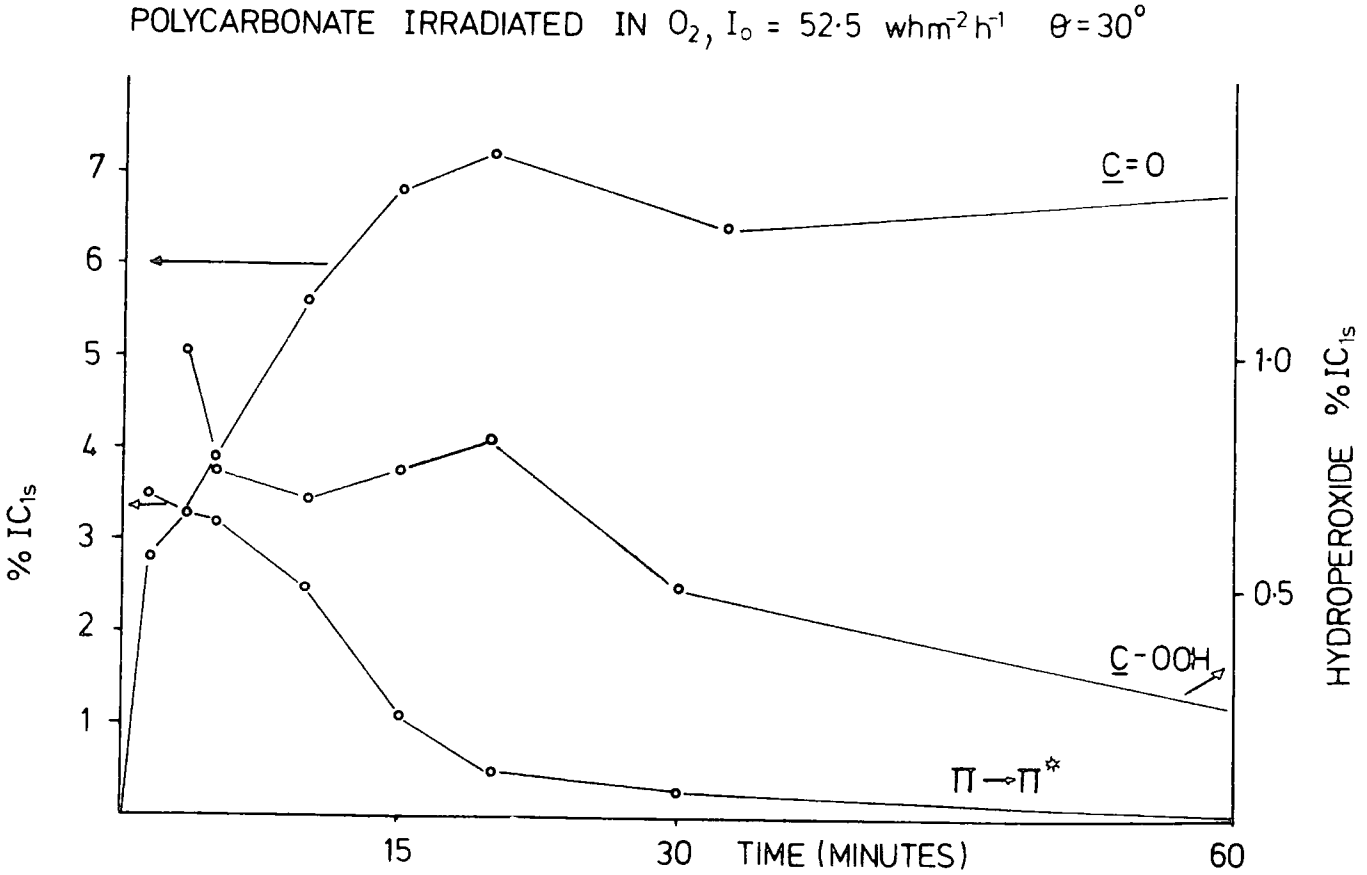

Figure 4.13 C=O, -COOH and Π→Π* shake-up components for polycarbonate samples irradiated in oxygen at photon fluxes (a) 5.7 Whm^{-2}h^{-1} (b) 52.5 Whm^{-2}h^{-1}

hydroperoxide is seen to build up to a maximum over a period of four hours and then declines. There is thus an induction period and the level of carbonyl structural features closely follows that for the hydroperoxide. The dramatic effect of increasing the photon flux is evident from a comparison of Figures 14.3(a) and (b). In this case the maximum in hydroperoxide concentration is obviously reached relatively early so that the induction period is not evident. The decrease in $\Pi \rightarrow \Pi^*$ shake-up is also clearly evident revealing that photo-oxidation also involves oxidation of the aromatic ring systems.

(c) Surface Chemistry as a function of Temperature

A distinctive feature of natural as opposed to model photo-degradation studies is the cyclic variation not only in photon flux impinging on the sample but also the temperature cycle. Therefore, preliminary studies of the change in surface chemistry for polycarbonate irradiated in an oxygen atmosphere as a function of temperature have been carried out.

Samples have been studied at three different temperatures (30^{o}, 50^{o} and 70^{o}C) for varying irradiation times with a photon flux of 52.5 $Whm^{-2}h^{-1}$ and the relevant data are displayed in Table 4.3. The percentage increase in O_{1s}/C_{1s} intensity ratio as a function temperature for a given dosage is surprisingly small, probably as a result of the balance between rate processes leading to oxidative functionalisation and desorption of low molecular weight materials from the surface. (It was previously noted in Section 4.3(a) that an equilibrium surface composition seems to be formed after a given irradiation time indicating an overall balance of this nature irrespective of temperature).

TABLE 4.3 Comparison of C_{1s} components and oxygen uptake for photooxidised polycarbonate films (Io = 52.5 $Whm^{-2}h^{-1}$) as functions of time and temperature.

Temperature (^{o}C)	Time (minutes)	C_{1s}	C-H	C-O	C=O	O-C=O	O ‖ O-C-O	$\Pi \rightarrow \Pi^*$	% O_{1s}/C_{1s} increase
30	5	1	0.65	0.20	0.04	0.05	0.03	0.03	74
	10	1	0.56	0.20	0.06	0.13	0.03	0.02	139
	20	1	0.51	0.22	0.07	0.17	0.02	0.01	188
50	5	1	0.61	0.17	0.05	0.12	0.03	0.02	136
	10	1	0.54	0.21	0.05	0.16	0.03	0.01	159
	20	1	0.48	0.20	0.08	0.20	0.03	0.005	240
70	5	1	0.59	0.20	0.04	0.12	0.03	0.02	135
	10	1	0.54	0.20	0.05	0.16	0.04	0.01	161
	20	1	0.52	0.20	0.05	0.20	0.025	0.005	226

The data in Table 4.3 reveals that the difference between the C_{1s} components for different temperatures as an indicator of functionality becomes smaller as the length of exposure to radiation increases. At low dosage, however, the main difference in going from 30° to 50° appears to be the increase in carboxylate functionalities produced (cf. data for 5 minutes' exposure). The data indicates much smaller differences between samples exposed at 50° and 70°C than between samples at 30° and 50°C. The C_{1s} components for samples exposed for 10 minutes at 30°C show a close similarity to those exposed at 70°C for 5 minutes, again indicating the relatively small apparent effect of temperature.

The extraneous infrared component in the lamp emission leads to a small rise in sample temperature for the higher lamp intensities. This amounts to equilibrium temperatures under the conditions of dynamic gas flow of 18°C and 30°C respectively for photon fluxes of 5.7 and 52.5 $Whm^{-2}h^{-1}$, ambient temperature being 17°C. The convolution of the small temperature dependence and the uv dosage effects are indicated in Figure 4.14 which reveals the large increase in oxidative functionalisation as a function of dosage for a fixed time period of exposure (15 minutes).

4.3.3 Reactions in Nitrogen

The investigations described above indicate that oxygen plays a crucial role in the surface photodegradation of Bisphenol A polycarbonate and as a comparison samples have been irradiated in a nitrogen atmosphere.

The C_{1s} and O_{1s} core level spectra for samples irradiated at an intermediate dosage ($\sim$30 $Whm^{-2}h^{-1}$) in a nitrogen

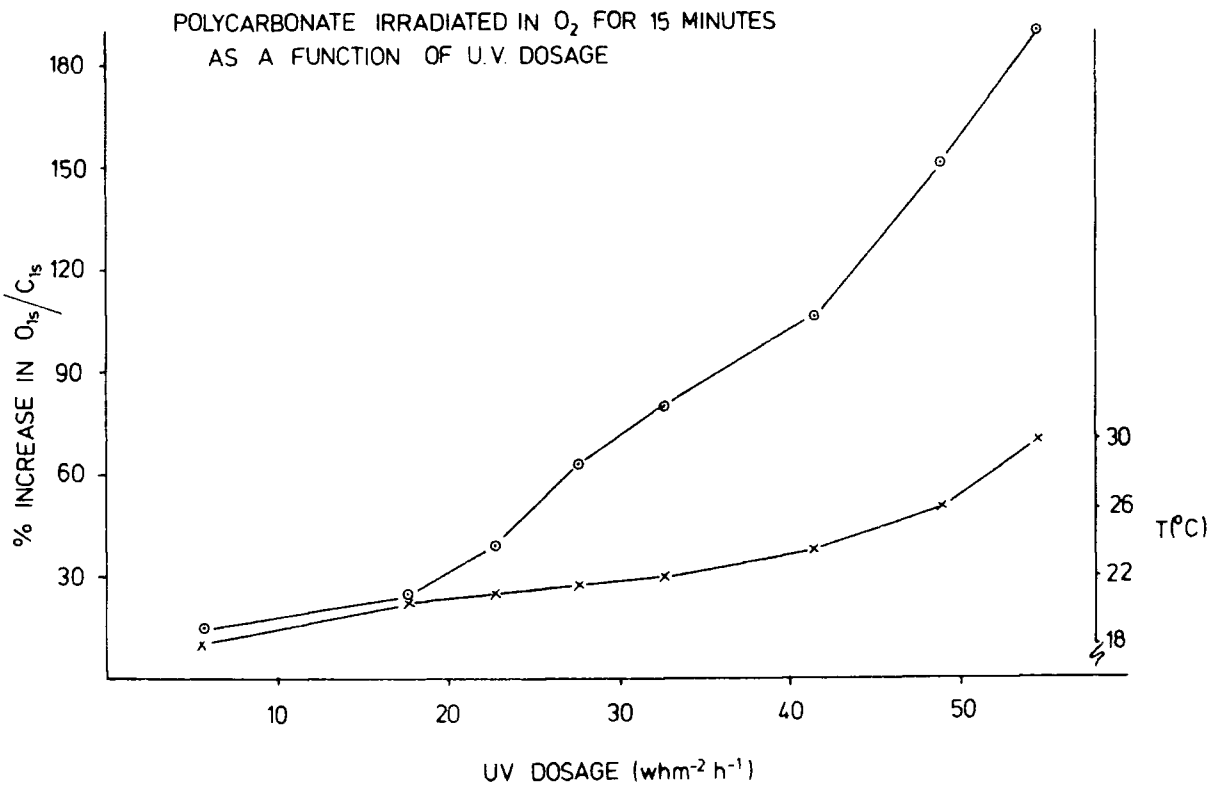

Figure 4.14 % increase in O_{1s}/C_{1s} intensity ratios for polycarbonate samples irradiated in oxygen as a function of uv dosage. (Also shown is the sample temperature as function of uv dosage).

atmosphere are displayed in Figure 4.15. Comparison with the core level spectra (Figure 4.5) for samples irradiated in oxygen at much lower levels of photon flux (5.7 Whm^{-2}h^{-1}) reveals the striking influence of the high partial pressure of oxygen at the polymer surface. It is clear from the data in Figure 4.15 that there is a low level of oxygen uptake for the sample irradiated in nitrogen and the component analysis in Figure 4.16 provides an immediate indication of the differences in oxidative functionalisation with respect to those samples irradiated in oxygen. The $\Pi \rightarrow \Pi^*$ shake-up satellite remains roughly constant showing that the aromatic residues remain intact.

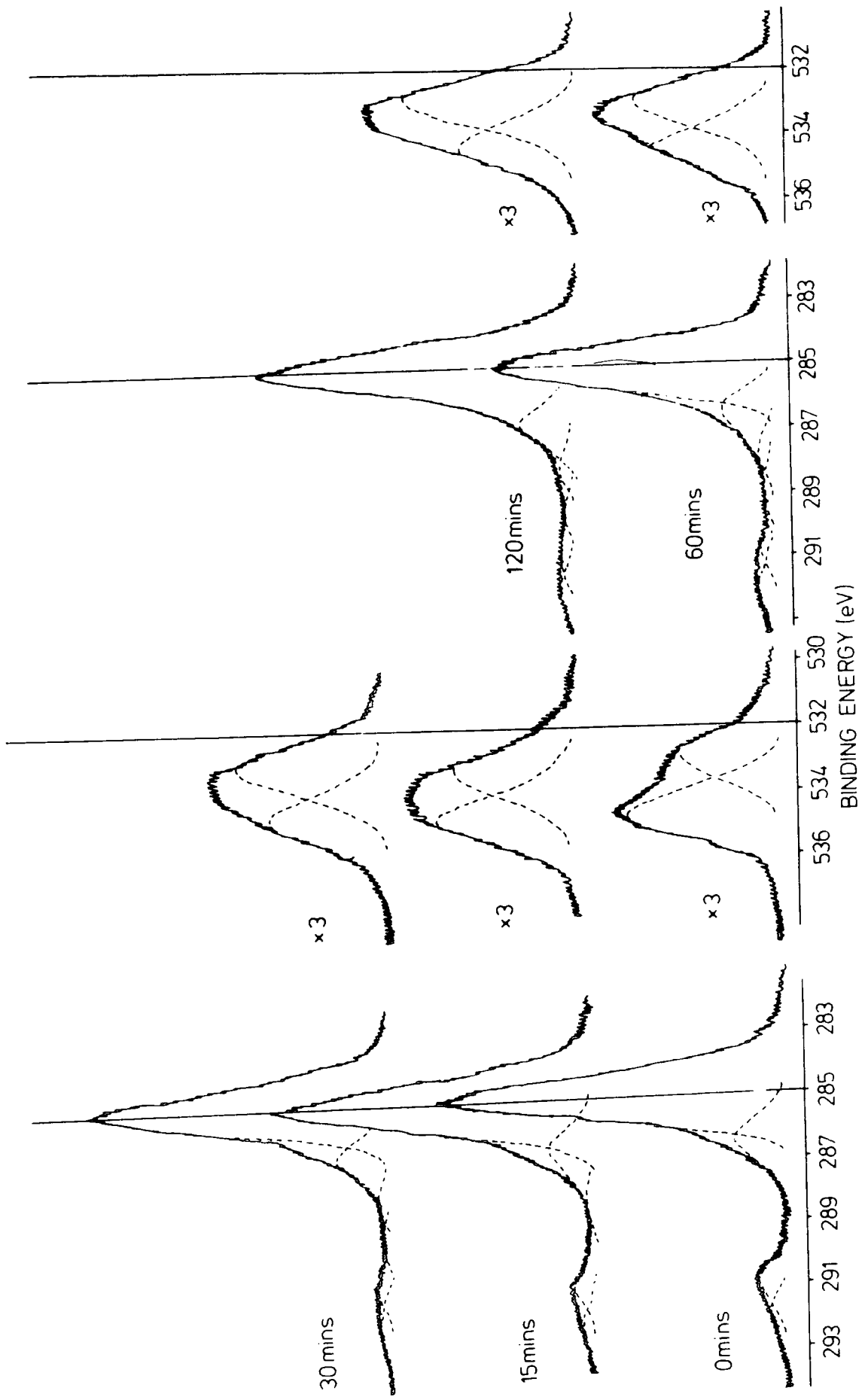

Figure 4.15. C_{1s} and O_{1s} levels ($Mg_{K\alpha 1,2}$) as a function of irradiation time for polycarbonate samples irradiated in nitrogen atmosphere.

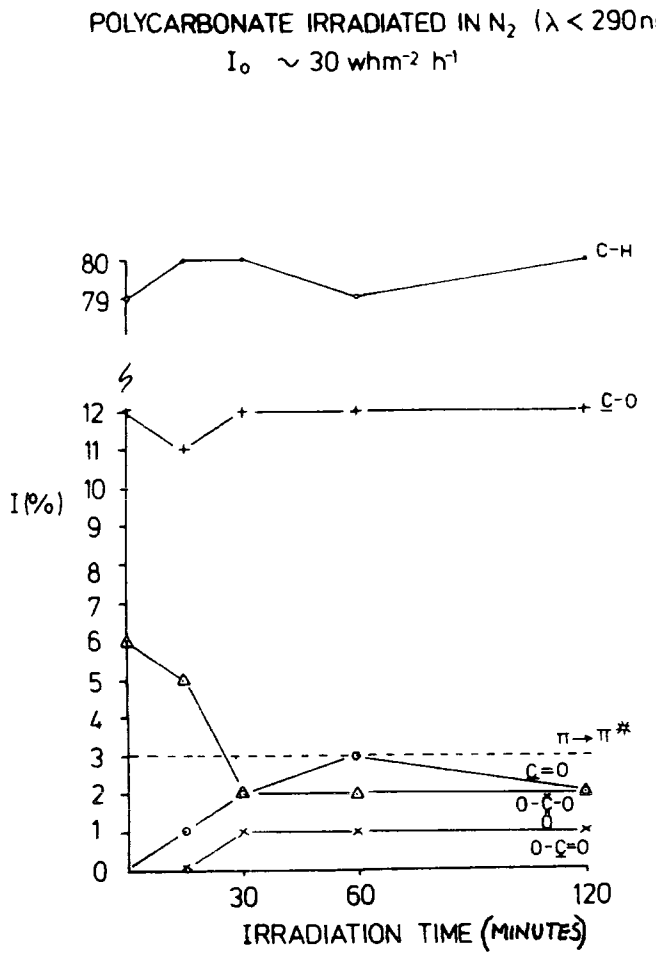

Figure 4.16 Components of the C_{1s} levels for polycarbonate irradiated in a nitrogen atmosphere.

The carbonate structural feature decreases whilst the carboxylate intensity increases and this is most readily accommodated by a photo-Fries rearrangement mechanism. There is a small contribution from >C=O structural features suggesting a low level of oxidation of the gem-dimethyl groups presumably arising from a low level of dissolved oxygen in the polymer film. This provides a solid state analogue of the solution phase photochemistry studies which have received so much attention in the literature,[160,161] and which also involves a photo-Fries rearrangement since the level of dissolved oxygen is also low. The low degree of oxygen uptake for the samples irradiated in nitrogen is also shown by comparison of the relative intensities

of the O_{1s} and C_{1s} levels and this is displayed in Figure 4.17. The level of oxygen incorporation for the samples irradiated in a nitrogen atmosphere is somewhat below that for samples irradiated at a much lower dosage in oxygen. This difference is highlighted by comparison of oxygen uptake at identical uv dosages for 15 minutes. The point to the top left hand corner of Figure 4.17 shows the oxygen uptake for a sample irradiated in oxygen. Whereas the sample irradiated in a nitrogen atmosphere shows little oxygen uptake that in oxygen shows ∿100% increase.

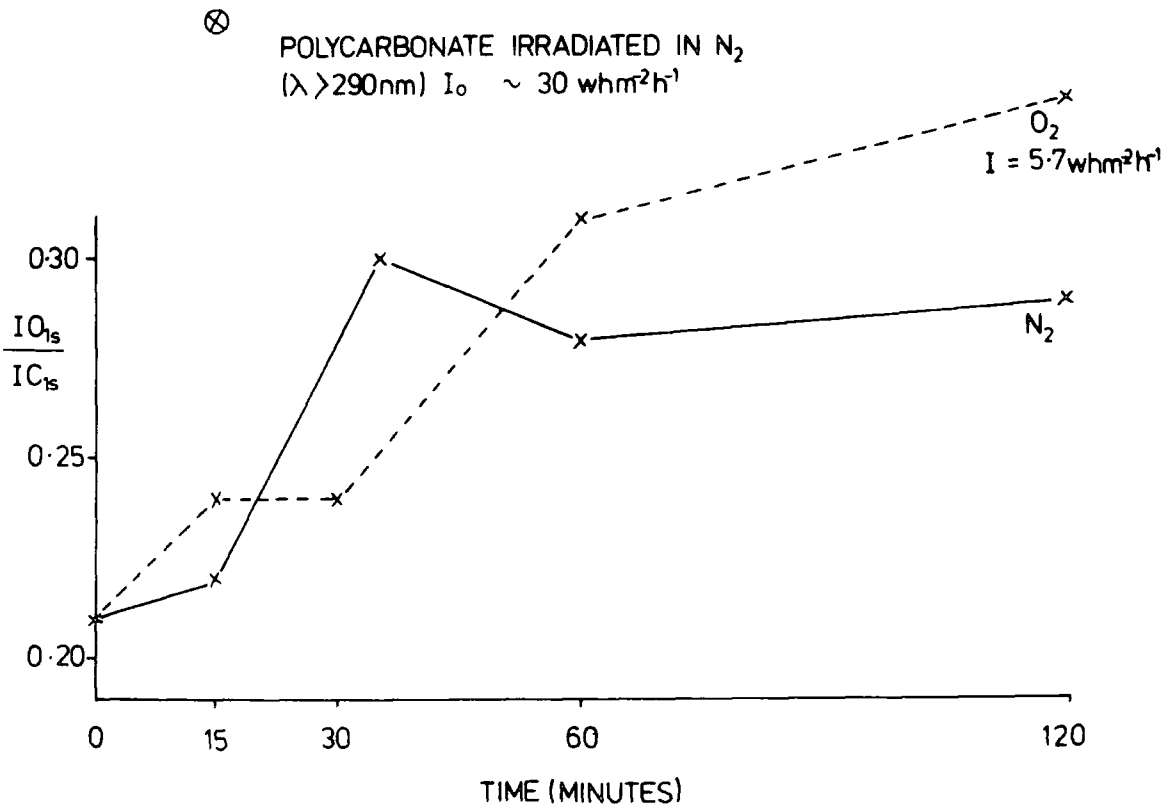

Figure 4.17 O_{1s}/C_{1s} intensity ratios as a function of irradiation time for polycarbonate in a nitrogen atmosphere, also shown are the corresponding ratios for irradiation in oxygen.

4.3.4 Conclusions

The striking differences in surface chemistry for samples irradiated in the presence or absence of oxygen reveals the important contribution provided by photooxidation in the photodegradation of Bisphenol A polycarbonate. The range of oxidative functionalities produced under the conditions employed in these studies and in particular the large oxygen uptake and loss of aromatic character are all consistent with a photodegradative pathway in which oxidations of both the gem-dimethyl groups and the aromatic ring systems are important. The role of the photo-Fries rearrangement is relatively small in the regions of the polymer close to the surface where the partial pressure of oxygen is high. The surface reactions may possibly be represented by the scheme in Figure 4.18. The mechanism by which aromatic ring oxidation takes place is still unknown. The possible involvement of singlet oxygen ($^1O_2$) in a ring opening reaction (as has been suggested by Ranby and Rabek for polystyrene)[206] is considered in detail in Chapter Six. However, these present studies provide strong confirmatory evidence for the scheme outlined by Factor and Chu[178] who by contrast studied the bulk phase after extended irradiation periods at elevated temperatures. The results presented in this chapter show that such reactions occur in the surface regions at ambient temperatures and at relatively low uv dosages.

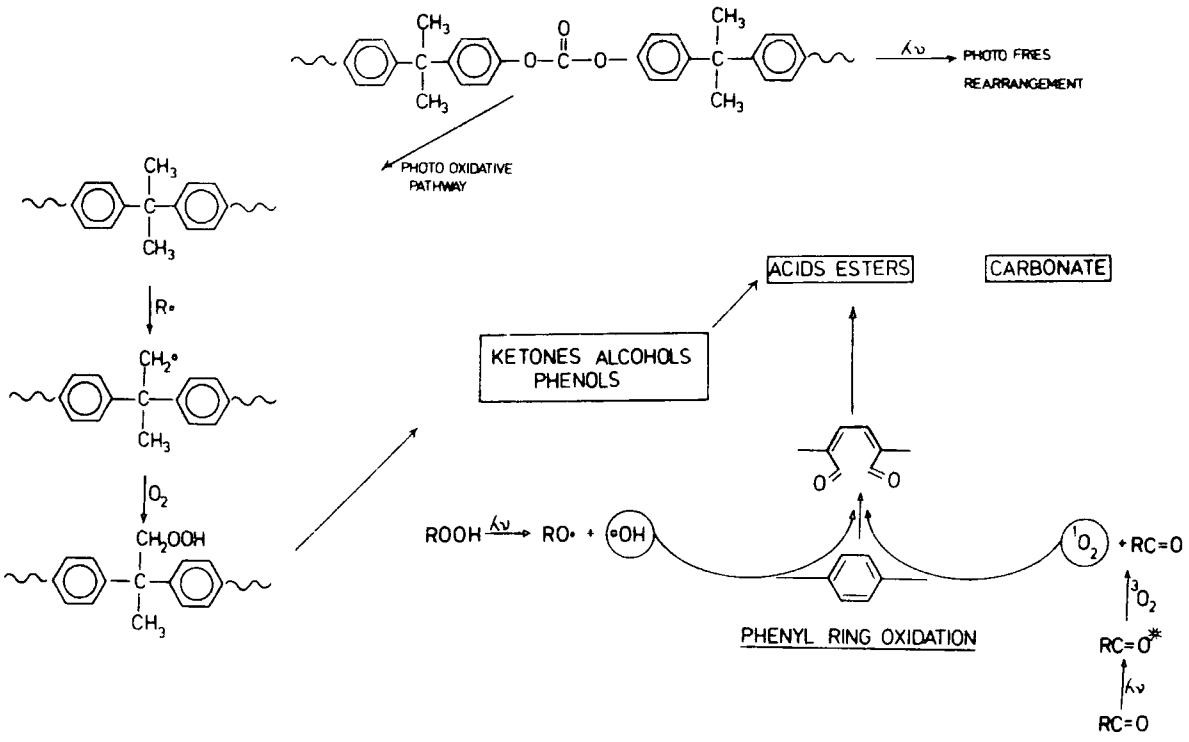

Figure 4.18 Schematic of the main photodegradative pathways for polycarbonate.

CHAPTER FIVE

THE PHOTOAGING OF BISPHENOL A POLYCARBONATE - PART III

SURFACE AND BULK ASPECTS OF THE NATURAL AND ARTIFICIAL PHOTODEGRADATION OF BISPHENOL A POLYCARBONATE AS REVEALED BY ESCA AND DIFFERENCE UV SPECTROSCOPY

5.1 Introduction

The investigations in Chapter Four revealed that oxidative pathways, as opposed to the main role in the photodegradation which had been previously assigned to photo-Fries rearrangements, are of primary importance in the uv induced degradation of Bisphenol A polycarbonate. These studies have shown that there are marked differences in surface chemistry dependent on the partial pressure of oxygen, however, the irradiations at wavelengths >290 nm have been confined to exposures in either pure nitrogen or oxygen environments.

As the exposure of polycarbonate to the natural environment is dependent in the most part on both the solar radiation and relative humidity, studies have been carried out to study the changes in surface chemistry of Bisphenol A polycarbonate films as a function inter alia of:

(i) Relative humidity for irradiations in air;

(ii) Partial pressure of oxygen, from a comparison of irradiations in oxygen, nitrogen and air;

(iii) Differences associated with static and dynamic gas flow.

In Chapter One the importance of natural weathering studies, to obtain real data on the stability of polymers in the natural environment, was discussed. 'Accelerated' or 'artificial' exposures are important in determining the mechanisms involved (fundamental and/or approximations of natural exposures) in the photodegradation of polymeric systems, however, care must be taken in the extrapolation of data in the prediction of natural weathering performance. Therefore samples have been exposed to natural weathering at sites of high uv intensity

and the data compared with that obtained from model studies.

5.2 Experimental

(a) Model Studies

To facilitate the study of the influence of relative humidity on the surface photooxidation (λ>290nm) of Bisphenol A polycarbonate, a graded seal pyrex window was attached to a pyrex dessicator (Figure 5.1). By placing silica gel (10% R.H.) or the requisite amount of distilled water (100% R.H.) in a petri dish as shown in Figure 5.1, the relative humidity inside the dessicator could be controlled. Polycarbonate films ($\sim$30μm) were then allowed to equilibriate for 1 hour before

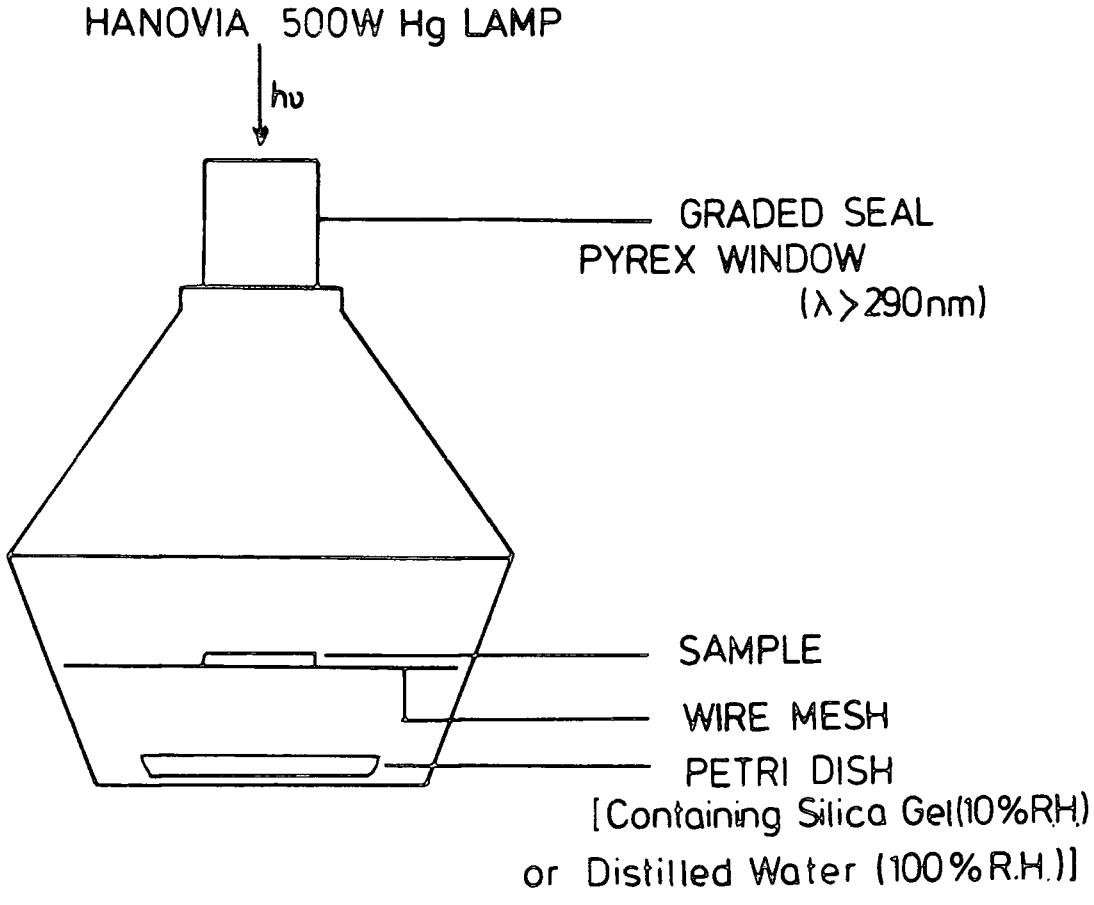

Figure 5.1 Schematic of reactor used for relative humidity studies.

exposure to the output of a 500W medium pressure Hg arc lamp for various periods of time. The incident photon flux was 20Whm^{-2}h^{-1}, measured as previously described in Chapter Four.

The conditions of the experiment pertain to a static air environment and for comparison samples were also exposed to static and dynamic oxygen and dynamic environments in the stainless steel reactor described in Chapter Four.

Polycarbonate films were also exposed to the output of a Philips 25W Black lamp (λmax ∿360nm) in air at ∿50% R.H. The photon flux at ∿20mm from the lamp was 0.24 Whm^{-2}h^{-1}.

It is not possible from the C_{1s} and O_{1s} profiles to directly delineate the formation of surface hydroxyl (C-OH) hydroperoxide and ether structural features which change the O_{1s}/C_{1s} intensity ratios in different manners. To facilitate the study of the formation of the former, it is possible to convert these groups to fluorinated esters by the direct reaction with trifluoracetic anhydride.[183] Irradiated samples were evacuated to ∿10^{-3} torr and then exposed to the vapour of trifluoroacetic anhydride for 15 minutes. Preliminary experiments on Phenoxy resin ∿(Ph-C(CH$_3$)$_2$-Ph-O-CH$_2$-CHOH-CH$_2$-O)$_n$ indicated that this exposure time is more than sufficient to label the C-OH groups completely at a depth of ∿50Å, (the approximate sampling depth of the ESCA experiment employing $Mg_{K\alpha}$ radiation). From a knowledge of the appropriate sensitivity factors the proportion of C-OH groups in the surface may be determined from the relative F_{1s}/C_{1s} intensity ratios. The labelling technique also produces distinctive CF_3 components in the C_{1s} envelope which provide a reference for the F_{1s}/C_{1s} ratio.

(b) Natural Weathering

In order to obtain data on the natural weathering of polymers, sites of exposure best suited to this purpose should have a high uv intensity and/or relative humidity. Polycarbonate samples were therefore exposed at three different locations.

For extended periods of exposure (6, 12 and 24 months), samples, kindly supplied by Dr. A. Davis (PERME, Waltham Abbey), were taken from two locations in Australia at a 45^{o} plane facing the equator. The sites, Joint Tropical Research Unit (JTRU), Innisfail, Queensland and JTRU, Cloncurry, Queensland correspond to Hot/Wet and Hot/Dry environments.

For information pertaining to the initial stages of degradation, polycarbonate films were exposed, by courtesy of Dr. J. Peeling, during May and June 1981, in a horizontal configuration 12 feet above the ground, in Dhahran, Saudi Arabia. As this location is situated on the Gulf Coast the relative humidity tends to be high.

Difference uv/visible spectra were recorded on a Unicam SP800 uv/visible spectrometer using unexposed polycarbonate film as the reference. A null difference was obtained for unexposed films recorded against the reference.

ESCA spectra were obtained on an AEI ES200B spectrometer employing $Mg_{K\alpha 1,2}$ radiation. It is interesting to note that for samples (unexposed and exposed) taken from 100% R.H. showed no evidence in the core level analysis for physi-sorbed water, although these samples took longer to pump down to better than 10^{-2} torr in the insertion lock of the spectrometer than those from 10% R.H. Integration of spectra was accomplished on a

Dupont 310 curve resolver. The $Au_{4f_{7/2}}$ level used for calibration purposes had a fwhm of 1.15eV. Binding energies were referenced to the C-H level at 285.0eV. Spectra were recorded at an electron take-off angle of 30^{o} corresponding to a sampling depth of $\sim 45\text{Å}$.

5.3 Results and Discussion

5.3.1 Introduction

The main emphasis of the work described in this chapter has been to investigate the photodegradation ($\lambda > 290$nm) of Bisphenol A polycarbonate in model studies, as functions of relative humidity, partial pressure of oxygen and gas flow, and natural weathering. In discussing these results it is convenient to consider the model studies first and then to compare these data and those obtained in Chapter Four with the effects of natural weathering.

5.3.2 Difference uv spectra

One of the most frequently employed techniques for monitoring changes in the bulk or solution phase chemistry of Bisphenol A polycarbonate has been uv-visible spectroscopy.[159-161, 178, 184, 185] As a preliminary, therefore, to the detailed investigation of surface chemistry as a function of reaction conditions, uv-visible difference spectroscopy has been employed to interrogate the changes occurring for irradiation of polycarbonate films under the following conditions, the uv flux and irradiation time being constant (20 $Whm^{-2}h^{-1}$ and 30 minutes respectively):

(i) Irradiation in air 10% R.H.

(ii) Irradiation in air 100% R.H.

(iii) Irradiation in nitrogen.

(iv) Irradiation in oxygen.

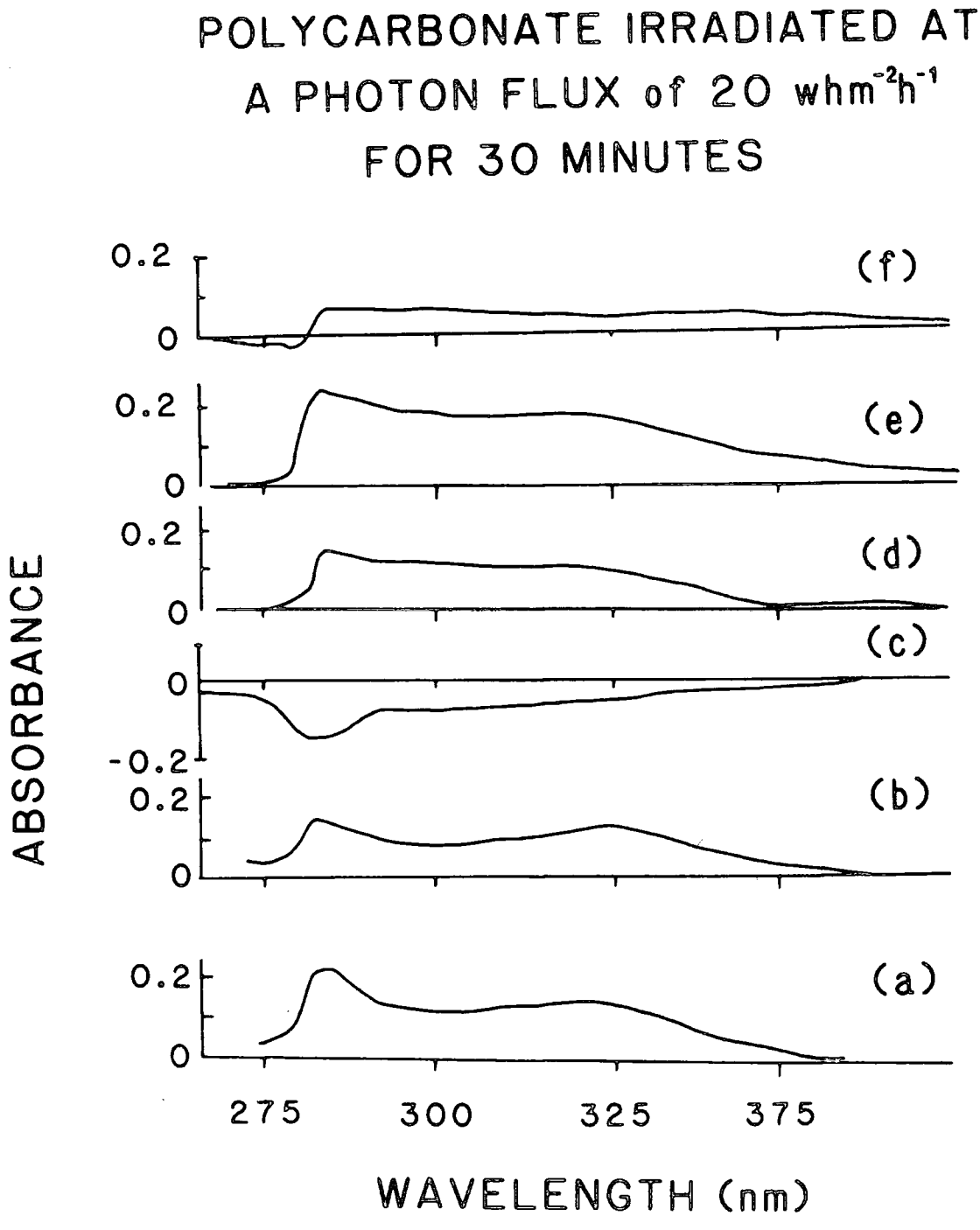

Figure 5.2 Difference uv spectra for polycarbonate samples irradiated (Io = 20 $Whm^{-2}h^{-1}$, λ>290nm) in various atmospheres for 30 minutes. (a) 10% R.H., (b) 100% R.H., (c) b-a, (d) N_2, (e) O_2, (f) e-d.

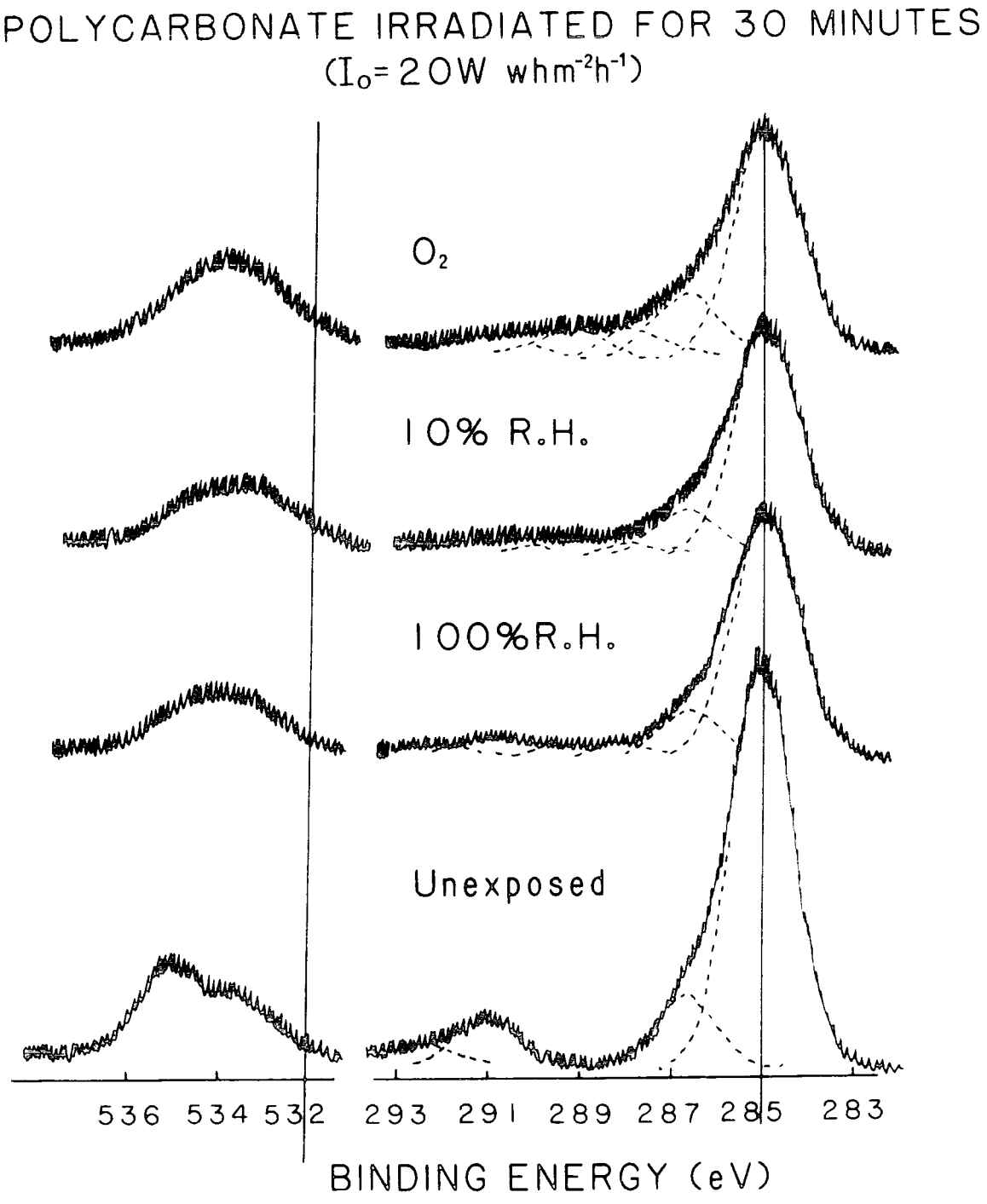

Figure 5.3 C_{1s} and O_{1s} core levels for unexposed polycarbonate and after 30 minutes' irradiation (Io = 20 Whm^{-2}h^{-1}) in various atmospheres.

The relevant spectra are displayed in Figure 5.2 and the corresponding ESCA spectra in Figure 5.3. (Directly recorded uv-visible spectra for the 30μm polycarbonate films in the region 275-400nm were essentially the same as those previously reported in the literature).[159,160,185]

The spectra for samples irradiated in air at different relative humidities show that water vapour has a substantial effect on the reaction and this is most clearly evident from the difference spectrum, Figure 5.2(c), between the samples irradiated in air at 10% and 100% R.H. The difference uv spectra of the samples irradiated in either an oxygen or nitrogen atmosphere, Figure 5.2(d) and (e) compared with the unirradiated material show the considerable increase in absorption coefficients in the region ∿280-400nm and the direct difference spectrum (e-d) reveals the significant effect of the interface environment. Comparison of the irradiation in air at 10% R.H. with irradiation in oxygen suggests a greater change for the latter. The difference uv spectra, therefore, reveal the importance of the interface in the overall photodegradation under differing conditions. In the absence of specific additional information it is difficult, on the basis of the uv data alone, to speculate on the exact nature of the chemical transformations responsible. However, the core level spectra reveal the substantial differences in oxidative functionalisation, at least in the surface regions for the samples irradiated under different conditions.

5.3.3 Comparison of Static versus Dynamic Reaction conditions

As a starting point in the investigation of the surface photodegradation of polycarbonate, under the various

conditions outlined in Section 5.3.2, it is convenient to consider the differences in surface chemistry on irradiation in static and dynamic oxygen atmospheres for the same photon flux and time. The data in Table 5.1 indicates that the reactions are similar, however, the dynamic flow seems to involve slightly greater oxidative functionalisation and hence a larger O_{1s}/C_{1s} intensity ratio. These results are indicative of photooxidation being the major degradative pathway as opposed to a photo-Fries rearrangement and agree with those previously discussed in Chapter Four.

TABLE 5.1 Comparison of C_{1s} components and O_{1s}/C_{1s} levels for polycarbonate films irradiated for 30 minutes in static and dynamic O_2 environments.

	Total C_{1s}	C-h	C-O	C=O	O-C=O	O-$\overset{O}{\overset{\|}{C}}$-O	$\Pi \rightarrow \Pi^*$	O_{1s}/C_{1s}
Static	100	70	15	3.5	6	3.5	2	0.39
Dynamic	100	65	17	6	7	3	2	0.45

5.3.4 Comparison of changes in surface chemistry as a function of conditions at constant photon flux

Examination of the results for polycarbonate irradiated at 20 $Whm^{-2}h^{-1}$ for 30 minutes in oxygen (dynamic and static) and air (10 and 100% R.H.) atmospheres show that the increase in oxidative functionalisation is greatest for irradiations in pure oxygen: the level of oxidation being highest, as already noted above, in the flow system. It is interesting to compare the components of the C_{1s} spectra as a function of irradiation conditions and this is shown in Table 5.2 where the reference is taken as the least oxidatively functionalised system, namely that involving irradiation in air at 100% R.H. The interesting

TABLE 5.2 Comparison of C_{1s} component intensities for polycarbonate films irradiated under various atmospheres taking those for 100% as the reference.
After 30 minutes' exposure, Io = 20 $Whm^{-2}h^{-1}$

	100% R.H.	10% R.H.	Static O_2	Dynamic O_2
$\frac{C-H}{C-H(100\%\ R.H.)}$	1	1	1	0.9
$\frac{C-O}{C-O(100\%\ R.H.)}$	1	1	1	1.1
$\frac{C=O}{C=O(100\%\ R.H.)}$	1	1.7	1.3	3
$\frac{O-C=O}{O-C=O(100\%\ R.H.)}$	1	1.6	2.3	2.5
$\frac{CO_3}{CO_3(100\%\ R.H.)}$	1	0.9	0.6	0.6
$\frac{\Pi\rightarrow\Pi^*}{\Pi\rightarrow\Pi^*(100\%\ R.H.)}$	1	0.9	0.6	0.5
O_{1s}/C_{1s} (initial, 0.26)	0.28	0.36	0.39	0.45

feature to emerge from this is that the C-H (aromatic ring system and gem dimethyl group) remains as a constant proportion of the total spectrum virtually independent of the relative humidity. The main changes occur in the C=O and O-C=O regions. Thus irradiations in a pure oxygen atmosphere give rise to increased levels of highly oxidised carboxylate structural features. Physi or chemi-sorption of water does not, therefore, give rise to artefacts in the ESCA spectra since otherwise the O_{1s}/C_{1s} ratios would be in an inverted order to those displayed in Table 5.2.

5.3.5 Reactions as a function of irradiation time

Relative humidity appears to have a dramatic effect not only on the overall distirubtion of functionalities but also on their relative rates of appearance and decay. The C_{1s} components for irradiations in air (100 and 10% R.H.) and oxygen (static) are displayed in Figure 5.4 as functions of irradiation time.

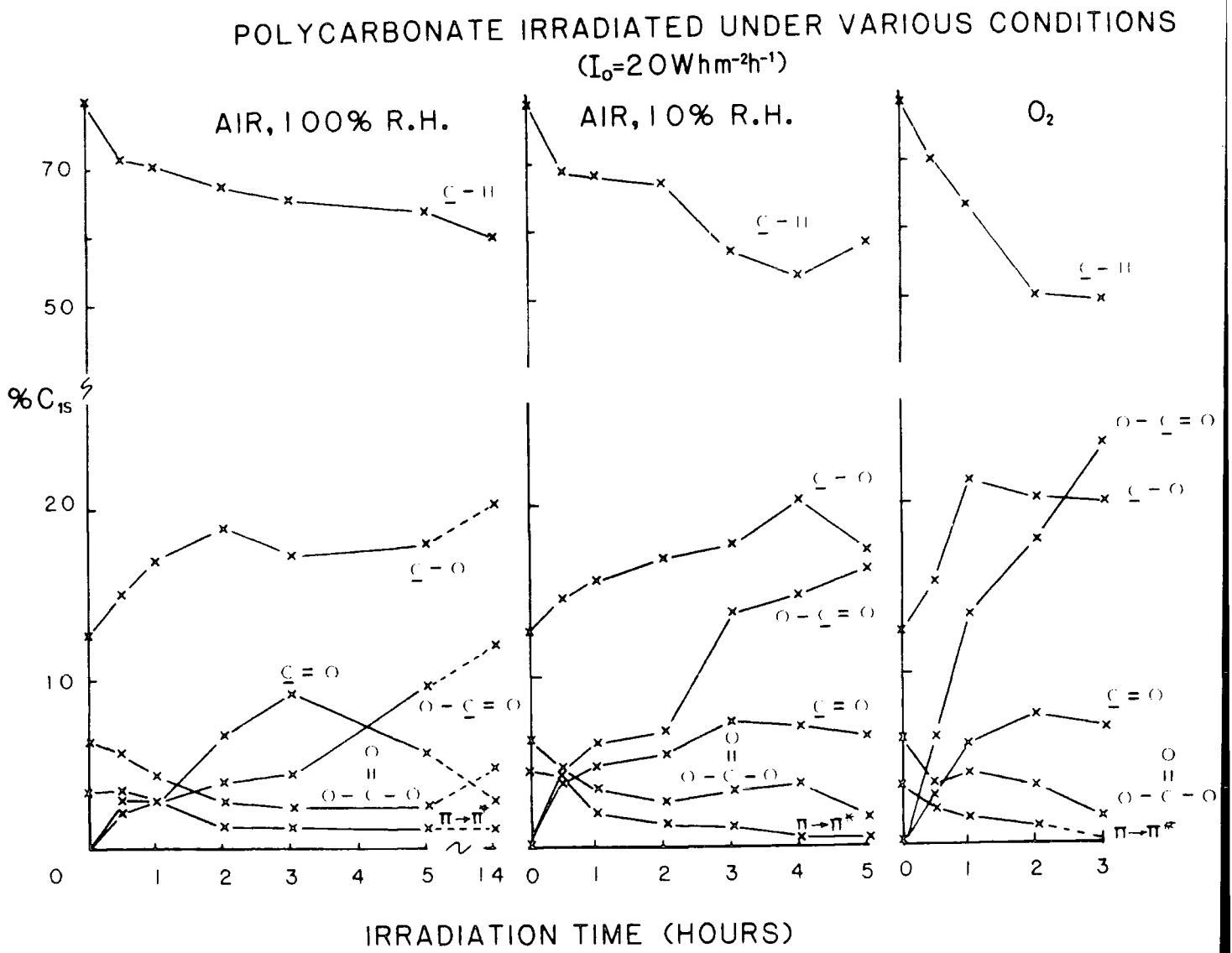

Figure 5.4 C_{1s} components for polycarbonate irradiated (I_o = Whm^{-2}h^{-1}) in various atmospheres as a function of time.

It is clear from these data that the initial rate of formation of carbonyl groups is greater than that for carboxylate during

irradiation at 100% R.H. The reverse trend exists for 10% R.H. and pure oxygen environments and reflects the influence of the partial pressures of both water and oxygen on the photooxidation process.

Superposition of Figures 5.4(a) and (b) indicate that a similar distribution of functional groups is obtained at 100% R.H. after ∿4 hours' exposure to those at 10% R.H. after ∿2 hours. The intermediate behaviour at 10% R.H. with respect to exposure in air at 100% R.H. and exposure in oxygen is evident from the comparison of Figures 5.4(a), (b) and (c). For irradiation in oxygen, the carboxylate structural feature for an extended period of exposure (>2.5 hours) is more predominant than carbonyl whilst for exposure to air at 100% R.H. the reverse is true.

The overall effect of changes in partial pressures of both oxygen and water on the level of oxygen uptake in the surface photodegradation of polycarbonate is clearly evidenced from the data in Figure 5.5 which shows the integrated O_{1s}/C_{1s} intensity ratios as a function of irradiation time under the various conditions. The initial oxygen uptake is highest for irradiation in oxygen and the maximum level of oxidative functionalisation in that case is reached (under the conditions of the experiment with a photon flux of 20 $Whm^{-2}h^{-1}$) after ∿1 hour. The corresponding build up for samples irradiated in air at R.H.'s of 10% and 100% is much slower.

Overall, the influence of both the partial pressures of oxygen and water on the photodegradation of polycarbonate may be observed from the bulk and surface viewpoints by means of difference uv and ESCA respectively. At high partial pressures

of oxygen and low relative humidity the main oxidative functionality to be formed during the early stages of exposure is the carboxylate structural feature. The results also reveal, as previously shown in Chapter Four, that photo-oxidation involves both the aromatic ring systems and the gem dimethyl groups.

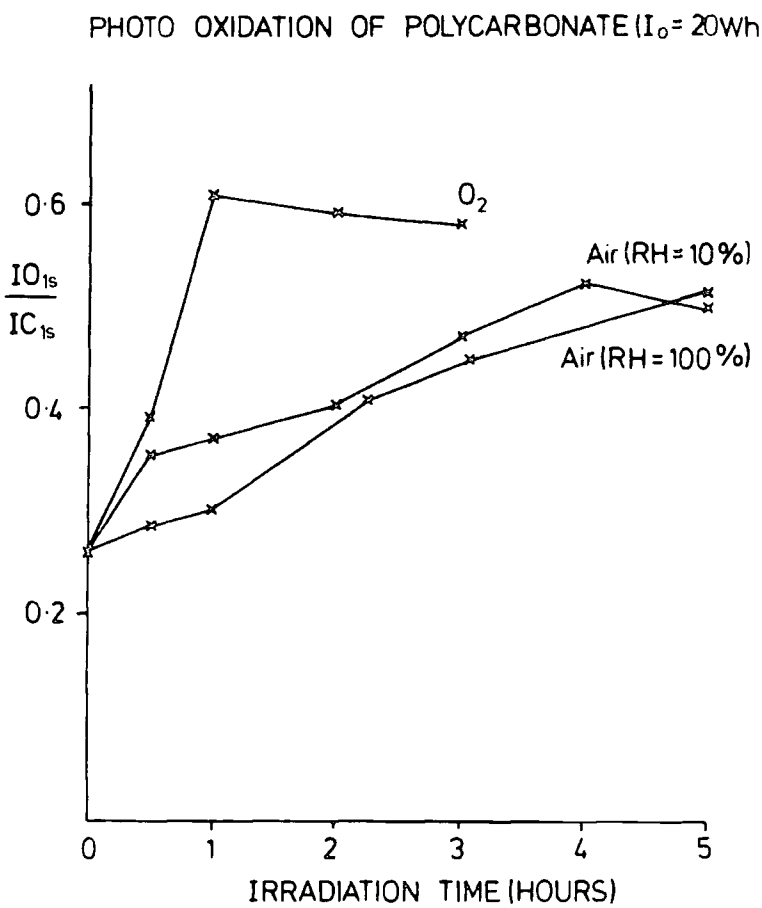

Figure 5.5 O_{1s}/C_{1s} levels as functions of irradiation time for polycarbonate films exposed to various atmospheres

5.3.6 Surface Hydroxyl group formation

The formation of phenolic structural features have been recently considered to be a major product in the natural

weathering of Bisphenol A polycarbonate.[184] Unfortunately the -OH functional group cannot be directly delineated in the surface from the C_{1s} and O_{1s} profiles. The binding energy for C-OH features in the C_{1s} core level at ∿286.6eV is also characteristic for all carbon atoms singly bonded to oxygen (e.g. ethers, hydroperoxides and esters). However, Hammond *et al*[183] have shown that these groups may be successfully studied by ESCA by the direct reaction with trifluoroacetic anhydride (TFAA) to form a fluorinated ester:

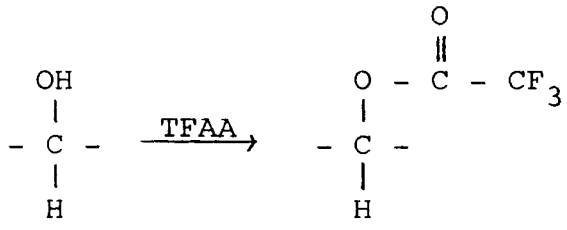

This reaction produces carboxylate and distinctive CF_3 features in the C_{1s} spectrum and with the uptake of 3 fluorine atoms for every C-OH group, relatively low levels of the latter may be readily detected by examination of the F_{1s} core level.

Since the recognition of this technique for examining hydroxyl features in the surfaces of model polymer systems, it has not been applied to the study of surface C-OH group formation during the oxidative degradation of polymers (e.g. photooxidation).

The ESCA spectra in Figure 5.6 reveal the C_{1s}, O_{1s} and F_{1s} core levels for unirradiated polycarbonate exposed to the vapour pressure of TFAA at 20°C for 15 minutes and after irradiation in air (10% R.H.) at a photon flux of 20 $Whm^{-2}h^{-1}$ for various periods of time. A low level of fluorine uptake is observed from the F_{1s} core level for the unirradiated material resulting in a small contribution to the C_{1s} envelope

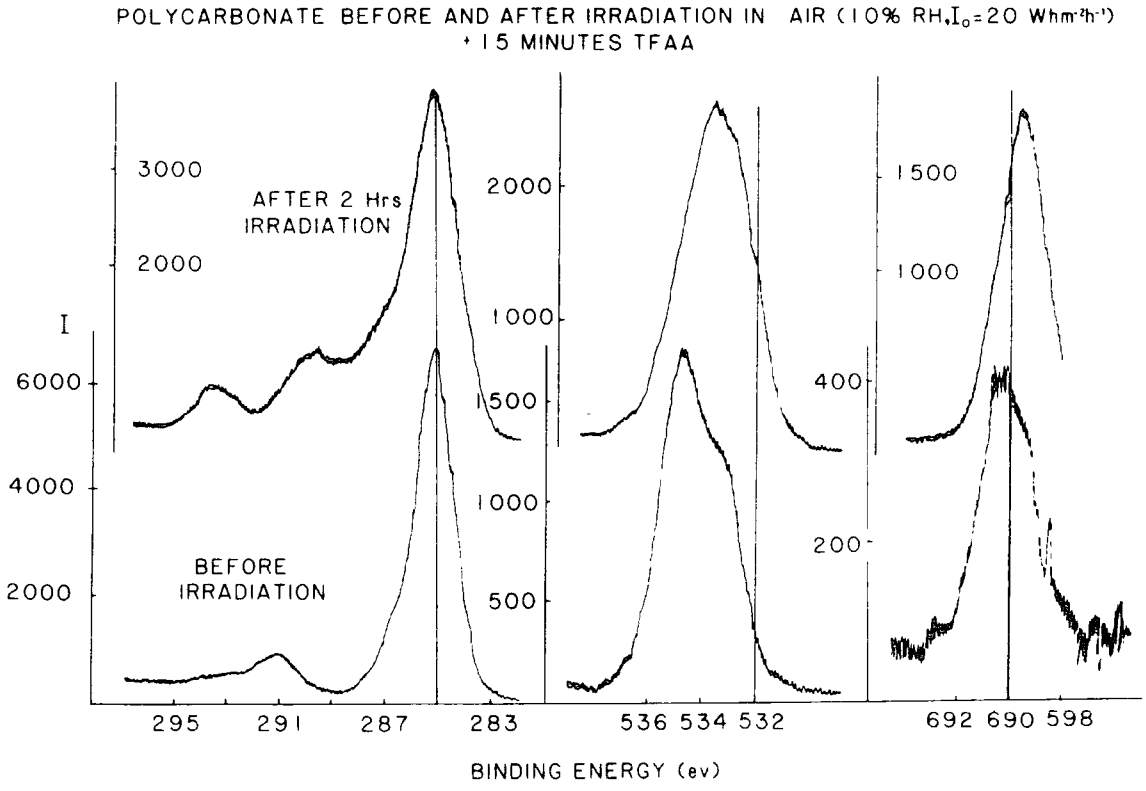

Figure 5.6 C_{1s}, O_{1s} and F_{1s} levels for polycarbonate and photooxidised polycarbonate films exposed to trifluoroacetic anhydride vapour for 15 minutes

arising from $\underline{C}F_3$ groups at ∿293.2 eV. From a knowledge of instrumentally dependent sensitivity factors the F_{1s}/C_{1s} intensity ratio corresponds to ∿1% $\underline{C}$-OH features in the surface. This is in good agreement with the intensity of the $\underline{C}F_3$ functionality. This low level of hydroxyl functionalisation in the unirradiated polycarbonate may be readily accounted for by phenol end groups in the polymer.

On exposure to uv irradiation (λ>290nm) followed by treatment with TFAA the intensity of the fluorine signal increases with concomitant increases in the complexity of the C_{1s} envelope indicative of a higher level of hydroxyl groups in the surface. The data in Figure 5.7 reveal the fluorine uptake as a function of irradiation time and for comparison the growth of the $\underline{C}$-O peak for the untreated irradiated material is also included. It is clear from this data that fluorine is smoothly incorporated into the surface with increasing irradiation time. The rate of uptake is greatest initially and after ∿3 hours the level of fluorine in the surface corresponds to a $\underline{C}$-OH functionalisation of ∿6%.

From the results discussed above it is clear that treatment of irradiated polycarbonate with TFAA enables surface hydroxyl group formation during photooxidation to be followed. It should be noted, however, that it is not possible to determine specifically the role of phenolic species in the degradative process.

5.3.7 Comparison of the difference uv spectra obtained for natural and artificial weathering

The natural and artificial weathering of Bisphenol A polycarbonate has been recently considered by Moore[184]

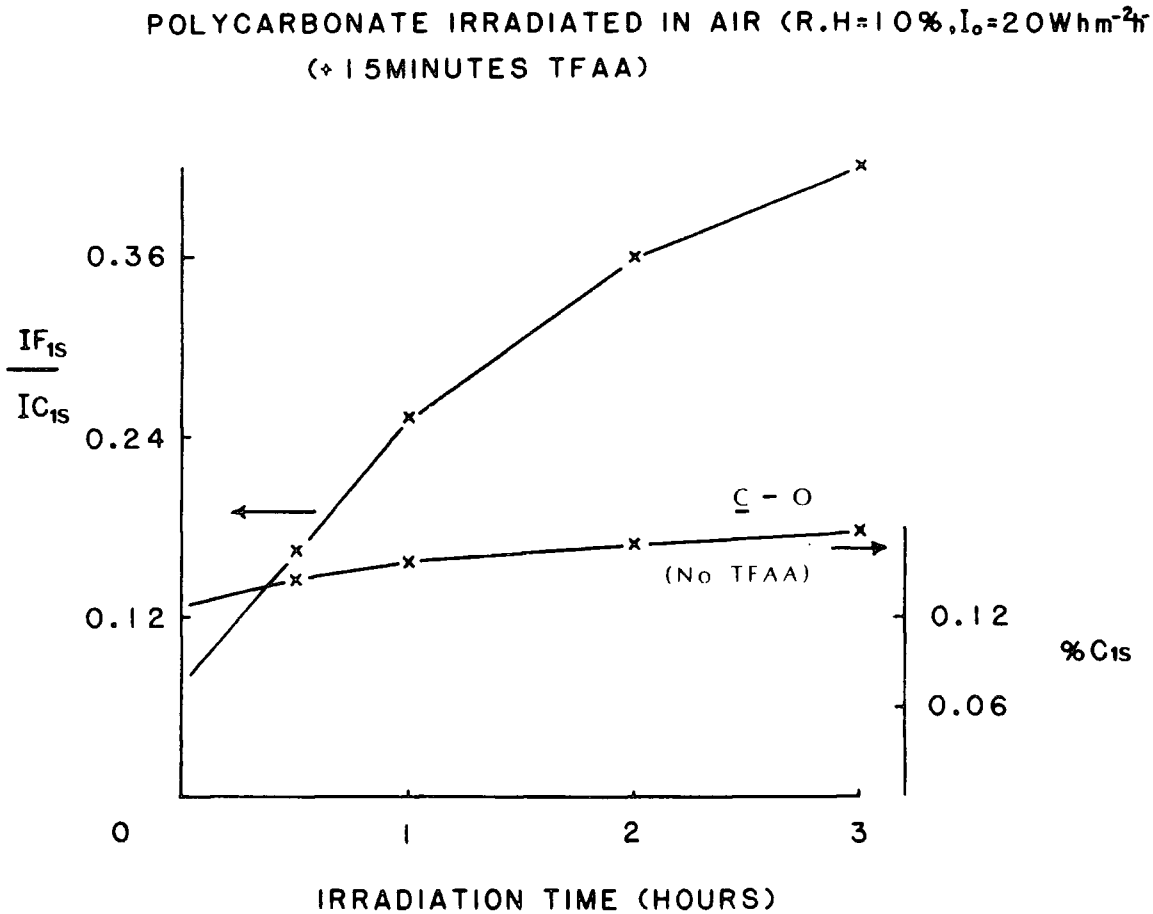

Figure 5.7 F_{1s}/C_{1s} intensity ratios for photooxidised polycarbonate films exposed to TFAA vapour. (Also shown are the C-O intensities for the untreated samples).

employing difference uv spectroscopy. Examination of the data presented suggests that different mechanisms are involved depending on the nature of the exposure, i.e. natural or artificial. It is, therefore, worthwhile to consider in some detail the aspects of natural and artificial weathering as studied by difference uv spectroscopy before examining and comparing the respective surface chemistries as revealed by ESCA.

The data in Figure 5.8 reveal the difference uv spectra obtained for polycarbonate films irradiated in oxygen at

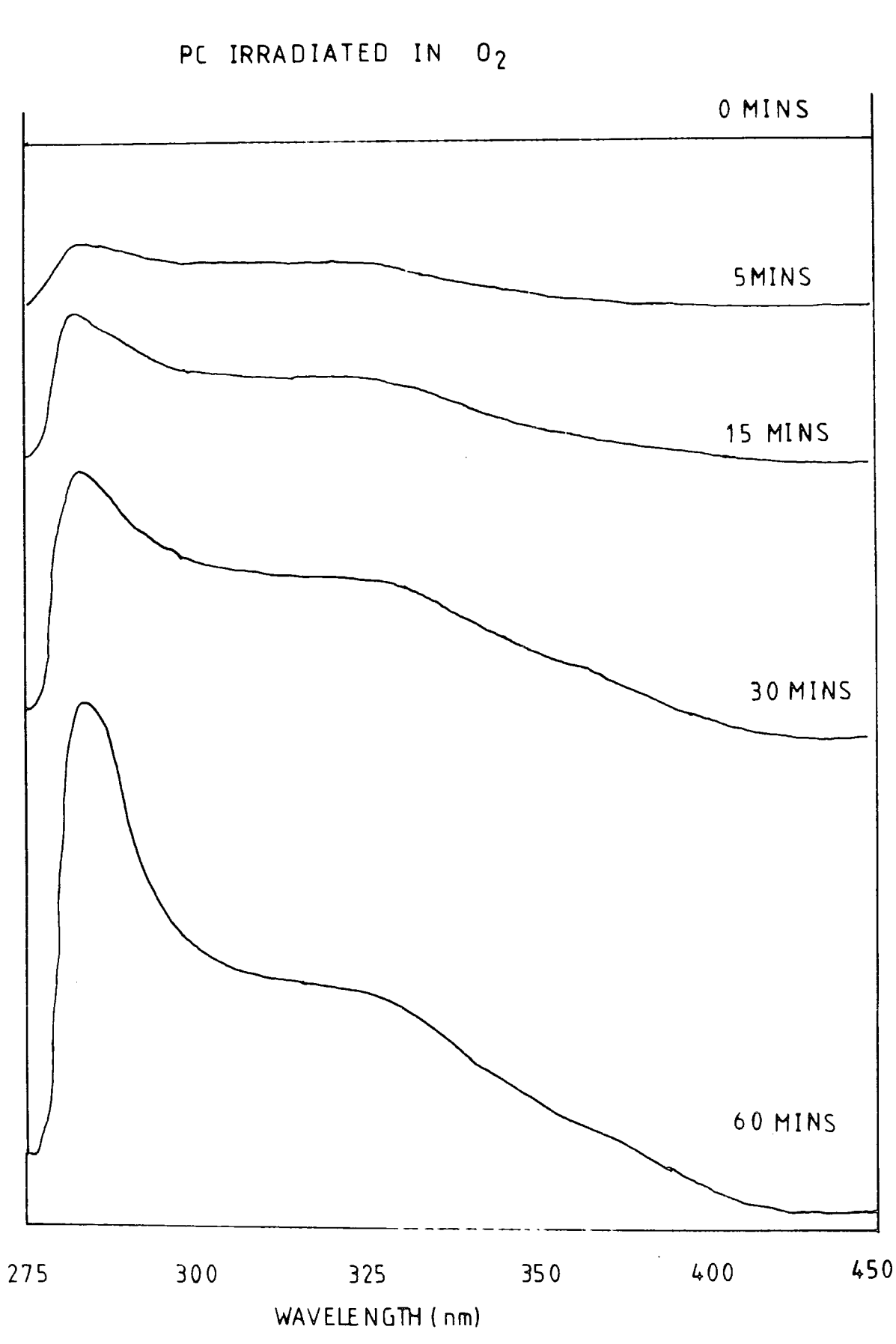

Figure 5.8 Difference uv spectra for polycarbonate samples irradiated in oxygen
($Io = 52.5\ Whm^{-2}h^{-1}$, $\lambda > 290nm$)

52.5 $Whm^{-2}h^{-1}$ for various periods of time and the profiles correspond well with those previously reported. The directly recorded absorption spectra are also in essential agreement with the trends discussed in the literature. These spectra correspond to a highly oxidised surface structure as revealed by the data presented in Chapter Four.

The interpretation of the uv spectra has previously centred on the wavelength assignments of absorbing species produced by a photo-Fries rearrangement mechanism. Peaks centred at ∿360 and ∿320 nm have designated as arising from dihydroxybenzophenone and phenyl salicylate species respectively.[159,160,184,185] Increases in absorption at these wavelengths are clearly seen from the data in Figure 5.8. The increase in absorption at ∿285 nm has been attributed to phenolic groups from the examination of the difference uv spectra obtained from polycarbonate films containing added Bisphenol A. As such the data presented here would be consistent with the literature[159,160,184,185] in the interpretation of a photo-Fries rearrangement, although, in the surface regions at least, extensive photooxidation has been shown to occur (cf. Chapter Four).

The uv difference spectra for polycarbonate films exposed to the natural environment in Dhahran, Saudi Arabia are displayed in Figure 5.9. The striking contrast between these spectra and those revealed in Figure 5.8 is readily observed. Increases in absorption at ∿285 and ∿360 nm occur as was seen in artificial weathering, however, at ∿320 nm a 'negative' peak is formed. This is indicative of 'bleaching', i.e. the loss of chromophoric species in the exposed samples. These results are in agreement with those obtained by Moore[184] for natural

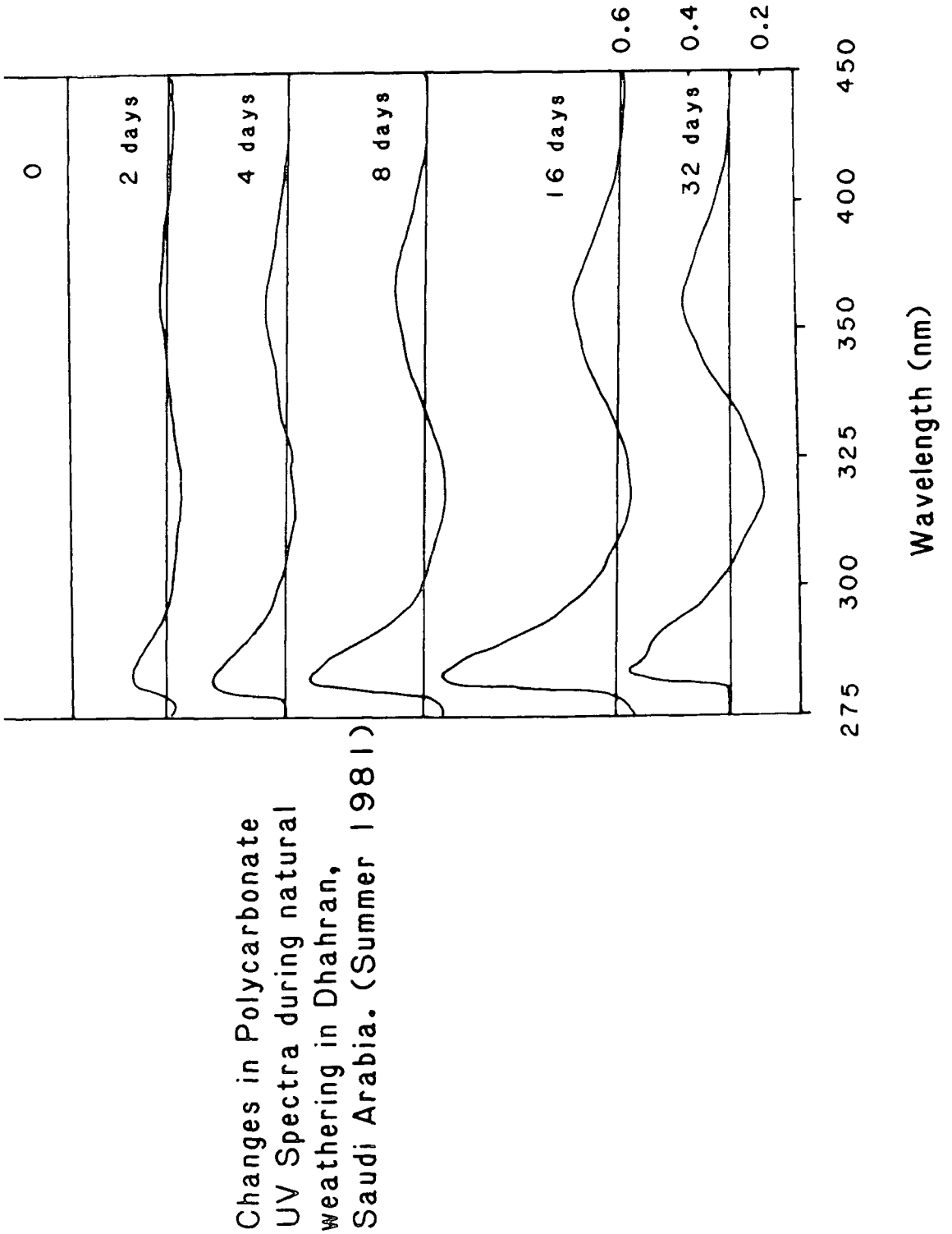

Figure 5.9 Difference uv spectra for polycarbonate samples weathered in Saudi Arabia

weathering in Schenectady, New York, U.S.A. and provide confirmation for the type of spectra expected to be obtained during the initial stages of the natural weathering of Bisphenol A polycarbonate. Unfortunately insufficient samples were available for examination of the difference uv for exposures over an extended period of time to confirm the observation in Moore's data that the 'bleaching' effect is of a 'transitory' nature.[184]

The assignment of a photo-Fries reaction predominating the natural weathering of polycarbonate is in the light of these data unreasonable.

In a study of the activation spectrum of polycarbonate, employing a Xenon arc lamp as the uv source, Mullen and Searle[185] observed a bleaching effect at 320 nm when 10-mil thick extended films were irradiated with wavelengths between 325 and 360 nm with a maximum effect at 343 nm. It is possible that the differences observed between natural and artificial weathering may be attributable to differences in spectral distribution and intensity. From a consideration of the distribution of the uv component of natural sunlight and the output of a medium pressure Hg arc lamp (cf. Chapter One) it is clear that the intensities of the shorter wavelengths (c.a. 300 nm) are greater for the latter.

To investigate the influence of the shorter wavelength on the photodegradation of polycarbonate, samples have been exposed in air (R.H. $\sim$50%) to the output of a fluorescent black lamp. The photon flux below 320 nm, as measured by the polysulphone technique, is low (I_o = 0.24 $Whm^{-2}h^{-1}$) and the wavelength of maximum intensity is $\sim$350 nm. The relevant difference uv spectra

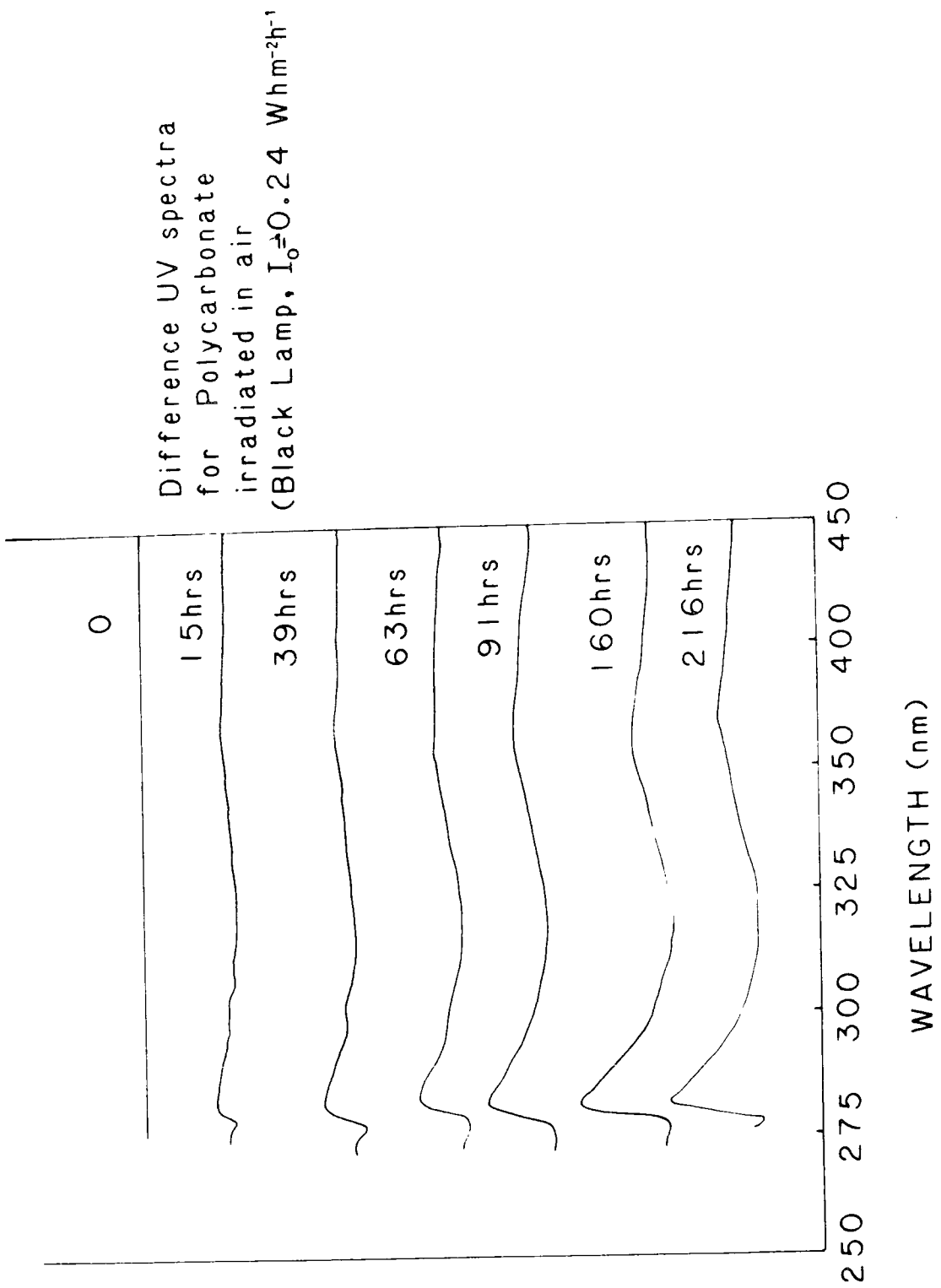

Figure 5.10 Difference uv spectra for polycarbonate samples irradiated in air (λ>290 nm, ∿50% R.H. Io = 0.24 Whm^{-2}h^{-1}) with a black lamp

for various times of irradiation are shown in Figure 5.10. The similarity to the spectra obtained for natural weathering is very striking indicating the effectiveness of the black lamp as an artificial source of ultraviolet light for approximating natural weathering from the bulk point of view.

In the absence of specific additional information it is not possible, on the basis of the uv data alone, to speculate on the nature of the chemical transformations involved. In the next section, however, the core level spectra reveal the substantial differences in chemistry between Hg arc irradiation (λ>290 nm) and natural weathering.

5.3.8 Comparison of the natural and artificial surface photoaging of polycarbonate

The changes in surface chemistry of polycarbonate films for irradiation in an oxygen atmosphere at a photon flux of 52.5 $Whm^{-2}h^{-1}$ (and 5.7 $Whm^{-2}h^{-1}$) have already been discussed in Chapter Four.

In summary, therefore, extensive oxygen incorporation in the surface occurs with increasing irradiation time. Oxidative functionalisation of the C_{1s} core level is seen, with carboxylate structural features being the most prominent oxidative functionality. The intensity of the carbonate structural feature decreases. Photooxidation involves both the gem dimethyl and phenyl moieties.

From the discussion in the previous section, where the difference uv spectra obtained for natural and artificial weathering were remarkably different, it is not unreasonable to expect that the changes in surface chemistry will also differ depending on the exposure conditions.

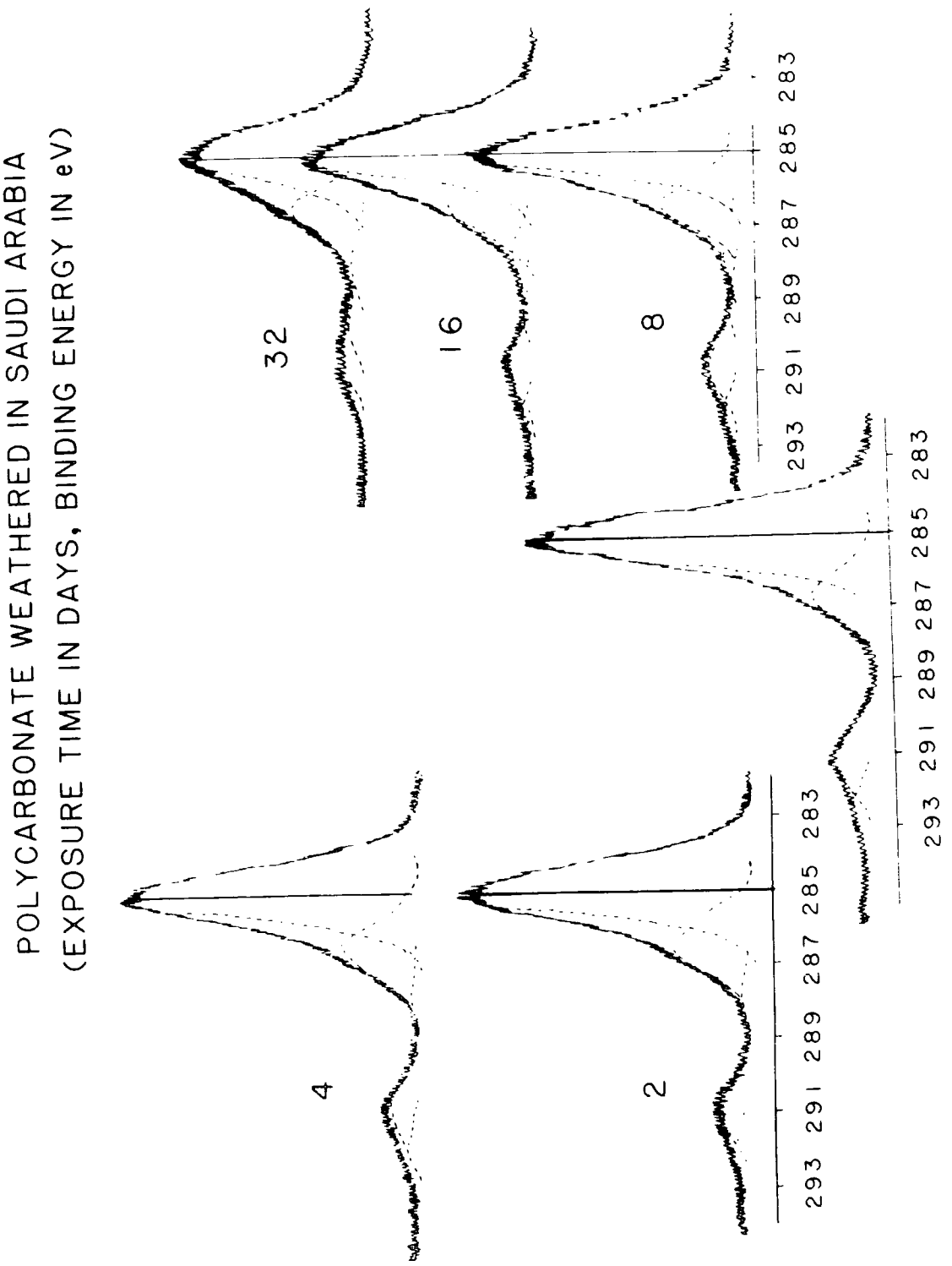

Figure 5.11 C_{1s} core levels for polycarbonate films weathered in Saudi Arabia

The ESCA spectra in Figure 5.11 reveal the changes in the C_{1s} core level for natural weathering in Dhahran. All the weathered samples had a major surface contamination as revealed by the ESCA data, in the form of silicon dioxide which originates from airborne particulates. Although the degree of contamination is variable, in general the quantity increases with exposure time and in consequence the O_{1s} spectra cannot be usefully employed in the data analysis. The C_{1s} core levels show a small increase in complexity on exposure arising from >C=O and O-C=O. The exact nature of the changes in surface chemistry are clearly shown in the C_{1s} component analysis in Figure 5.12. The C-H component (gem dimethyl groups and aromatic ring systems) decreases in intensity on exposure.

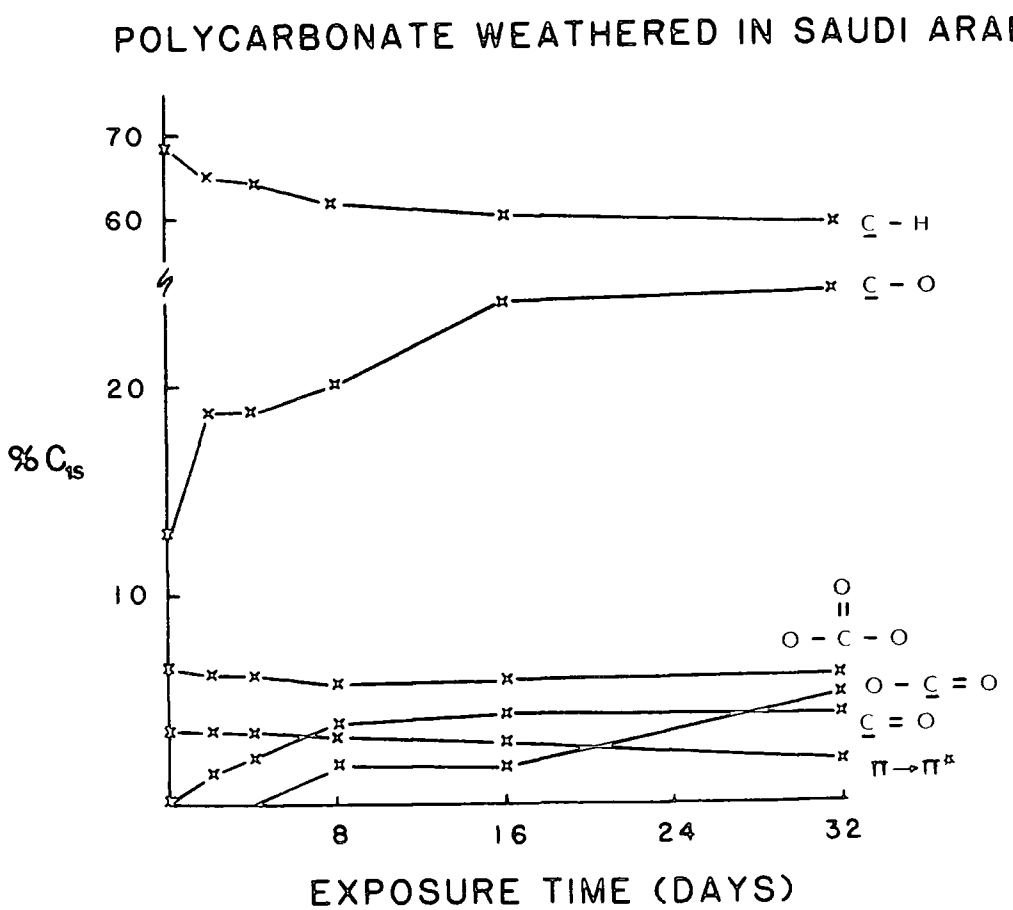

Figure 5.12 C_{1s} components for the spectra in Figure 5.11

The C-O functionality increases in intensity as does the carbonyl structural feature. Carboxylate groups do not appear until after 8 days although after 32 days' exposure the intensity is slightly greater than that for the >C=O functionality. A striking difference for natural weathering as opposed to the data for artificial weathering (Hg lamp) is the change in carbonate functionalisation. In the latter case this group decreases in intensity in the early stages whereas the data in Figure 5.12 clearly shows that there is only a slight decrease. For the photo-Fries rearrangement to occur, the carbonate moiety must be involved and hence its intensity would be expected to decrease. Thus in the present case the level of carbonyl and carboxylate groups cannot be explained by such a mechanism and hence arise from photo-oxidation of the gem dimethyl groups and in part (from the small decrease in $\Pi \rightarrow \Pi^*$ shake-up intensity, diagnostic of the aromaticity) the aromatic ring system. These data show that the mechanism for natural surface photoaging is somewhat different from that for artificial exposures and hence confirm the trends observed from the difference uv spectra.

For comparison the ESCA spectra in Figure 5.13 reveal the C_{1s} and O_{1s} core levels for polycarbonate films irradiated in air (∿50% R.H.) with the black lamp (Io = 0.25 $Whm^{-2}h^{-1}$). All the samples revealed a very low level of surface contamination as evidenced by the appearance of an Si2p peak in the ESCA spectra at a binding energy of ∿102.0 eV. As such the O_{1s} signal will have contributions to its intensity arising from this contamination, however this amount may be estimated and from a knowledge of the relevant instrument dependent

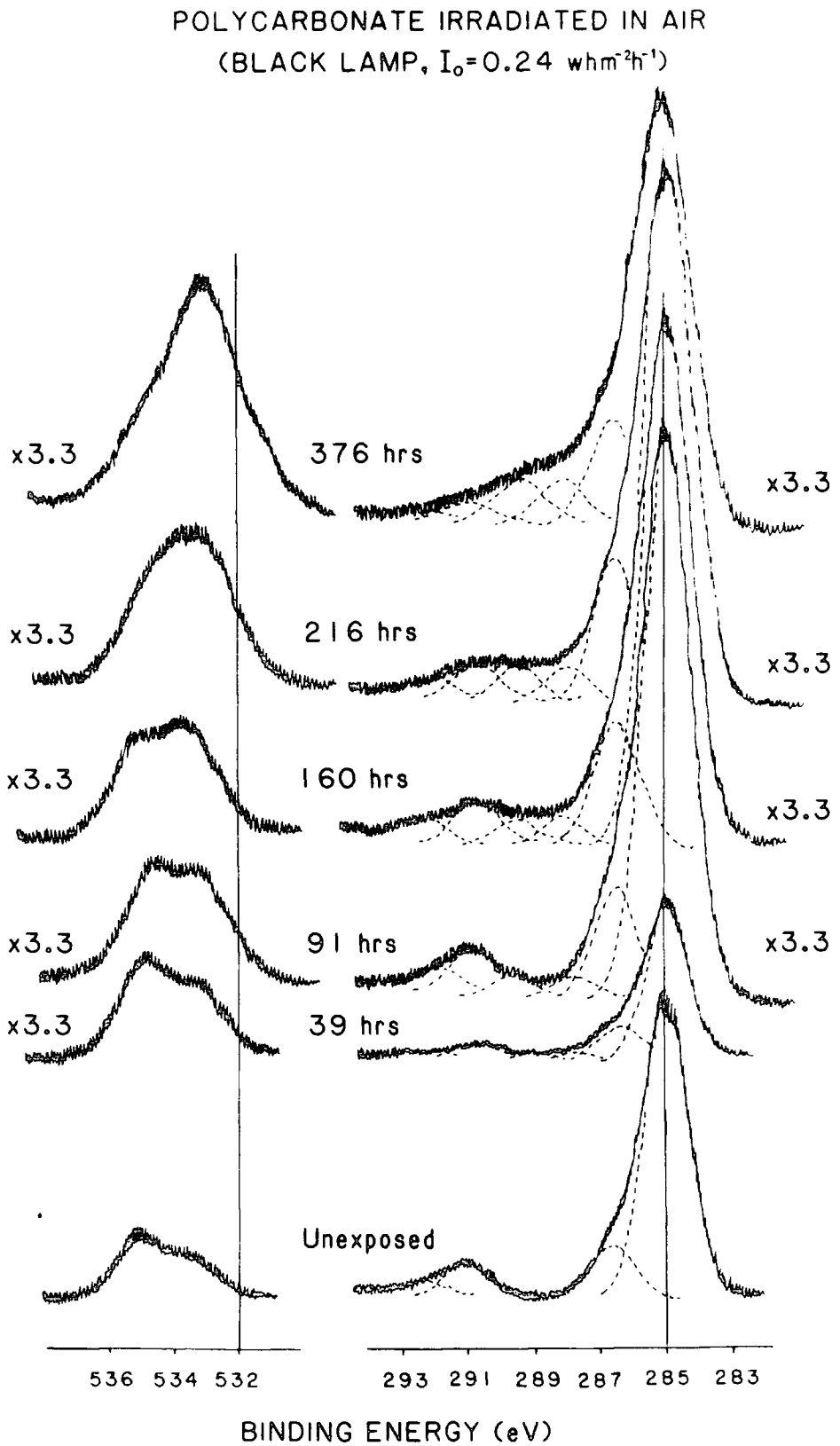

Figure 5.13 C_{1s} core levels for polycarbonate films exposed to a black lamp for various periods of time

sensitivity factors a corrected O_{1s}/C_{1s} intensity ratio can be determined and this is shown in Figure 5.14. The C_{1s} core

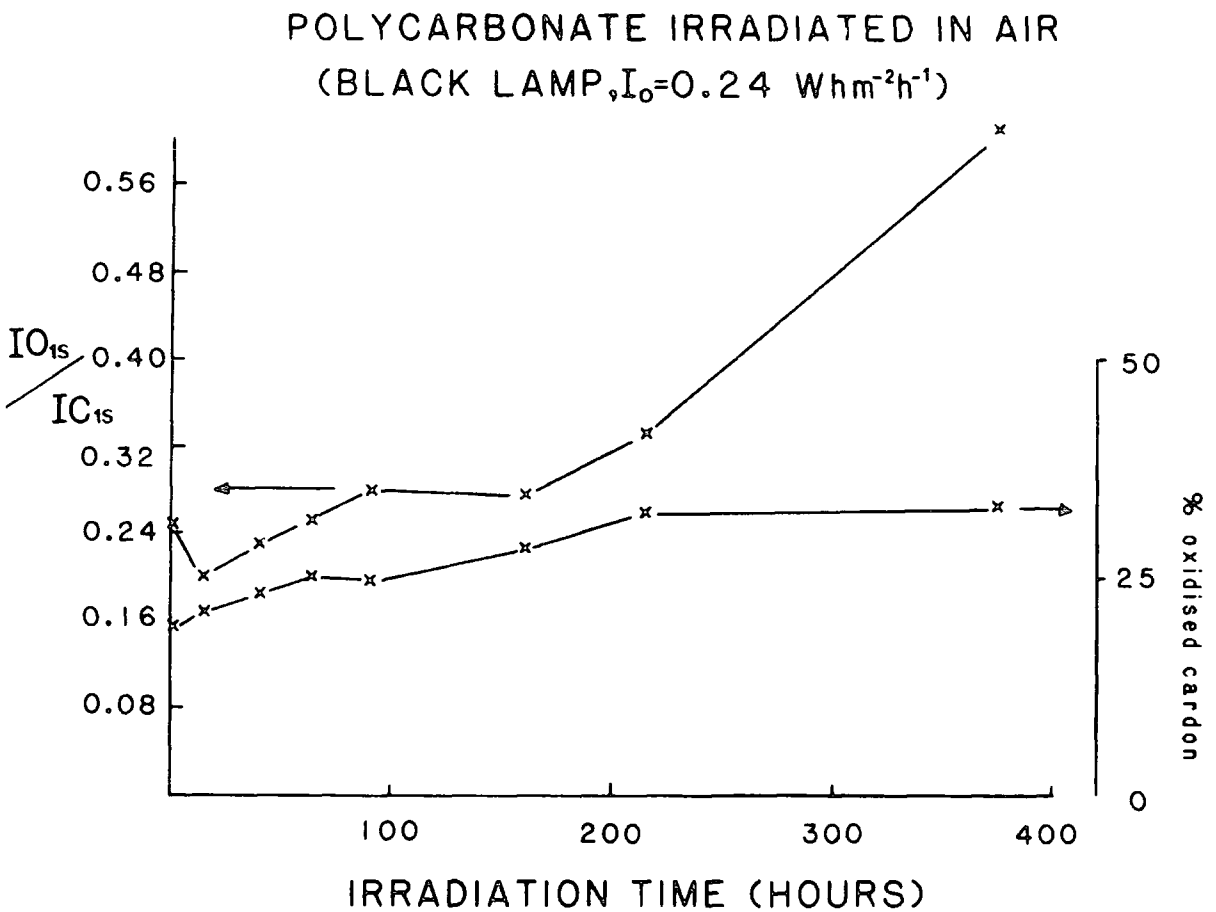

Figure 5.14 O_{1s}/C_{1s} intensity ratios and percentage contributions to the total C_{1s} signal arising from oxidative functionalities for polycarbonate films exposed to a black lamp.

level spectra in Figure 5.13 reveal that, from a starting profile of components arising from C-H, C-O, O-C(=O)-O and $\Pi \rightarrow \Pi^*$ shake-up satellite environments, additional functionalities due to >C=O and O-C=O groups appear on irradiation. The O_{1s}/C_{1s} intensity ratios in Figure 5.14 show that, in the initial stages of exposure, a slight decrease from the starting value occurs

but that on prolonged exposure overall oxygen uptake takes place. From these data and a consideration of the relative proportion of the C_{1s} signal arising from oxidative functionalities (also shown in Figure 5.14) it is clear that photo-oxidation represents the major contribution to the overall degradation process.

The nature of the oxidative functionalisation becomes clear from the C_{1s} component analysis in Figure 5.15 for the spectra in Figure 5.13. In the initial stages a slight decrease in the carbonate moiety occurs with a concomitant increase in C-O and decrease in C-H functionalities.

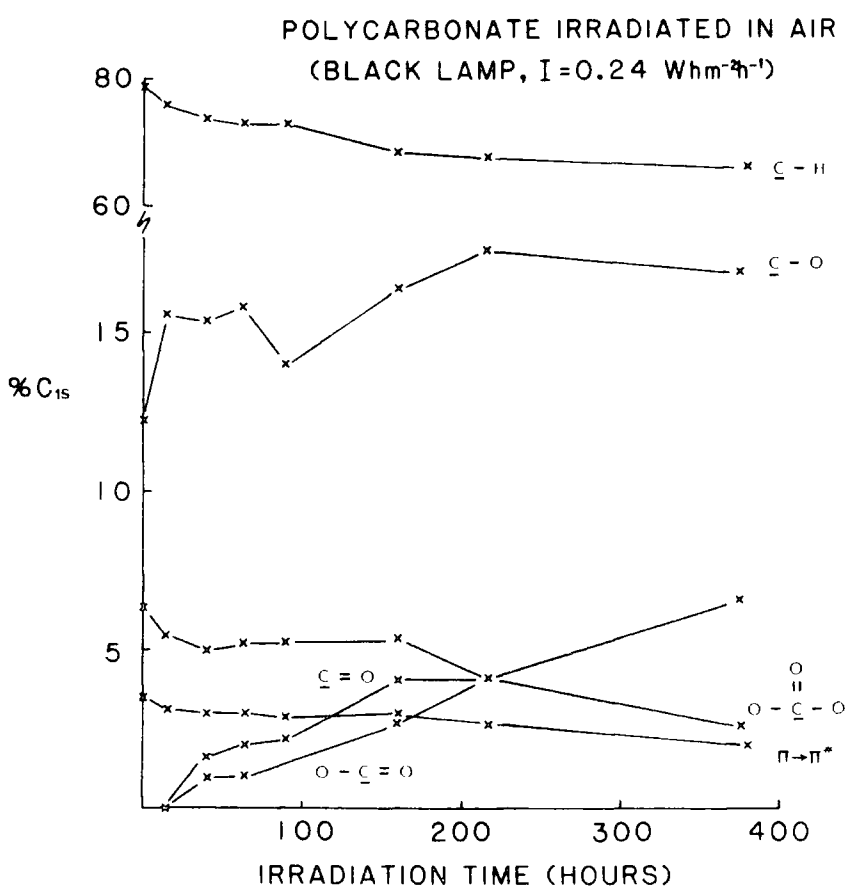

Figure 5.15 C_{1s} components for the spectra in Figure 5.13

Carbonyl and carboxylate features do not appear until after ∿39 hours' exposure. In conjunction with the relevant O_{1s}/C_{1s} intensity ratios it is feasible that in the preliminary stages of irradiation that the predominant reaction involves cleavage of the carbonate group to form phenolic and possibly ether species. However, over the period 39-176 hours' exposure the carbonate and shake-up satellite component intensities remain relatively constant whereas the >C=O and O-C=O functionalities increase. This is indicative that photooxidation of the gem dimethyl groups during this period is the major reaction. On prolonged exposure (∿ 176 hours) the >C=O and O-C=O components continue to increase in intensity whilst both the O-C(=O)-O and $\Pi \rightarrow \Pi^*$ contributions to the C_{1s} signal decrease. This suggests that the degradative process now involves the carbonate group and the aromatic ring system.

Overall the data clearly reveal that photooxidation and not a photo-Fries mechanism is the predominant reaction and that the process is extremely complex. The nature of the changes in surface chemistry for the exposures to the black lamp are not dissimilar to those obtained in natural weathering and hence for approximating natural exposures, this type of lamp is invaluable for studying the photoaging of Bisphenol A polycarbonate.

As discussed earlier, Moore[184] has considered the formation of phenolic groups to be of major importance in polycarbonate photoaging. For comparison a sample, irradiated for 216 hours with the black lamp, was treated with trifluoroacetic anhydride to label surface hydroxyl groups, as discussed in Section 5.3.6. The contribution of C-OH structural features

to the C_{1s} signal after 216 hours' exposure was found to be ∿2%. From a consideration of the data in Figure 5.15 it is clear that C-OH groups are not under these conditions of exposure a major product of photodegradation in the surface regions.

The question as to why the results obtained from the irradiation of polycarbonate films with a Hg lamp (λ>290nm) differ from those for natural and black lamp exposures has still not been fully resolved. The initial impetus for studying polycarbonate photodegradation with the black lamp was to examine the changes in bulk and surface chemistries with a uv source with relatively low output below 320nm, the major emission occurring in the region between ∿320 and ∿360nm, thus providing a comparison with the data obtained by Mullen and Searle[185] for the activation spectra for 10-mil thick films of polycarbonate. However, on consideration of the corresponding data for 0.1 mil thick films[185] doubt must be placed on the importance of the wavelength dependence above 320nm on the nature of the photodegradation occurring in the surface regions at least. The bleaching effect, for the 10-mil samples, at ∿320nm for irradiating wavelengths 325nm-360nm was attributed to sample thickness as were the range of wavelengths causing photodegradation (230nm-430nm). In contrast, for the thin films, no such bleaching was found and the longest wavelength causing photodegradation was ∿320 nm. The incident radiation in the surface is essentially unattenuated and consequently it is unlikely that wavelengths ∿320 nm will be responsible for the initial photodegradation in these regions. Therefore, the differences in the observed surface chemistries may be due to the variations in the intensities in the region 290nm-320nm of

the uv sources utilised. Photon fluxes <320nm in natural sunlight can exceed 4 Wm^{-2} such that the use of incident radiation at ∿6 Wm^{-2} from an Hg arc is not unreasonable. However, in the latter case the contributions to the flux arising from wavelengths ca. 300nm and at 313nm are more intense than in natural sunlight. The possible consequence of this is that the number and nature of radicals formed per unit time may differ for artificial weathering and hence influence the type of reaction mechanism involved. Evidence for this can, to some extent, be seen from a comparison of the changes in surface chemistry of polycarbonate films irradiated with similar total photon fluxes arising from black lamp and Hg arc emissions (air, 40-50% R.H.). The relevant data is shown in Table 5.3. It is clearly evident that oxidative functionalisation and oxygen uptake are more extensive for the mercury arc lamp exposure.

TABLE 5.3 Comparison of the C_{1s} components and O_{1s}/C_{1s} intensity ratios for polycarbonate samples exposed to a black lamp and a mercury arc lamp for similar total photon fluxes.

	Total C_{1s}	C-H	C-O	C=O	O-C=O	CO_3	$\Pi \rightarrow \Pi^*$	O_{1s}/C_{1s}
Hg arc lamp (1 hour, 20 $Whm^{-2}h^{-1}$)	100	71	16	5	5	2	1	0.36
Black lamp (91 hours, 0.24 $Whm^{-2}h^{-1}$)	100	74	14	2	2	5	3	0.28

Samples irradiated in air with the Hg lamp at much lower photon fluxes (1.2 and 0.8 $Whm^{-2}h^{-1}$) reveal difference uv spectra of a similar nature to those obtained for exposures in

oxygen (Io = 52.5 $Whm^{-2}h^{-1}$) and air (Io = 20 $Whm^{-2}h^{-1}$). It has been shown above that the contrast between black and Hg lamp exposures as revealed by difference uv spectroscopy reflects differences in surface chemistries as revealed by ESCA. Thus for these low lamp intensity exposures it is to be expected that the trends in surface photodegradation will follow (although at a much slower rate) those observed for higher incident fluxes. This indicates the importance of the contributions to the total flux arising from the wavelengths in the region 290-320 nm on the nature of the photodegradation. As such the data presented above strongly suggests that for a close correspondence to natural weathering, artificial uv sources should employ wavelengths and relative intensities comparable to sunlight.

5.3.9 Prolonged Natural Weathering

The data presented in the previous section revealed the changes in bulk and surface chemistry during the early stages of natural weathering (∿1 month) in Saudi Arabia. It is of interest, however, to examine the surface chemistries of polycarbonate samples weathered for extended periods of time (6, 12 and 24 months). The C_{1s} core levels displayed in Figure 5.16 reveal the changes occurring in the surface region for exposures in Australia at 2 different sites corresponding to hot/wet (H/W) and hot/dry (H/D) conditions. Although, after 6 months' weathering, the appearances of the C_{1s} spectra for the 2 sites are similar it is clear that those for 12 and 24 months differ and reflect the variations in the respective relative humidities. The nature of the changes are more apparent from the C_{1s} component analyses in Figure 5.17.

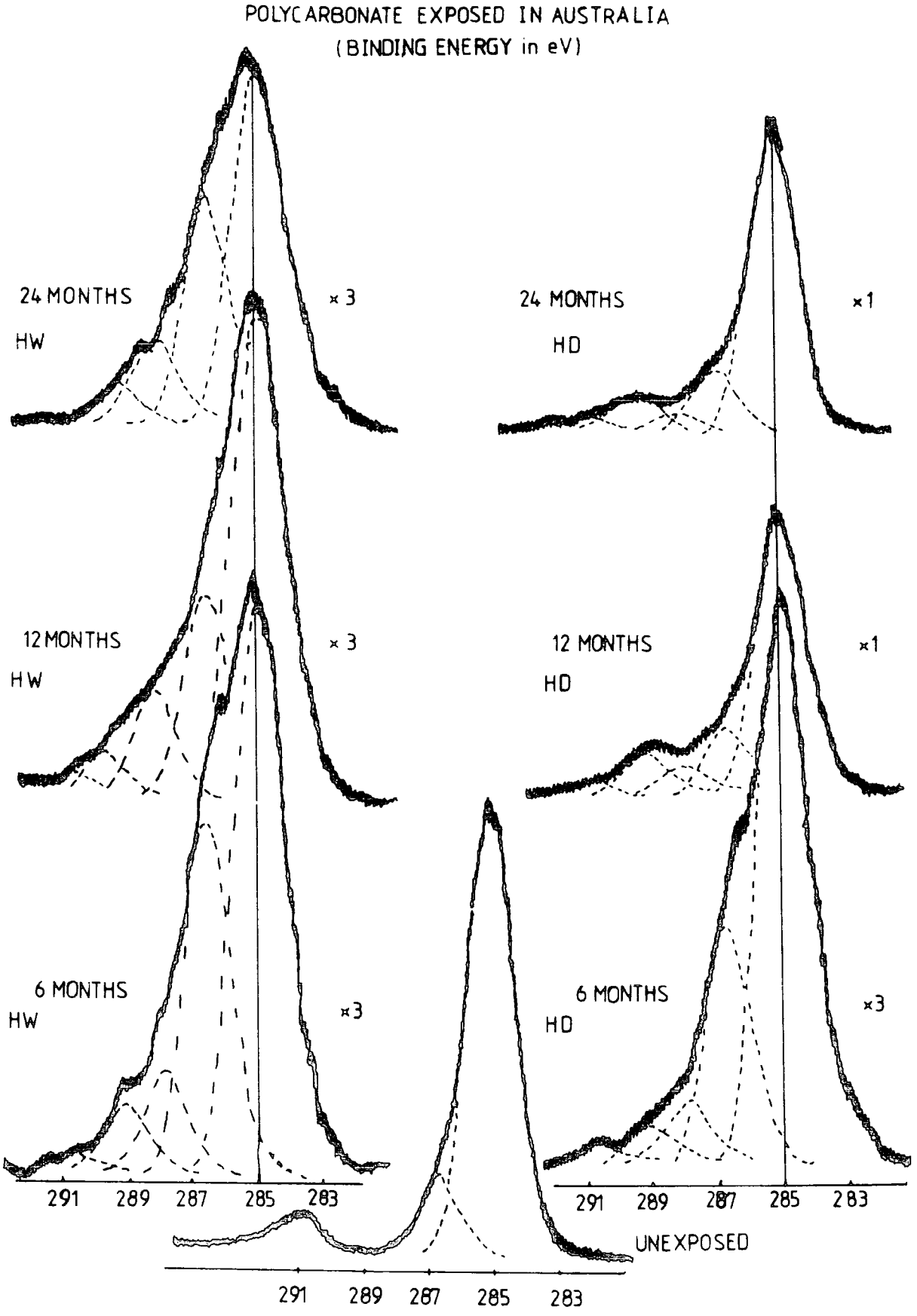

Figure 5.16 C_{1s} core levels for polycarbonate samples weathered in Australia at Hot/Wet and Hot/Dry sites

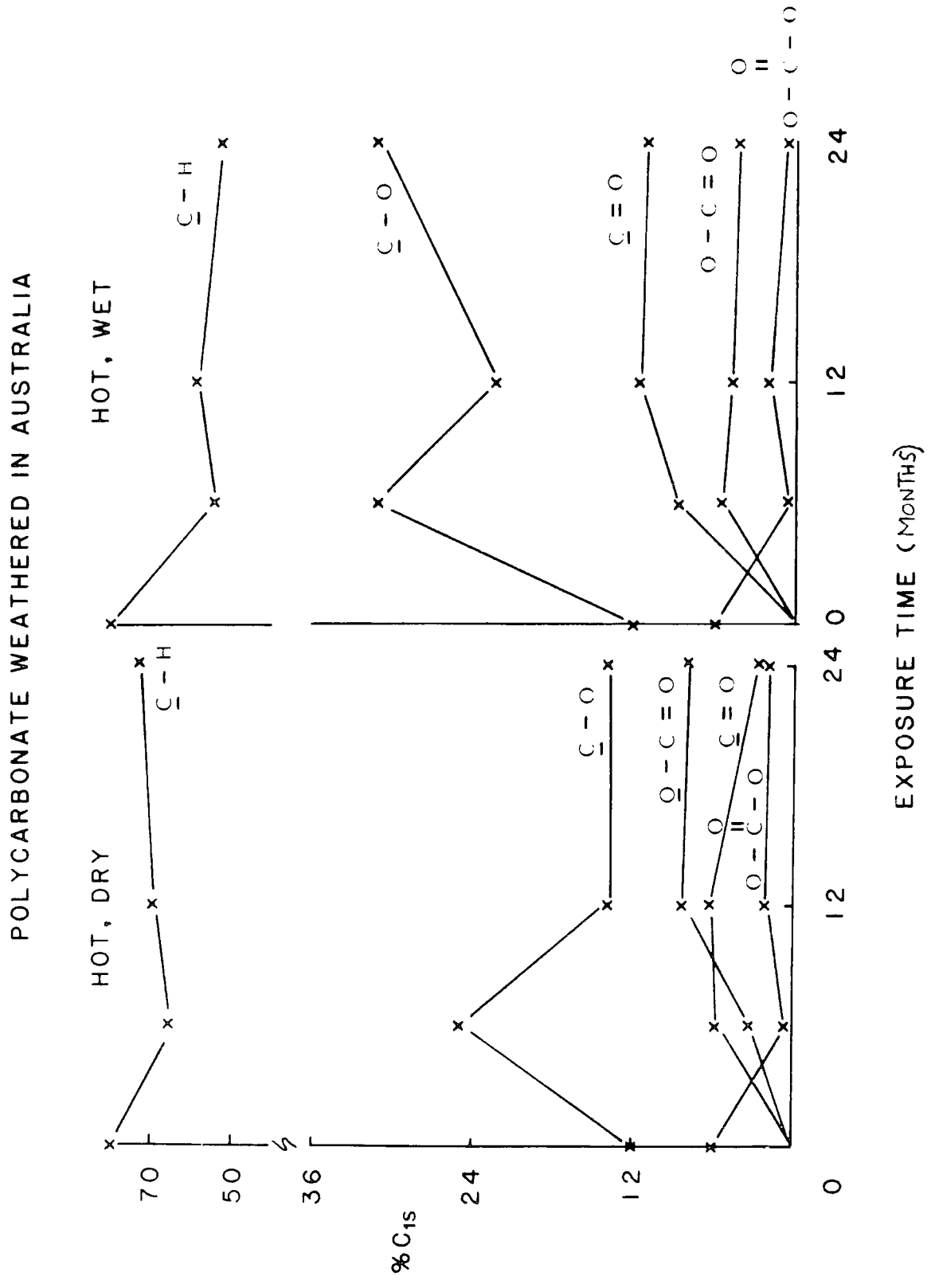

Figure 5.17 C_{1s} components for the spectra in Figure 5.16

The similarity in the nature of the surface after 6 months' exposure at the two locations is highly evident from the intensities arising from C-H, C-O, C=O, O-C=O and O-C(=O)-O components. The intensity of the C-O functionality is more intense for the H/W exposure. It is clear from these data that extensive photodegradation has occurred. Even allowing for the fact that surface erosion probably takes place and thus the surface examined may not be the same as the original sample, the trends in carbonyl and carboxylate formation over 24 months reflect those found in the model studies where photoaging was studied as a function of relative humidity. As such the carboxylate feature is predominant over the carbonyl component after 12 and 24 months' exposure in H/D conditions with the reverse trend being the case for H/W weathering.

5.4 Conclusions

The data discussed in Section 5.3 highlights the following features of polycarbonate photoaging.

(i) Natural and artificial weathering in the surface regions occurs via photooxidation and not by photo-Fries re-arrangement and mechanisms. This is also the case for the bulk photoaging albeit natural or black lamp exposures. It may well be the case for Hg arc lamp irradiations (λ>290nm) although in the absence of specific additional information this cannot be shown directly from the difference uv spectra.

(ii) The changes in bulk and surface chemistries, as evidenced by difference uv spectroscopy and ESCA respectively, induced by uv irradiation are strongly dependent on the partial pressures of water and oxygen.

(iii) Surface photooxidation involves both the gem dimethyl groups and aromatic ring systems.

(iv) For close correlation to natural weathering, the artificial weathering of Bisphenol A polycarbonates should employ uv sources having an emission in the region 290-320nm of comparable distribution and relative intensity as sunlight.

CHAPTER SIX

THE PHOTOAGING OF BISPHENOL A POLYCARBONATE - PART IV

SURFACE ASPECTS OF THE OXIDATION OF BISPHENOL A POLYCARBONATE FILMS, INDUCED BY REACTIVE OXYGEN SPECIES, AS REVEALED BY ESCA.

6.1 Introduction

The natural weathering of polymers is a very complex process. Although photooxidation is generally regarded as the predominant cause of degradation, reactions with reactive gaseous compounds (e.g. O_3, SO_2 and NO_2), present as atmospheric pollutants, may also play an important part. The role of photooxidation in the photoaging of Bisphenol A polycarbonate has been considered in Chapters Four and Five and it is therefore of interest to consider the surface aspects of the degradation induced by some of the reactive species (namely ozone and singlet oxygen) that have received attention in the literature.[188-190]

Ozone is produced in the upper atmosphere by the ultraviolet photolysis of oxygen.[190] The resulting oxygen atoms then combine with oxygen molecules to form ozone. A layer of ozone at an altitude between ∿12 and 22 miles has been formed with concentrations as high as 500 parts per hundred million (pphm). This layer acts as an efficient filter of the short wavelengths of solar radiation (<290nm) and protects life at the earth's surface from the harmful effects of ultraviolet light. As a result of winds, ozone which has diffused into the troposphere is brought down to the earth's surface.[191] Local concentrations vary widely, depending on locality and weather conditions although they are normally higher in coastal regions.

Ozone reacts with virtually all polymers, the rate of attack being strongly dependent on the structure of the material. The reaction with solid polymers occurs mainly at the surface [192,193,194] and as such a knowledge of the changes in surface

chemistry is of prime importance. Thus the first part of the results and discussion in Section 6.3 considers a preliminary investigation of the surface ozonation of polycarbonate with the aid of ESCA.

Since the proposal, by Trozzolo and Winslow,[195] that singlet oxygen may play a possible role in the oxidative photodegradation of polyethylene, the study of singlet oxygen reactions with polymers has been the centre of considerable interest in the literature.[10,188,189] In the case of polyethylene, singlet oxygen is postulated as arising from the quenching of $n \rightarrow \Pi^*$ triplet states of ketone groups by molecular oxygen.[195] However, it should be noted that there is no experimental evidence for this process.

Two out of the various higher states of excited oxygen molecules were considered by Herzberg[19] to consist of singlet oxygen, namely, $^1O_2$ ($^1\Delta_g$) and $^1O_2$ ($^1\Sigma^+_g$). These two singlet states have excitation energies with respect to the ground state of $\sim$22.5 and $\sim$37.5 kcal mole^{-1} respectively. In the gas phase (under low pressure) the $^1\Delta_g$ state is extremely long-lived (ca. 45 min.) whereas the $^1\Sigma^+_g$ state has a much shorter lifetime (ca. 7 sec.).[10] Thus, in general, it is the former species which is considered to be involved in the oxidative degradation of polymers.

Levels of singlet oxygen, in the p.p.m. range, have been identified in urban atmospheres,[196,197] consequently polymers which are affected by singlet oxygen need to have these reactions taken into account when their ageing in contaminated atmospheres is being studied.

As, in the case of ozonation, singlet oxygen reactions occur predominantly at the surface[198] of a solid polymer although the literature[188] has not considered to any great extent the nature of the reactions at the gas/solid interface ESCA has been shown to be of prime importance as a technique for the study of polymer surface degradation[45-52] and in this chapter it has been utilised to investigate some aspects of the surface oxidation of Bisphenol A polycarbonate induced by ozone and singlet oxygen.

6.2 Experimental

6.2.1 Ozonation

Ozonated samples of Bisphenol A polycarbonate and polysulphone films (30μm) were kindly supplied by Dr. J. Peeling (Dhahran, Saudi Arabia). The samples were exposed to ozone from an ozonator (Ozone Research and Equipment Corporation) for various periods of time in a purged pyrex vessel. The gas flow throughout the experiment was maintained at 0.52 $lmin^{-1}$. The ozone concentration, determined by iodometric-thiosulphate titration, was 0.27 mole %.

6.2.2 Singlet Oxygen

Singlet oxygen was generated by the microwave discharge technique.[199] Oxygen at a pressure of 2 torr was passed through a quartz tube (12.5mm) encircled by a microwave discharge cavity, see Figure 6.1. The microwave power is supplied by an Electro-Medical Supplies generator at 60W and a frequency of 2450 MHz. Singlet oxygen, atomic oxygen and ozone are produced. The concentration of the latter two may be essentially removed by continual distillation of Hg vapour

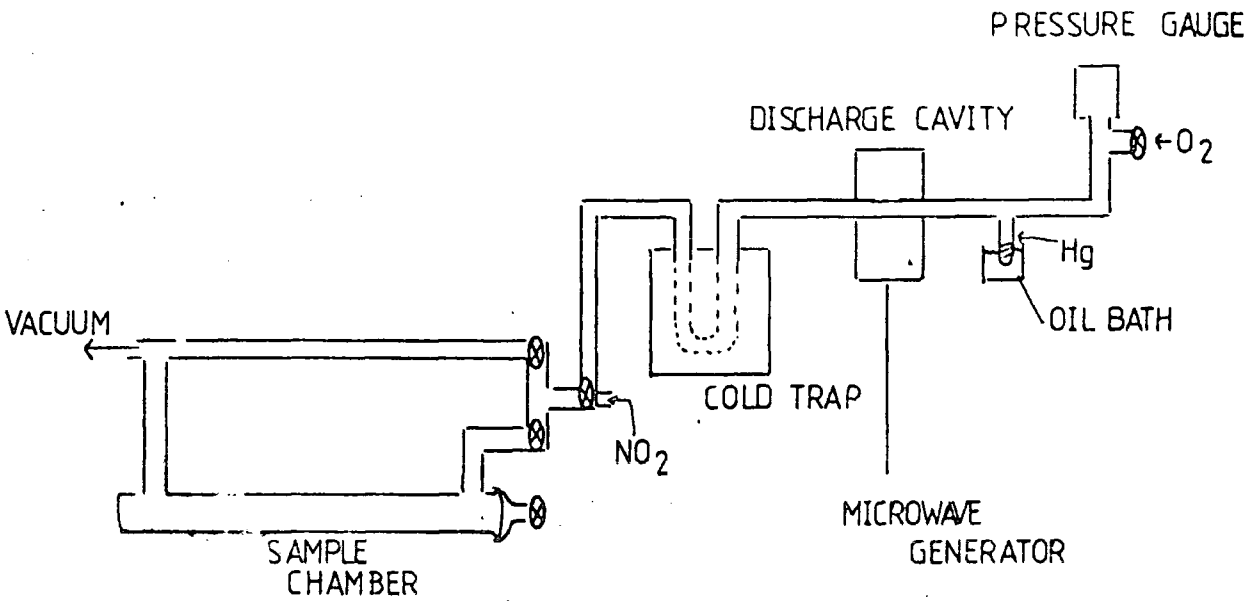

Figure 6.1 Schematic of the flow system used to study the reactions of reactive oxygen species with polymers.

through the discharge region. A ring of mercuric oxide is formed inside the quartz tube downstream of the discharge. The effluent was passed through a dry ice/acetone cold trap ($-78^{o}C$), to remove mercury vapour, and passed to the sample region. The effluent was monitored for atomic oxygen at the sample position, in separate experiments, by the addition of nitric oxide. The fluorescence which arises from the reaction:

$$NO + O \longrightarrow NO_2 + h\nu$$

was not observed in the present case. However, a low level

of atomic oxygen, estimated to be $\sim 1 \times 10^{-4}$ of the singlet oxygen concentration, has been shown to be present in the effluent from an oxygen discharge even with the presence of mercury vapour. To remove the residual atomic oxygen contamination nitrogen dioxide may be added to the stream beyond the discharge region. This is a very rapid reaction and follows the scheme:

$$NO_2 + O \longrightarrow NO + O_2$$

$$NO + O \longrightarrow NO_2 + h\nu$$

A bypass system has been incorporated to allow the discharge to stabilise before exposing the sample to the effluent. The sample chamber is surrounded by a water jacket enabling this region to be heated to $\sim 80^{o}C$.

The experimental procedure consisted of placing a polymer film mounted on an ESCA probe tip, by means of double sided scotch tape, into the reaction chamber and evacuating the whole system to $\sim 10^{-3}$ torr with an Edwards ED50 two-stage rotary pump. After flushing with oxygen at the required pressure for ~ 5 minutes and ensuring that the flow is directed through the bypass system, the microwave discharge is initiated with an Edwards H.F. Tester and allowed to stabilise for 15 minutes before passing the effluent over the sample.

As will become apparent from the results and discussion, when mercury vapour is used as the only means of removal of atomic oxygen and ozone extensive surface oxidation occurs which may arise from a low level of contamination due to the former species. To investigate the effect of oxygen atoms on polycarbonate a flow system, based on the design for the singlet oxygen generator described above, was constructed. This

essentially consists of replacing the microwave cavity with a mercury arc lamp, the dry ice/acetone cold trap with liquid nitrogen and the oxygen by nitrous oxide.

The production of atomic oxygen arises from the mercury sensitised photlysis of nitrous oxide (N_2O) at $\sim$254nm.[44] By passing N_2O through the system at $\sim$2 torr with the continual distillation of mercury vapour, a very small level of oxygen atoms are produced. This is evidenced by the contrast in pressures on either side of the liquid nitrogen cold trap. The pressure in the sample region is $\sim 10^{-3}$ torr although an accurate measurement was not possible due to range of the Edwards Pirani gauge employed.

ESCA spectra were recorded with an AEI ES200B spectrometer using $Mg_{K\alpha_{1,2}}$ radiation. Under the conditions employed the $Au_{4f_{7/2}}$ level at 84.0 eV used for calibration purposes had a full width at half maximum (FWHM) of 1.2 eV. Spectra were obtained at electron take-off angles of $\theta=30^{\circ}$ and $\theta=70^{\circ}$ corresponding to sampling depths of $\sim 45\mathring{A}$ and $\sim 12\mathring{A}$ respectively. Binding energies were referenced to the C-H component at 285.0 eV. Line shape analysis of complex spectral envelopes was achieved using a DuPont 310 curve resolver.

6.3 Results and Discussion

6.3.1 Ozonation

Previous investigations, pertaining to changes in bulk chemistry, of the ozonation of Bisphenol A polycarbonate in the solid state[200] and solution phase[192] reveal contrasting degrees of reactivity. It is of interest to compare these data with those obtained for polystyrene.[10,192] The rate of

ozonation for the latter polymer appears to be greater in the solid state than that in solution whereas the converse situation exists for polycarbonate. An ESCA study of the surface ozonation of polystyrene films[193] has in fact revealed that extensive oxygen uptake and hence oxidative functionalisation occurs. If the trends observed in bulk chemistry are followed then it is to be expected that the changes in the surface chemistry of polycarbonate on ozonation will not be as great as those for polystyrene.

The ESCA spectra in Figure 6.2 reveal the C_{1s} core levels for polycarbonate before and after treatment ozone. From an initial profile due to peaks arising from C-H (gem dimethyl and phenyl moieties), C-O, O-C(=O)-O and $\Pi \rightarrow \Pi^*$ shake-up components, additional features due to >C=O and O-C=O functionalities appear on exposure indicative of oxygen uptake. All the samples revealed a varying degree of surface contamination as evidenced by the presence of a signal arising from the Si_{2p} core level ($\sim$102.2 eV). This contamination contributes to the O_{1s} envelope and consequently useful information on oxygen uptake cannot be obtained solely from the O_{1s} levels themselves.

The nature of the changes in the C_{1s} signal are revealed in the component analysis in Figure 6.3. The C-H feature decreases in intensity with concomitant increases in C-O, >C=O and O-C=O functionalities. After an initial decrease in the carbonate moiety the level remains relatively constant indicative that this functionality does not play a predominant role in the ozonalysis of polycarbonate. The $\Pi \rightarrow \Pi^*$ shake-up satellite, diagnostic of the aromaticity present, decreases in intensity with increasing ozone exposure such that the level after 32 hours is only $\sim$35% of the initial value. These results,

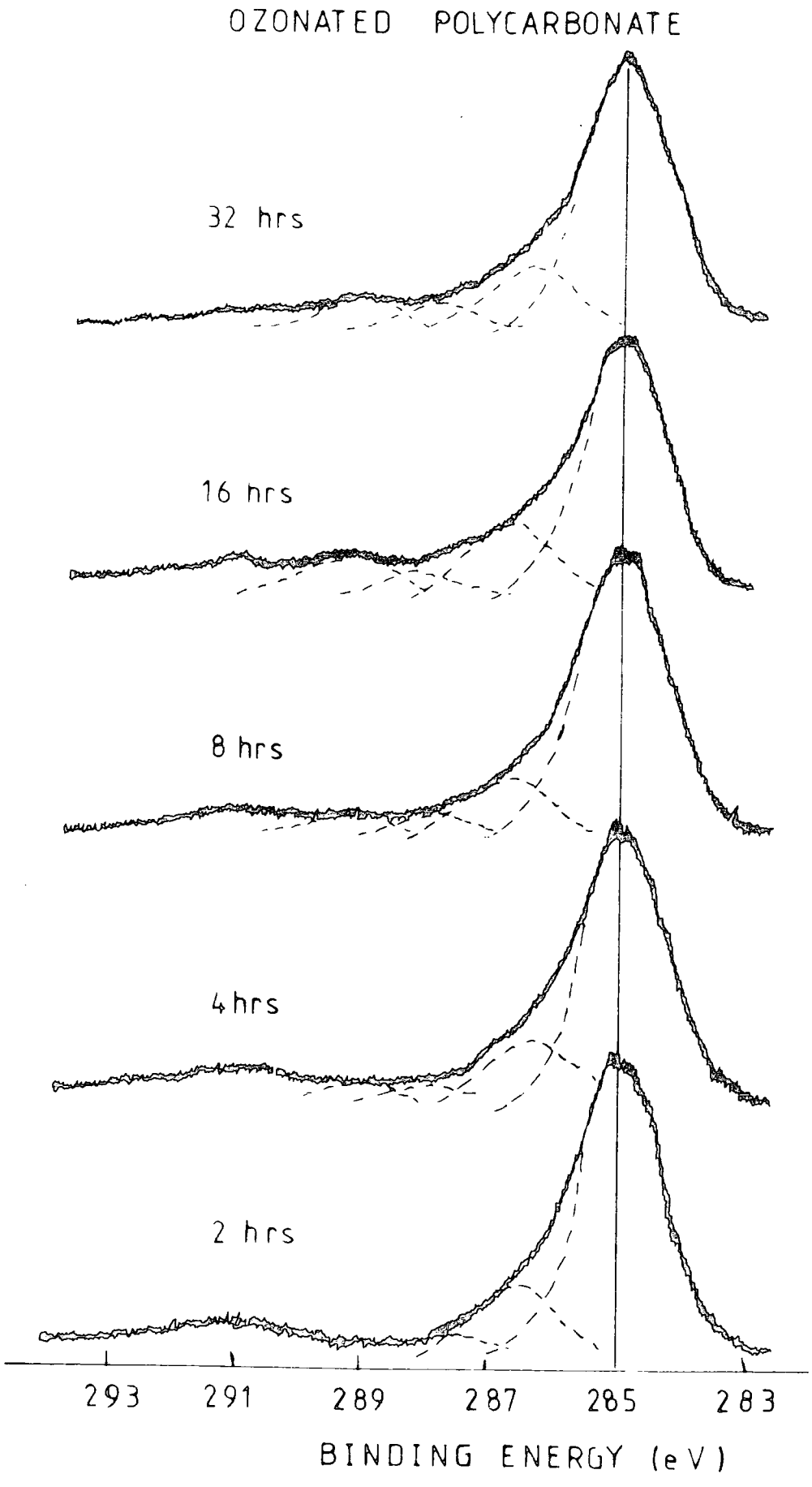

Figure 6.2 C_{1s} core levels for ozonated polycarbonate samples

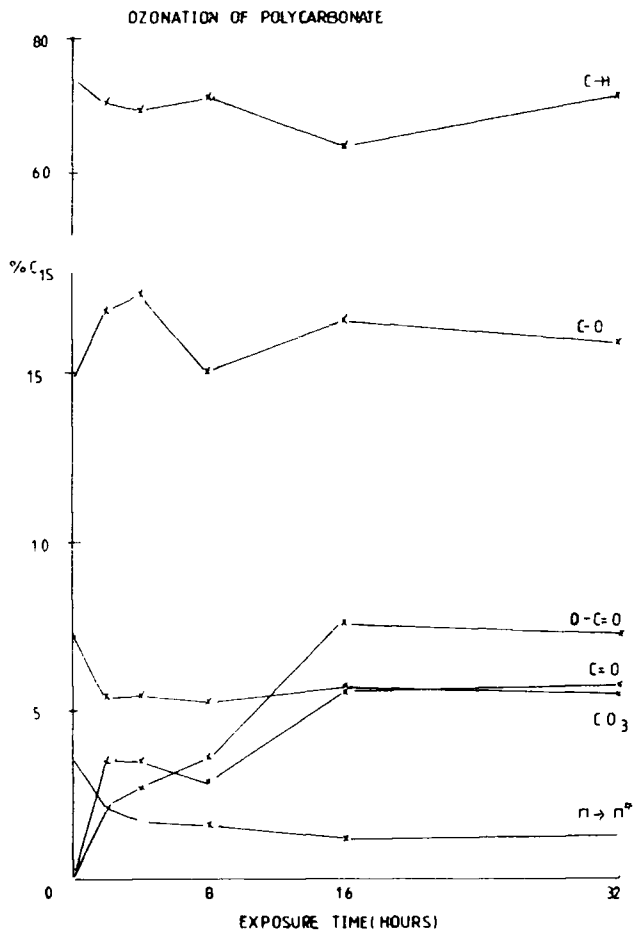

Figure 6.3 C_{1s} components for the spectra in Figure 6.2

therefore suggest that polycarbonate ozonolysis in the surface regions involve both the gem dimethyl groups and aromatic ring systems. It is interesting to note that the extent of reaction of polycarbonate after 32 hours' exposure is not as great as that for polystyrene after two hours under the same degradation conditions. Consequently, the initiation of oxidative degradation in the natural environment by ozone is of greater importance for the latter system.

Electron spin resonance (esr) studies of polycarbonate ozonation have revealed radical formation indicating that the formation of peroxy radicals is the predominant reaction over

the formation of aromatic ozonides.[192] It is not possible from the data in Figure 6.3 to delineate the relative predominance of either reaction, however, the decrease in the shake-up satellite intensity suggests that the latter mechanism, in the degradative processes, is of importance in the surface regions.

6.3.2 Microwave discharge oxidation of polycarbonate

Prior to the consideration of the results pertaining to singlet oxygen reactions, this section is involved with the study of the changes in surface chemistry of polycarbonate films exposed to the effluent of a microwave initiated oxygen discharge. The reactive oxygen species reaching the sample consist of atomic oxygen, singlet oxygen and ozone. This method has been previously utilised to study the reactions of atomic oxygen with a variety of organic materials,[201] including polymers,[202] but is generally acknowledged as not being very representative of the reactions involved due to the presence of the other reactive oxygen species.

The ESCA spectra in Figure 6.4 reveal the changes in the C_{1s} and O_{1s} core levels at electron take-off angles of 30 and 70^{o} of polycarbonate films after treatment with the effluent of a microwave oxygen discharge (60W, 2 torr). The increases in complexity of the C_{1s} signal and relative intensity of the O_{1s} envelope provide evidence for intensive oxygen uptake. The spectra for 15 minutes' exposure reveal that the extent of reaction is greater at $\theta=70^{o}$ and the surface specificity of the oxygen uptake is readily apparent from a comparison of the carbon:oxygen stoichiometries as displayed in Table 6.1. This trend is in essential agreement with that found for the radio-

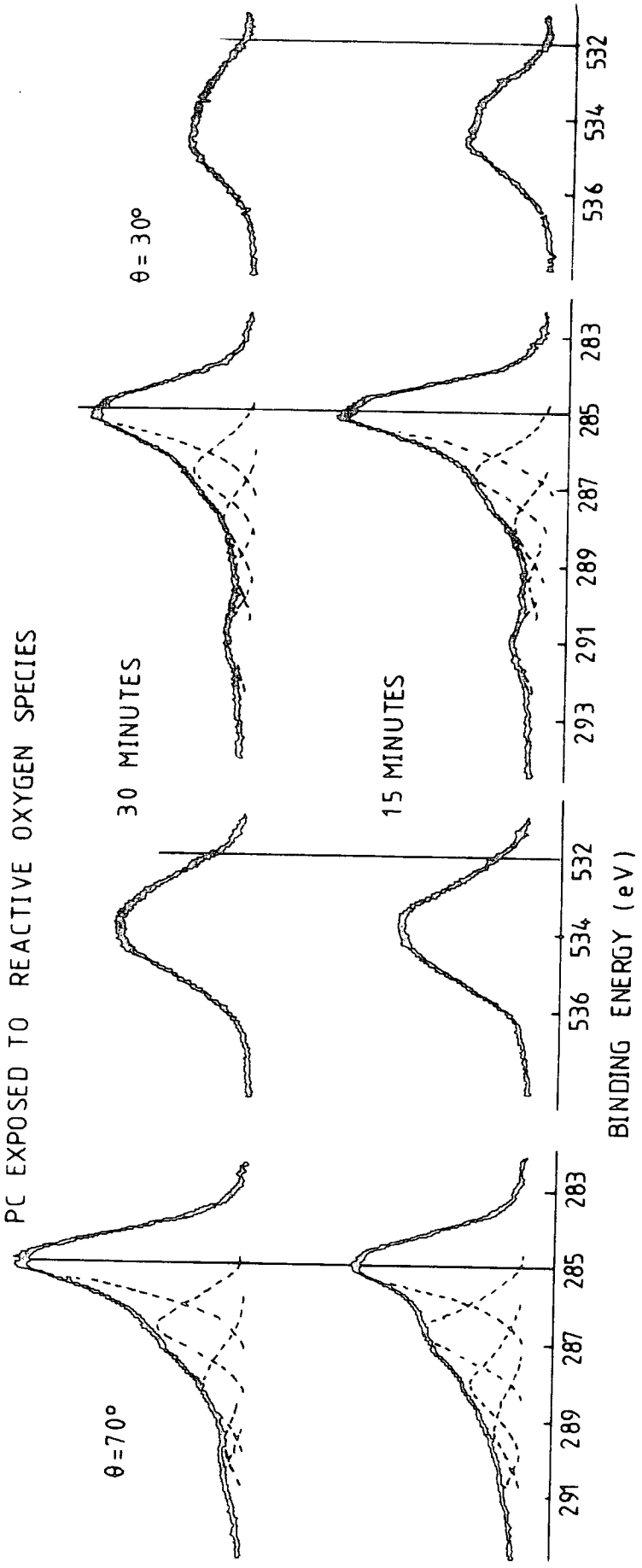

Figure 6.4 C_{1s} and O_{1s} core levels for polycarbonate samples exposed to the effluent of an oxygen microwave discharge.

frequency induced plasma oxidation of polymers.[182]

TABLE 6.1 C:O stoichiometries for polycarbonate films exposed to the effluent of an oxygen microwave discharge

	C:O stoichiometry	
Time	$\theta=30^{o}$	$\theta=70^{o}$
15 minutes	$C_1:O_{0.31}$	$C_1:O_{0.47}$

TABLE 6.2 C_{1s} components for polycarbonate films exposed to the effluent of an oxygen microwave discharge

		Total C_{1s}	C-H	C-O	C=O	O-C=O	CO_3	$\Pi\rightarrow\Pi^*$
	0	100	76	14	0	0	7	3
$\theta=70^{o}$	15	100	48	26	14	7	4.5	0.5
	30	100	61	22	10	2.5	4	0.5
	0	100	76	13	0	0	7	4
$\theta=30^{o}$	15	100	60	20	10	2.0	6	2.0
	30	100	58	20	11	4	5	2

The nature of the changes in C_{1s} envelope are revealed in the component analysis in Table 6.2. At a take-off angle of 70^{o} after 15 minutes' exposure, carbonyl and carboxylate features are evident contributing 14 and 7% respectively to the total C_{1s} intensity. The carbonate and $\Pi\rightarrow\Pi^*$ shake-up components have decreased in intensity indicating chain scission at the former and oxidation of the latter. Exposure for a further 15 minutes results in a decrease in oxygen content which is reflected by decreases in the contributions of the various oxidised carbon species and an increase in the C-H component at 285.0eV. This is representative of the ablation of the surface.

On examination of the data for comparable exposures for a take-off angle of 30^{o} the lower degree of reaction is readily apparent. The lesser extent of oxidative functionalisation is highlighted by the higher level of carbonate and shake-up features in comparison to those for $\theta=70^{o}$.

6.3.3 Singlet Oxygen ($^{1}\Delta O_{2}$)

The reactions of singlet oxygen ($^{1}\Delta O_{2}$) with polymers have been the centre of considerable interest in the literature.[188,202,203] For the study of such reactions with polymers in the solid state, $^{1}\Delta O_{2}$ is normally generated by means of a microwave initiated oxygen discharge.[199] To remove the atomic oxygen and ozone before the effluent from the discharge reaches the sample, mercury is continually distilled through the excitation region. The ring of mercuric oxide is formed on the sides of the quartz tube just beyond the microwave cavity. The oxygen atom concentration under these conditions is believed to be less than 10^{-4} of that for the singlet oxygen.[199]

The C_{1s} and O_{1s} core levels in Figure 6.5 ($\theta=70^{o}$) reveal the changes in the surface chemistry of polycarbonate films exposed to a stream of singlet oxygen (60W, 2 torr) for various periods of time. The increases in complexity of the C_{1s} envelope and intensity of the O_{1s} signal reveal extensive oxidation of the surface. The oxygen uptake is more apparent from a consideration of the relative O_{1s}/C_{1s} intensity ratios in Figure 6.6. For comparison the relevant data for an electron take-off angle of 30^{o} are also included. From these data it is clear that the oxygen uptake is greater for $\theta=70^{o}$ indicative of the surface specificity of the oxidative processes. It is

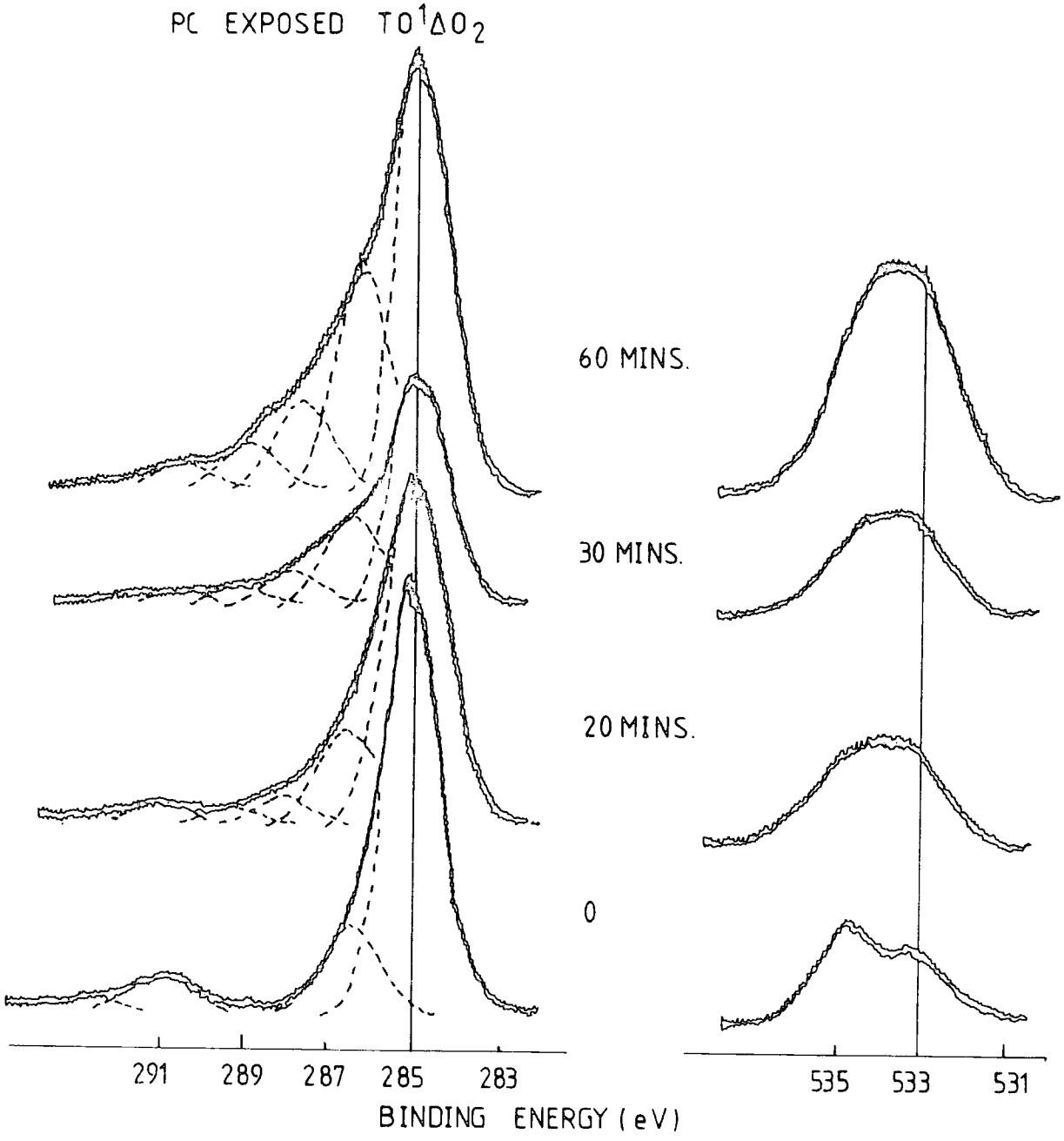

Figure 6.5 C_{1s} and O_{1s} core levels for polycarbonate films exposed to "Singlet Oxygen" for various periods of time ($\theta = 70^{o}$)

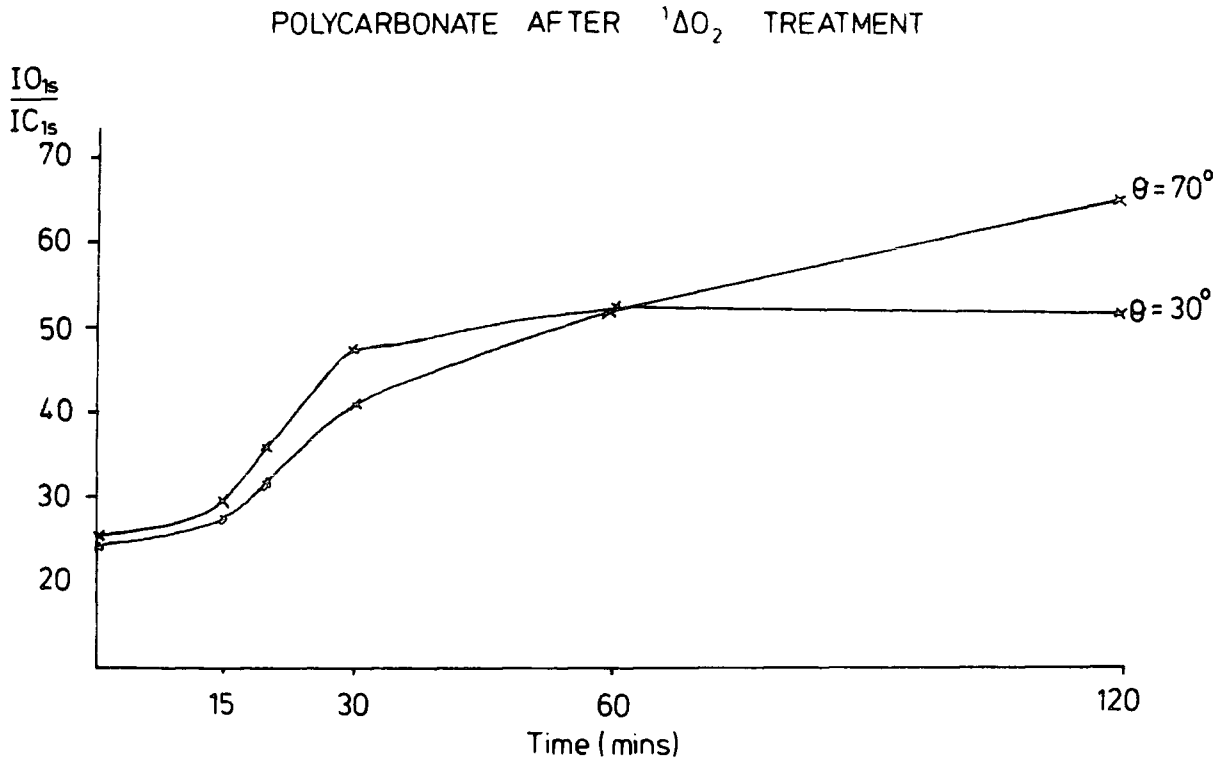

Figure 6.6 O_{1s}/C_{1s} intensity ratios for polycarbonate samples exposed to "Singlet oxygen" (θ=70 and 30°) for various periods of time.

also interesting to note that the oxygen uptake follows an autocatalytic mechanism with an induction period of ∿15 minutes. A steady state situation is reached after ∿60 minutes' exposure representative of the balance between oxidation processes and desorption of low molecular weight species.

Examination of the C_{1s} component analysis displayed in Figure 6.7 also reveals the autocatalytic nature of the reactions involved. Increases in the C-O, C=O and O-C=O functionalities are evident. The formation of the carbonyl component is a factor of ∿2 greater than the carboxylate group

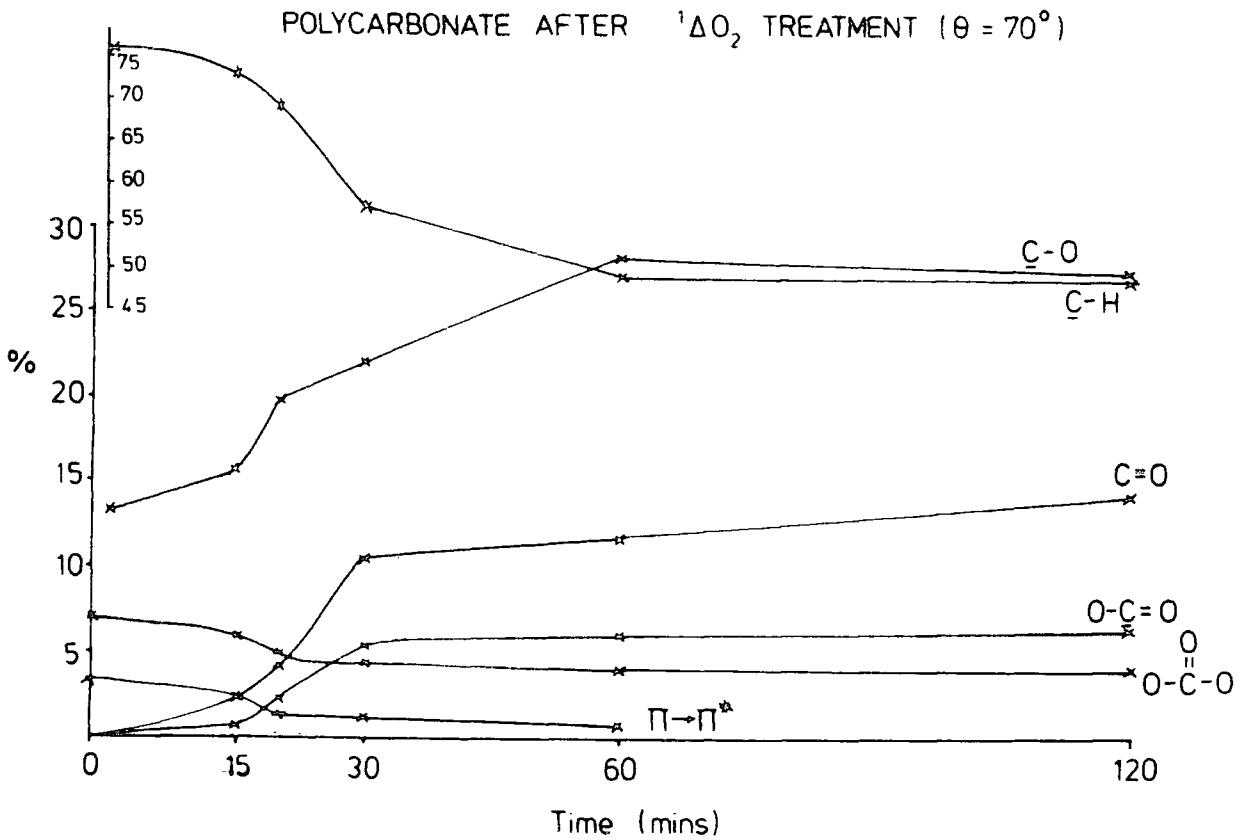

Figure 6.7 C_{1s} components for polycarbonate films exposed to "singlet oxygen" for various periods of time.

which contrasts with the results obtained for photooxidation (cf. Chapter Four) where the latter is more predominant than the former in a highly ozidised surface. The C-H, O-C-O and $\Pi \rightarrow \Pi^*$ shake-up components decrease in intensity autocatalytically. The latter functionality is not evident after $\sim$2 hours indicative of the loss of aromaticity during the oxidative processes.

It is of interest to compare the nature of the oxidised surface obtained for similar degrees of oxygen uptake for polycarbonate films exposed to the effluent of an oxygen microwave discharge with and without the continuous distillation of mercury

through the discharge region. The appropriate data is revealed in Table 6.3. There are distinct similarities in the distribution of the C_{1s} components for the two surfaces which indicates similar reaction mechanisms. The data in fact suggest that the "singlet oxygen" reaction is the same as that for the microwave initiated oxygen discharge degradation as described in the previous section but that it occurs at a much slower rate. The extent of oxidation in the subsurface ($\theta=30^{o}$) is greater for the exposure with continuous mercury distillation.

TABLE 6.3 Comparison of the C_{1s} components and O_{1s}/C_{1s} intensity ratios for polycarbonate films exposed to the effluent of an oxygen microwave discharge with and without continuous Hg distillation

Time	Total C_{1s}	C-H	C-O	C=O	O-C=O	CO_3	$\Pi\rightarrow\Pi^*$	O_{1s}/C_{1s}
15 minutes (without Hg)	100	48	26	14	7	4.5	0.5	0.63
120 minutes (with Hg)	100	48	27	14	6	5	0	0.65

The "singlet oxygen" exposures described above were carried out at $20^{o}C$. To investigate the effect of temperature on the induction period, polycarbonate films were oxidised at $60^{o}C$. The relative oxygen to carbon intensity ratios displayed in Figure 6.8 reveal the oxygen uptake for exposures at 20 and $60^{o}C$ ($\theta=70^{o}$). It is clear from these data that the induction period is not affected by elevating the temperature. However, when oxidation occurs the rate is dramatically increased and an equilibrium state is reached at much earlier stage. The contrast in the degree of oxidation at the two temperatures is reflected in Table 6.4 where the C:O stoichiometries for polycarbonate films for 60 minute exposures are displayed.

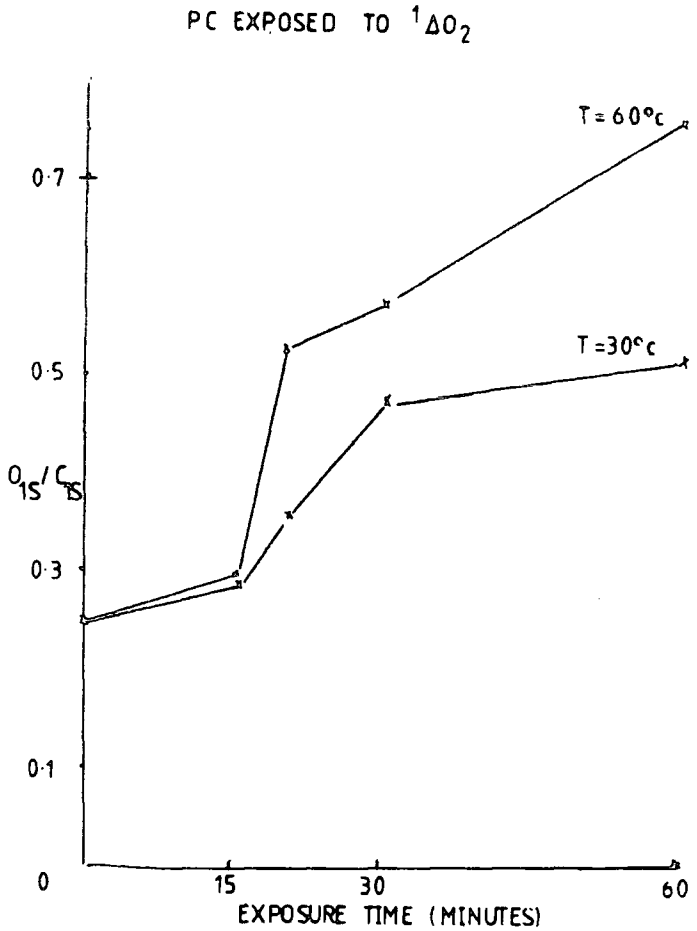

Figure 6.8 O_{1s}/C_{1s} intensity ratios for polycarbonate films exposed to "singlet oxygen" for various periods of time as a function of temperature.

TABLE 6.4 C:O stoichiometries for oxidised polycarbonate films (60 minutes' exposure)

Temperature	C:O stoichiometry
20	$C_1:O_{0.39}$
60	$C_1:O_{0.53}$

As noted above the nature of the oxidised polycarbonate surfaces for exposures to the microwave discharge effluent, with and without the continuous distillation of mercury vapour, are

remarkably similar. These data suggest that the mercury vapour does not remove oxygen atoms to a sufficient extent to prevent participation in the degradative processes. It has been reported in the literature that residual traces of atomic oxygen can lead to anomalous results in the quenching of singlet oxygen by hydrocarbons.[199] The results discussed above, therefore, appear to reflect the extremely small level of oxygen atoms reaching the sample. Previously reported studies in the literature,[204] where the removal of atomic oxygen relies solely on the reaction with mercury vapour may also suffer from reactions in the surface due to this species.

Residual traces of atomic oxygen may be removed by the continuous titration of nitrogen dioxide (NO_2) into the flow system beyond the discharge region. The reactions, described in the experimental section, will give rise to a weak green glow at the inlet valve when viewed in complete darkness. No such glow was observed in the experiments reported here. In the absence of sensitive instrumentation to detect weak chemiluminescent reactions, the amount of NO_2 required can only be obtained on a trial and error basis. Initial runs revealed that an autocatalytic reaction, although to a much lesser extent, was still occurring. This suggested that atomic oxygen was still present but with a greatly reduced concentration.

On increasing the amount of NO_2 added to the system, no change in the C_{1s} and O_{1s} core levels could be detected even after 5 hours' exposure. The N_{1s} core level was examined to reveal any contamination arising from the NO_2, however no signal arising from this level could be detected. This strongly suggests that singlet oxygen does not react with Bisphenol A

polycarbonate under the conditions of these experiments. However, it is possible that the amount of NO_2 titrated may have significantly reduced the singlet oxygen concentration via the following reaction:

$$NO_2 + 3(^1\Delta O_2) \longrightarrow NO_2^* + 3O_2$$

A white glow may be emitted due to a slow energy transfer process.[199] No glow was detected but to ensure that reactive oxygen species (i.e. $^1\Delta O_2$) were reaching the sample, solution cast films of cis-polyisoprene, well known for its reactivity with singlet oxygen,[205] were placed downstream of the polycarbonate samples.

Hydroperoxides are believed to be formed in the reaction of singlet oxygen with olefins possessing an allylic hydrogen (the ene reaction) and cis-polyisoprene is thought to react in this manner.[205] The ESCA spectra in Figure 6.9 reveal the C_{1s} and O_{1s} core levels before and after $^1\Delta O_2$ treatment for cis polyisoprene films placed downstream of the polycarbonate sample position. Although a small degree of surface oxidation is evident from the spectra for the unexposed material, oxygen uptake on $^1\Delta O_2$ treatment is readily apparent. The intensity of the $\Pi \rightarrow \Pi^*$ shake-up component (diagnostic of the double bonds in the system) as evidenced by the expanded regions of the C_{1s} levels, decreases indicative of oxidation occurring at the double bonds of cis-polyisoprene.

The nature of the changes in surface chemistry are revealed in Table 6.5. Decreases in the intensities of the $\underline{C}$-H and $\Pi \rightarrow \Pi^*$ components are concomitant with increases in the $\underline{C}$-O and $>\underline{C}$=O functionalities and consequently an increase in the relative O_{1s}/C_{1s} intensity ratio. The presence of $^1\Delta O_2$ reaching

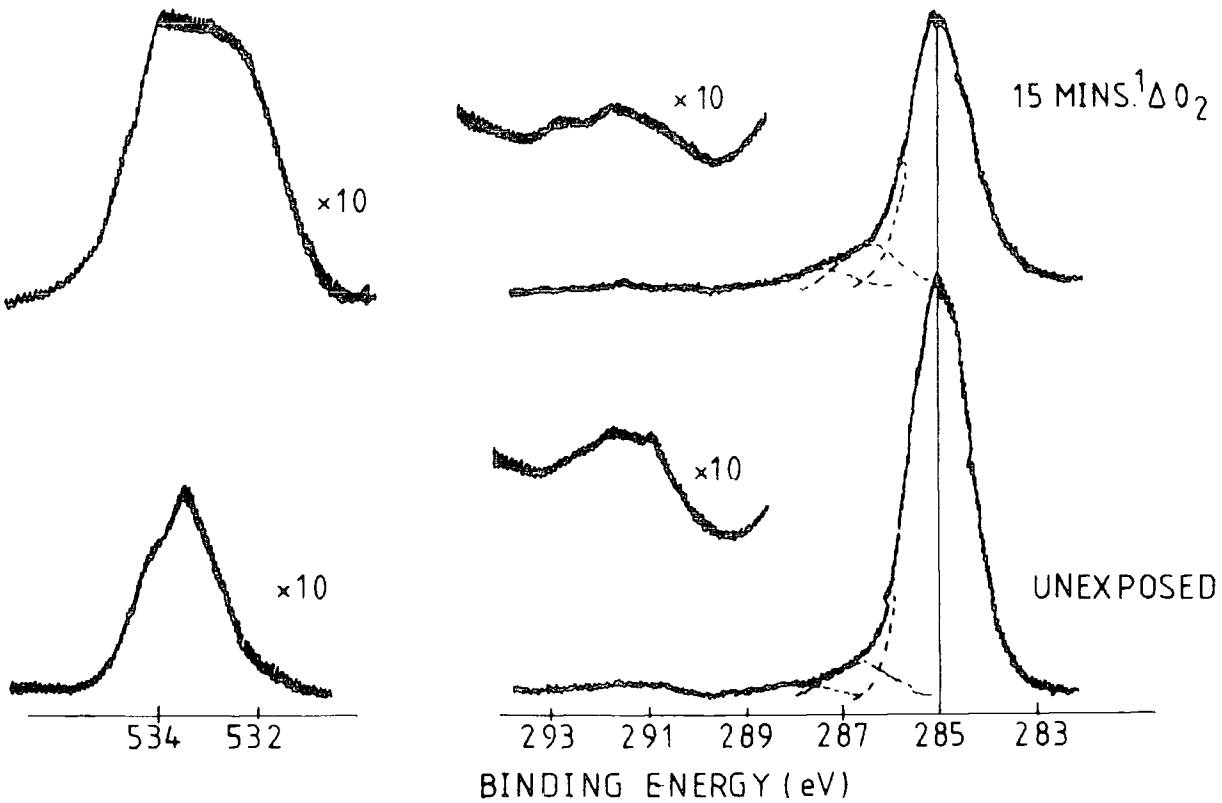

Figure 6.9 C_{1s} and O_{1s} core levels for cis-polyisoprene and cis-polyisoprene exposed to "singlet oxygen".

TABLE 6.5 C_{1s} components and O_{1s}/C_{1s} intensity ratios for cis-polyisoprene and cis-polyisoprene exposed to $^1\Delta O_2$

Time (Minutes)	Total C_{1s}	C-H	C-O	C=O	O-C=O	CO_3	$\Pi \rightarrow \Pi^*$	O_{1s}/C_{1s}
0	100	91	5	1	0	0	3	0.062
15	100	83	12	4	0	0	1	0.237

the sample region is thus confirmed. The data, therefore, suggest that under the present experimental conditions singlet oxygen does not react with Bisphenol A polycarbonate and conseq-

uently does not play a role in the oxidative degradation of this polymer and confirm the results for solution phase studies.

6.3.4 Atomic Oxygen

The results discussed in the previous section indicated the dramatic influence on the degradative mechanisms of polycarbonate surfaces when low levels of atomic oxygen are present in the effluent from a microwave oxygen discharge. It is, therefore, of interest to examine the changes in the surface chemistry of polycarbonate films exposed to a low level of pure atomic oxygen in a flow system of similar design to the singlet oxygen generator. This was achieved by the uv photolysis of N_2O as described in Section 6.2.

The C_{1s} and O_{1s} core levels in Figure 6.10 reveal the changes in the surface on exposure of polycarbonate films to oxygen atoms for various periods of time. These spectra correspond to an electron take-off angle of 70^{o}. The characteristic 2:1 doublet of the O_{1s} signal changes on exposure for 60 minutes to an envelope not as well defined. The nature of the contributions to the C_{1s} envelope are more apparent from the component analysis in Table 6.6. It is clear from these data that the C-H and $\pi \rightarrow \pi^*$ components are essentially unchanged and only small differences from the initial values for the C-H, C-O and O-$\overset{O}{\overset{\|}{C}}$-O functionalities are evident.

Examination of the corresponding O_{1s}/C_{1s} intensity ratios reveal that the intensity of the oxygen signal decreases with increasing exposure time. Although a component analysis of the O_{1s} core level is difficult, an approximate fit may be obtained by employing two peaks corresponding to O-C and O=C environments and these data and those for the total O_{1s}/C_{1s} ratios

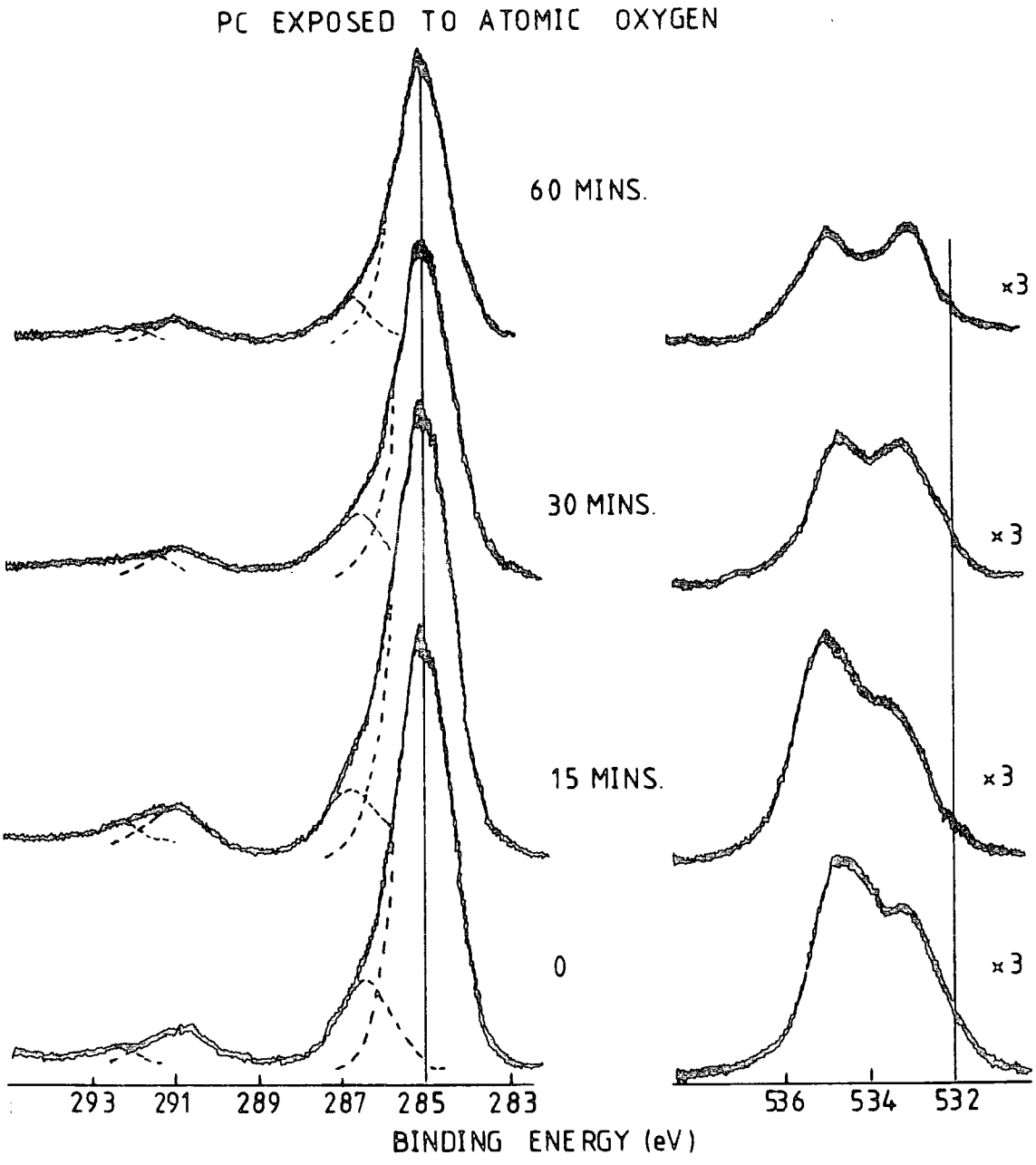

Figure 6.10 C_{1s} and O_{1s} core levels for polycarbonate films exposed to atomic oxygen for various periods of time ($\theta=70^{o}$)

TABLE 6.6 C_{1s} components for polycarbonate films exposed to atomic oxygen

Time	Total C_{1s}	C-H	C-O	C=O	O-C=O	CO_3	$\Pi \rightarrow \Pi^*$
0	100	79	12	0	0	6	3
15	100	79	13	0	0	5	3
30	100	80	12	0	0	5	3
60	100	81	11	0	0	5	3

are shown in Figure 6.11. It is evident that after 60 minutes' exposure that the O-C and O=C intensities have decreased and the relative ratio between the two environments is ∿1.7:1 (cf. the 2:1 ratio for the starting material).

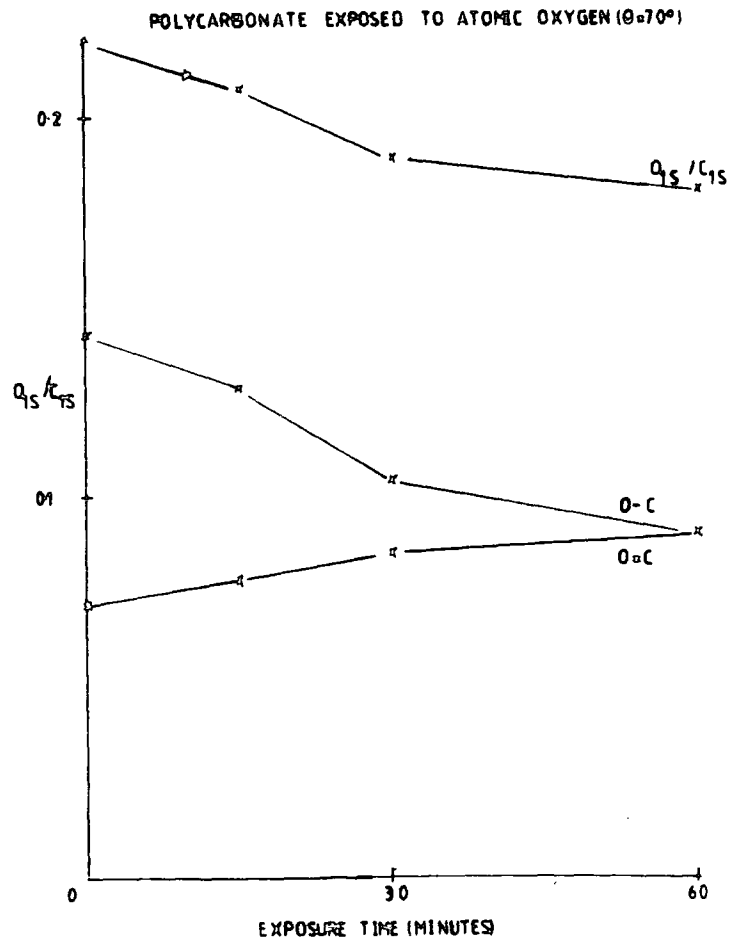

Figure 6.11 Changes in the O_{1s}/C_{1s} intensity ratios and the O-C and O=C components of the O_{1s} signal for polycarbonate films exposed to atomic oxygen ($\theta=70^{\circ}$)

The corresponding spectra for a take-off angle of 30° were recorded immediately after those at 70°. However, the analysis of the O_{1s}/C_{1s} ratios suggested that anomalous results were being obtained (i.e. inconsistent increases and decreases in the intensity of the O_{1s} signal). On rerunning the spectra for $\theta=70^{\circ}$ after 60 minutes' exposure (i.e. the spectra were recorded in the sequence $\theta=70^{\circ}$, 30°, 70°) it was found that the O_{1s}/C_{1s} intensity ratio had increased relative to the first run. This suggested that the X-ray irradiation of the sample was initiating a reaction in the surface regions and consequently fresh samples are required for an angular dependence study. The data in Figure 6.12 reveal the changes in the O_{1s}/C_{1s} ratios and the respective contributions arising from O-C and O=C environments. It can be readily seen that there are similar trends for $\theta=30^{\circ}$ and $\theta=70^{\circ}$.

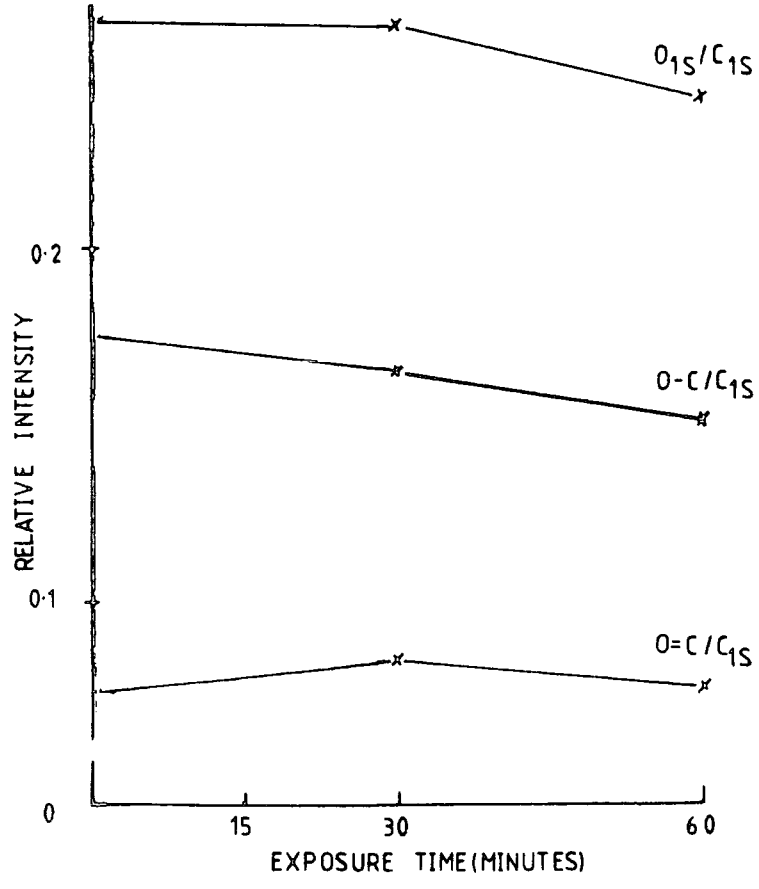

Figure 6.12 Changes in the O_{1s}/C_{1s} intensity ratios and the O-C and O=C components of the O_{1s} signal for polycarbonate films exposed to atomic oxygen ($\theta=30^{\circ}$)

To investigate the effect of X-rays on the exposed surface the C_{1s} and O_{1s} core levels at $\theta=70^{o}$ were recorded as a function of X-ray irradiation time for a polycarbonate sample exposed to atomic oxygen for 60 minutes. The relevant C_{1s} component analysis is shown in Table 6.7. The corresponding changes in the O_{1s} signal are revealed in Figure 6.13. After ∿30 minutes' exposure to the X-rays the proportions of the C_{1s} components are the same as the starting material. The O_{1s}/C_{1s} intensity ratio increases with time and approaches the value for the unexposed polycarbonate. However, the O-C/O=C ratio does not obtain the characteristic 2:1 value.

TABLE 6.7 C_{1s} components for polycarbonate films exposed to atomic oxygen for 1 hour as a function of X-ray irradiation time

X-ray irradiation time (minutes)	Total C_{1s}	C-H	C-O	C=O	O-C=O	CO_3	$\Pi\rightarrow\Pi^*$
0	100	81	11	0	0	5	3
12	100	78	13	0	0	6	3
22	100	78	13	0	0	6	3
32	100	79	12	0	0	6	3

The data suggest that the X-rays are interacting with a labile species in the surface. It is not possible to determine the nature of this species from the data presented above. It has been reported that the highly oxygenated peroxide link in dibenzoyl peroxide is very unstable to the $Mg_{K\alpha}$ radiation employed in the ESCA experiment[198] and it is possible that a labile peroxide feature is formed in the

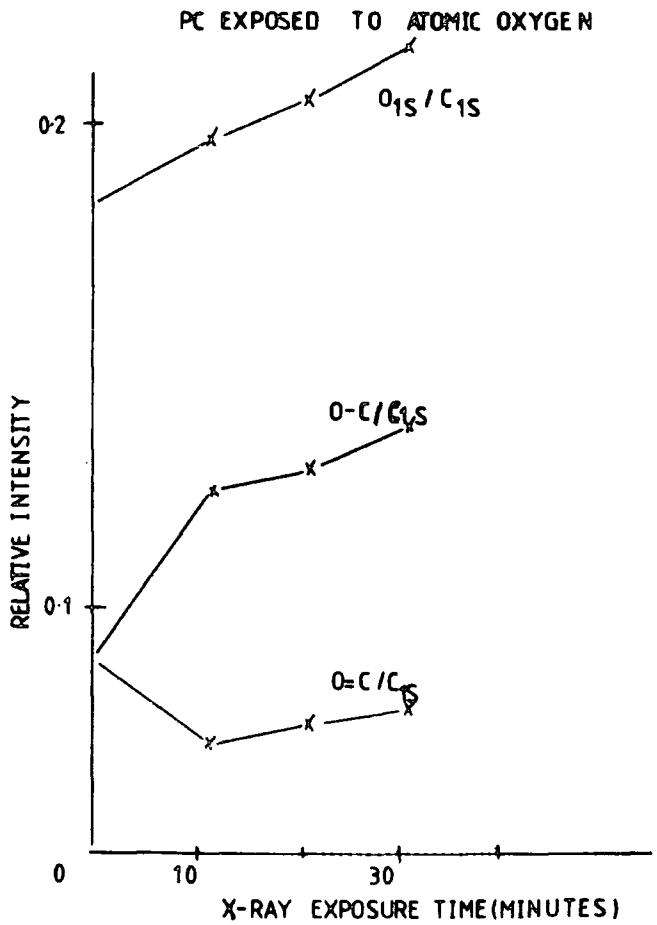

Figure 6.13 Changes in the O_{1s}/C_{1s} intensity ratios and the O-C and O=C components of the O_{1s} signal, for a polycarbonate film exposed to atomic oxygen for 1 hour, as a function of X-ray irradiation time ($\theta=70^{o}$).

surface of polycarbonate.

Overall the reaction of polycarbonate with the effluent of an oxygen microwave discharge containing a low level of oxygen atoms is an extremely complex process arising from a combination of singlet oxygen, atomic oxygen and molecular oxygen interactions.

CHAPTER SEVEN

SURFACE ASPECTS OF THE NATURAL AND ARTIFICIAL PHOTOAGING OF POLYSTYRENE FILMS AS REVEALED BY ESCA

7.1 Introduction

One of the most extensively investigated polymers, with respect to photodegradation and photooxidation, is polystyrene. A considerable body of literature[49,204,206-217] has been published over the years but a consistent theory has failed to emerge and in some cases contradictory hypotheses have been presented. This accentuates the complexity of the mechanisms involved.

Previous studies on the photooxidation of polystyrene films have primarily involved the monitoring of changes in bulk chemistry.[204,206-217] In order to obtain information pertaining to the oxidative processes involved in natural weathering, model studies should employ uv radiation of wavelengths >290nm. As such the reported investigations utilising wavelengths <290nm are of limited value as different mechanisms may well be involved. For example 254nm radiation is able to directly excite the pendant phenyl groups of polystyrene:[49,204,213-217] a situation which is unlikely to occur with sunlight at the earth's surface. It is currently believed that the initiation of photooxidation for λ>290nm is due to the absorption of light by chromophoric impurities, e.g. hydroperoxides[218,219] and carbonyl groups.[218-220] The possibility of oxygen-polymer charge-transfer complexes, extending the uv absorbance tail of polystyrene above 300nm, being involved in the initiation stage has also been considered.[204,213]

As all solids interact with their environment via the surface, a knowledge of the changes in chemistry at the gas/solid interface is of prime importance. This chapter, therefore, considers in some detail the surface aspects of the photooxidation

of polystyrene films as revealed by ESCA. Model studies employing wavelengths >290nm have been compared to the data for natural exposures.

7.2 Experimental

Orientated polystyrene films (Dow Chemical Co.) (25μm) were exposed to uv radiations (λ>290nm) in atmospheres of oxygen (dynamic) and air (static) as previously described in Chapters Four and Five. Surface hydroperoxide formation was followed by the SO_2 labelling technique (cf. Chapter Four).

Natural weathering exposures were carried out in Dhahran, Saudi Arabia by the courtesy of Dr. J. Peeling. Two starting dates were employed, namely September 1980 and April 1981.

ESCA spectra for each sample were obtained on an AEI ES200 B spectrometer employing $Mg_{k\alpha_{1,2}}$ radiation. The FWHM for the $Au_{4f_{7/2}}$ level at 84.0 eV, used for calibration purposes, was 1.2 eV. Line shape analyses were carried out with the aid of a DuPont 310 curve resolver. Binding energies were referenced to the C-H component at 285.0 eV.

7.3 Results and Discussion

7.3.1 Reactions in Oxygen

(a) Studies as a function of light intensity and irradiation time

As a starting point for the investigation of the changes in surface chemistry during photooxidation (λ>290nm) it is convenient to consider the irradiation of polystyrene films in a flowing oxygen atmosphere at a photon flux of 10 $Whm^{-2}h^{-1}$. The relevant C_{1s} and O_{1s} core levels are displayed in Figure 7.1.

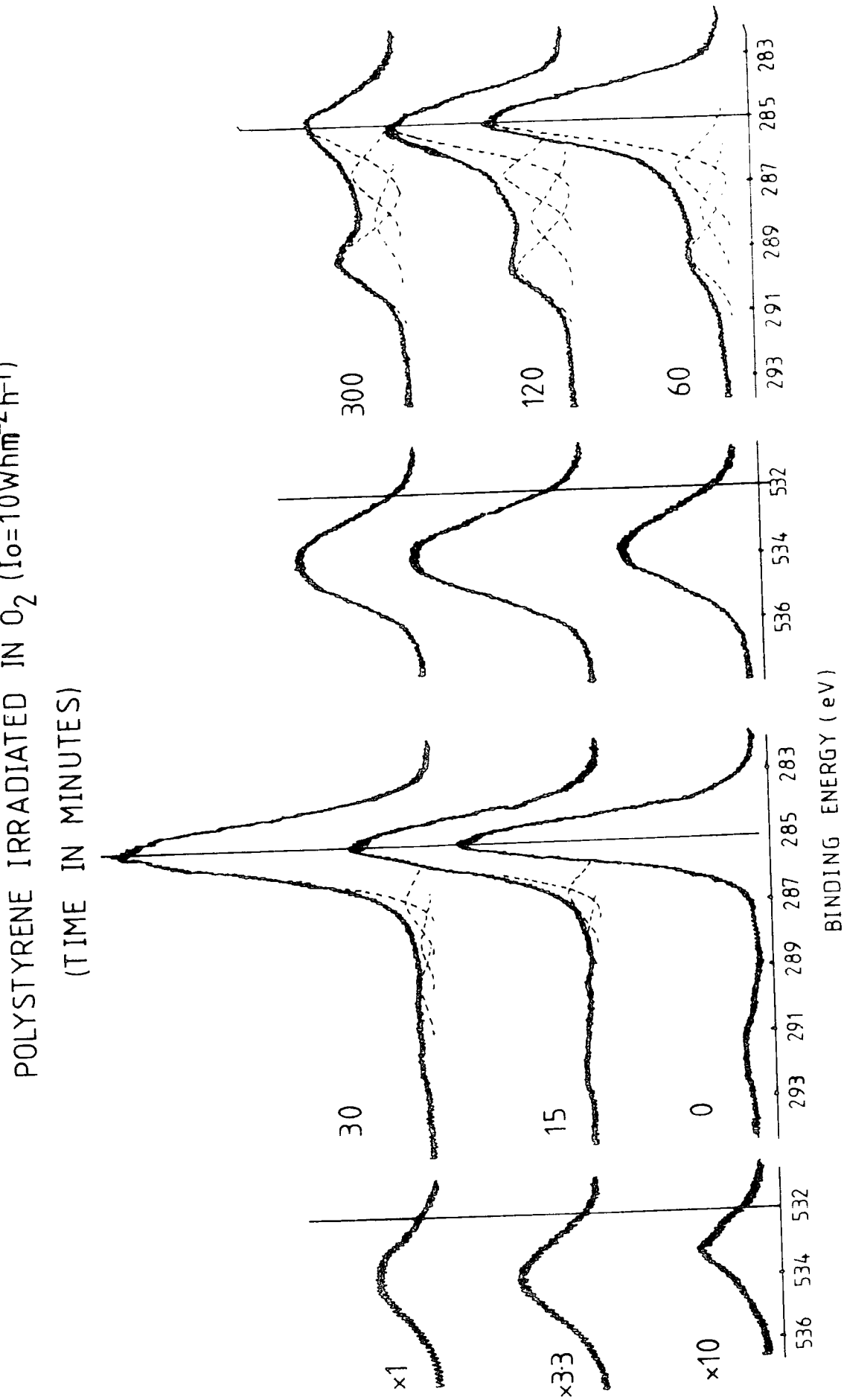

Figure 7.1 C_{1s} and O_{1s} core levels for polystyrene films exposed to uv irradiation (λ>290nm, Io=10Whm^{-2}h^{-1}) for varying periods of time

From a starting C_{1s} profile consisting of a main photoemission peak at 285.0 eV (arising from the C-H components in the backbone chain and pendant phenyl groups) and a $\pi \rightarrow \pi^*$ shake-up satellite centred at ∿292.3 eV (diagnostic of the aromaticity in the system) additional peaks appear during irradiation. These components arise from C-O, >C=O and O-C=O functionalities and are indicative of extensive photooxidation. The corresponding O_{1s} signal of low intensity in the unexposed material indicates that a small degree of surface oxidation is present although no corresponding C_{1s} component could be detected. The intensity of this signal increases on exposure.

Studies of the photooxidation of polystyrene utilising wavelengths >300nm have shown that an induction period exists for oxygen uptake.[209,214] It can be clearly seen from a consideration of the relative O_{1s}/C_{1s} intensity ratios displayed in Figure 7.2 that an induction period is not evident for photooxidation (λ>290nm) in the surface regions. Oxygen incorporation into the surface is rapid and this is also evidenced by the contribution to the total C_{1s} intensity made by the oxidised carbon species as is also shown in Figure 7.2.

After two hours irradiation there is a marked decrease in the rate of oxygen uptake and is indicative of a steady state situation representing a balance between further photooxidation and the evolution of low molecular weight species. From a knowledge of the appropriate instrumental sensitivity factors the C:O stoichiometry after ∿2 hours' irradiation is ∿2:1.

The nature of the oxidative functionalisation is more apparent from the examination of the C_{1s} component analysis in Figure 7.3 for the spectra in Figure 7.1. The C-H component

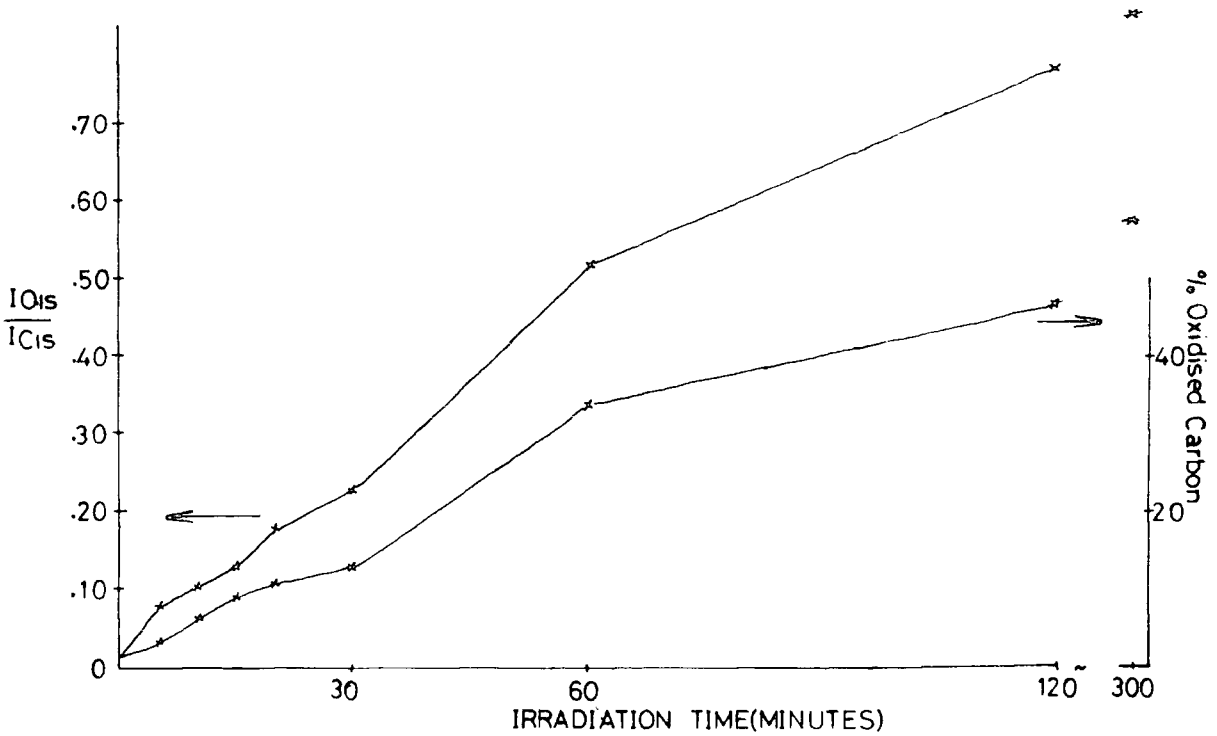

Figure 7.2 O_{1s}/C_{1s} intensity ratios and % oxidised carbon atoms contributing to the total C_{1s} signal for the spectra in Figure in 7.1.

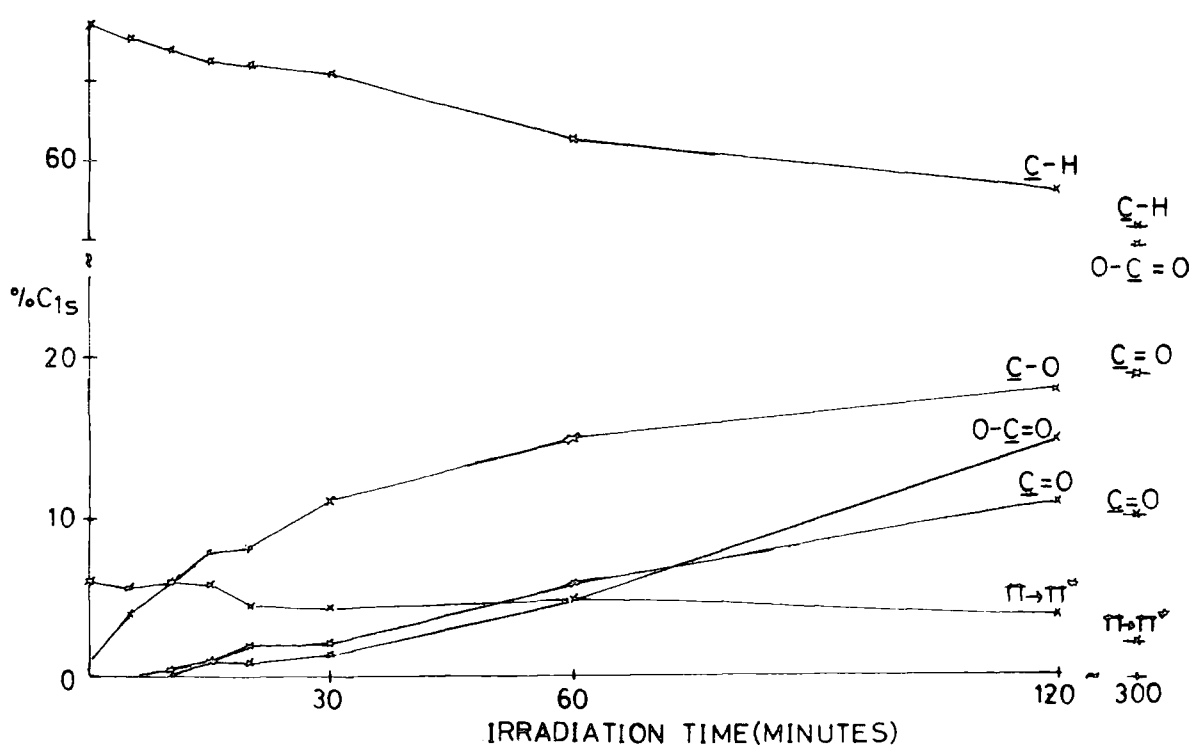

Figure 7.3 C_{1s} component analysis for the spectra in Figure 7.1.

(carbon not directly bonded to oxygen) decreases in intensity with increasing irradiation time. There are concomitant increases in C-O, C=O and O-C=O functionalities and a decrease in the $\Pi \rightarrow \Pi^*$ shake-up satellite. The extent of oxidative functionalisation and the loss of shake-up structure are indicative of the oxidation of the pendant aromatic ring. It has been suggested by Kovačević *et al*[214] that oxidation of the benzene ring may occur during longwave length irradiation (λ>300nm) of polystyrene films and the data discussed above provide confirmatory evidence that such a reaction is present in the surface regions at least.

A feature of the bulk photooxidation of polystyrene at wavelengths >290nm, that has been reported in the literature, is the presence of an induction period.[208,214] The oxygen uptake in the surface regions, as previously noted above, does not indicate an induction period, however, examination of the formation of C=O and O-C=O functionalities, as shown in Figure 7.3, reveal that the former appear after ~10 minutes' exposure and the latter after ~15 minutes. The initial oxygen uptake may therefore reflect the formation of hydroperoxides and this is considered in greater detail in the next section.

For comparison purposes Figure 7.4 shows the core level spectra for polystyrene films irradiated for varying times at a higher photon flux of 52.5 $Whm^{-2}h^{-1}$. A significantly greater extent of oxidation is apparent for a given irradiation time compared to the lower photon flux.

The component analysis in Figure 7.5 reveals the same trend with a much higher build up of C-O and O-C=O structural features at earlier stage than for the low lamp intensity.

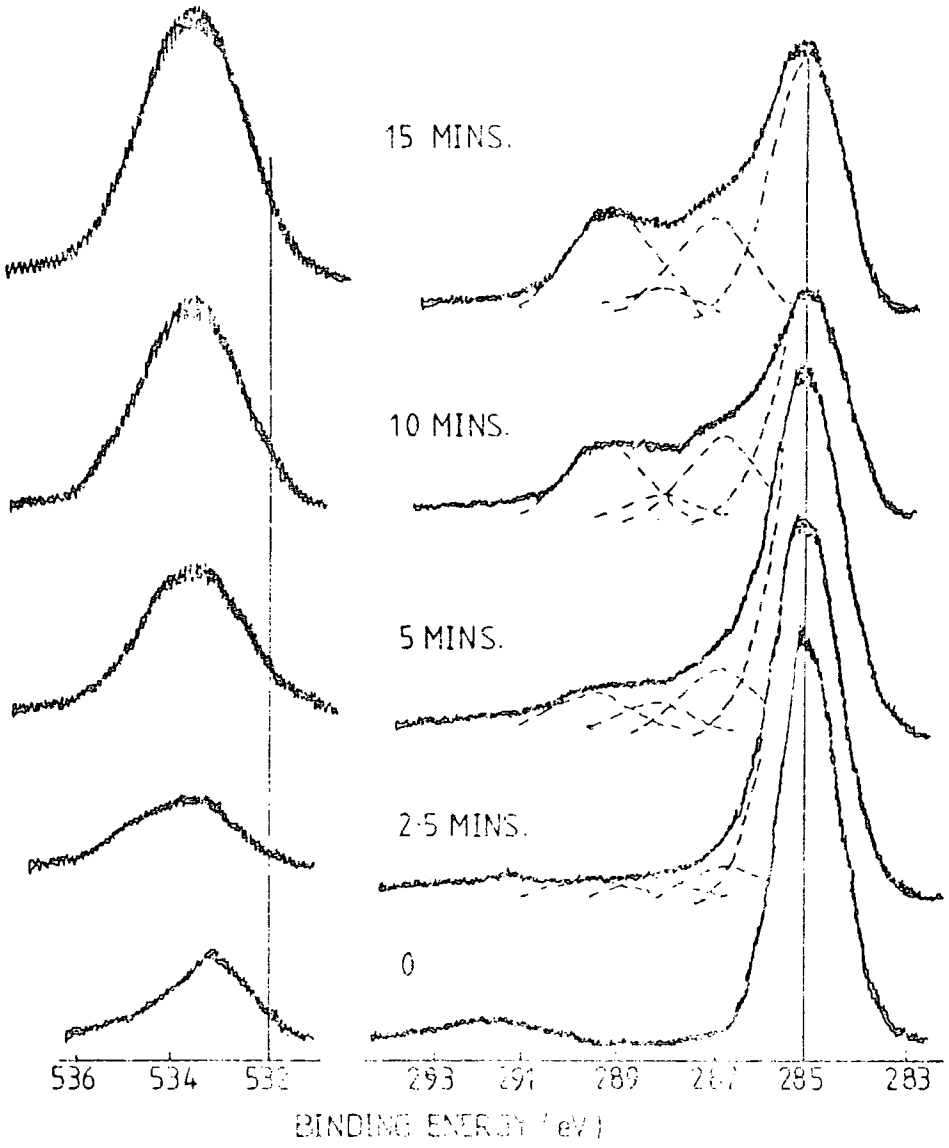

Figure 7.4 C_{1s} and O_{1s} core levels for polystyrene films irradiated in O_2 (λ>290nm, Io=52.5 $Whm^{-2}h^{-1}$)

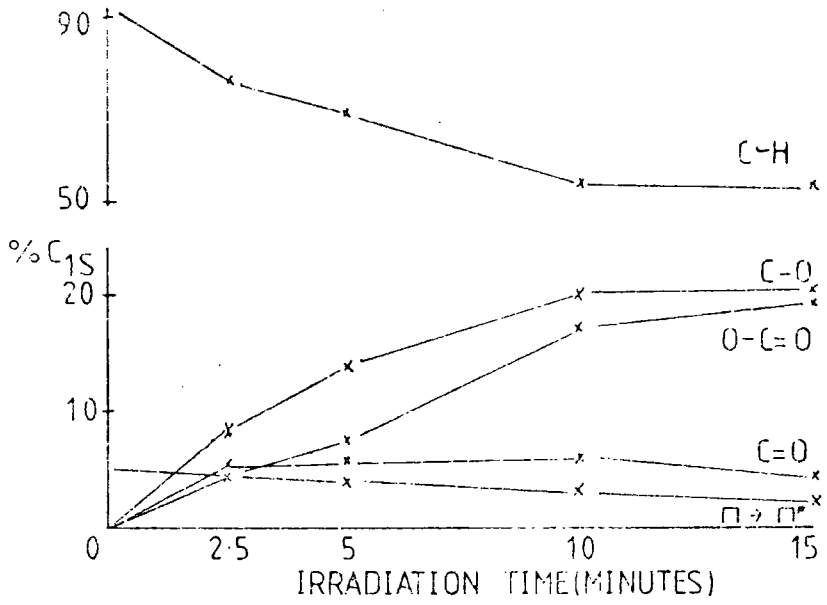

Figure 7.5 C_{1s} components for the spectra in Figure 7.4.

It is of interest to draw a comparison in terms of functionality distribution and oxygen uptake for comparable total fluxes received for samples irradiated at the higher and lower lamp intensities and this is shown in Table 7.1. It can be readily seen that the extent of oxidative functionalisation, in particular the levels of O-C=O groups, and hence the intensity of the oxygen signal are greater at the higher photon flux. These data suggest that the initiation mechanisms for photo-oxidation are very sensitive to the intensity of radiation and that the nature of the oxidised surface is not linearly dependent on the level of the incident flux. This becomes more apparent from a consideration of the data presented in Figure 7.6 where the various C_{1s} components for polystyrene films irradiated for a fixed period of time (15 minutes), are displayed

as a function of the incident photon flux.

TABLE 7.1 Component distributions and oxygen uptakes for polystyrene films exposed to similar total photon fluxes at high and low lamp intensities.

	Total C_{1s}	C-H	C-O	C=O	O-C=O	$\Pi \rightarrow \Pi^*$	O_{1s}/C_{1s}
60 minutes ($10 Whm^{-2} s h^{-1}$)	100	64	15	6	10	5	0.52
10 minutes ($52.5 Whm^{-2} s h^{-1}$)	100	54	20	6	17	3	0.73

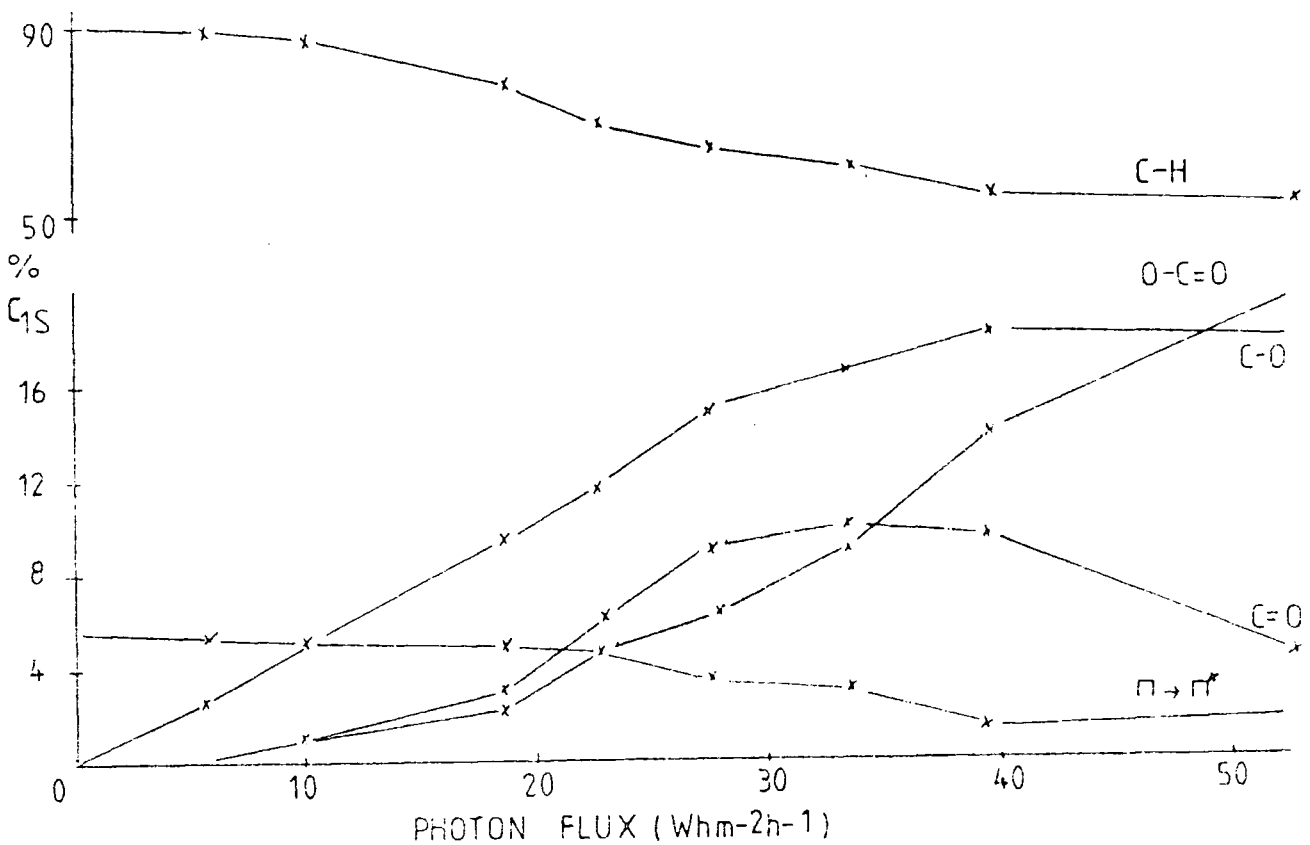

Figure 7.6 C_{1s} components for polystyrene films irradiated for 15 minutes in oxygen as a function of photon flux

The decrease in C-H and increase in C-O functionalities occur steadily with increasing photon flux although they both appear to reach a constant level at $\sim 39 Whm^{-2}h^{-1}$. Of particular interest are the formation of the C=O and O-C=O components. The induction period as evidenced from the data in Figure 7.3 is also apparent in the present case. The level of carbonyl functionalities present after 15 minutes' exposure is greater than that for the carboxylate for increasing fluxes up to $\sim 33\ Whm^{-2}h^{-1}$. The intensity of the former then decreases with increasing photon flux whilst the latter continues to rise. The $\Pi \rightarrow \Pi^*$ shake-up satellite, diagnostic of the aromaticity present in the system, is also seen to decrease. It is interesting to note that the centroid of this peak tends to move to lower binding energy with increasing flux. A similar situation also exists for irradiations as a function of time (i.e. at $10 Whm^{-2}h^{-1}$ with increasing time). These observations coupled with the fact that although the surface is extensively oxidised the intensity of this component tends to be relatively high, may be consistent with the formation of carbonate structural features.

(b) Surface Hydroperoxide Formation

The formation and subsequent decomposition of hydroperoxides are believed to be of primary importance in the bulk photooxidation of polystyrene.[218,219] As it was noted above, the oxygen uptake during the initial stages of irradiation was reflected by an increase in the intensity of the C-O component in the C_{1s} spectra. This may be indicative of the formation of hydroperoxides in the surface. In Chapter Four a technique for the labelling of these groups by the direct reaction with SO_2 was

described enabling a semi-quantitative study of surface hydroperoxide formation to be made. This technique has been utilised to study the role of hydroperoxides in the surface photooxidation of polystyrene films (λ>290nm, 10 $Whm^{-2}h^{-1}$).

The ESCA spectra in Figure 7.7 reveal the S_{2p} core levels for photooxidised films exposed to sulphur dioxide. Although four component peaks are apparent, the spin-orbit splitting of the S_{2p} level gives rise to a doublet due to contributions from $S_{2p_{1/2}}$ and $S_{2p_{3/2}}$ levels in the ratio of 1:2, only two chemical environments of sulphur are present. These correspond to sulphones ($\sim$168.0 eV) and sulphates ($\sim$169.2 eV): the latter arising from the reaction of SO_2 with hydroperoxides.

From a knowledge of the instrumentally dependent sensitivity factors the intensity of the sulphate component may be directly related to the hydroperoxide level in the surface (i.e. C-OOH) and the data in Figure 7.8 reveal the formation of these groups as a function of time. A low level of functionalisation in the unexposed material is present, but on exposure it rapidly increases and reaches a maximum after $\sim$30 minutes. The growth in the carbonyl component is also shown in Figure 7.8 for comparison. It is readily apparent that the hydroperoxide level reaches its maximum whilst the C=O functionality has only attained $\sim$20% of the ultimate value. These data confirm that hydroperoxides are formed in the initial stages of surface photooxidation of polysryrene films.

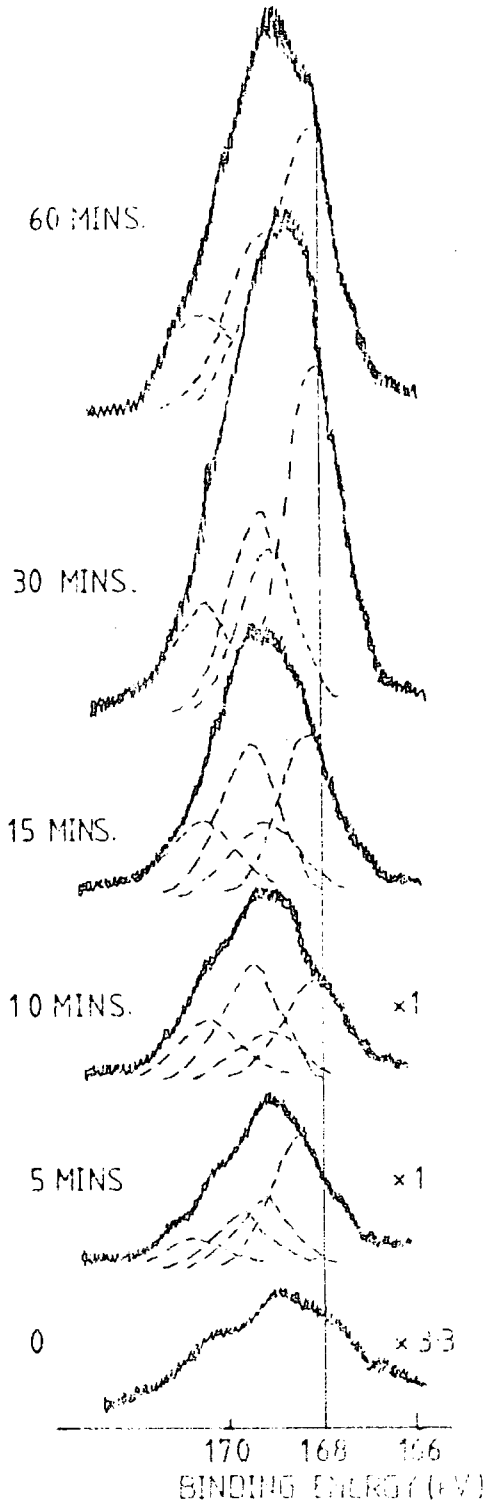

Figure 7.7 S_{2p} core levels for photooxidised polystyrene films exposed to SO_2.

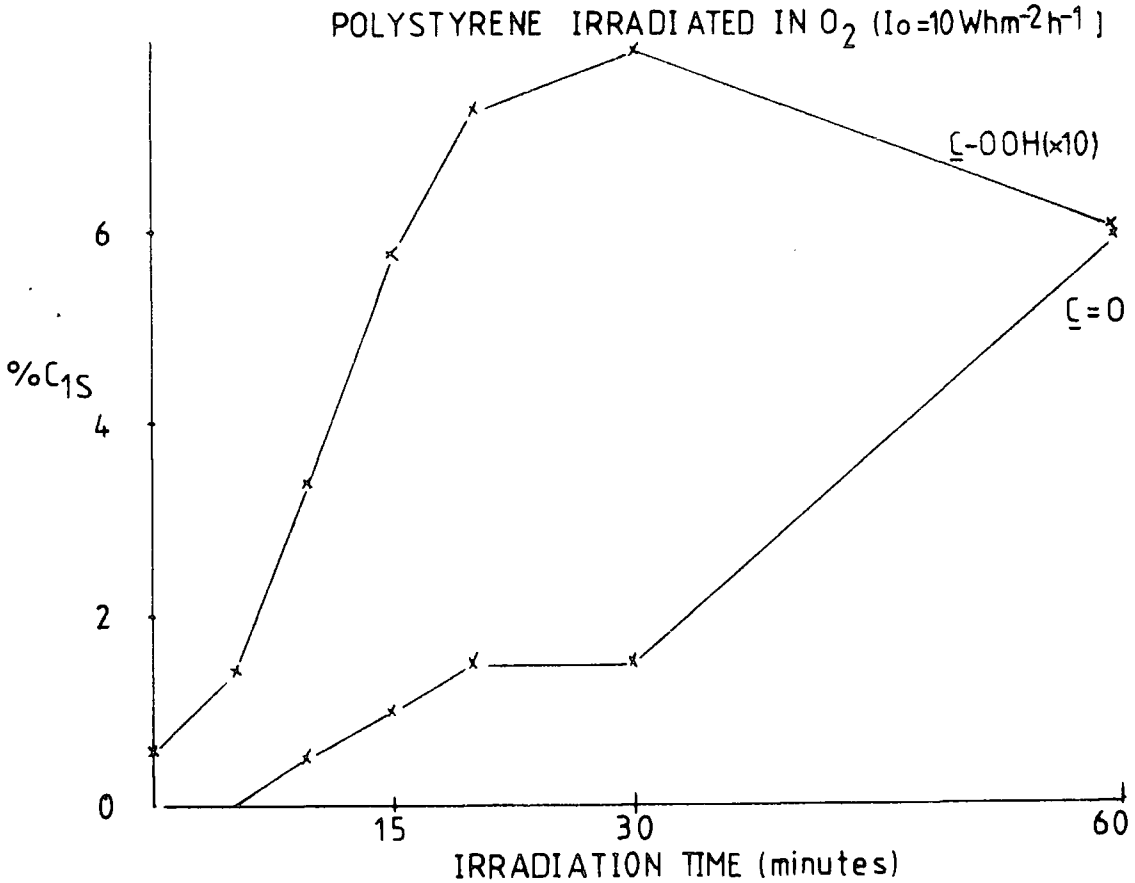

Figure 7.8 C-OOH levels in the surface of photooxidised polystyrene films (I_o = 10 Whm^{-2}h^{-1})

(c) Surface Chemistry as a function of Temperature

The experimental conditions employed in the literature for photooxidation studies can vary considerably, e.g. photon flux and temperature. The former has been considered in relation to polystyrene films above and in this section the influence of elevated temperature on the nature of the surface chemistry during photooxidation.

The data in Table 7.2 reveal the distributions of the various C_{1s} components and the relative O_{1s}/C_{1s} intensity ratios for polystyrene films irradiated with a photon flux of 52.5 Whm^{-2}h^{-1} for various periods of time at 30°, 50° and 70°C.

TABLE 7.2 Comparison of the C_{1s} components and O_{1s}/C_{1s} intensity ratios for polystyrene films irradiated in O_2 (Io = 52.5 $Whm^{-2}h^{-1}$) as functions of temperature and time.

T (^oC)	Time (minutes)	Total C_{1s}	C-H	C-O	C=O	O-C=O	$\Pi \rightarrow \Pi^*$	O_{1s}/C_{1s}
30	2.5	100	76	8	5	6	5	0.2
	5	100	69	14	6	8	3	0.46
	10	100	54	20	6	17	3	0.73
	15	100	0.53	21	4	20	2	0.80
50	2.5	100	83	8	2.5	2.5	4	0.2
	5	100	70	14	4	9	3	0.44
	10	100	58	17	6	17	2	0.65
	15	100	49	22	5	22	2	0.77
70	2.5	100	83	8	2	3	4	0.16
	5	100	74	11	5	7	3	0.38
	10	100	58	19	4	17	2	0.71
	15	100	55	22	3	18	2	0.75

On increasing the temperature from 30^o to 50^oC the main difference in the component distribution is seen to arise in the increased intensity of the carboxylate functionality at the higher temperature. At 70^oC this level is reduced to below that at 30^oC. These results indicate that temperature under the conditions of the experiment has only a small effect. This may well arise as a result of the balance between rate processes leading to oxidative functionalisation and desorption of low molecular weight materials from the surface. Indeed the data

in Table 7.2 appear to show that the oxidative processes are enhanced on increasing the temperature to 50°C from 30°C whereas desorption rates are enhanced at 70°C.

(d) The role of singlet oxygen ($^1\Delta O_2$) in the surface oxidation of polystyrene films

The results discussed above revealed that the irradiation of polystyrene films with wavelengths >290nm in a pure oxygen atmosphere leads to extensive oxygen uptake in the surface regions. Oxidation of the carbon atoms in the backbone chain cannot alone account for the degree of uptake. At a photon flux of 10 $Whm^{-2}h^{-1}$, 5.5% of the C_{1s} signal after ~5 hours' exposure arises from components due to carbon atoms directly bonded to oxygen. Examination of the $\Pi \rightarrow \Pi^*$ shake-up satellite, diagnostic of the aromaticity of the pendant phenyl group, reveals a decrease in intensity during photooxidation indicative of this moiety being oxidised. This process could account for the extent of oxygen uptake and has been postulated for bulk[204,214] and surface[49] photooxidation studies utilising wavelengths <290nm. In these cases the reaction probably arises from the direct excitation of the benzene ring.

However, Ranby and Rabek[204] have suggested that singlet oxygen ($^1\Delta O_2$) may be responsible for the ring opening reaction. It is possible that the observed ring oxidation in the surface at wavelengths >290nm could arise from such a reaction between the phenyl moiety and $^1\Delta O_2$ and this is considered in detail below.

The C_{1s} and O_{1s} core levels for an electron take-off angle of 70°, displayed in Figure 7.9 reveal the changes in the surface chemistry of polystyrene films exposed to a stream of singlet

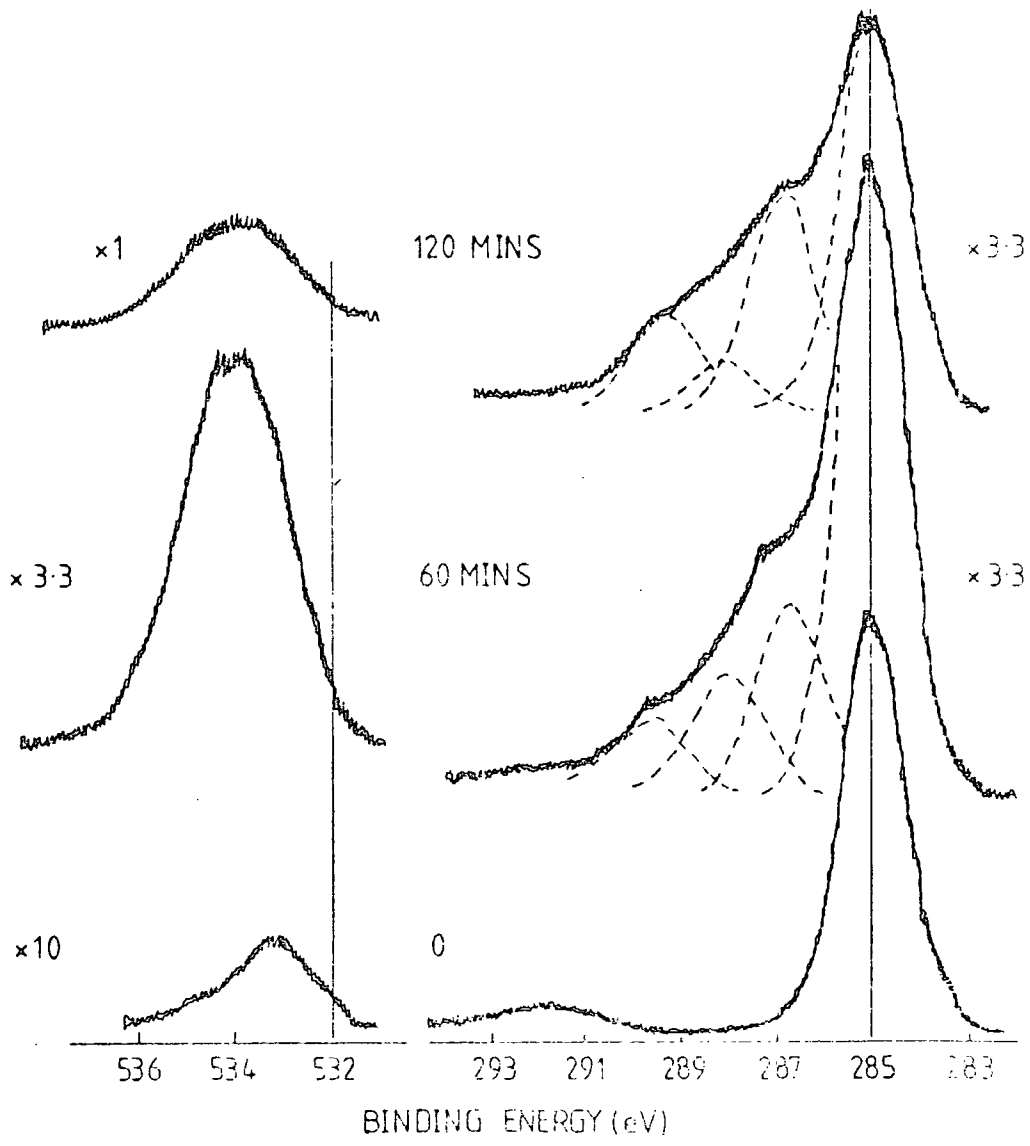

Figure 7.9 C_{1s} and O_{1s} core levels for polystyrene films exposed to "singlet oxygen" ($\theta = 70^{o}$).

oxygen from a microwave discharge for 60 and 120 minutes. (The conditions of the experiment employed were 60W, 2 torr and the atomic oxygen and ozone also produced were removed by the continuous distillation of mercury through the discharge region as described in Chapter Six). Oxygen incorporation into the surface is evident from the increase in the complexity of the C_{1s} signal, arising from C-O, C=O and O-C=O components, and the increase in the intensity of the O_{1s} envelope.

The nature of the surface is more apparent from the C_{1s} component analysis and the relative O_{1s}/C_{1s} intensity ratios in Table 7.3. The distribution of components are in essential agreement to those reported by Dilks[198] and are not dissimilar to the results obtained for Bisphenol A polycarbonate (c.f. Chapter Six).

TABLE 7.3 C_{1s} components and O_{1s}/C_{1s} intensity ratios for the spectra in Figure 7.9

	Time	Total C_{1s}	C-H	C-O	C=O	O-C=O	$\pi\rightarrow\pi^*$	O_{1s}/C_{1s}
$\theta=70^{\circ}$	0	100	92	2	0	0	6	0.0
	60	100	61	19	12	7	1	0.58
	120	100	53	27	7	11	2	0.73
$\theta=30^{\circ}$	0	100	93	1	0	0	6	0.02
	60	100	69	13	10	5	3	0.40
	120	100	66	15	10	6	3	0.40

The surface specificity of the oxidation is revealed from the consideration of the data obtained with an electron take-off angle of 30° also shown in Table 7.3. Both the degree of oxidative functionalisation and oxygen uptake are greater at $\theta=70^{\circ}$.

From the discussions presented in Chapter Six, it is unlikely that the effluent reaching the polystyrene films is completely free of contaminant reactive oxygen species (i.e. atomic oxygen). Consequently experiments were repeated over a five hour exposure period with NO_2 also being added to the effluent to remove residual traces of oxygen atoms. No oxidation of polystyrene could be detected with ESCA. Control experiments where cis-polyisoprene films were exposed downstream of polystyrene revealed oxidation of the former and not the latter indicative of singlet oxygen reaching the samples (cf. Chapter Six).

These results show that polystyrene does not react with singlet oxygen and are in agreement with the conclusions of MacCallum and Rankin.[202] Consequently singlet oxygen is not responsible for the observed ring opening reaction in polystyrene films.

Weir[212] has proposed that phenyl ring oxidation is due to attack by hydroxy radicals resulting from the decomposition of hydroperoxides.

$$ROOH \xrightarrow{h\nu} RO\cdot + \cdot OH$$

From the study of surface hydroperoxide formation during the photooxidation of polystyrene films (λ>290nm, Io = $Whm^{-2}h^{-1}$) it is apparent that the decrease in the $\Pi \rightarrow \Pi^*$ shake-up satellite does not begin until the rate of hydroperoxide formation is high and this may well support the hydroxy radical theory. The nature of the reaction in the surface during photooxidation are of an extremely complex nature and Figure 7.10 displays a scheme for some of the possible processes.

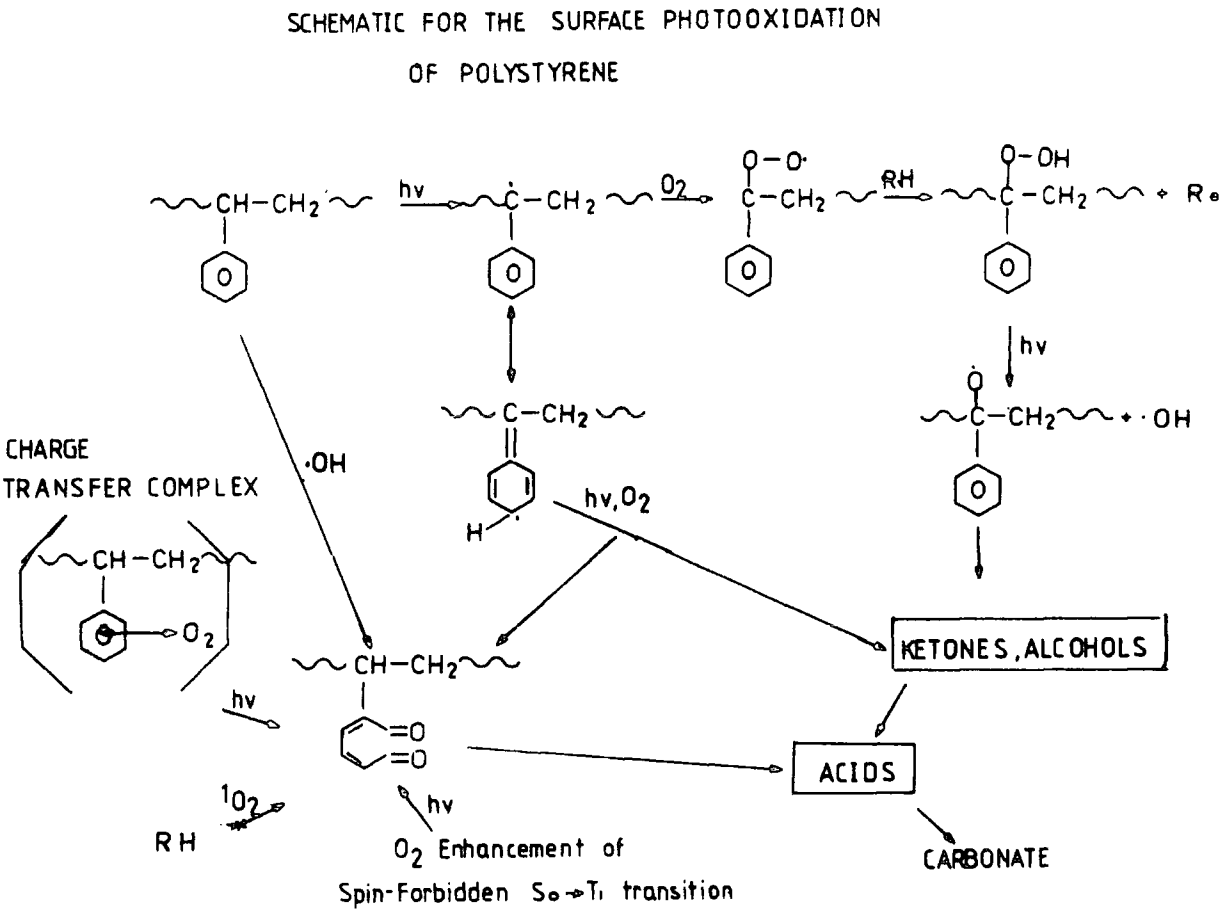

Figure 7.10 Scheme for some of the possible reactions occurring in the surface of polystyrene films during photooxidation.

7.3.2 Reactions in Air

(a) Continuous Irradiation

In Chapter Five the photooxidation of Bisphenol A polycarbonate was considered as a function of the partial pressure of oxygen and the rate and extent of reaction was shown to be strongly dependent on this factor. It is of interest, therefore, to consider the photooxidation of polystyrene films in air. The exposures were carried out in a static environment and as shown in Chapter Five direct comparison of the results with those obtained for irradiations in a dynamic oxygen atmosphere should be treated with caution.

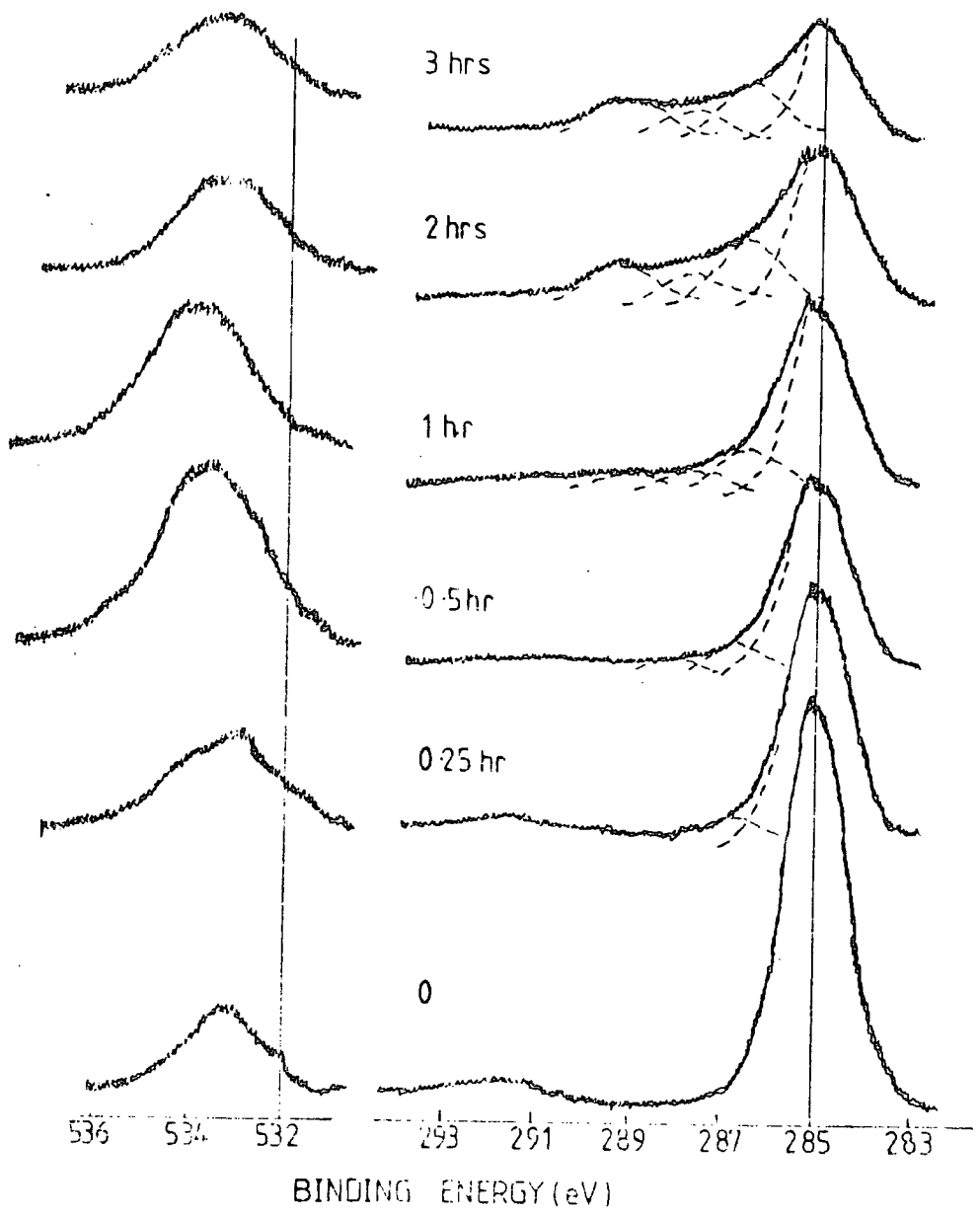

Figure 7.11 C_{1s} and O_{1s} core levels for polystyrene films irradiated in air (Io = 20 $Whm^{-2}h^{-1}$, 10% R.H.)

The ESCA spectra in Figure 7.11, displaying the C_{1s} and O_{1s} core levels for polystyrene films exposed to an incident photon flux of 20 $Whm^{-2}h^{-1}$ (λ>290nm) in air (10% R.H.), reveal that extensive photooxidation has taken place. The C_{1s} component analysis in Figure 7.12 reveal the formation of C-O, C=O and O-C=O functionalities as a function of irradiation time. The C-H and $\Pi \rightarrow \Pi^*$ components are also seen to decrease.

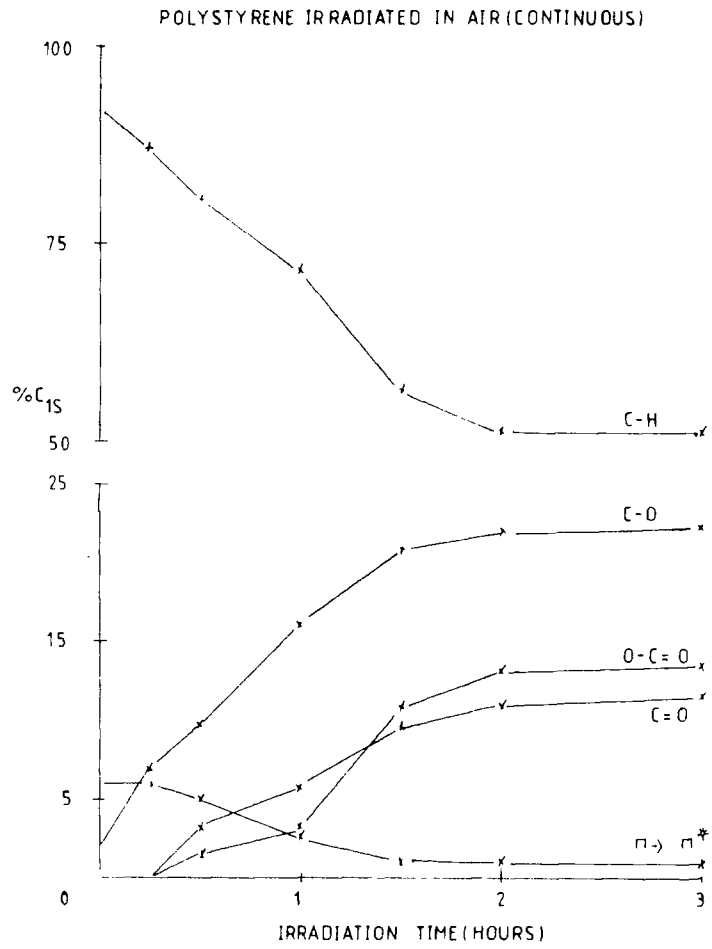

Figure 7.12 C_{1s} component analysis for the spectra in Figure 7.11.

The initial increase in the C-O component without concomitant increases in carbonyl and carboxylate groups is indicative of hydroperoxide formation. As was also evident from irradiations in pure oxygen an induction period is apparent for the formation of carbonyl and carboxylate groups with the rate for the former being greater than that for the latter.

The mechanisms involved in the photooxidation of polystyrene films in air appear to be of a similar nature to those in oxygen. The main difference between the two conditions arises from the rate and extent of reaction. This is highlighted on comparing the surface stoichiometries for similar total photon fluxes. In oxygen after 2 hours' exposure at 10 $Whm^{-2}h^{-1}$ the carbon to oxygen ratio is ∿1:0.5 and in air (1 hour at 20 $Whm^{-2}h^{-1}$) the corresponding value is 1:0.16. Even after 2 hours' exposure in air the C:O ratio of ∿1:0.31 is well below that for 2 hours in O_2 at a much lower photon flux and this emphasises the sensitivity of the photooxidation processes in the surface to the partial pressure of oxygen at the interface.

(b) Cyclic Irradiation

The results presented so far have concentrated on the use of continuous irradiation. Solar radiation is of a cyclical nature and it is possible that during the hours of darkness reactions take place which may well influence the kinetics and mechanisms of photooxidation. In the model studies discussed above a highly reactive surface will remain on termination of exposure and hence some of dark reaction is to be expected. To investigate the effect of cyclic irradiation, polystyrene films

were exposed to ultraviolet light (λ>290nm, Io = 20 $Whm^{-2}h^{-1}$ and 10% R.H.) for cycles of 15 minutes (i.e. 15 minutes' exposure followed by 15 minutes' darkness, etc.) such that the samples received a total flux as those described in the previous section.

The C_{1s} component analysis in Figure 7.13 reveals the nature of the oxidative functionalisation during cyclical exposure and are very similar to those for continuous irradiation. It is interesting to note that the induction periods for carbonyl and carboxylate functionalities are longer under the present conditions.

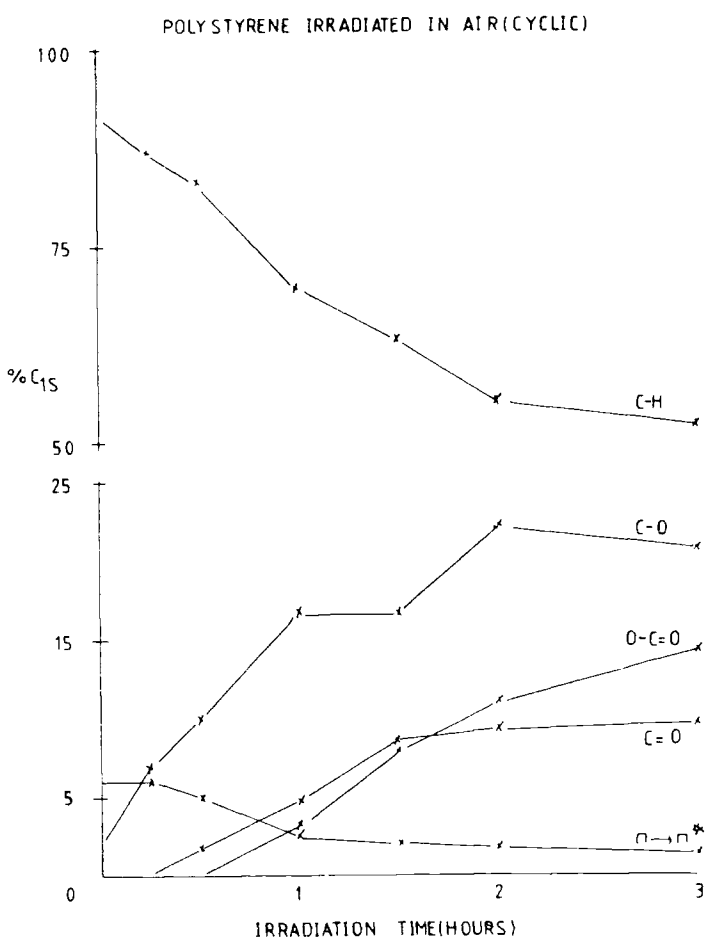

Figure 7.13 C_{1s} component analysis for polystyrene films exposed to cyclic irradiation (Io = 20 $Whm^{-2}h^{-1}$, 10% R.H.).

Comparison of the relative O_{1s}/C_{1s} intensity ratios for continuous and cyclical exposures and the corresponding contributions to the C_{1s} signal arising from oxidative species as shown in Figure 7.14 are very revealing. It is evident that oxygen incorporation into the surface occurs at a slower rate during cyclic irradiation and as such indicate that dark reactions are occurring.

Post irradiation effects have been previously observed in bulk studies of polystyrene and are believed to consist of two first order reactions.[215-217] The fast reaction is due to the decomposition of hydroperoxides (known to be present due to their ability to initiate the polymerisation of methyl methacrylate)[221] and it has been suggested that the slow reaction is due to the cis-trans isomerisation of a benzalacetophenone formed by the decomposition of the hydroperoxide.

In order to obtain information on post irradiation effects in the surface, polystyrene films were exposed to continuous irradiation for 30 minutes and the ESCA spectra were then recorded immediately and after 15, 45 and 90 minutes in the dark. The changes in the O_{1s}/C_{1s} intensity ratios displayed in Figure 7.15 reveal that two stages are involved. Over the first 45 minutes the oxygen content in the surface decreases (possibly reflecting hydroperoxide decomposition and cross-linking) and after 90 minutes the level has returned to the initial value present on immediate analysis. The differences in the C_{1s} components are very small and in the absence of additional data it is not possible to determine the precise nature of the dark reactions involved.

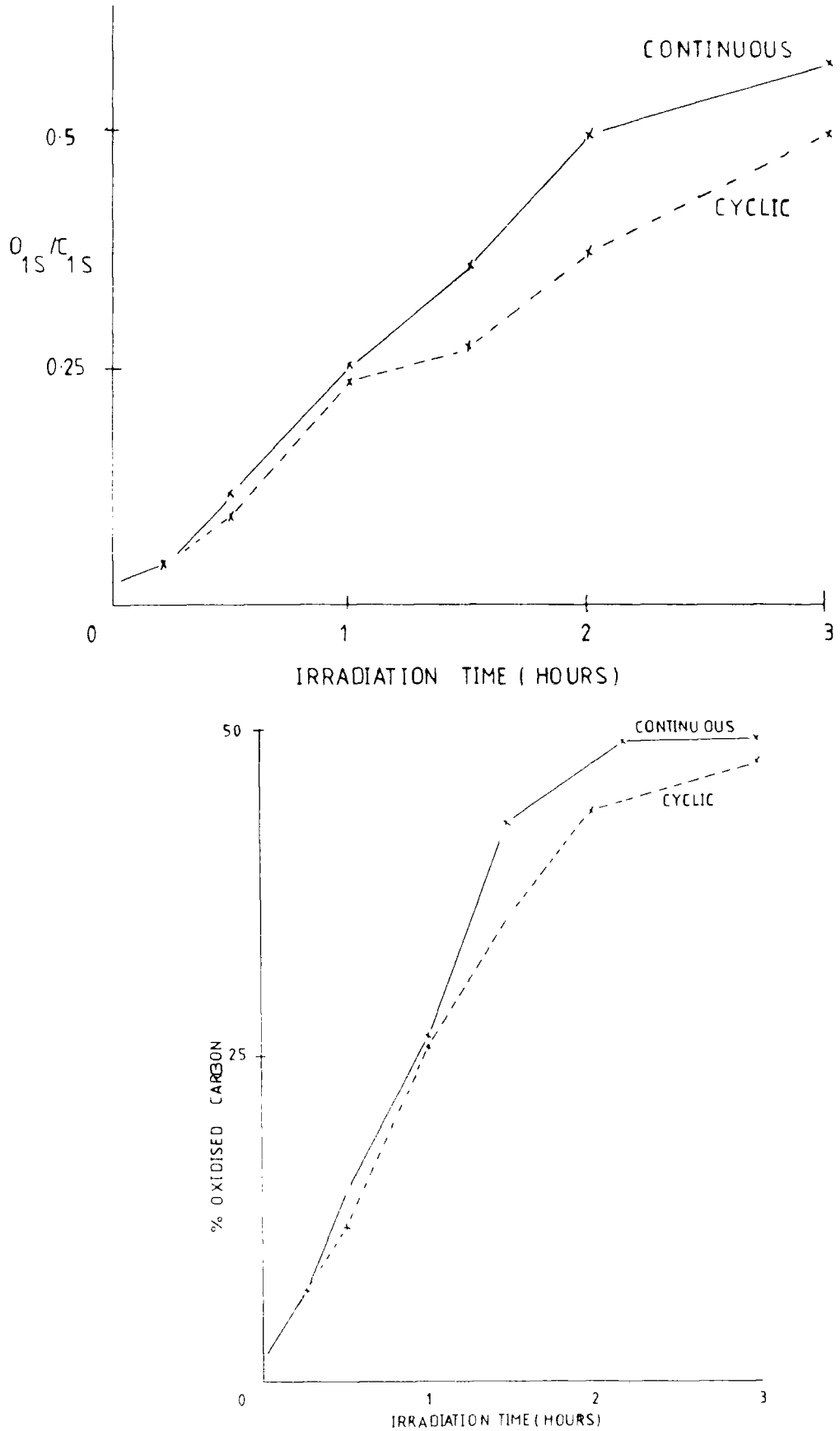

Figure 7.14 Comparison of the O_{1s}/C_{1s} intensity ratios and % contributions arising from oxidative functionalities for polystyrene films exposed to continuous and cyclic irradiation.

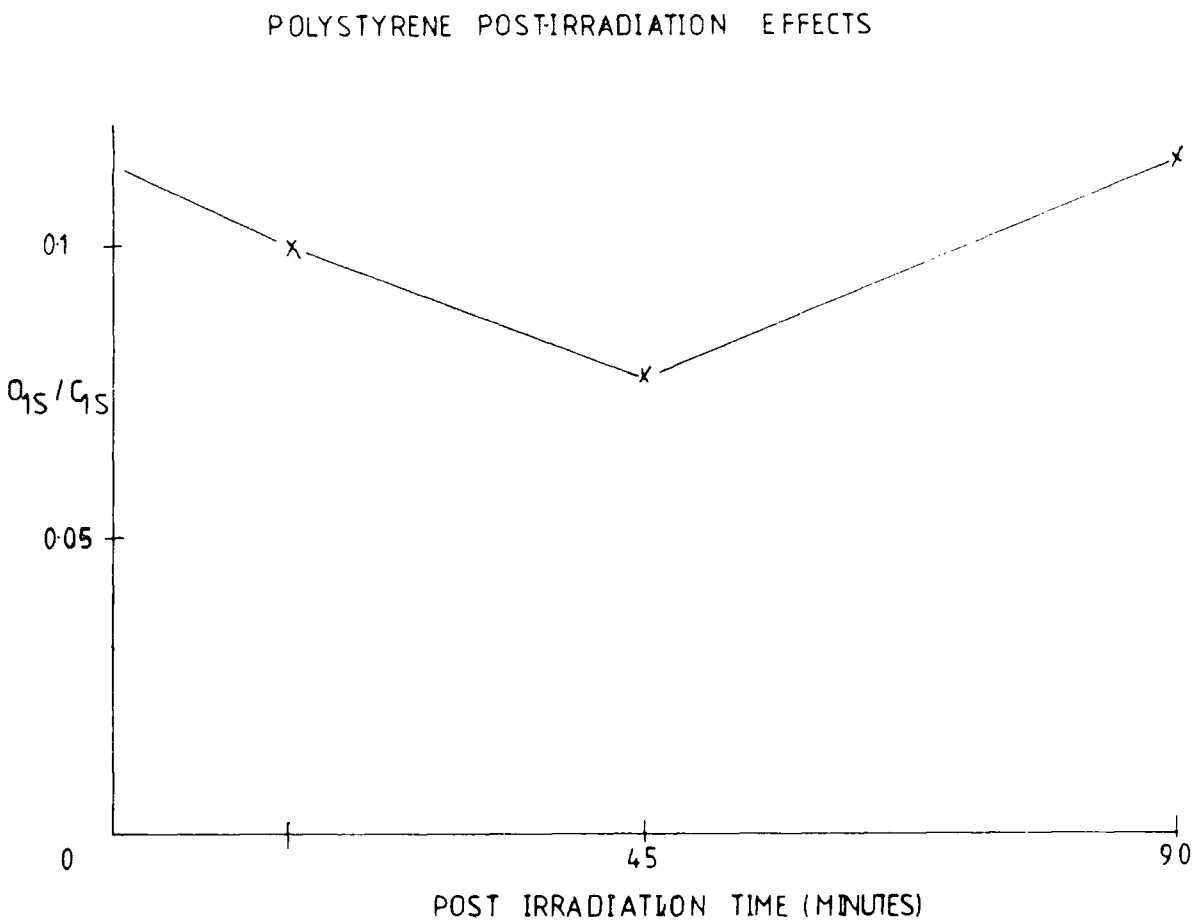

Figure 7.15 O_{1s}/C_{1s} intensity ratios for polystyrene films irradiated for 30 minutes (Io = 20 $Whm^{-2}h^{-1}$, 10% R.H.) and left in the dark for various periods of time.

From the data in Figure 7.15 it would appear that irradiation for another 30 minutes after 15 and 90 minutes in the dark should give rise to oxygen uptakes to a lesser and similar extent respectively with respect to 60 minutes' continuous exposure. This is confirmed from the data in Table 7.4. It is apparent that the length of the dark period strongly influences the rate of photooxidation during cyclic irradiation.

TABLE 7.4 O_{1s}/C_{1s} intensity ratios for polystyrene films irradiated for 30 minutes and re-irradiated for a further 30 minutes after being left in the dark for various periods of time. (For comparison the relevant ratio for 60 minutes' continuous irradiation are also included).

Dark period (minutes)	O_{1s}/C_{1s}
15	0.22
90	0.26
(60 minutes' continuous exposure)	0.25

7.3.3 Natural Weathering

In the previous sections the photooxidation of polystyrene films was considered under various model conditions. The discussions presented in Chapter Five highlighted the caution required when comparing model studies to natural exposures therefore to complement the above data polystyrene films have been weathered in Dhahran, Saudi Arabia.

The C_{1s} core levels displayed in Figure 7.16 reveal the changes in surface chemistry during natural weathering for starting dates in September 1980 and April 1981. No useful information can be obtained from a consideration of the O_{1s} signal due to the presence of a variable quantity of surface contamination in the form of deposited sand (SiO_2) which contributes to the total intensity of this core level.

The increase in complexity of the C_{1s} envelope during exposure is due to components arising from C-O, C=O and O-C=O functionalities. The nature of the changes are more

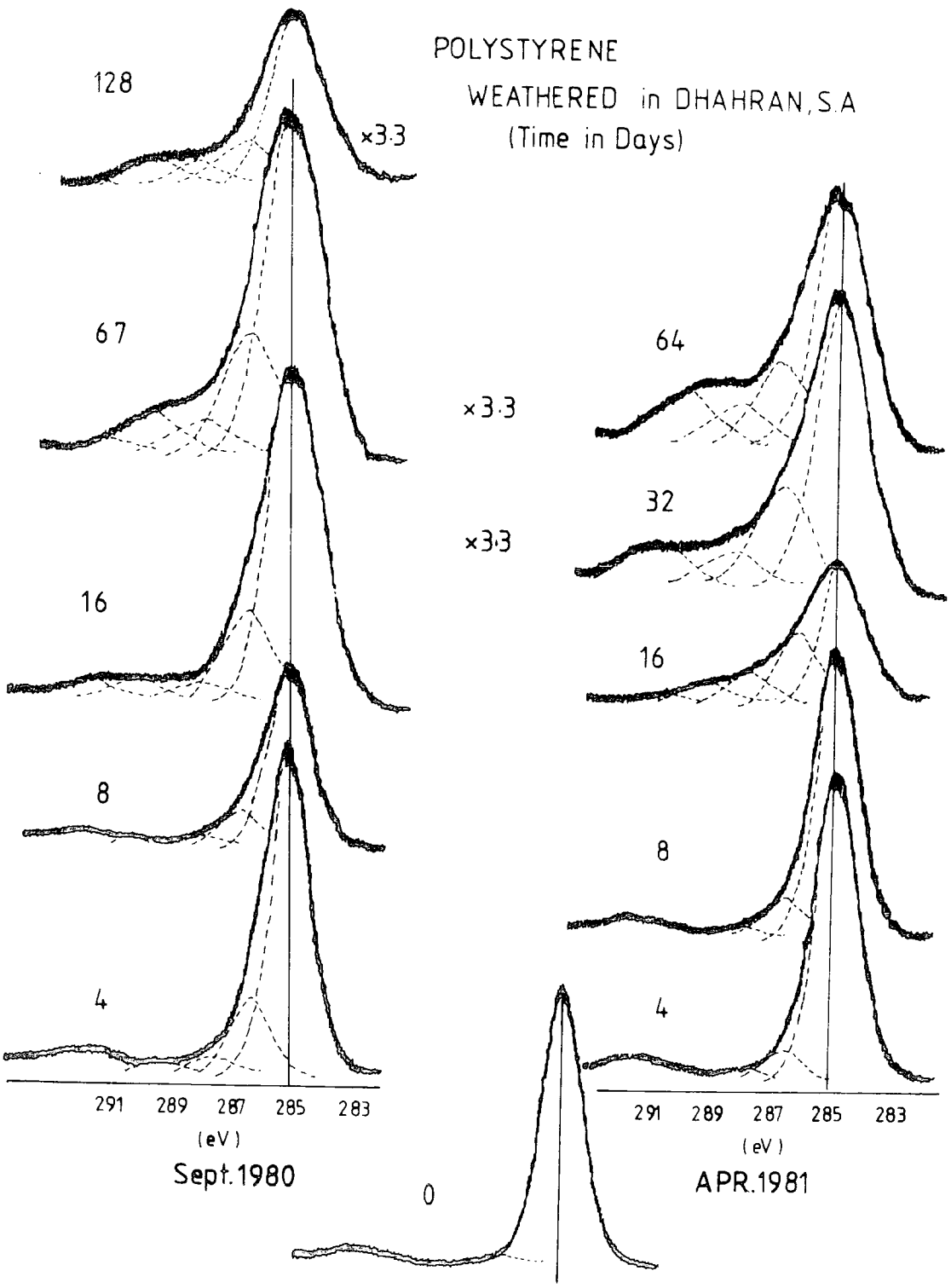

Figure 7.16 C_{1s} core levels for polystyrene films weathered in Dhahran, Saudi Arabia, (starting dates September 1980 and April 1981).

apparent from a consideration of the distributions of the various components as displayed in Figure 7.17. Considering the data for the September 1980 starting date first, it can be readily seen that the C-O component increases in intensity rapidly in the initial stages of exposure. As was observed in the model studies the rate of carbonyl formation is greater than that for carboxylate. No induction period for the C=O and O-C=O groups is apparent at the sampling times utilised in this study. The $\Pi \rightarrow \Pi^*$ shake-up satellite decreases in intensity indicative of the oxidation of the aromatic ring.

The data for April 1981, as in September 1980, reveal the high intensity of the C-O functionality. However, an induction period is evident for carbonyl and carboxylate formation: the latter appearing at a later stage than the former and is in agreement with the data obtained for the model studies utilising cyclic irradiation. The rate of photooxidation is much slower than for September 1980. Although the differences in temperature and relative humidity for the two starting dates may influence the distributions of components (Figures 7.18 and 7.19 respectively) the contrast between them does not appear to be sufficient to account for the variation in rate. Recent photon flux measurements, using the polysulphone technique, indicate that the uv component of solar radiation in Dhahran in September is a factor of $\sim$2 greater than that in April.[231] Consequently the differences in photon flux can account for the contrast in the observed reaction rates.

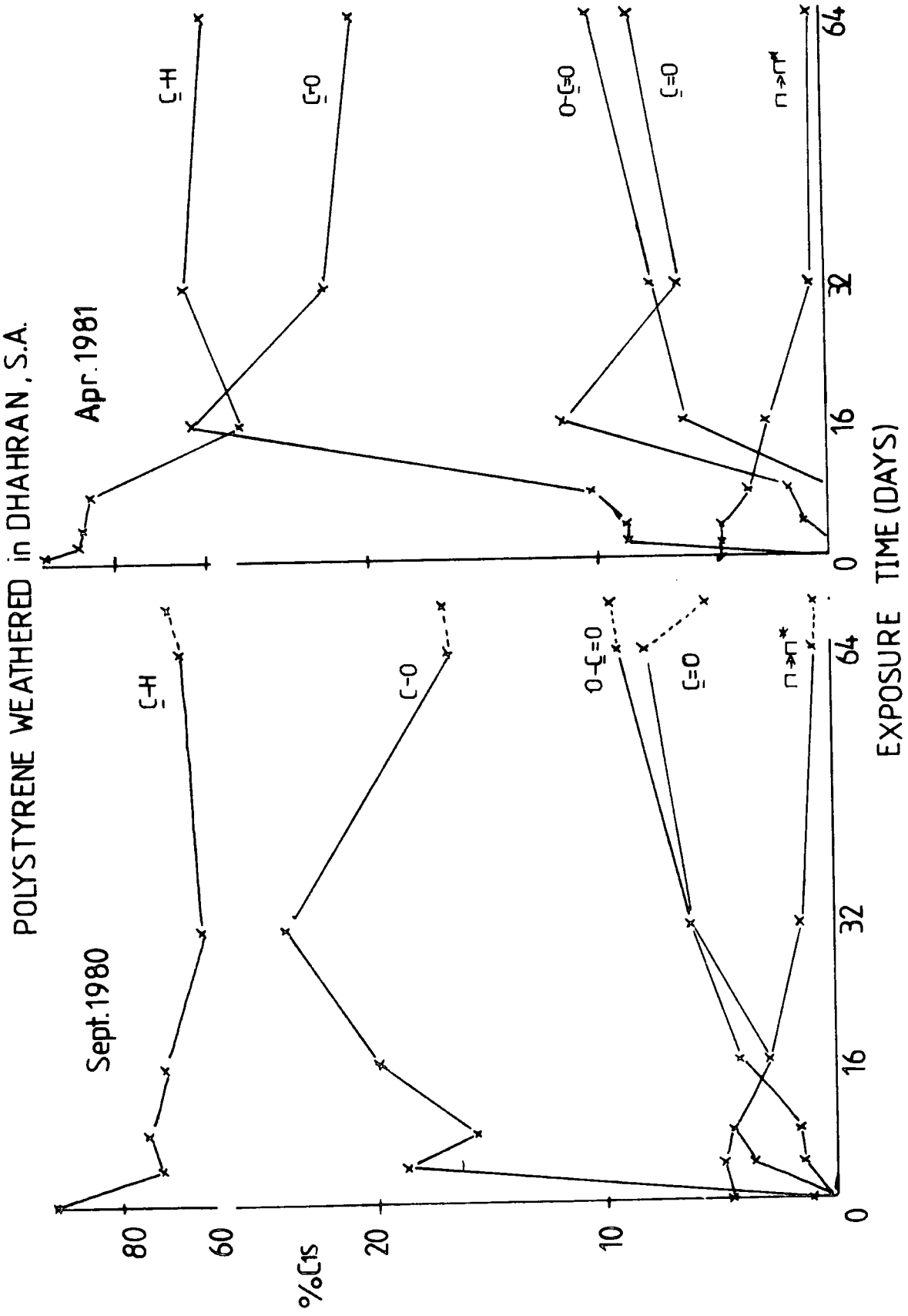

Figure 7.17 C_{1s} component analysis for the spectra in Figure 7.16

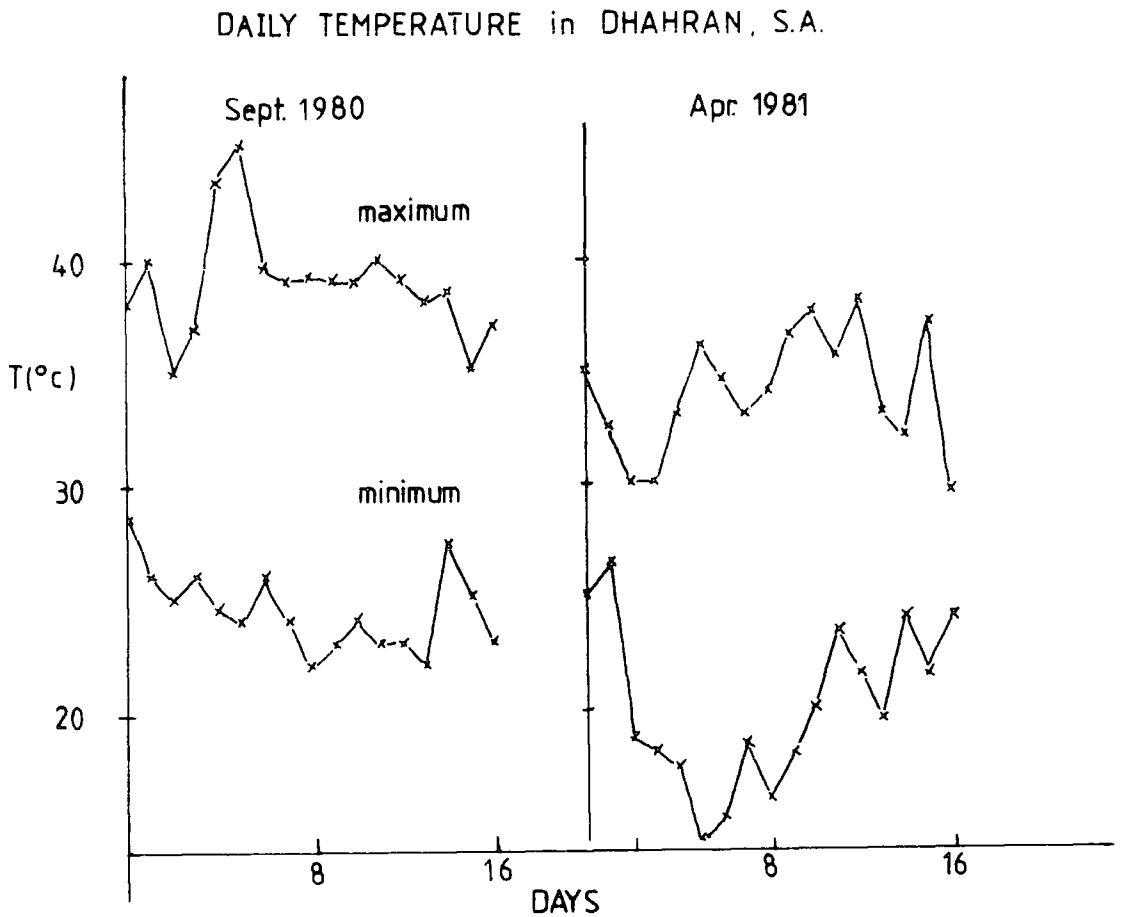

Figure 7.18 Variation in daily temperature during the first 16 days of polystyrene weathering

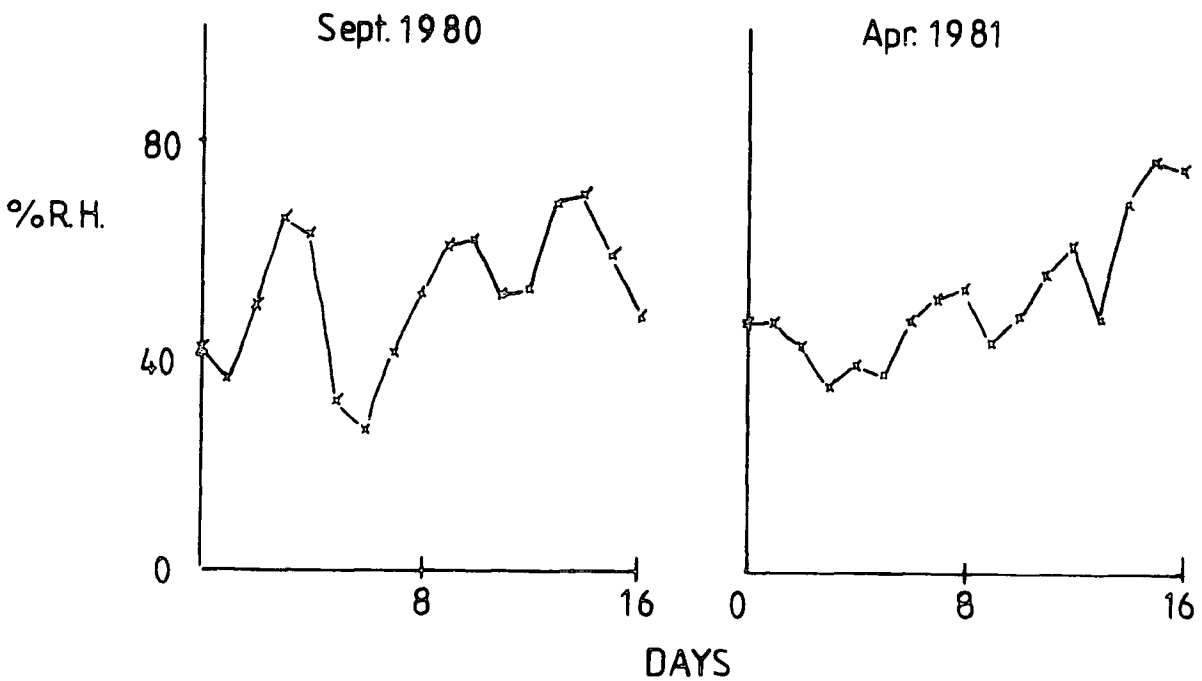

Figure 7.19 Variation in daily relative humidity during the first 16 days of polystyrene weathering

7.4 Conclusions

Model photooxidation studies (λ>290nm) of polystyrene films have revealed that extensive oxygen uptake occurs in the surface. The reactions involve the formation of hydroperoxides in the initial stages and induction periods for the formation of carbonyl and carboxylate features are evident. The extent of reaction can only be explained by oxidative processes involving the main chain and the pendant phenyl groups as evidenced by the decrease in intensity of the $\Pi \rightarrow \Pi^*$ shake-up satellite. Singlet oxygen does not react with polystyrene.

Photooxidation is strongly dependent on the partial pressure of oxygen at the solid/gas interface. Cyclic irradiation, as opposed to continuous, gives rise to a slower reaction rate. Natural weathering studies reveal similar trends in the changes in surface chemistry to the model studies. The higher observed level of C-O groups in relation to the C=O and O-C=O features may well be a result of the higher relative humidities experienced during natural exposures.

CHAPTER EIGHT

SURFACE ASPECTS OF THE NATURAL AND ARTIFICIAL PHOTOAGING OF BISPHENOL A POLYSULPHONE AS REVEALED BY ESCA

8.1 Introduction

The photoaging of Bisphenol A polysulphone has been the centre of some interest in the literature.[40-42, 51,52,221,222] The changes induced by artificial and natural ultraviolet exposures have been investigated from both the bulk[40-42,221,222] and surface points of view.[51,52]

The data from ir studies and analysis of the evolved gases have been interpreted in terms of random bond scission occurring at all bonds except the aromatic C-H and C-C bonds as shown in Figure 8.1.[221]

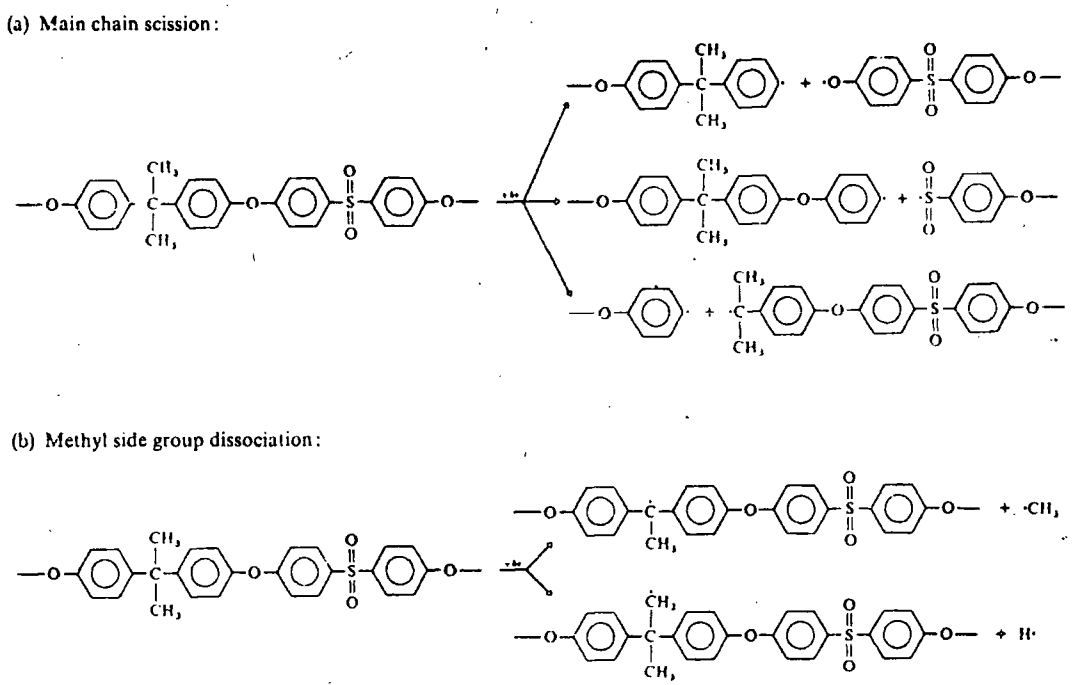

Figure 8.1 Scheme for bond-scission processes in polysulphone during photooxidation

Of particular interest has been the use of polysulphone as a uv monitor for solar radiation and artificial light sources for wavelengths below 320nm.[40-42] That polysulphone is sensitive only to wavelengths below this value has been shown from the examination of the activation spectrum. The change in optical density at 330nm gives a measure of the incident radiation dose.

Previous ESCA studies have examined the changes in surface chemistry of polysulphone after prolonged exposure to natural weathering in San José, U.S.A.[52] and Durham, England.[224] Model photooxidation studies have been conducted in static atmospheres of oxygen utilising incident radiation greater than 230nm.[51] In this chapter the photodegradation of Bisphenol A polysulphone in oxygen and nitrogen atmospheres such that λ>290nm is considered. Photooxidation has been studied as functions of irradiation time, light intensity and temperature and comparisons made with the changes involved in natural weathering in Dhahran, Saudi Arabia.

8.2 Experimental

The photodegradation of Bisphenol A polysulphone films ($\sim$40μm) in oxygen and nitrogen atmospheres (λ>290nm) were carried out in the stainless steel reactor described in Chapter . For comparison, photooxidation has also been studied at λ>240nm by utilising the quartz zero path length window shown in Figure 4.3 (Chapter Four).

The photochemistry of sulphurdioxide (λ>290nm) has been studied by irradiation of Bisphenol A polycarbonate ($\sim$40μm) in a flowing atmosphere of SO_2 (B.D.H. Chemicals) and the immediate examination of the changes in surface chemistry.

Natural weathering exposures were carried out in Dhahran, Saudi Arabia as described in Chapter Four. The starting date was 10 September 1980.

ESCA spectra were recorded on an AEI ES 200B and Kratos ES 300 spectrometer using $Mg_{K\alpha_{1,2}}$ radiation. Under the experimental conditions employed in these studies the respective full width at half maximum for the $Au_{4f_{7/2}}$ level at 84.0 eV were 1.2 and 1.1 eV. The spectra were deconvoluted and integrated using a DuPont 310 curve resolver. Binding energies were referenced to the hydrocarbon component at 285.0 eV. Angular dependence studies were carried out by examination of the ESCA spectra obtained at electron take-off angles of 30 and 70° corresponding to sampling depths of ∿40 and ∿12Å. The results have shown that photooxidation at these depths are essentially homogeneous and consequently the data discussed in the section below are for those obtained at 30°.

The uv and ir spectra for the natural weathering exposures were recorded on a Unicam SP800 uv/visible spectrometer and a Perkin Elmer ir spectrometer respectively.

8.3 Results and Discussion

The main emphasis of this work has been to investigate reactions at the gas solid interface at wavelengths >290nm in oxygen and nitrogen atmospheres and to draw comparisons with natural weathering. It is convenient in discussing the results to consider each of the environments separately.

8.3.1 Reactions in Oxygen

(a) Studies as functions of light intensity and irradiation time

As a starting point for the investigation of the changes

in surface chemistry of polysulphone films, the irradiation in a flowing oxygen atmosphere at an incident photon flux of 5.7 $Whm^{-2}h^{-1}$ is considered. The ESCA spectra in Figure 8.2 reveal the C_{1s}, O_{1s} and S_{2p} core levels for the unexposed starting material and the subsequent changes on exposure.

The initial C_{1s} profile consists of three components due to carbon not bonded to oxygen at 285.0 eV, carbon singly bonded to oxygen at ∿286.4 eV and a shake-up satellite centred at ∿291.5 eV diagnostic of the aromaticity present in polysulphone. A component arising from carbon bonded to sulphur is also present at ∿286.0 eV but has not been resolved in this case due to the difficulty in fitting this peak as changes occur in surface chemistry. The O_{1s} core level reveals a 1:1 doublet consistent with ether and sulphone oxygens. The corresponding S_{2p} envelope displays a 1:2 doublet, arising from the spin orbit splitting of the S_{2p} level, at binding energies indicative of a sulphone group.

On irradiation in oxygen the C_{1s} envelope increases in complexity due to peaks arising from carbonyl and carboxylate groups. The carboxylate is seen to clearly dominate with respect to the carbonyl during exposure. The O_{1s} level increases in relative intensity and the clearly defined doublet disappears as the nature of the signal becomes more complex. The S_{2p} core level broadens on exposure and may be resolved in terms of two chemical environments with the $S_{2p_{3/2}}$ centroids at ∿168.0 eV and 169.3 eV indicative of sulphone and sulphate groups respectively. This has been previously observed in the natural weathering of polysulphone.[52] These results clearly indicate that extensive oxygen incorporation into the surface of polysulphone has occurred.

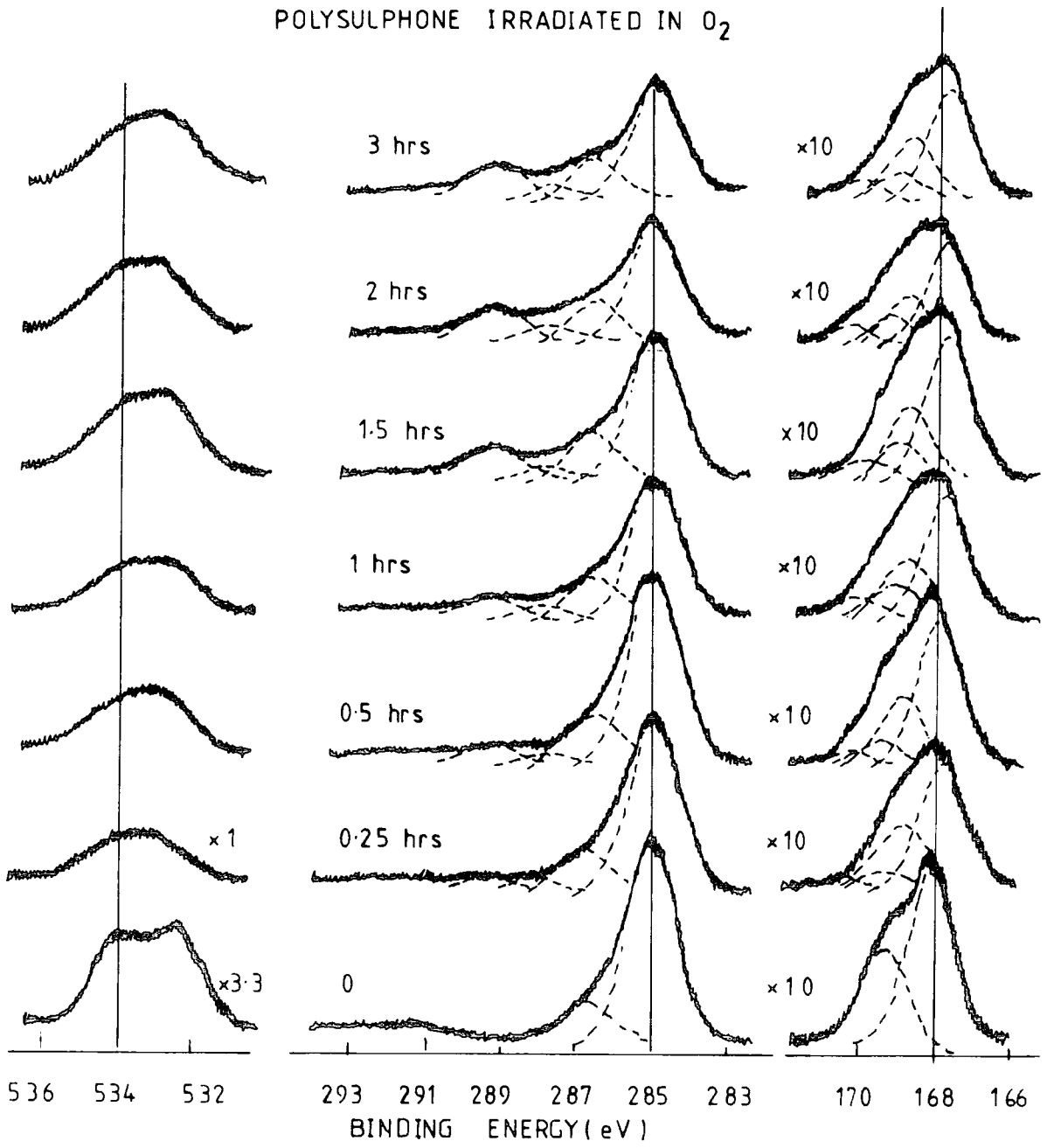

Figure 8.2 C_{1s}, O_{1s} and S_{2p} core levels for polysulphone films irradiated in oxygen (Io = 5.7 $Whm^{-2}h^{-1}$, λ>290nm).

The changes in the relative O_{1s}/C_{1s}, S_{2p}/C_{1s} and S_{2p}/O_{1s} ratios as a function of time are shown in Figure 8.3. The oxygen uptake starts to level off after ∿2 hours and this is also reflected in the S_{2p}/O_{1s} intensity ratio. The total sulphur content appears to increase slightly reflecting that the desorption of low molecular weight carbon species is greater than for sulphur dioxide. This is in essential agreement with the results obtained from the analysis of evolved gases.[222,223]

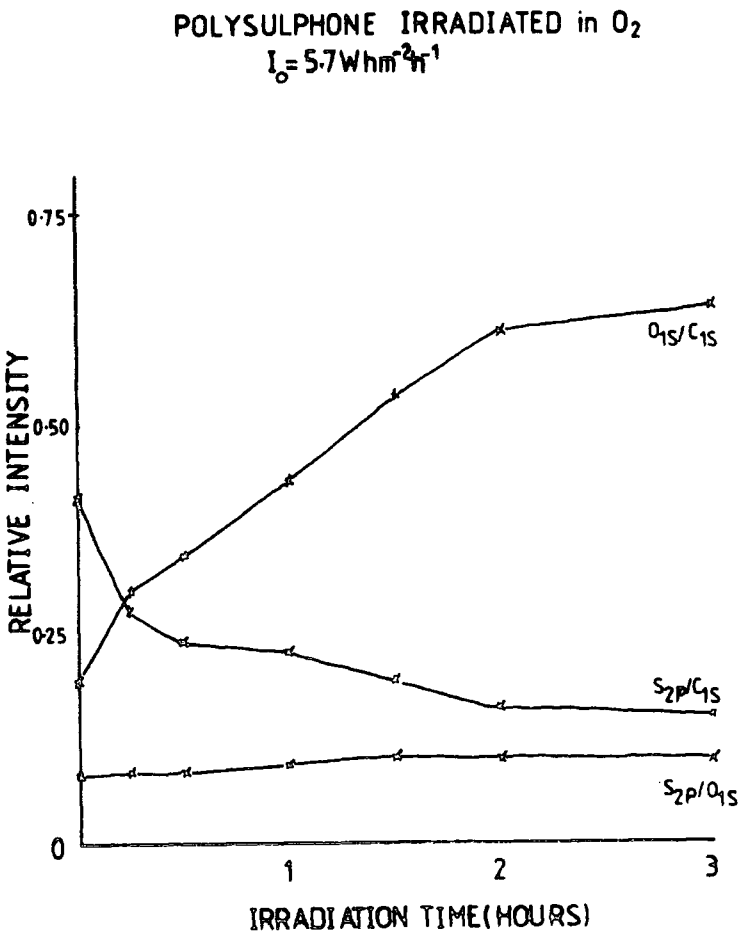

Figure 8.3 O_{1s}/C_{1s}, S_{2p}/C_{1s} and S_{2p}/O_{1s} intensity ratios for the spectra in Figure 8.2.

The nature of the oxidised surface is more clearly revealed in the C_{1s} component analysis displayed in Figure 8.4. The C-H component (phenyl and methyl groups) decreases in intensity with corresponding increases in C-O, >C=O and O-C=O functionalities: the latter representing ∿16% of the C_{1s} profile after three hours' irradiation. The $\Pi \rightarrow \Pi^*$ intensity also decreases indicative of a loss in the aromatic content present in the surface. The data, therefore, suggest oxidation of both the dimethyl moiety and the aromatic ring system. That the shake-up satellite increases in intensity after the initial increase may well be consistent with a small degree of carbonate formation.

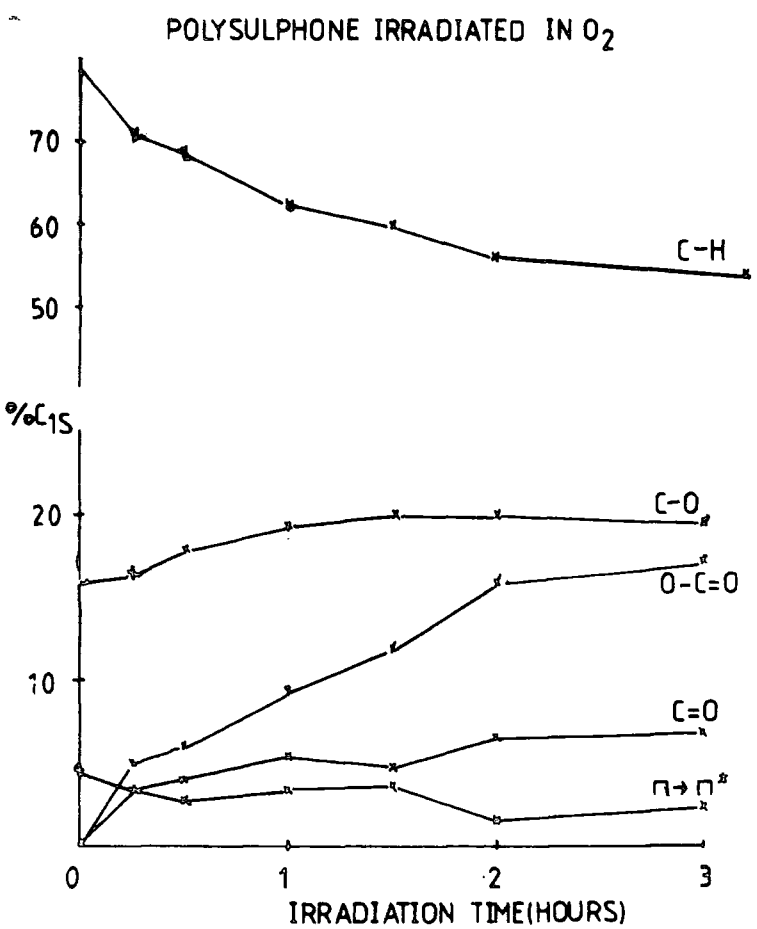

Figure 8.4 C_{1s} component analysis for the spectra in Figure 8.2.

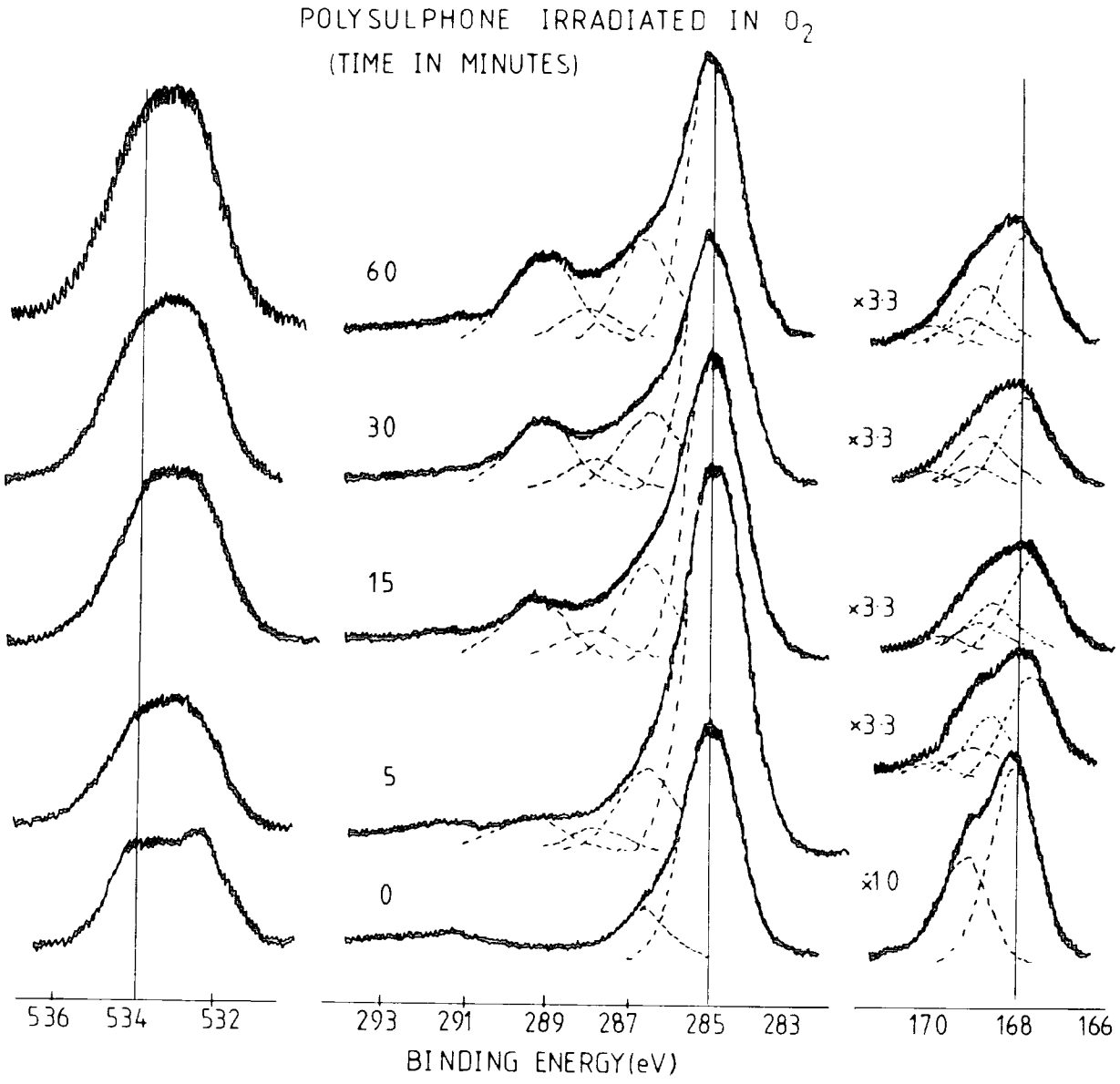

Figure 8.5 C_{1s}, O_{1s} and S_{2p} core levels for polysulphone films irradiated at a higher photon flux of 27.4 $Whm^{-2}h^{-1}$.

The core levels shown in Figure 8.5 reveal the changes in polysulphone films after irradiation for various times at a higher photon flux of 27.4 $Whm^{-2}h^{-1}$. A greater degree of oxygen uptake is evident than for a comparable irradiation time at a lower lamp intensity. Two sulphur environments are also evident. The data in Figure 8.6 display the corresponding O_{1s}/C_{1s}, S_{2p}/C_{1s} and S_{2p}/O_{1s} intensity ratios. It is readily apparent that the oxygen uptake starts to plateau after ∿60 minutes' irradiation. The C_{1s} component analysis reveals a similar trend for that at 5.7 $Whm^{-2}h^{-1}$ with a higher build-up of C=O and O-C=O structural features at an earlier stage. From a starting C:O stoichiometry of ∿1:0.15 after 1 hour's irradiation the oxygen content has risen by ∿125% in the case of lower light intensity and ∿300% for the higher intensity.

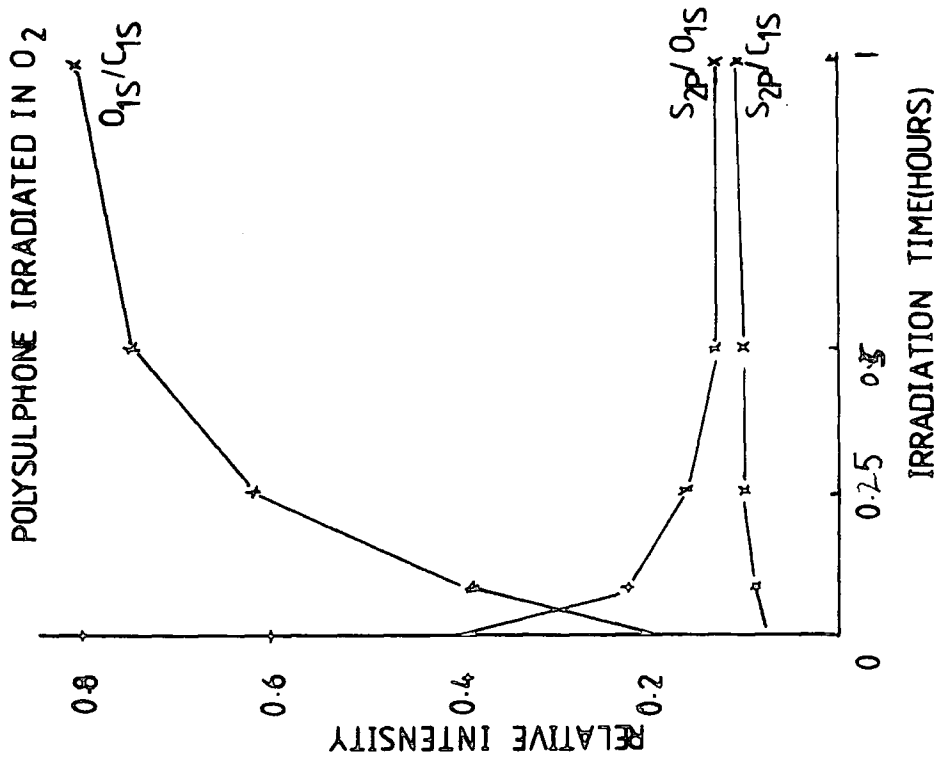

Figure 8.6 O_{1s}/C_{1s}, S_{2p}/C_{1s} and S_{2p}/O_{1s} intensity ratios for the spectra in Figure 8.5.

In order to obtain a more comprehensive view of the effect of light intensity on the component distribution the data in Table 8.1 displays the relevant functionalities for comparable total fluxes received at higher and lower lamp intensities. The distribution is remarkably similar, the main differences occurring in the carbonyl and carboxylate functionalities and hence total oxygen signal.

TABLE 8.1 Comparison of the C_{1s} components and O_{1s}/C_{1s} intensity ratios for polysulphone films exposed to similar total photon fluxes from low and high lamp intensities

	Total C_{1s}	C-H	C-O	C=O	O-C=O	$\Pi \rightarrow \Pi^*$	O_{1s}/C_{1s}
60 minutes ($Io=5.7 Whm^{-2}h^{-1}$)	100	63	19	6	9	3	0.43
15 minutes ($Io=27.4 Whm^{-2}h^{-1}$)	100	60	19	6	12	3	0.63

The effect of light intensity on the rate of oxygen uptake is shown in Figure 8.7 for irradiations at 27.4, 13.5 and 5.7 $Whm^{-2}h^{-1}$. From these data it appears that the initial rate is roughly linear with photon flux.

The data in Figure 8.8 represents the changes in the relative oxygen and sulphur levels on irradiation for 15 minutes at varying photon flux. Oxygen incorporation into the surface increases steadily with lamp intensities up to $\sim$35 $Whm^{-2}h^{-1}$. Irradiation at higher photon flux reveals essentially no change indicative of a steady state condition representative of a balance between photooxidation and desorption of low molecular species. The relative sulphur intensity does not change a

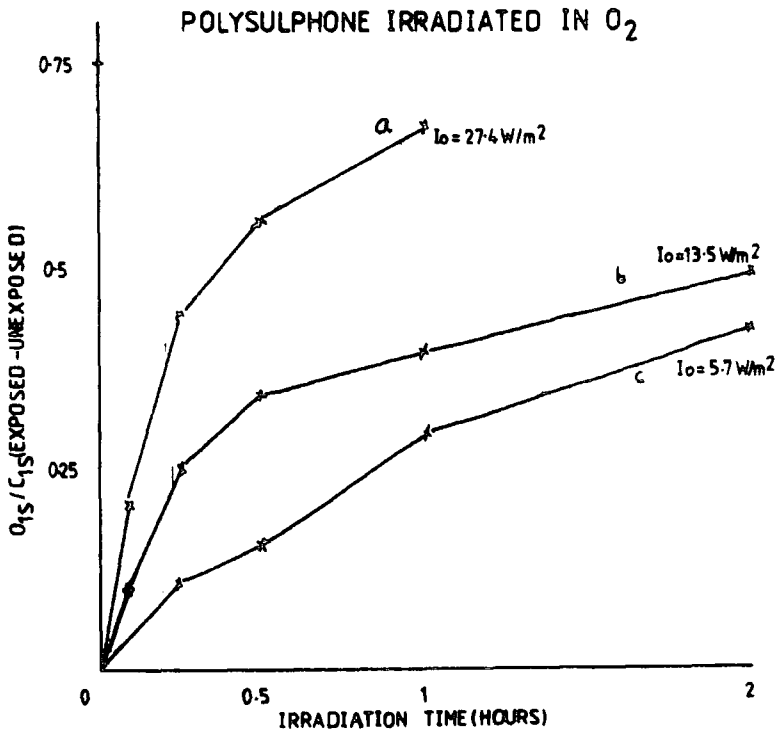

Figure 8.7 Oxygen uptake in polysulphone films irradiated at three different intensities (a) 5.7Whm^{-2}h^{-1}, (b) 13.5Whm^{-2}h^{-1} and (c) 27.4Whm^{-2}h^{-1}.

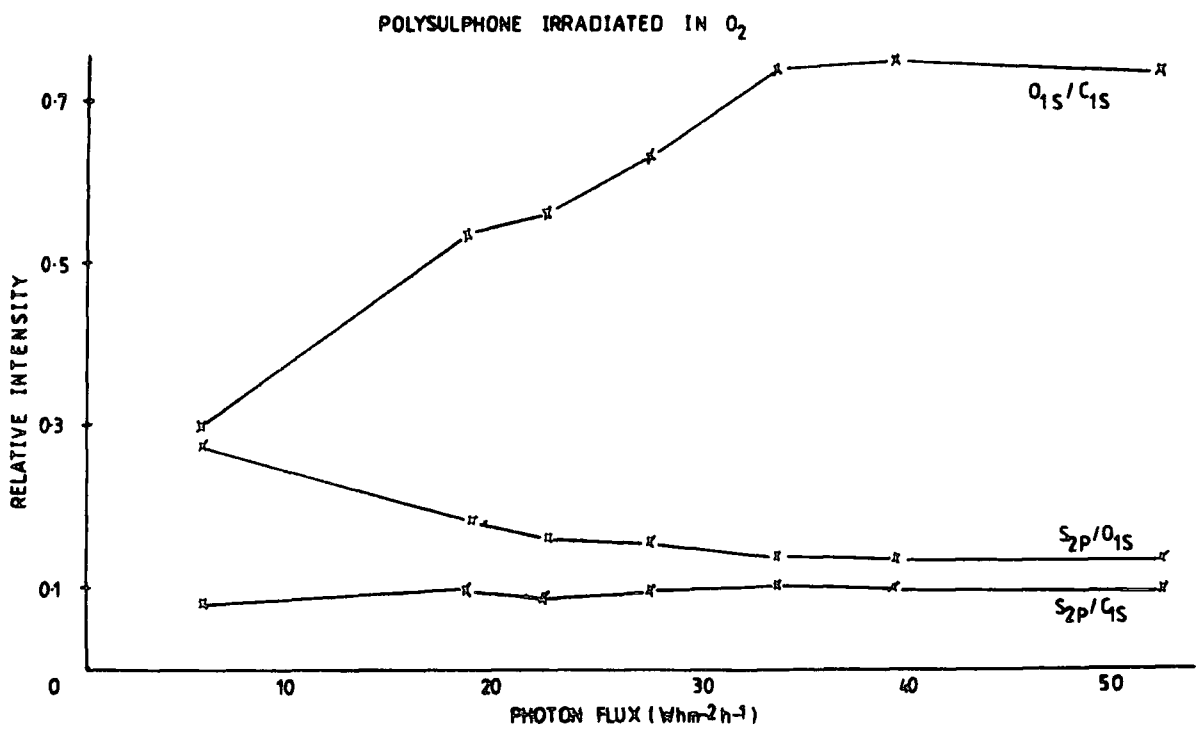

Figure 8.8 O_{1s}/C_{1s}, S_{2p}/O_{1s}, S_{2p}/C_{1s} intensity ratios for polysulphone films irradiated for 15 minutes at various photon fluxes

a great deal over the range of light intensities employed. The corresponding C_{1s} component analysis displayed in Figure 8.9 reveals that the major difference, arising from irradiation at higher photon flux, is an increase in the intensity of the carboxylate functionality and consequently a decrease in C-H and C=O components.

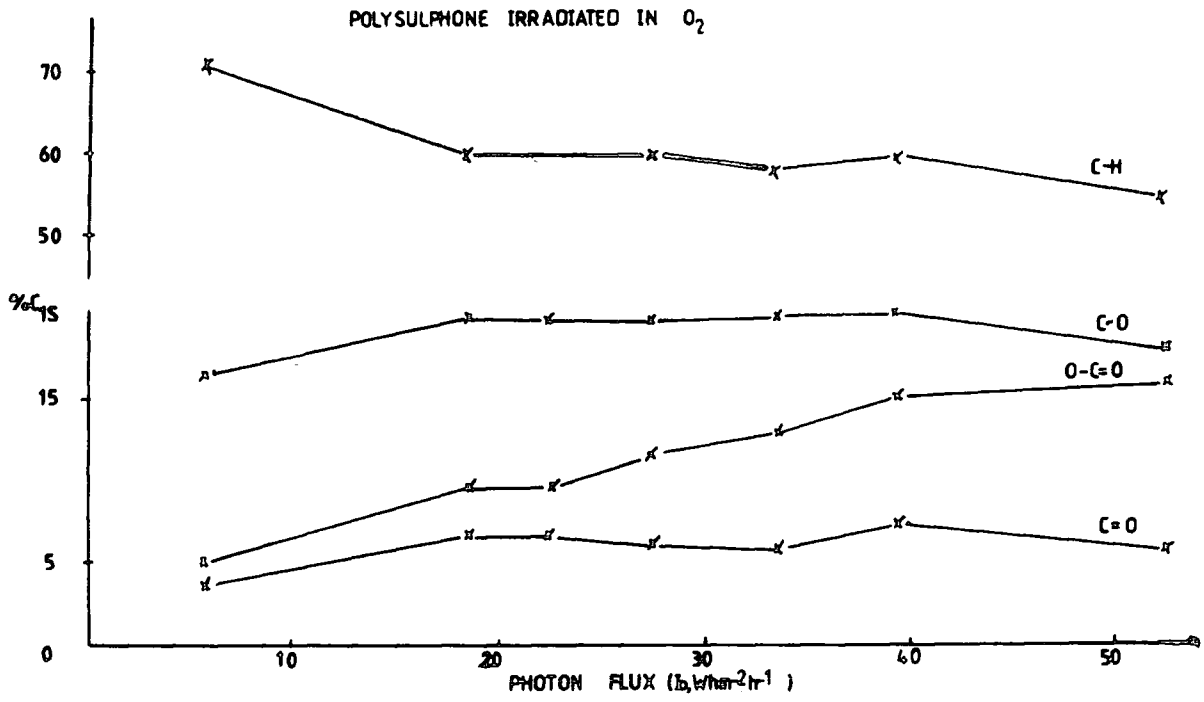

Figure 8.9 C_{1s} components for polysulphone films irradiated for 15 minutes at various photon fluxes.

(b) Surface Hydroperoxide formation

In the previously discussed photooxidation studies of polycarbonate and polystyrene films, hydroperoxide formation was followed by the conversion of these groups to sulphates by

the direct reaction with SO_2. However, as has been discussed in the previous section, the S_{2p} core level broadens during the photooxidation of polysulphone giving rise to two sulphur environments corresponding to sulphone and sulphate. The sulphate component arises from the reaction of SO_2, released by chain scission on either side of the sulphone group, with hydroperoxides. As such polysulphone appears to provide its own internal labelling of these groups.

The data in Figure 8.10 displays the total relative S_{2p} intensity and the contributions to this arising from the sulphone and sulphate components as a function of irradiation time for photon fluxes of 5.7 and 27.4 $Whm^{-2}h^{-1}$. It is apparent from Figure 8.10(a) that the rise in the intensity of the sulphate component and hence hydroperoxide formation, is gradual. Irradiation at higher photon flux reveals a sharp increase in sulphate content and reaches a maximum at an earlier stage than that for a similar total photon flux at lower lamp intensity. This trend is also reflected in the total sulphur content and may well reflect the greater rate of rate of desorption of low molecular weight carbon species from the surface at higher photon flux.

(c) Surface Chemistry as a function of Temperature

The changes in surface chemistry as described above were due to irradiations over a temperature range of 18-22^{o}C for photon fluxes of 5.7 amd 27.4 $Whm^{-2}h^{-1}$. Natural weathering exposures in Dhahran, Saudi Arabia are typically subjected to temperatures in excess of 30^{o}C. The bulk photooxidation of polysulphone is essentially invariant to temperatures up to $\sim$50^{o}C.[225] However, this may not be the case at the surface, consequently, preliminary studies have been conducted to investigate the surface

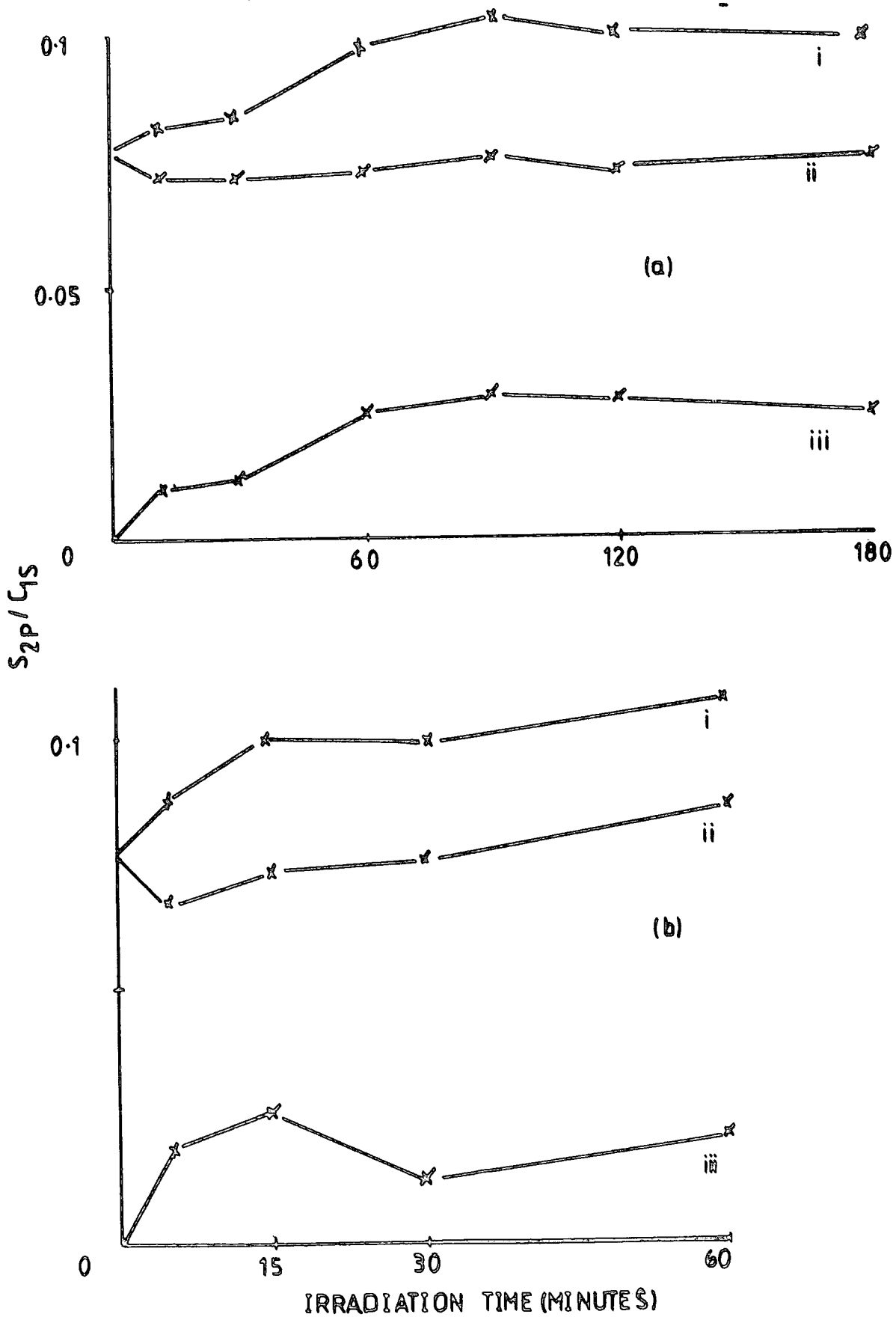

Figure 8.10 S_{2p}/C_{1s} intensity ratios for polysulphone films irradiated at two photon fluxes (a) 5.7 $Whm^{-2}h^{-1}$ and (b) 27.4 $Whm^{-2}h^{-1}$. (i) Total sulphur, (ii) Sulphone component and (iii) Sulphate component.

photooxidation of polysulphone at temperatures of 30, 50 and 70°C at a photon flux of 27.4 $Whm^{-2}h^{-1}$ and the relevant data are displayed in Table 8.2.

TABLE 8.2 % C_{1s} components, O_{1s}/C_{1s} and S_{2p}/C_{1s} intensity ratios for polystyrene films irradiated with an incident photon flux of 27.4 $Whm^{-2}h^{-1}$ as functions of time and temperature.

T(°C)	Time (minutes)	C-H	C-O	C=O	O-C=O	$\Pi \rightarrow \Pi^*$	O_{1s}/C_{1s}	S_{2p}/C_{1s}
30	5	68	18	3	7	4	0.48	0.09
	10	63	18	6.5	9	3.5	0.56	0.09
	15	58	20	7	12	3	0.69	0.10
	20	62	17	5	13	3	0.62	0.09
50	5	69	17	5	6	3	0.43	0.08
	10	66	16	5	10	3	0.52	0.09
	15	60	19	6	12	3	0.70	0.10
	20	59	20	6	12	3	0.69	0.09
70	10	63	19	6	9	3	0.54	0.08
	15	61	18	6	12	3	0.63	0.08
	20	62	18	6	12	2	0.62	0.09

The differences in the relative O_{1s}/C_{1s} intensity ratio on increasing the reaction temperature from 30 to 50°C are remarkably small reflecting a balance between desorption processes and photo-oxidation. The corresponding C_{1s} component analysis reveals that the carbonyl and carboxylate levels are also similar. The data for irradiation at 70°C shows a similar trend, in fact the C_{1s} components after 10 minutes' exposure at 30° and 70°C are comparable and highlight the small effect of elevating the temperature.

Comparison of the oxygen uptake at 22°C and 30°C, as shown in Figure 8.11, reveals a greater rate at the higher temperature in the initial stages. This increase however, does not reflect the approximation of an increase in reaction temperature of 10° doubling the rate. Examination of the C_{1s} components shows that at 30°C the carboxylate intensity is larger than that at 22°C.

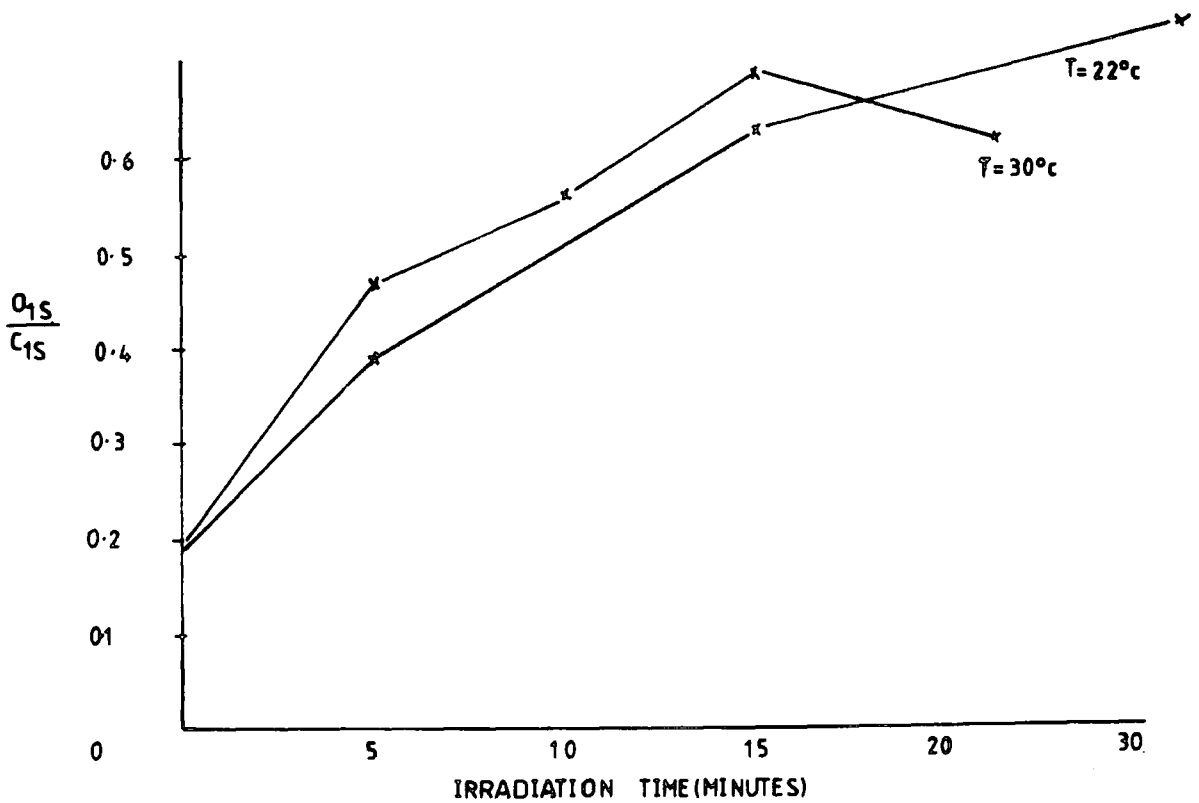

Figure 8.11 Comparison of oxygen uptakes for polysulphone irradiated at 22° and 30°C for varying periods of time

(d) Comparison of irradiations at λ>290nm and λ>240nm

A previously reported study of the surface photooxidation of polysulphone involved irradiations in a static oxygen atmosphere

and wavelengths >230nm.[51] Analysis of the oxidised carbon functionalities in the surface revealed that in the initial stages carbonyl and carboxylate functionalities are formed at comparable rates. Photooxidation at wavelengths >290nm in a flowing oxygen atmosphere as discussed above clearly reveals that the rate of O-C=O formation is faster than carbonyl indicating that different mechanisms are involved. In order to verify that these differences occur under the present experimental conditions, polysulphone films were exposed to ultraviolet light at wavelengths >240nm. This was achieved by replacing the pyrex window in the stainless steel reactor with a zero path length quartz window. The distance between the lamp and the sample was determined such that the incident light intensity for λ>290nm was 13.5 $Whm^{-2}h^{-1}$.

The C_{1s}, O_{1s} and S_{2p} core levels displayed in Figure 8.12 reveal the typical changes that occur during exposure (λ>240nm) for various periods of time. The C_{1s} envelope increases in complexity with components arising from carbonyl and carboxylate functionalities and with the increasing intensity of the O_{1s} signal it is evident that extensive photooxidation has occurred. The changes in the relative O_{1s}/C_{1s}, S_{2p}/C_{1s} and S_{2p}/O_{1s} intensity ratios are shown in Figure 8.13 as a function of irradiation time. Oxygen incorporation into the surface is rapid and a steady state is reached after 1 hour's exposure. The S_{2p}/C_{1s} level decreases in the initial stages indicative of the desorption of SO_2, however on extended exposure, it rises probably due to an increased rate in the loss of oxidised carbon species.

The main interest in these results is the relative rates of formation of the carbonyl and carboxylate components. The

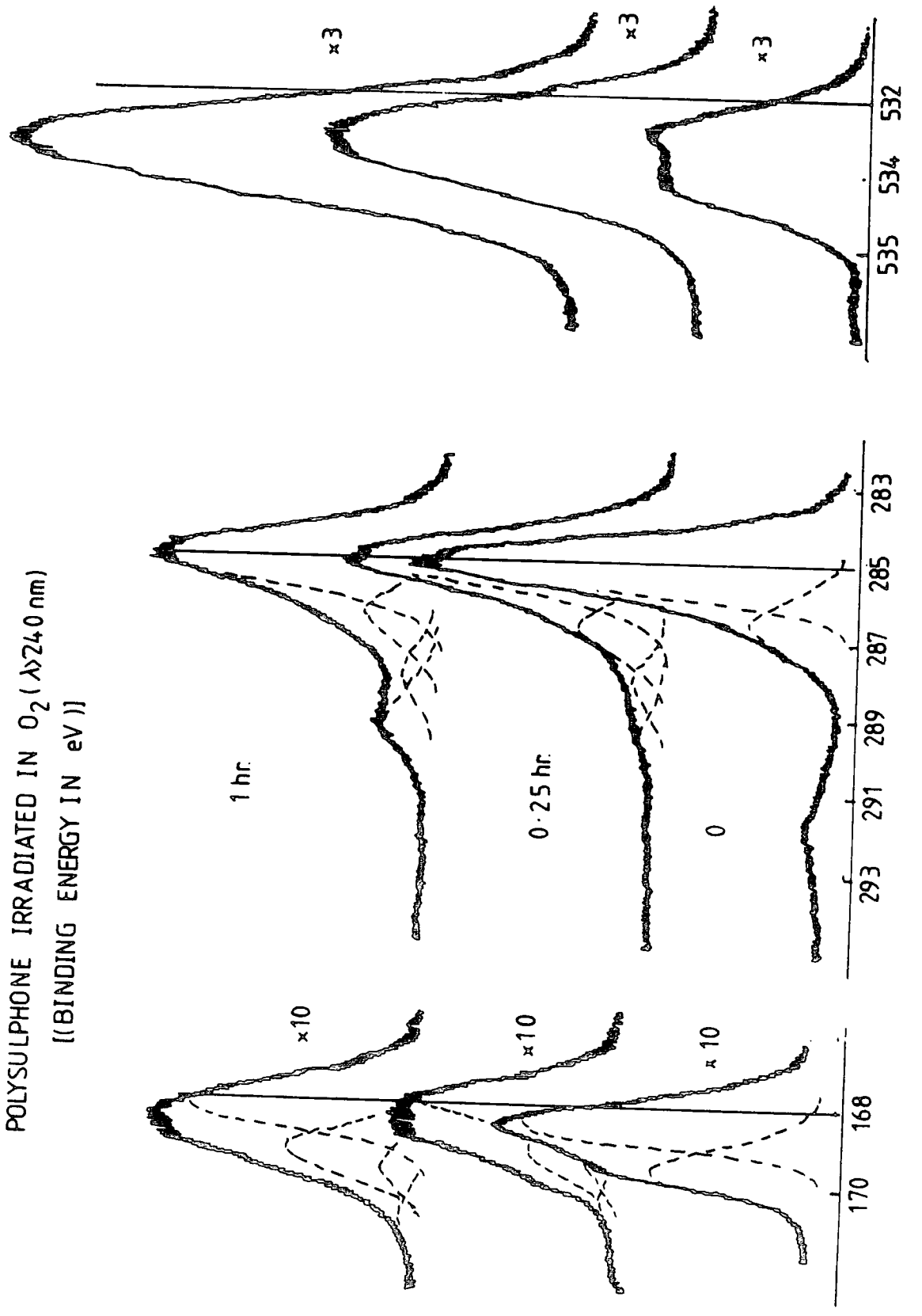

Figure 8.12 C_{1s}, O_{1s} and S_{2p} core levels for polysulphone films irradiated (λ>240nm) for various periods of time

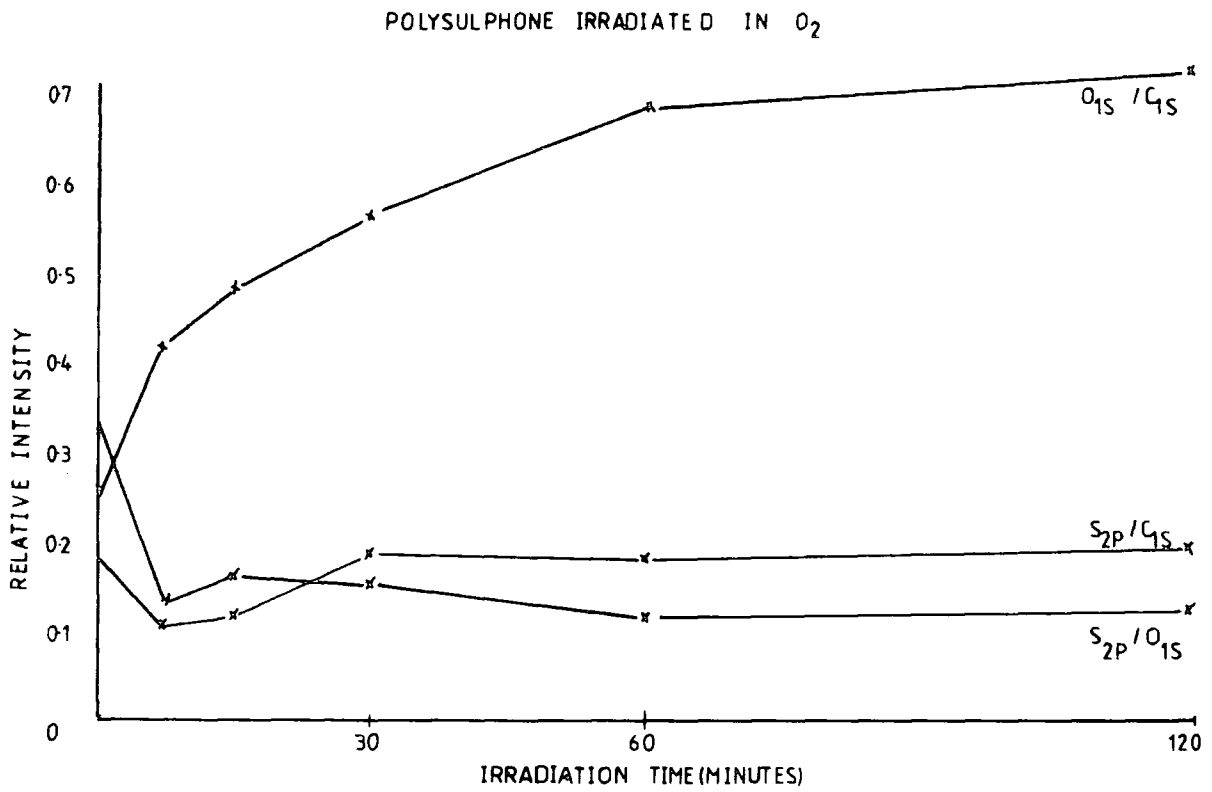

Figure 8.13 O_{1s}/C_{1s}, S_{2p}/C_{1s} and S_{2p}/O_{1s} intensity ratios for polysulphone films irradiated (λ>240nm) for various periods of time.

relevant data are displayed in Figure 8.14 (for comparison the corresponding data for λ>290nm are included). Figure 8.14(b) reveals that initially carbonyl formation is more rapid than carboxylate. The decrease in the intensity of the former on extended exposure corresponds to an increase in carboxylate indicative that these groups arise from the further photooxidation of carbonyl groups. Irradiation at λ>290nm reveals that the trend for λ>240nm is reversed. This clearly indicates that two different mechanisms are involved. This is understandable on consideration of the relative wavelength distributions.

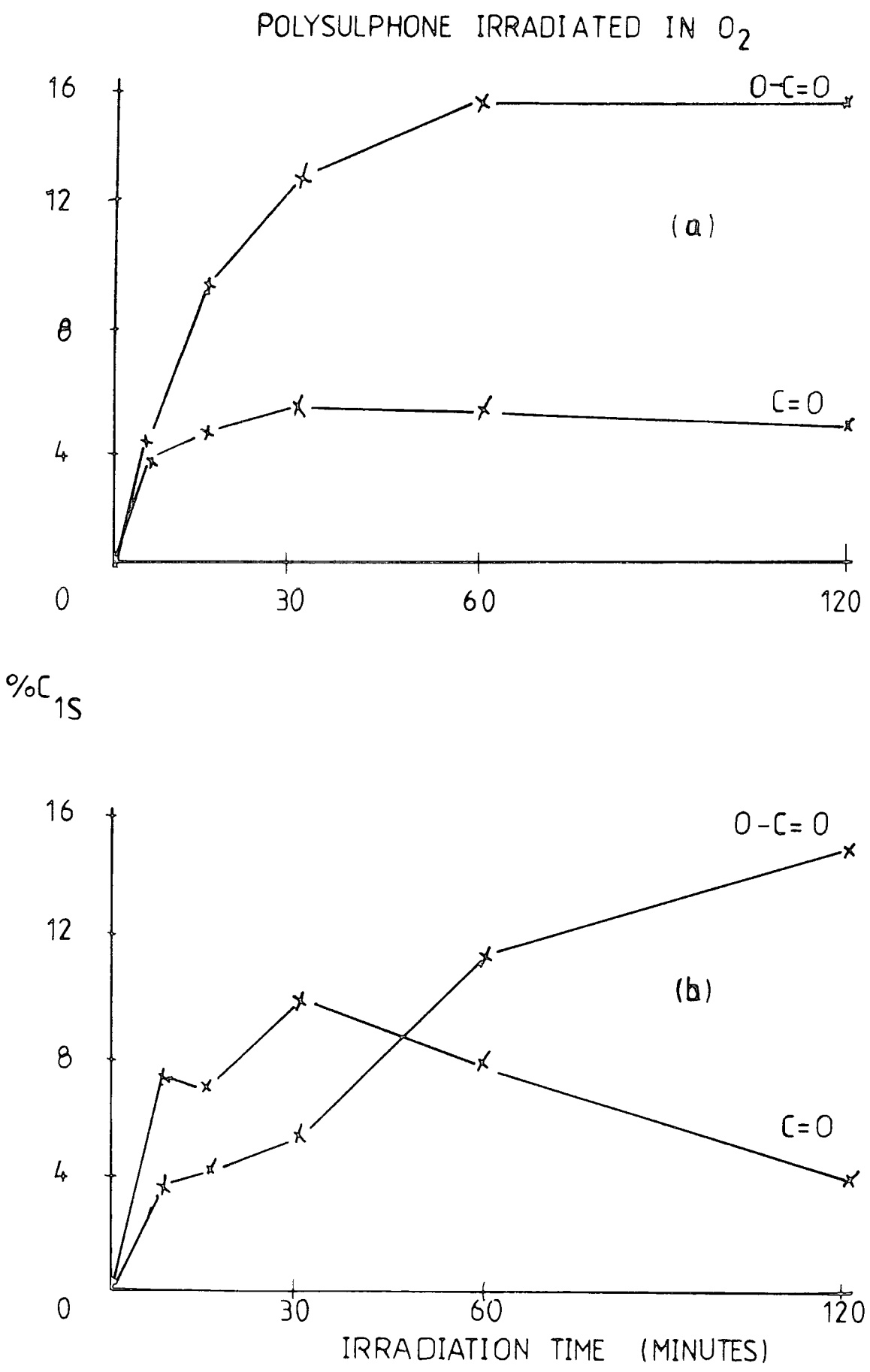

Figure 8.14 Comparison of the formations of carbonyl and carboxylate components (a) λ>290nm, (b) λ>240nm.

At λ>240nm, the 254nm band emitted from the Hg arc lamp will reach the sample and as polysulphone absorbs strongly in this region it is likely that the phenyl rings will be directly excited and participate in the photooxidation mechanism. Evidence for the oxidation of these groups arises from the observed decrease in intensity of the $\Pi \rightarrow \Pi^*$ shake-up satellite. The mechanism proposed by Ranby and Rabek[204] for the ring opening of the pendant phenyl group in polystyrene gives rise to carbonyl groups (cf. Chapter Seven). If such a mechanism occurs in polysulphone then the increase in carbonyl functionality would be expected to occur at a faster rate than for the carboxylate.

Decrease in the $\Pi \rightarrow \Pi^*$ component during irradiation at λ>290nm has also been observed. Direct excitation of the phenyl groups under these conditions is not possible and consequently a different mechanism must be involved if the observed $\Pi \rightarrow \Pi^*$ decrease is a true representation of the oxidation of the aromatic groups at these wavelengths. Evidence for these reactions may be obtained from the consideration of the photooxidation of an aromatic polysulphone which does not contain the gem dimethyl moiety of Bisphenol A polysulphone. This is discussed in the next section where the photooxidation of polyethersulphone (-Ph-SO_2-Ph-O) is considered.

(e) <u>The surface photooxidation of polyethersulphone</u>

Comparison of the uv absorption spectra for Bisphenol A polysulphone and polyethersulphone, as revealed in Figure 1.3 (Chapter One), shows that the latter polymer absorbs light below 350nm and the former below 320nm reflecting the influence of the aromatic isopropylidene link. The differences in changes in

in the ultraviolet absorptions of these two polymers on photooxidation have already been noted by Davis and Gardiner.[225] A laser flash photolysis study has shown that one of the primary photochemical processes in polyethersulphone is the formation of a phenoxy radical by bond cleavage at the diphenyl oxygen group.[226]

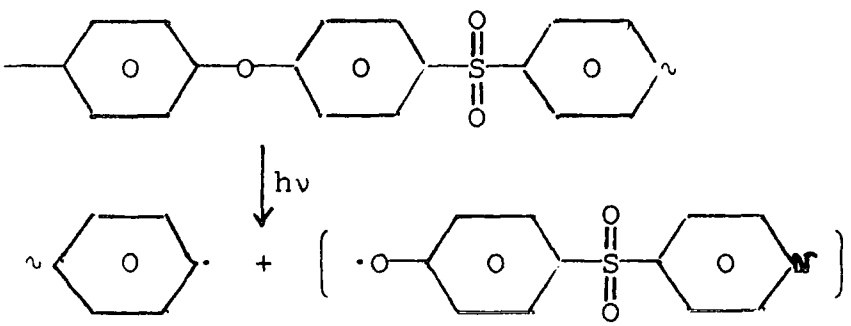

Transient species

The changes in surface chemistry during photooxidation have not as yet been reported. The ESCA spectra displayed in Figure 8.15 reveal the C_{1s}, O_{1s} and S_{2p} core levels of polyether sulphone before and after irradiation (λ>290nm) at a photon flux of 27.4 $Whm^{-2}h^{-1}$ for varying periods of time. The C_{1s} envelope for the starting material reveals photoemission peaks at 285.0 and 286.4 eV corresponding to C-H and C-O species. As previously noted, due to the overlapping nature of C-H and C-O components it is convenient not to resolve the peak at ∿286.0 eV arising from carbon bonded to sulphur. A shake-up satellite centred at 291.8 eV is also evident indicative of the aromaticity present in the polymer.

On exposure the complexity of the C_{1s} envelope increases with the appearance of carbonyl and carboxylate groups. The O_{1s} level changes from a distinctive 1:2 doublet to a more symmetrical envelope. The observed changes are consistent with oxygen incorporation into the surface. This is more readily

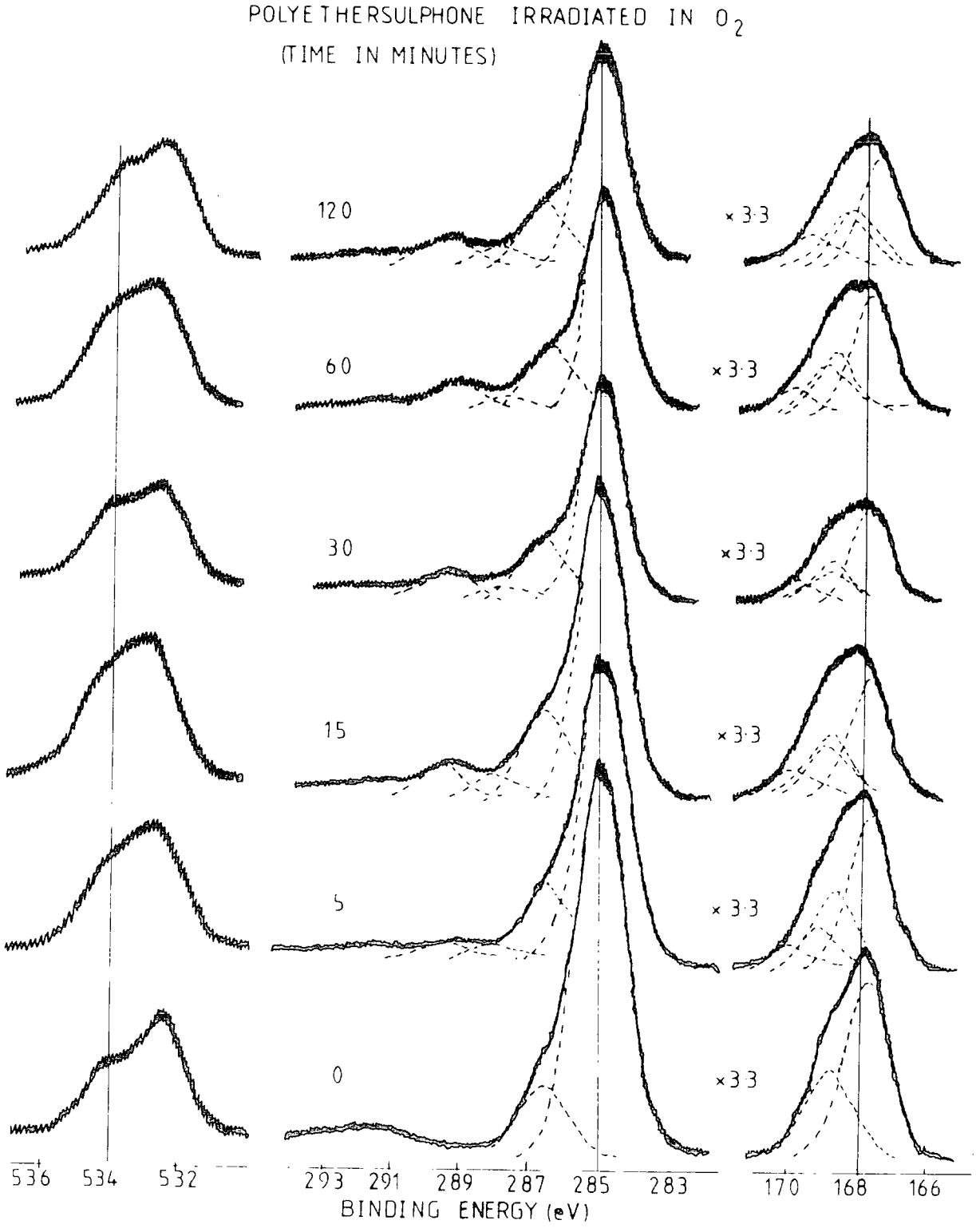

Figure 8.15 C_{1s}, O_{1s} and S_{2p} core levels for polyethersulphone films irradiated in O_2 (λ>290nm, Io = 27.4Whm^{-2}h^{-1})

apparent from the relative O_{1s}/C_{1s} intensity ratios shown in Figure 8.16. A maximum is obtained after an hour's exposure corresponding to a ∿100% increase in oxygen content.

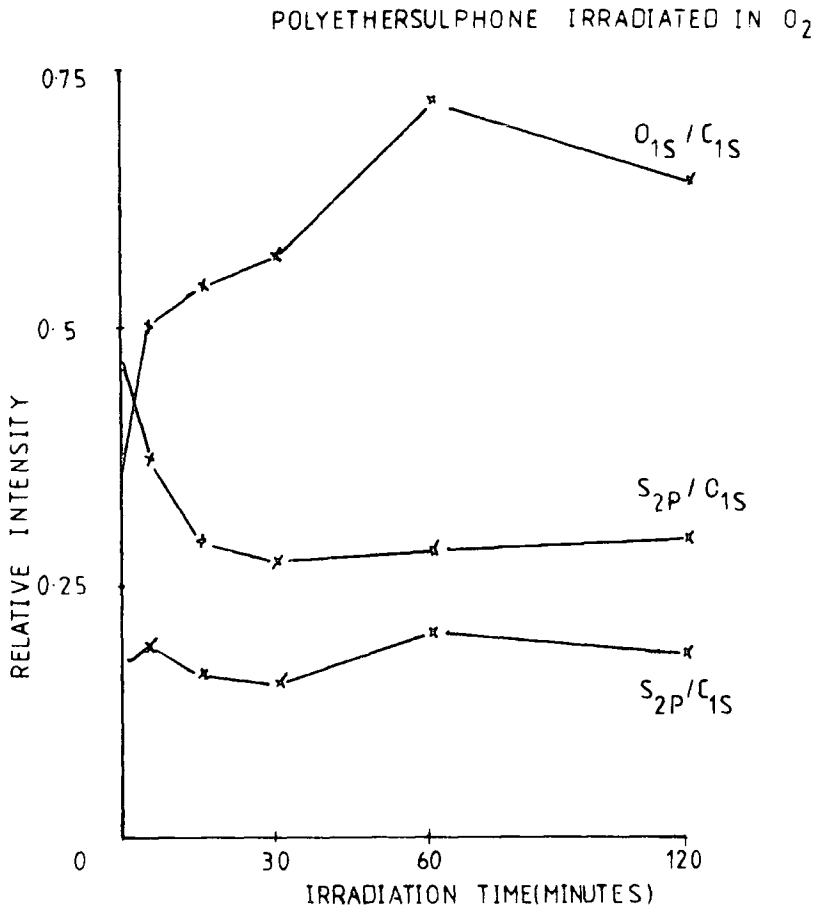

Figure 8.16 O_{1s}/C_{1s}, S_{2p}/C_{1s} and S_{2p}/O_{1s} intensity ratios for the spectra in Figure 8.15.

The S_{2p}/C_{1s} ratio, also shown in Figure 8.16 fluctuates around the initial value but remains essentially unchanged after extended exposure. As in the case of Bisphenol A polysulphone, this is indicative of the loss of oxidised carbon species occurring at a faster rate than that for SO_2. Examination of the S_{2p} core levels in Figure 8.15 reveals a broadening on exposure arising from an additional component at ∿169.2 eV which may be assigned to sulphate groups. This gives direct evidence for the formation

of hydroperoxide groups on the aromatic rings.

The nature of the surface oxidation becomes more apparent from a consideration of the C_{1s} component analysis displayed in Figure 8.17. The C-H component (phenyl carbon not bonded to oxygen) decreases as a function of irradiation time whilst the C-O, >C=O and O-C=O functionalities increase in intensity.

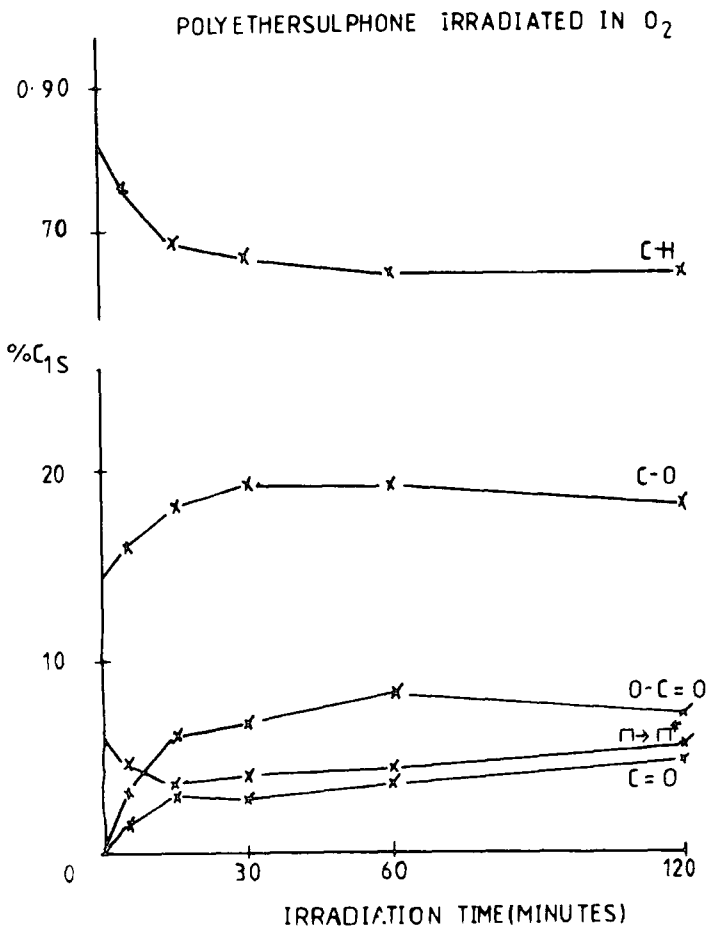

Figure 8.17 C_{1s} components for the spectra in Figure 8.15

The Π→Π* component initially decreases in intensity indicative of loss in the aromatic content. This, along with the presence of carbonyl and carboxylate groups is evidence for the photo-oxidation of the phenyl groups. The rise in intensity of the shake-up peak in the later stages of exposures may well be due

to a low level of carbonate functionalisation occurring at ∿290.8 eV.

It is clear from these results that photooxidation of polyethersulphone at λ>290nm involves the direct oxidation of the aromatic rings. As observed in polysulphone, the rate of carbonyl formation is less than that for carboxylate and this suggests similar mechanisms. The ∿Ph-SO_2-Ph-O∿ group within polysulphone thus contributes to the oxygen uptake but from a comparison of the relative rates this is not as great as that for the aromatic isopropylidene group.

8.3.2 Reactions in Nitrogen

The investigations described above have indicated the importance of oxygen in the surface photodegradation of polysulphone and for comparison irradiations have been carried out in a flowing nitrogen atmosphere.

The core levels in Figure 8.18 reveal the changes in the C_{1s}, O_{1s} and S_{2p} envelopes for exposure with an incident photon flux of 13.5 $Whm^{-2}h^{-1}$. It is clear from this data that there is a low level of oxygen uptake and the nature of this is revealed in the C_{1s} component analysis displayed in Figure 8.19. A small level of carbonyl and in the later stages carboxylate functionalisation is evident. The $\Pi \rightarrow \Pi^*$ shake-up satellite remains essentially constant showing that the aromatic rings remain intact.

The low degree of oxygen uptake for irradiations in nitrogen is also shown by comparison of the relative O_{1s}/C_{1s} intensity ratios as revealed in Figure 8.20. Also shown, along with the S_{2p}/C_{1s}, S_{2p}/O_{1s} ratios, are the relevant data for oxygen

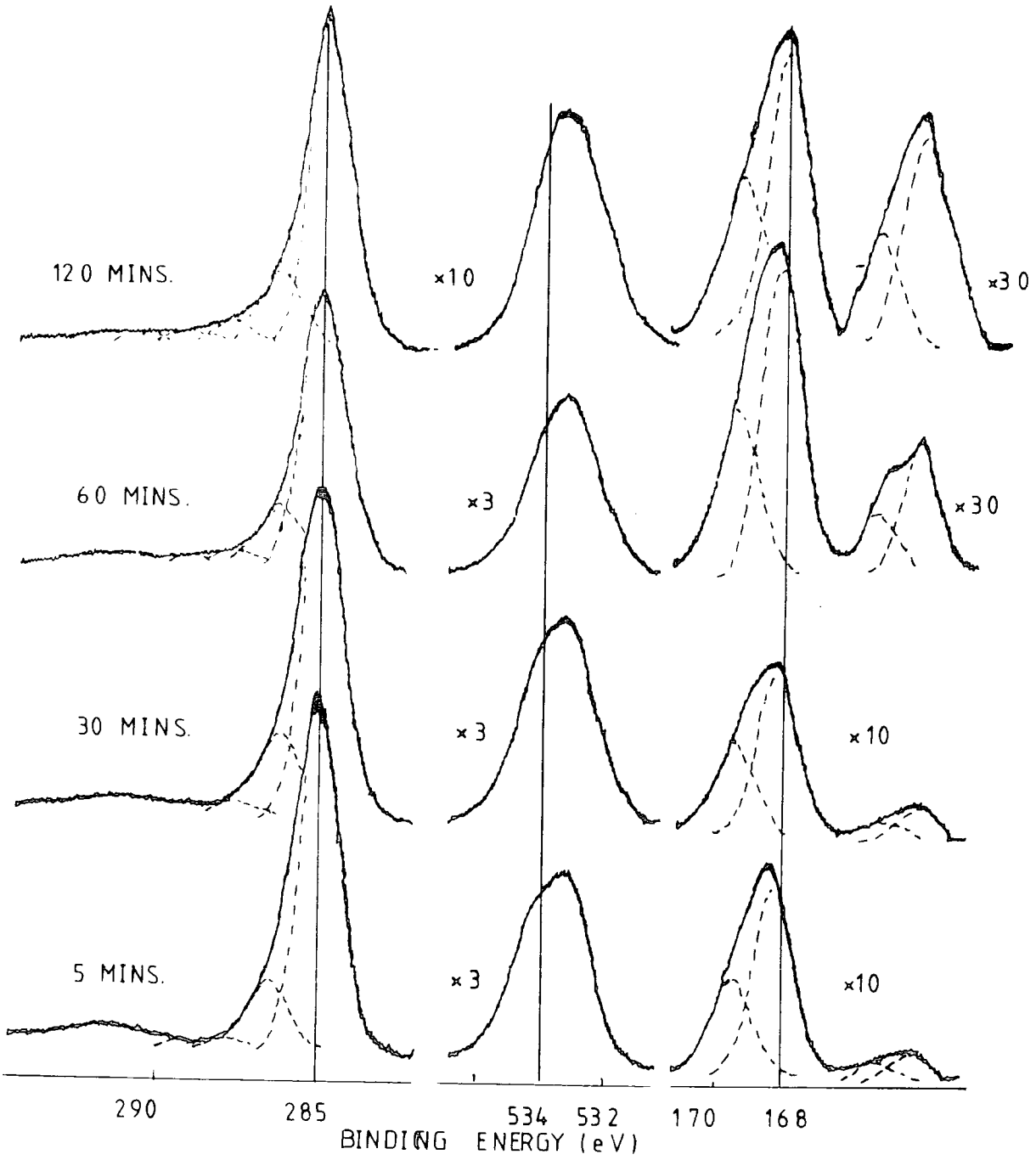

Figure 8.18 C_{1s}, O_{1s} and S_{2p} core levels for polysulphone films irradiated in nitrogen (λ>290nm).

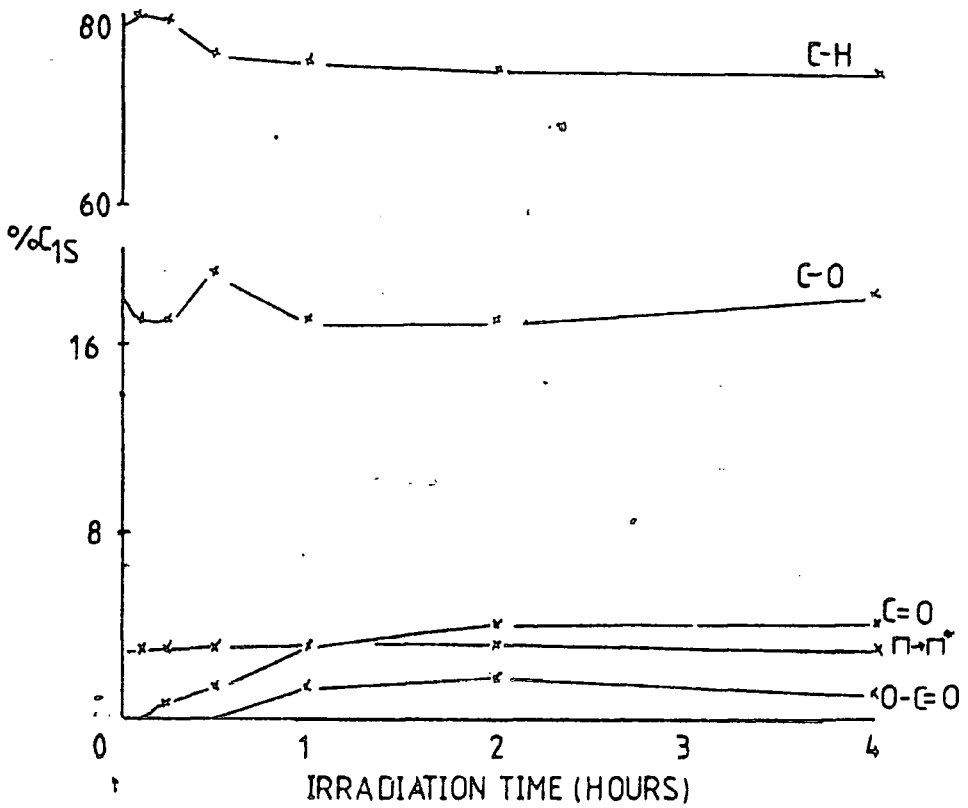

Figure 8.19 C_{1s} component analysis for the spectra in Figure 8.18.

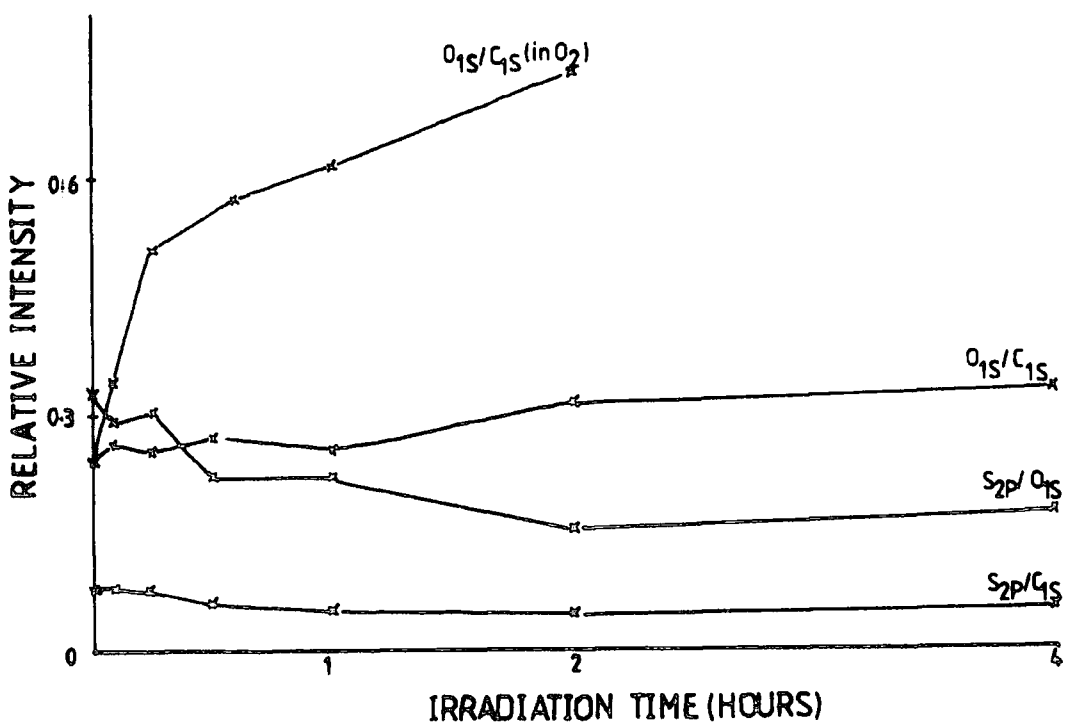

Figure 8.20 O_{1s}/C_{1s}, S_{2p}/C_{1s} and S_{2p}/O_{1s} intensity ratios for the spectra in Figure 8.18.

uptake for comparable irradiations in oxygen. These data highlight the importance of the partial pressure of oxygen in the photodegradation process.

The most striking reature of the irradiation of polysulphone in nitrogen may be observed in the S_{2p} core levels displayed in Figure 8.18. As exposure time increases, the S_{2p} signal decreases in intensity concomitant with appearance of a new peak at binding energy of ∿164.0 eV, representative of a sulphide group. After 4 hours' exposure this peak is of the same intensity as the sulphone, although it should be noted that the overall S_{2p} signal has decreased by ∿30% from that in the starting material. The changes in the S_{2p} core level as a function of time are displayed in Figure 8.21.

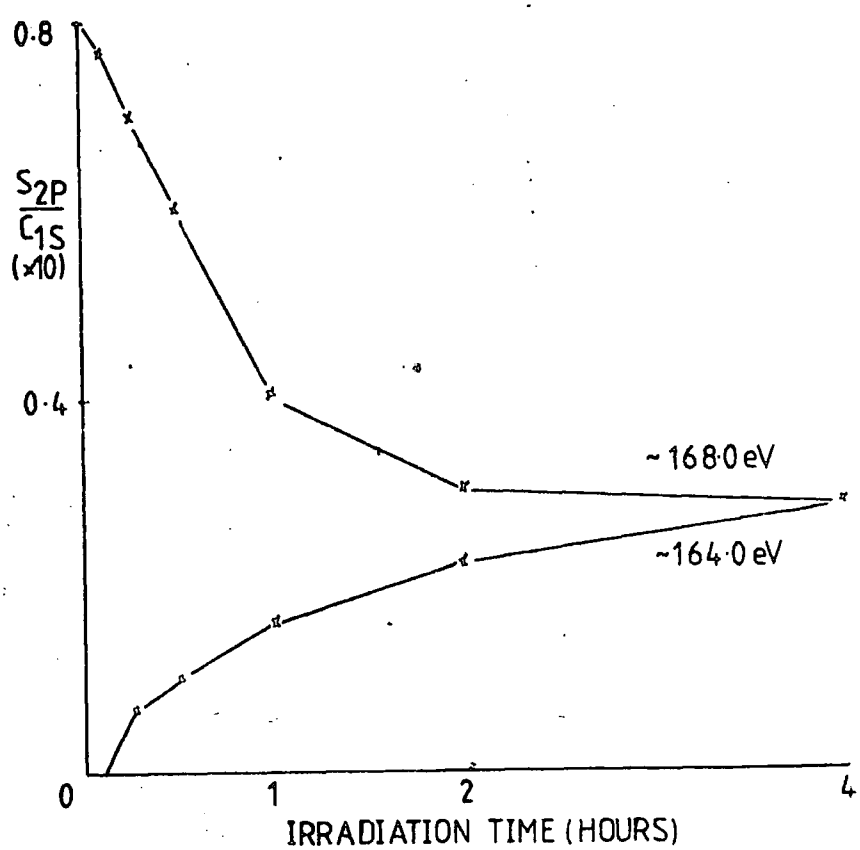

Figure 8.21 Components of the S_{2p} core levels for polysulphone films irradiated in nitrogen for various periods of time.

These results suggest a photoreduction reaction of the sulphone group which may arise from the photochemistry of liberated SO_2. Such a reaction has not been previously observed and the detection in these experiments may well be due to the surface sensitivity of ESCA.

For comparison polysulphone has been irradiated for an hour in low vacuum and the relevant core levels are displayed in Figure 8.22.

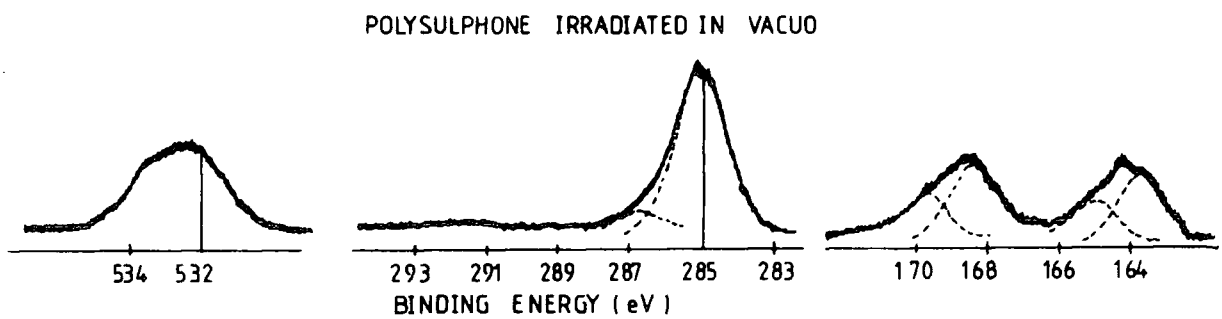

Figure 8.22 C_{1s}, O_{1s} and S_{2p} core levels for polysulphone films irradiated in vacuum.

The low binding energy sulphur component is again evident. The C_{1s} component analysis in Table 8.3 indicates the presence of a low degree of oxidative functionalisation which is reflected in

a small increase in the O_{1s} signal. The large decrease in the C-O intensity is indicative of chain scission at the ether linkages and this is also apparent in the increased C-H component. It is also interesting to note that sequential irradiation of polysulphone in nitrogen or vacuum for an hour followed by one hour in oxygen shows no evidence of the low binding energy sulphur component.

TABLE 8.3 C_{1s} component distributions for polysulphone films irradiated in vacuum

Time (minutes)	Total C_{1s}	C-H	C-O	C=O	O-C=O	$\Pi \rightarrow \Pi^*$	O_{1s}/C_{1s}	S_{2p}/C_{1s}
0	100	79	16	0	0	5	0.22	0.09
60	100	87	8	0.5	0.5	4	0.25	0.07

In order to investigate the effect of the irradiation of SO_2 at wavelengths >290nm, films of Bisphenol A polycarbonate have been exposed in a flowing SO_2 atmosphere. The ESCA spectra in Figure 8.23 display the C_{1s}, O_{1s} and S_{2p} core levels for exposures of 30 and 120 minutes. The C_{1s} envelope shows very little change but the distinctive 2:1 doublet of the unexposed O_{1s} signal has changed to ∿1:1. The presence of the S_{2p} envelope after exposure is very revealing and displays 3 chemical environment arising from components at ∿169.2, 168.0 and 164.0 eV. The low binding energy component increases on longer exposure.

The C_{1s} component analysis along with the O_{1s}/C_{1s} and S_{2p}/C_{1s} intensity ratios displayed in Table 8.4 reveal more clearly the nature of the changes in surface chemistry. The increase in C-O functionalisation will in part arise from the presence of C-S bonds as sulphur is incorporated into the surface.

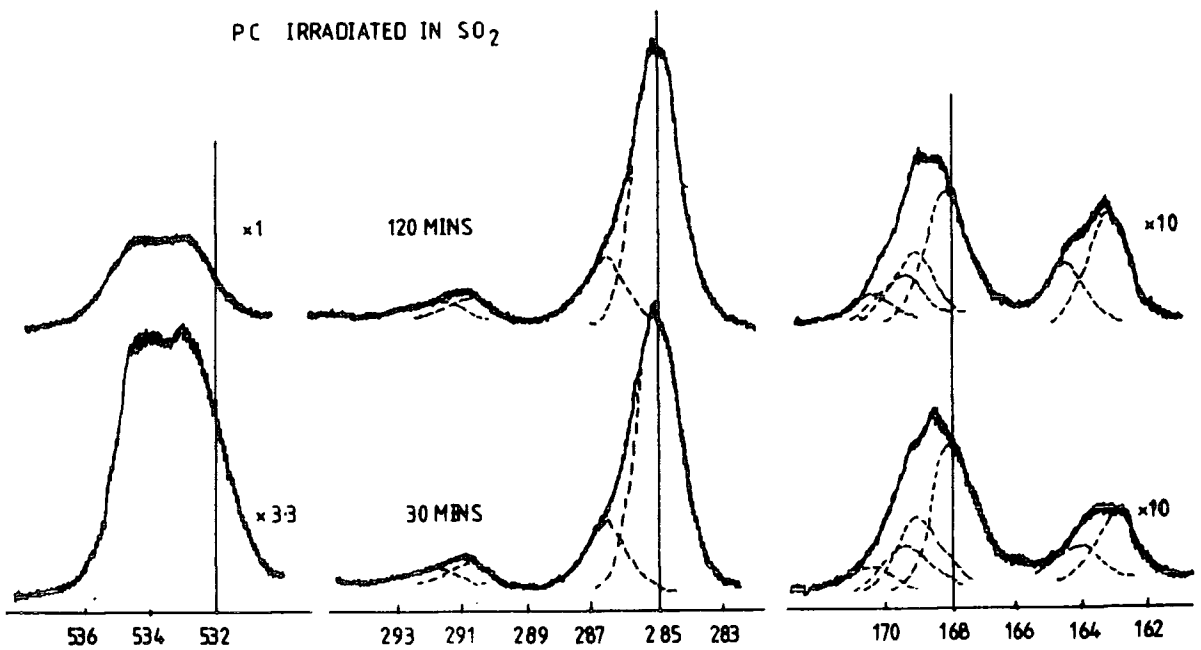

Figure 8.23 C_{1s}, O_{1s} and S_{2p} core levels for polycarbonate films irradiated in a flowing SO_2 atmosphere

The major change in the C_{1s} envelope is the decrease in O-$\underset{\underset{O}{\|}}{C}$-O groups with increasing exposure time. This suggests that the main chain scission occurs at the carbonate group. The $\Pi \rightarrow \Pi^*$ shake-up satellite remains relatively constant implying that the aromatic rings remain intact.

The total S_{2p} level increases in overall intensity between 30 and 120 minutes' exposure. As is apparent from Table 8.4 this increase arises from the component at 164.0 eV. The components due to sulphate and sulphone (at 169.2 and 168.0 eV respectively) remain roughly the same and this is also reflected

TABLE 8.4 Component distributions for C_{1s} and S_{2p} core levels and O_{1s}/C_{1s} intensity ratios for polycarbonate films irradiated in SO_2.

Time (Mins.)	C-H	C-O	C=O	O-C=O	CO_3	$\pi\rightarrow\pi^*$	O_{1s}/C_{1s}	S_{2p}/C_{1s}		
								SO_2	SO_4	S
0	78	13	0	0	6	3	0.27	0.002	0.002	
30	75	18	0	0	4	3	0.48	0.018	0.059	0.025
60	78	16	0	0	3	3	0.49	0.019	0.055	0.044

in the O_{1s}/C_{1s} level.

The data suggest that the main reaction arising from irradiation in SO_2 is the formation of sulphone functionalities and that the low binding energy component is a secondary and slower reaction. As such this probably arises from reactions mainly involving the newly formed sulphone group. On comparison with the results for polysulphone, the component at ∿164.0 eV therefore arises from the sulphone group and not liberated SO_2.

8.3.3 Surface Aspects of the Natural Weathering of Polysulphone

The discussion in Section 8.3.1 has considered in some detail the changes in surface chemistry induced by irradiation (λ>290nm) in pure oxygen. The formation of carboxylate functionalities were shown to be the main photooxidation products. Loss of aromaticity was also observed. In this section the changes observed in polysulphone during natural weathering in Dhahran, Saudi Arabia are considered in terms of bulk and surface chemistry and the results compared with those discussed above.

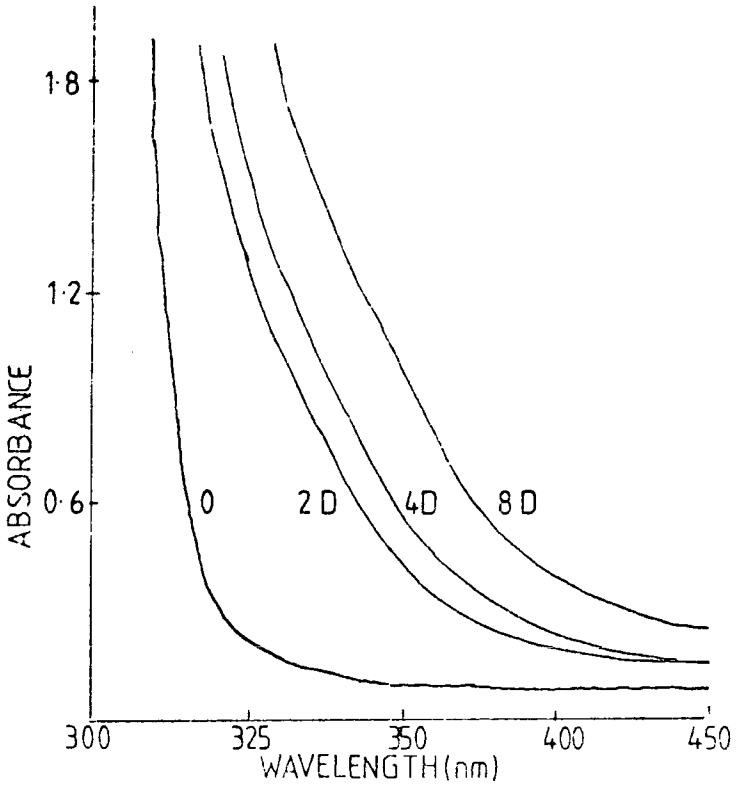

Figure 8.24 UV absorption spectra for polysulphone films weathered in Dhahran, Saudi Arabia.

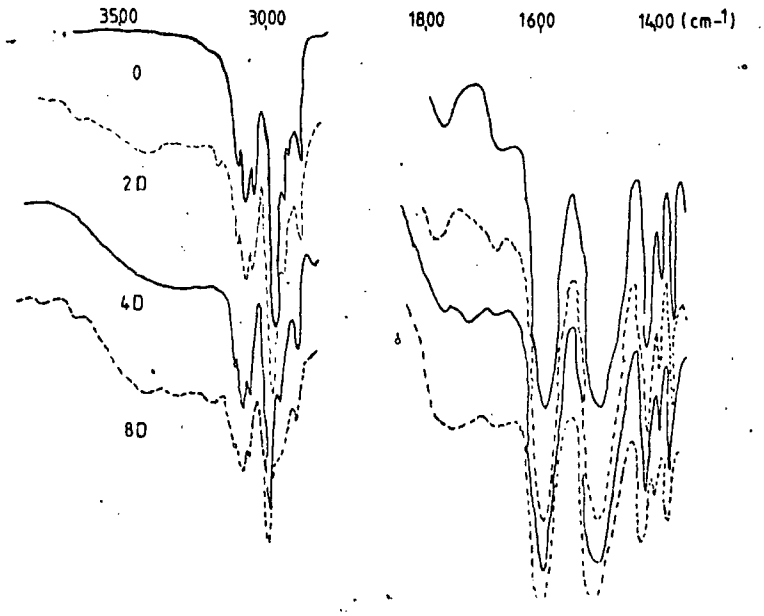

Figure 8.25 IR spectra for polysulphone films weathered in Saudi Arabia.

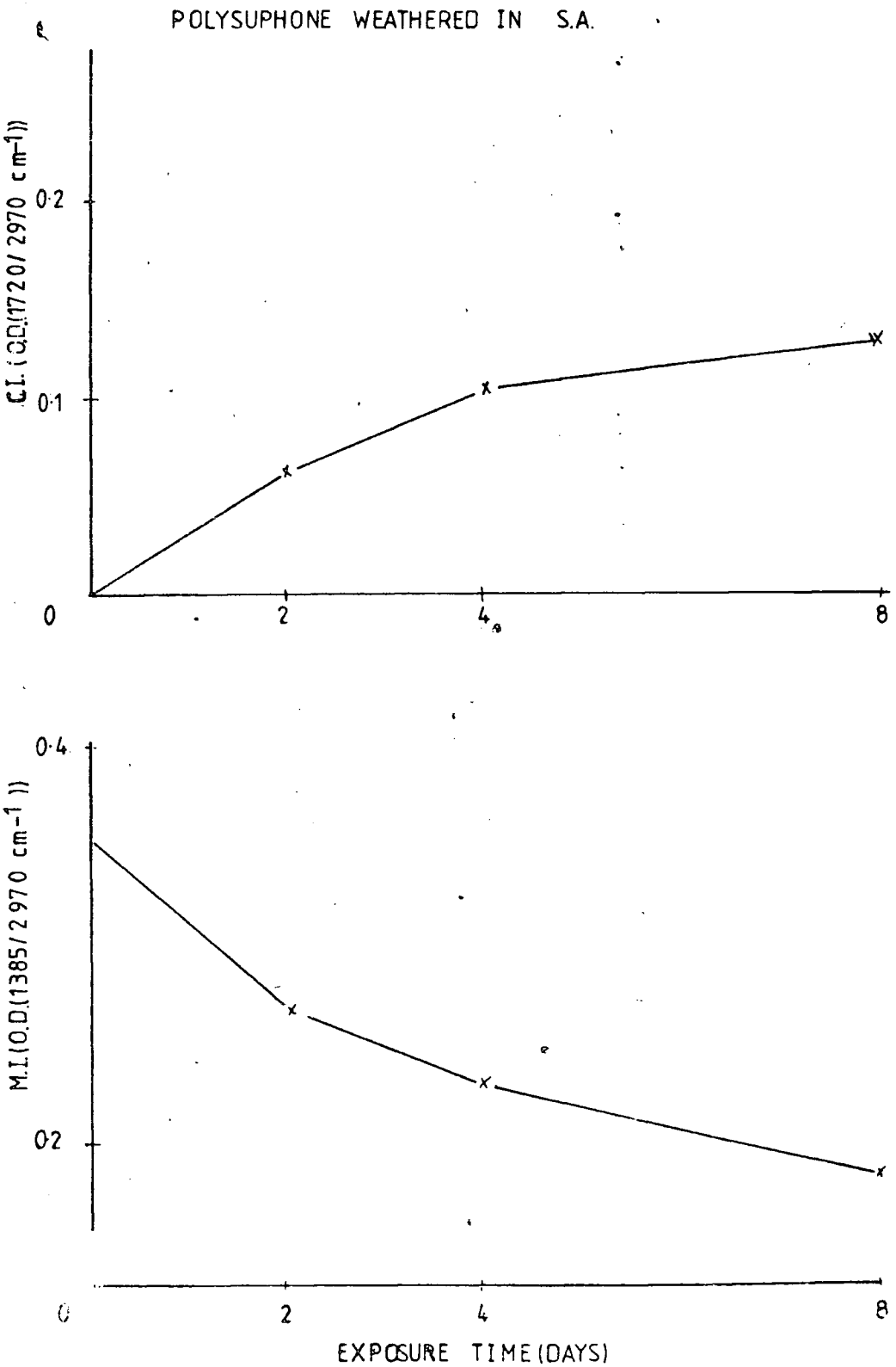

Figure 8.26 Methyl group and carbonyl group indexes for the spectra in Figure 8.25

(a) Bulk Chemistry

As a starting point in the investigation of the natural weathering of polysulphone, the uv and ir spectra for films exposed over the first eight days have been recorded and are displayed in Figures 8.24 and 8.25 respectively. The ir spectra reveal broad absorptions in the hydroxyl and carbonyl regions indicative of the formation of photooxidation products. The methyl group absorption at 1385 cm^{-1} decreases in intensity and this is revealed more clearly in Figure 8.26. The carbonyl index is also shown for comparison. The changes in absorbance at 330 nm as a function of time are displayed in Figure 8.27. It should be noted that these measurements were recorded ∿1 week after exposure and has been previously reported a dark reaction occurs which increases the absorbance at 330nm by ∿5%.[226]

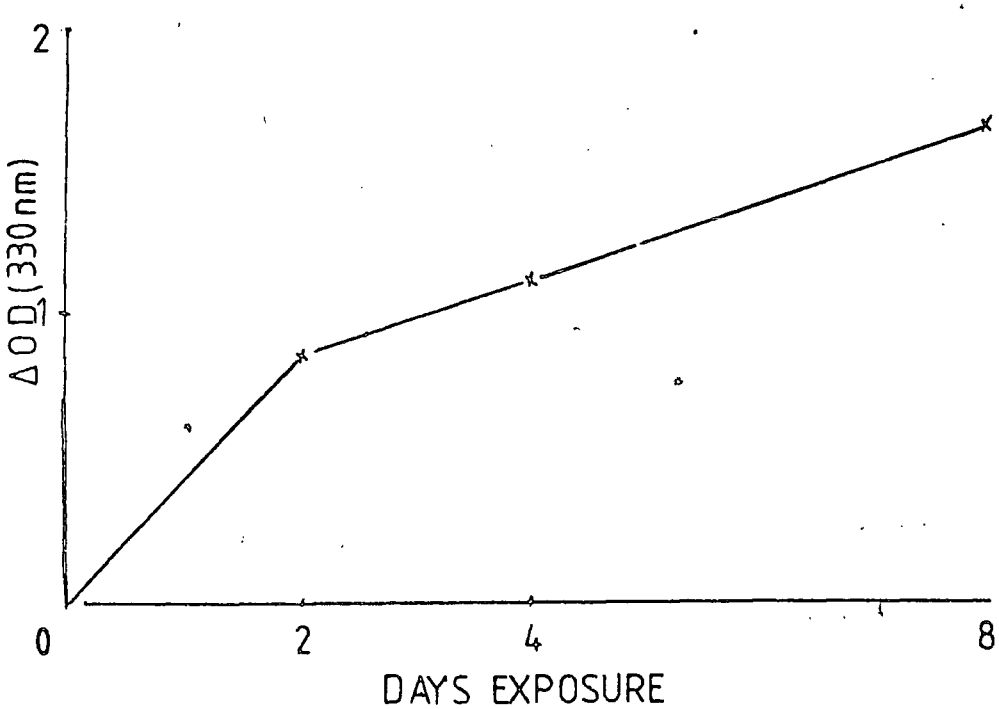

Figure 8.27 Changes in absorbance at 330nm for the spectra in Figure 8.24

The data reveals that the rate of change in the uv and ir regions are greatest over the first two days of exposure. This may reflect the attenuation of the incident radiation due to extensive changes in the surface chemistry as will be considered below.

(b) Surface Chemistry

The ESCA spectra for the C_{1s} and S_{2p} core levels for films exposed to direct sunlight in a horizontal configuration are displayed in Figure 8.28. For all the weathered samples, the ESCA data reveal a major surface contamination in the form of silicon dioxide which originates from airborne particles. The quantity is variable, although in general the amount increases with exposure time, and in consequence the O_{1s} spectra cannot be usefully employed in the data analysis. However, it has been shown that the contributions to the C_{1s} signal arising from oxidised carbon species reflect in general the trends shown by the O_{1s}/C_{1s} intensity ratio (cf. Chapters, 4, 5 and 6). The relevant data along with that for the relative S_{2p}/C_{1s} intensity ratios are displayed in Figure 8.29.

Oxygen incorporation into the surface steadily increases over the first 16 days. The corresponding sulphur content fluctuates about the value for the starting material. On extended exposure the S_{2p} signal decreases but this may be due to extraaneous material being deposited on the surface as will be discussed later. Broadening of the sulphur envelope occurs on exposure arising from two chemical environments, namely sulphone and sulphate. The presence of sulphate functionalities is consistent with the formation of hydroperoxides in the surface.

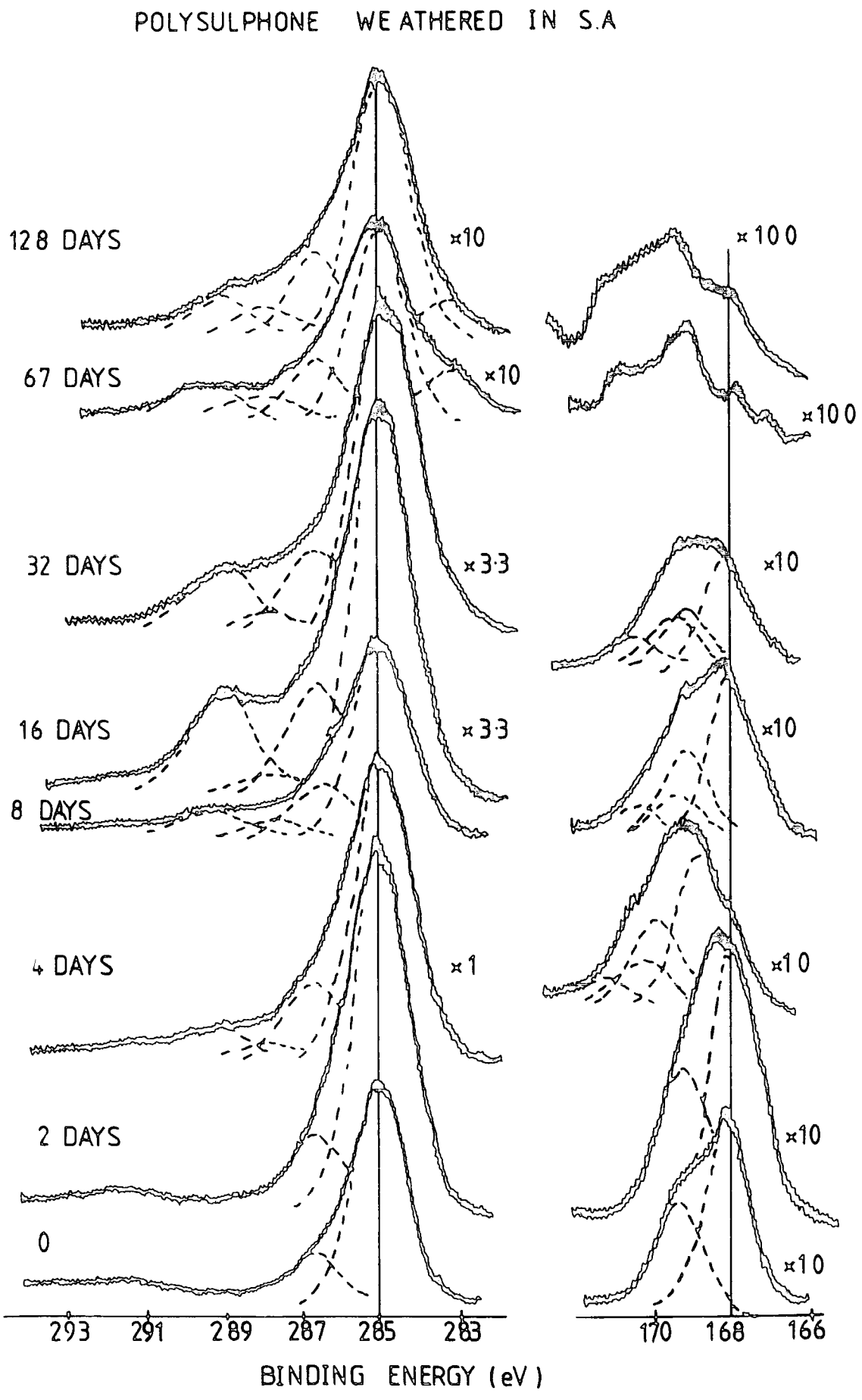

Figure 8.28 C_{1s} and S_{2p} core levels for polysulphone films weathered in Saudi Arabia

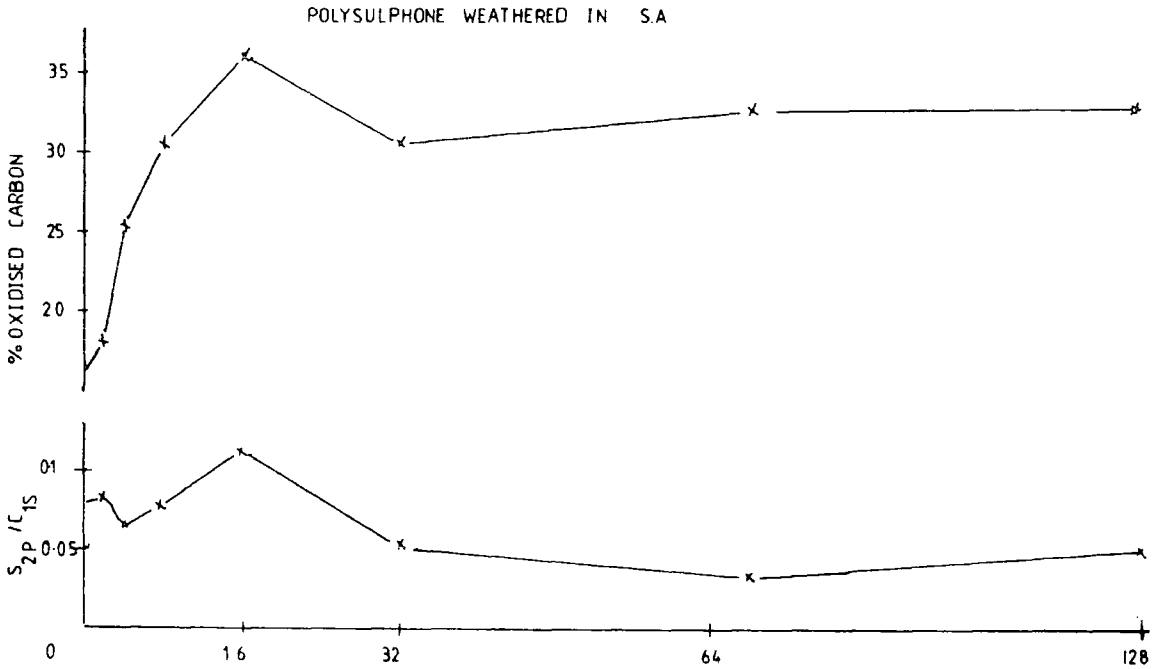

Figure 8.29 % contribution to the C_{1s} envelope arising from oxidative functionalities and S_{2p}/C_{1s} intensity ratios for the spectra in Figure 8.28.

As can be seen from the spectra in Figure 8.28 the C_{1s} envelope increases in complexity and the nature of the changes are revealed in Figure 8.30. The C-H component (representative of the phenyl and methyl groups) decreases in intensity as a function of exposure time. Increases occur for carbonyl and carboxylate functionalities with the latter formed at a greater rate. After 16 days this group represents ∿15% of the total carbon content in the surface which agrees well with the data obtained from model photooxidation studies for an extensively photooxidised surface. The degree of >C=O and O-C=O functionalisation cannot be readily accommodated in terms of reactions

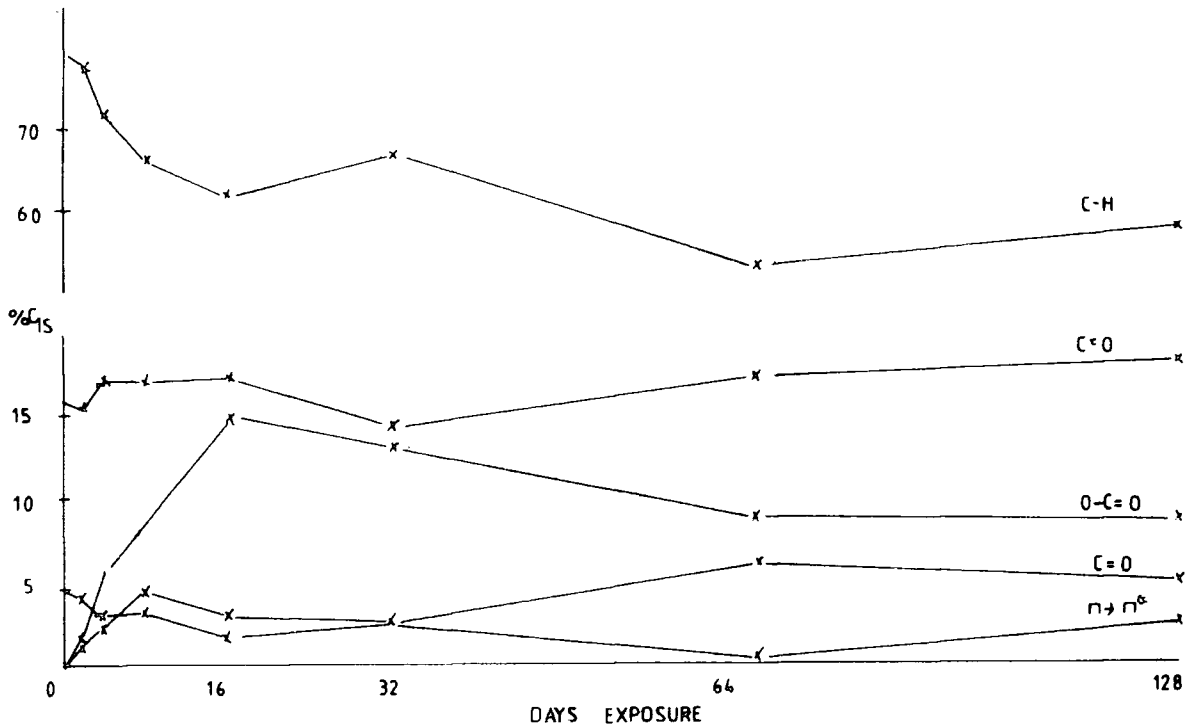

Figure 8.30 C_{1s} component analysis for the spectra in Figure 8.28

involving the methyl groups alone. The $\Pi \rightarrow \Pi^*$ shake-up satellite decreases in intensity during this period and suggests oxidation of the aromatic rings. That the carboxylate rate is greater than the carbonyl is indicative of a similar mechanism occurring in natural weathering as that in the model studies.

The data displayed in Figure 8.31 reveals the changes in the C_{1s} envelopes (in histogram form) occurring during the first 16 days of exposure in comparison to the daily variations in temperature and relative humidity. The minimum temperature does not fall below 26°C and the maximum fluctuates around 40°C. The conditions involve high temperatures but as has been shown in the model studies this does not drastically affect the com-

position of the surface. The relative humidity varies considerably but does not appear to influence the photo-oxidation in an observable manner. It is worthwhile noting that during the total 128 days' exposure, no precipitation was recorded.

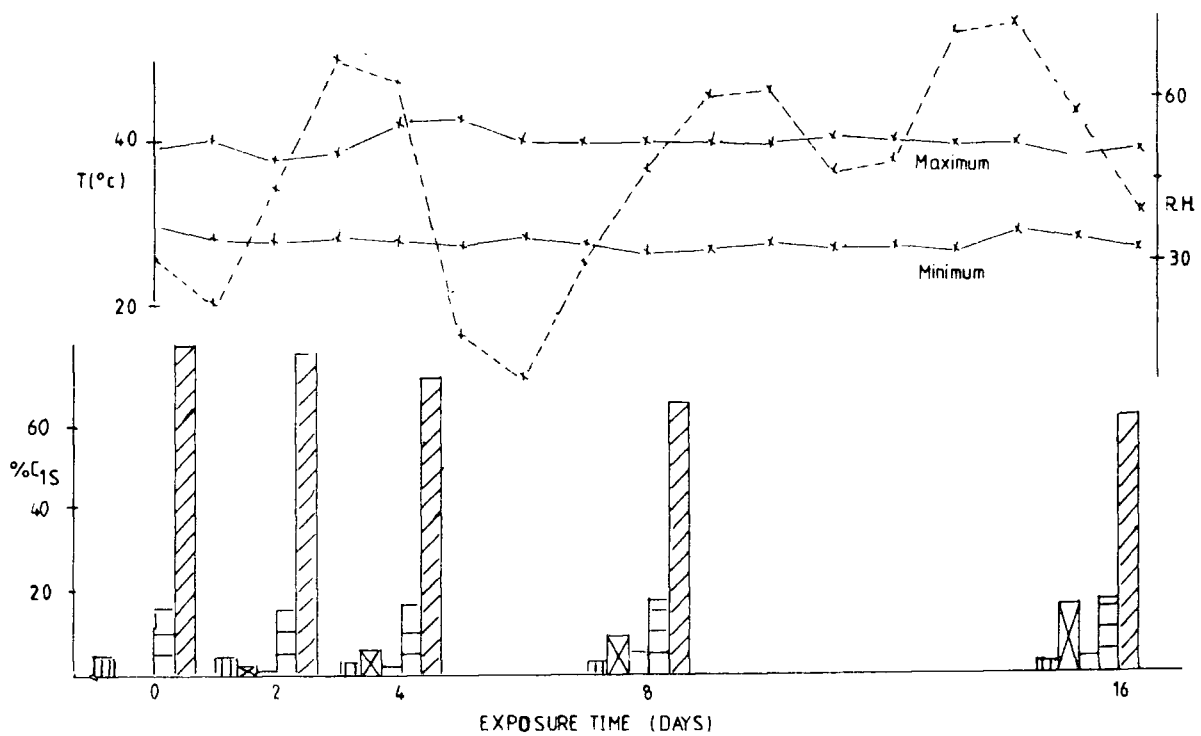

Figure 8.31 Comparison of the variations in temperature relative humidity and C_{1s} components during the exposure of polysulphone films in Saudi Arabia

On extended exposure beyond 16 days, continued deterioration of the surface is observed resulting from ablation of the polymer and the deposition of extraaneous material (e.g. sand). This C_{1s} spectra in Figure 8.28 reveal after 67 and 128 days the presence of a component to the low binding energy side of

the main photoemission peak at 285.0 eV. This is indicative of the deposition of carbon on to the surface. That this is present only at the surface is shown by the C_{1s} and S_{2p} core levels in Figure 8.32 representative of the scraped surface for the sample after 67 days' exposure. The C_{1s} signal shows no evidence for the low binding energy component. There is only a small degree of oxidative functionalisation in the form of carbonyl and carboxylate groups. The $\Pi \rightarrow \Pi^*$ satellite has an intensity comparable to the starting material suggesting that the phenyl groups are still intact. The data reveal by comparison, the surface specificity of the extensive photo-oxidation observed during the first 16 days' exposure and hence the sensitivity of the ESCA experiment.

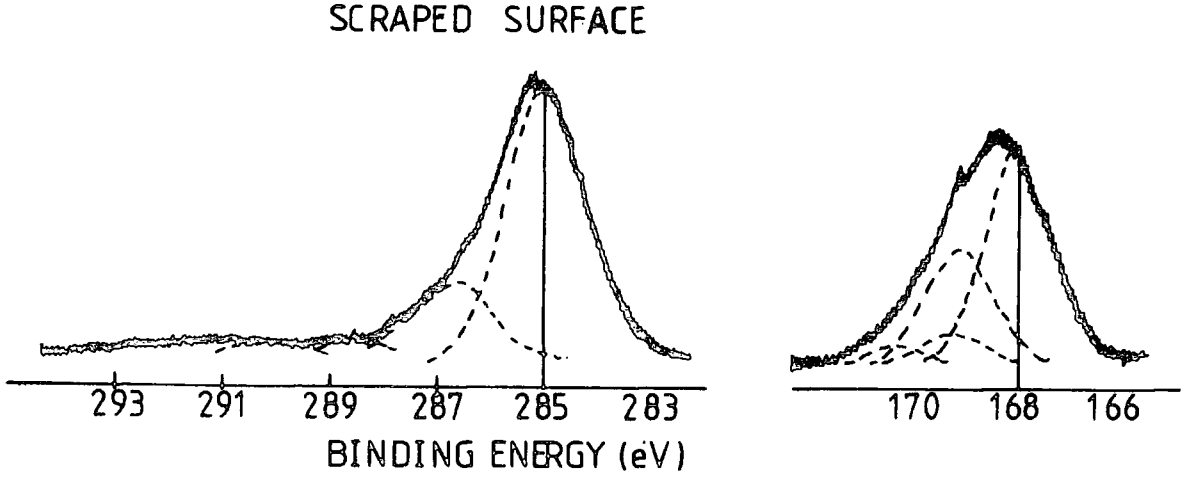

Figure 8.32 C_{1s} and S_{2p} core levels for the scraped surface of polysulphone weathered for 67 days.

Furthermore, a small N_{1s} signal is detected after 32 days, suggesting that nitrogen containing pollutants (e.g. NH_3, NO_2) may be incorporated into the surface. This has also been observed for samples exposed under pyrex for prolonged periods in California, but not for the fully exposed polymer.[52] The observation for the present study for direct exposure may well be attributable to the shorter sampling time.

8.4 Conclusions

Irradiation of Bisphenol A polysulphone films (λ>290nm) in an oxygen atmosphere gives rise to extensive oxygen uptake in the surface. The reaction mechanism involves the dimethyl and sulphone groups as well as the aromatic ring system. From a comparison of the photooxidation of polyethersulphone, it appears that photooxidation of the gem dimethyl moieties occurs at a faster rate than that for the phenyl groups. The S_{2p} core levels broaden on exposure, and can be resolved into components arising from sulphate and sulphone environments. The former occur as a result of the reaction of sulphur dioxide (released by chain scission on either side of the sulphone group) with hydroperoxides.

Natural weathering studies reveal that the changes in surface chemistry are of a similar nature to those in the model exposures and hence similar mechanisms are involved.

CHAPTER NINE

SURFACE ASPECTS OF THE PHOTOAGING OF POLYPHENYLENE OXIDE, PHENOXY RESIN AND POLYETHERKETONE AS REVEALED BY ESCA

9.1 Introduction

In Chapters 4-8 the surface aspects of the photooxidation (λ>290nm) of Bisphenol A polycarbonate, Bisphenol A polysulphone, polyethersulphone and polystyrene were considered in some detail. Extensive photooxidation, involving the aromatic ring systems, was observed in all these systems and it is, therefore, of interest to consider if these trends exist in other aromatic polymers that have received some attention in the literature.

Polyphenylene oxide (PPO) is well known for its rapid photooxidation both in model and natural weathering studies with respect to the surface[51,52] and bulk.[40,227-229] The increase in absorbance at 340nm has been utilised to monitor the solar uv component at a number of sites around the world.[40] The surface degradation for irradiation in a pure oxygen atmosphere (λ>290nm) as functions of irradiation time, photon flux and temperature are reported here for the first time along with data for natural weathering in Saudi Arabia.

Bisphenol A based phenoxy resin has also received consideration with respect to photooxidation in the bulk[223,230] but no data has reported to date for the changes occurring in the surface. The results for irradiations in a pure oxygen atmosphere ($Io = 5.2\ Whm^{-2}h^{-1}$, λ>290nm) are compared with those obtained for polycarbonate and polysulphone.

The photooxidation of polyetherketone (PEEK) has not yet been reported in the literature. The interest in the present study arises from two main points of view:

(a) the only non-aromatic carbon, in the pure polymer, is a carbonyl group. As such for oxygen uptake during photooxidation to occur this must involve the phenyl moieties

and provide further direct evidence for the oxidative attack of the aromatic ring system in the surface,

(b) the heat curing of phenoxy resin in air is believed to oxidise the isopropylidene unit to form aromatic carbonyl groups that can initiate photooxidation. As can be seen from Figure 9.1 this structure is not dissimilar to the repeat unit of PEEK. It is conceivable that such a structure may also arise during the photooxidation of Bisphenol A based polymers which can then initiate the phenyl group oxidation.

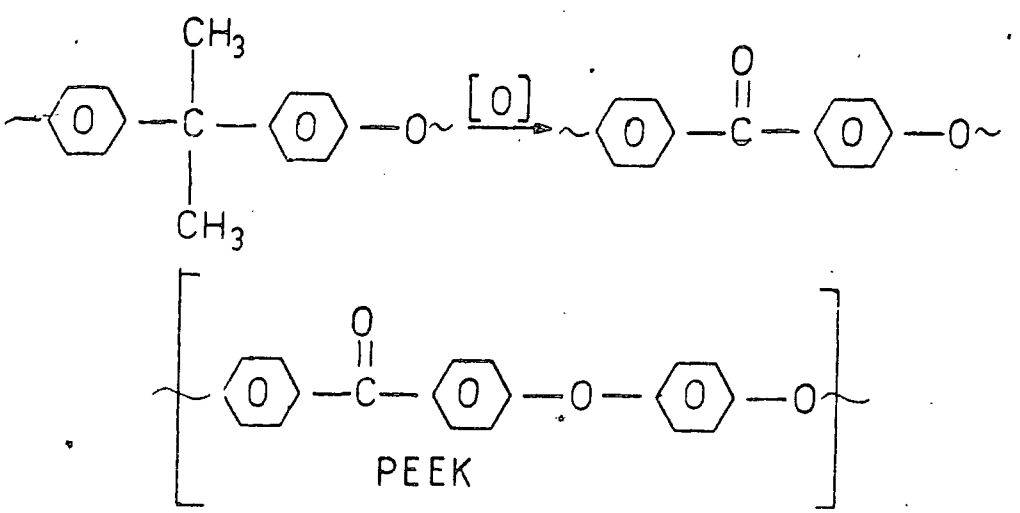

Figure 9.1 The oxidation of the isopropylidene unit in phenoxy resin. (The structure of PEEK is also shown for comparison).

9.2 Experimental

PPO, phenoxy resin and PEEK films were exposed to the output of a 500W Hanovia medium pressure Hg arc lamp via a pyrex window (λ>290nm) in a flowing oxygen atmosphere as previously described in Chapter Four.

Surface hydroperoxide formation during the photooxidation of PPO was followed by monitoring the component at ~169.2 eV in the S_{2p} core level after the direct reaction of these groups with SO_2 as described in Chapter Four. PPO films were weathered in Dhahran, Saudi Arabia as described in Chapter Five. The exposures started in April 1981.

To examine the role of the hydroxy functionality in the aliphatic ether portion of the chain in phenoxy resin, films were exposed to the vapour pressure (T=20^{o}C) of acetyl chloride for 15 minutes prior to irradiation in a similar manner to the treatment of Bisphenol A polycarbonate with trifluoroacetic anhydride as described in Chapter Five.

ESCA spectra for each sample were recorded on an AEI ES200B spectrometer employing $Mg_{k\alpha_{1,2}}$ radiation. The $Au_{4f_{7/2}}$ line at 84.0 eV used for calibration purposes had a FWHM of 1.2 eV. All the results discussed in the next section were recorded at an electron take off angle of θ=30^{o}. The corresponding data at θ=70^{o} revealed similar changes to those at θ=30^{o}. The spectra were deconvoluted and integrated using a DuPont 310 curve resolver. Binding energies were referenced to the C-H component at 285.0 eV.

9.3 Results and Discussion

9.3.1 Polyphenylene oxide

The C_{1s} and O_{1s} core levels in Figure 9.2 reveal

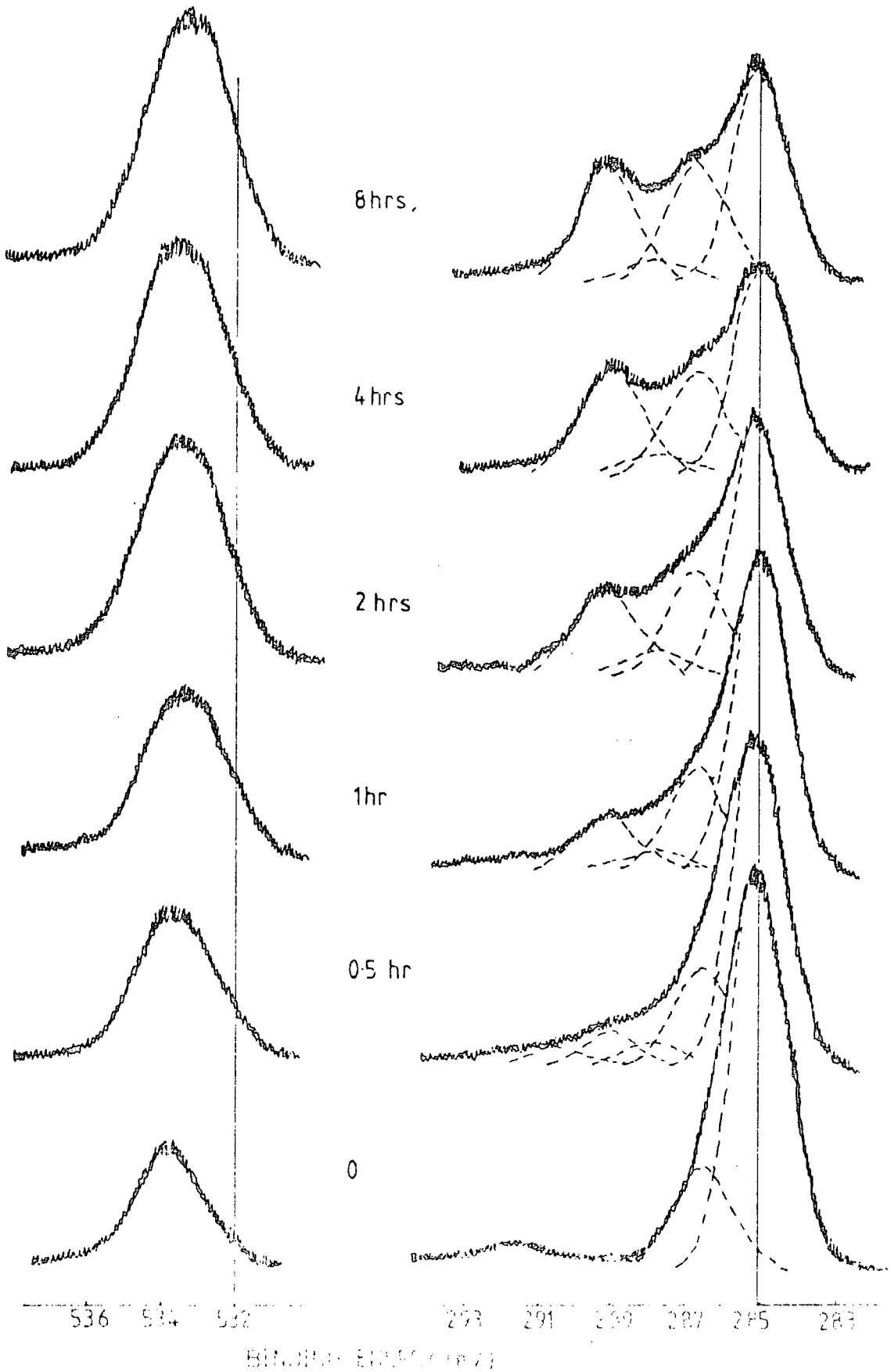

Figure 9.2 C_{1s} and O_{1s} core levels for photooxidised PPO films (Io = 5.7 $Whm^{-2}h^{-1}$, λ>290nm).

the changes in the surface chemistry during the irradiation (λ>290nm) of PPO for various periods of time at a photon flux of 5.7 $Whm^{-2}h^{-1}$. The C_{1s} level of the starting material, consisting of 2 main photoionisation peaks arising from C-H (methyl groups and the phenyl moiety) at 285.0 eV and C-O at ∿286.5 eV components and a shake-up satellite at ∿291.6 eV, rapidly increases in complexity with additional contributions from C=O and O-C=O functionalities. These data along with the increase in O_{1s} signal intensity reveal that extensive photooxidation has taken place. This is also readily apparent from the comparison of the relative O_{1s} and C_{1s} intensity ratios and from a consideration of the percentage contributions to the C_{1s} envelope arising from oxidative functionalities displayed in Figure 9.3.

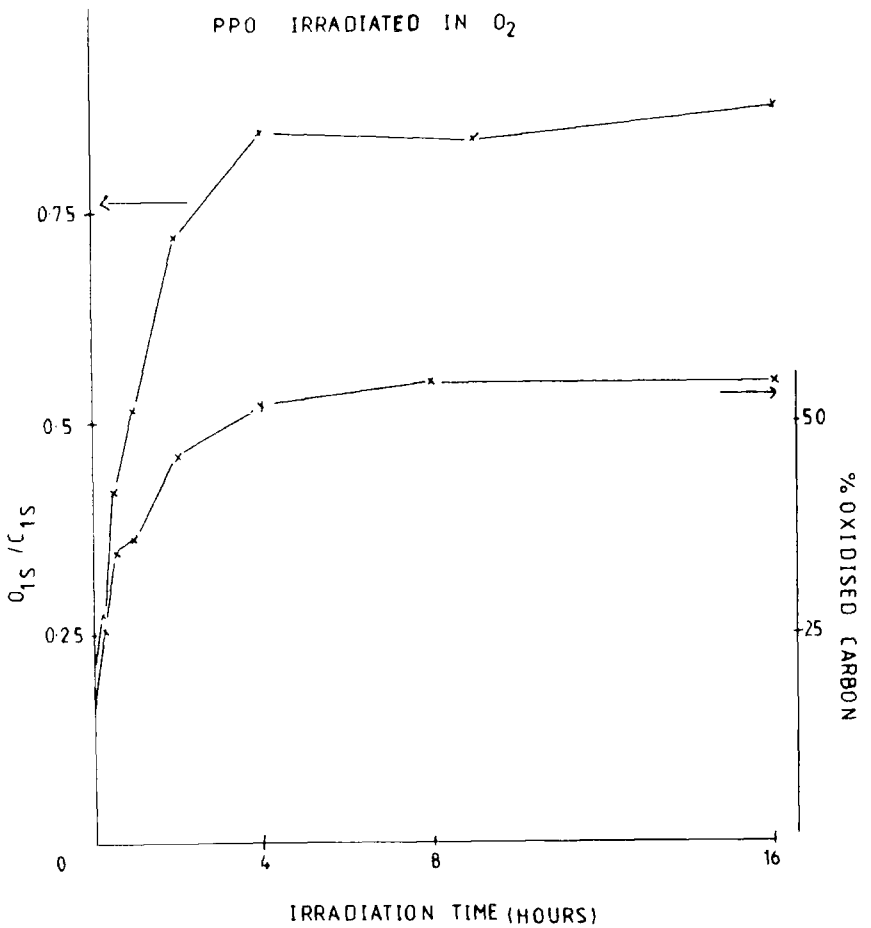

Figure 9.3 O_{1s}/C_{1s} intensity ratios and % contribution to the C_{1s} envelope arising from oxidative functionalities for the spectra in Figure 9.2.

A steady state situation arises after ∿4 hours' irradiation representative of a balance between further photooxidation and desorption of low molecular weight species from the surface. From a starting stoichiometry of $C_1:O_{0.125}$, after 16 hours' exposure this has changed to $\sim C_1:O_{0.5}$ indicative of the extensive oxygen uptake that has taken place.

The nature of the oxidative functionalisation occurring in the surface is evident from a consideration of the C_{1s} component analysis for the spectra in Figure 9.2 as displayed in Figure 9.4. The C-H component decreases in intensity as a function of irradiation time whilst the C-O, C=O and O-C=O functionality increase in intensity. The carboxylate component becomes a dominant feature of the surface structure. After

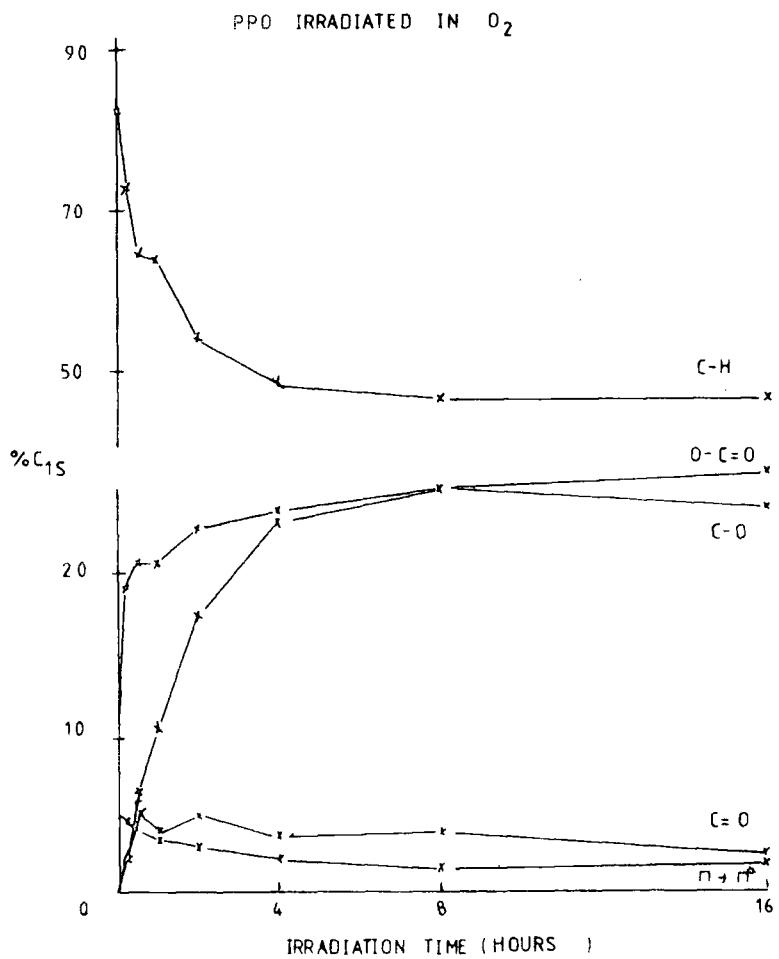

Figure 9.4 C_{1s} component analysis for the spectra in Figure 9.2.

16 hours' exposure this functionality contributes ∿27% to the total C_{1s} intensity. The $\Pi \rightarrow \Pi^*$ shake-up satellite also decreases in intensity. Although conversion of the methyl groups to carboxylic acids and esters will decrease the probability of the shake-up transition, the extent of oxidative functionalisation, over 50% after ∿4 hours' exposure, indicates that oxidative attack of the aromatic ring is also involved. The centroid of the $\Pi \rightarrow \Pi^*$ component shifts to lower binding energy during exposure and this may well be due to a low level of carbonate formation as noted in polystyrene and polysulphone (cf. Chapters Seven and Eight).

For comparison purposes, PPO films have been exposed to a higher photon flux of 52.5 $Whm^{-2}h^{-1}$. The greater extent of oxidation present for a given irradiation time compared to the lower photon flux is evident from the O_{1s}/C_{1s} intensity ratios in Figure 9.5. An equilibrium surface oxygen to carbon ratio is evident after ∿15 minutes' exposure. On examination of the relevant C_{1s} components displayed in Figure 9.6 it is clear that a higher level of $\underline{C}$=O features are formed at the higher photon flux compared with exposures at 5.7 $Whm^{-2}h^{-1}$ indicative of differences in reaction mechanisms.

The data in Figure 9.7 reveal the changes in the O_{1s}/C_{1s} intensity ratios for PPO films irradiated for 15 minutes as a function of lamp intensity. As the photon flux increases the change in oxygen content of the surface moves towards a steady state situation as already noted for irradiations as a function of time and this reflects the high reactivity of PPO in the surface regions.

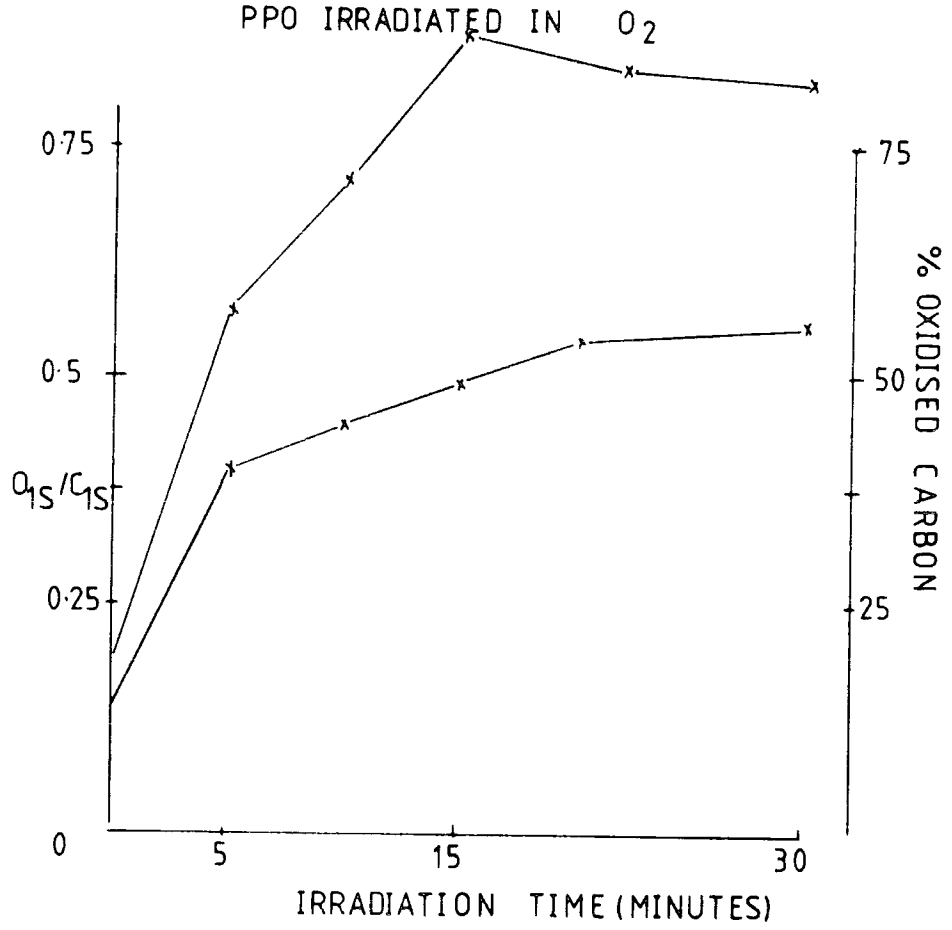

Figure 9.5 O_{1s}/C_{1s} intensity ratios for PPO films irradiated at a higher photon flux of 52.5 $Whm^{-2}h^{-1}$.

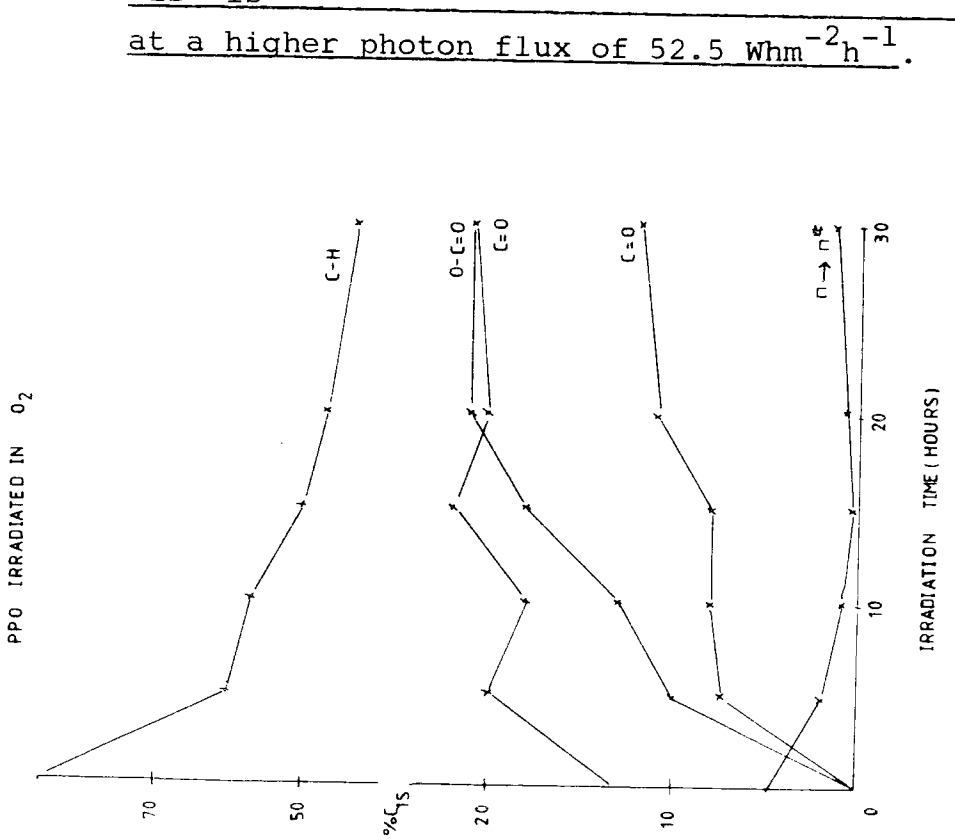

Figure 9.6 C_{1s} component analysis for PPO films irradiated at a higher photon flux of 52.5 $Whm^{-2}h^{-1}$.

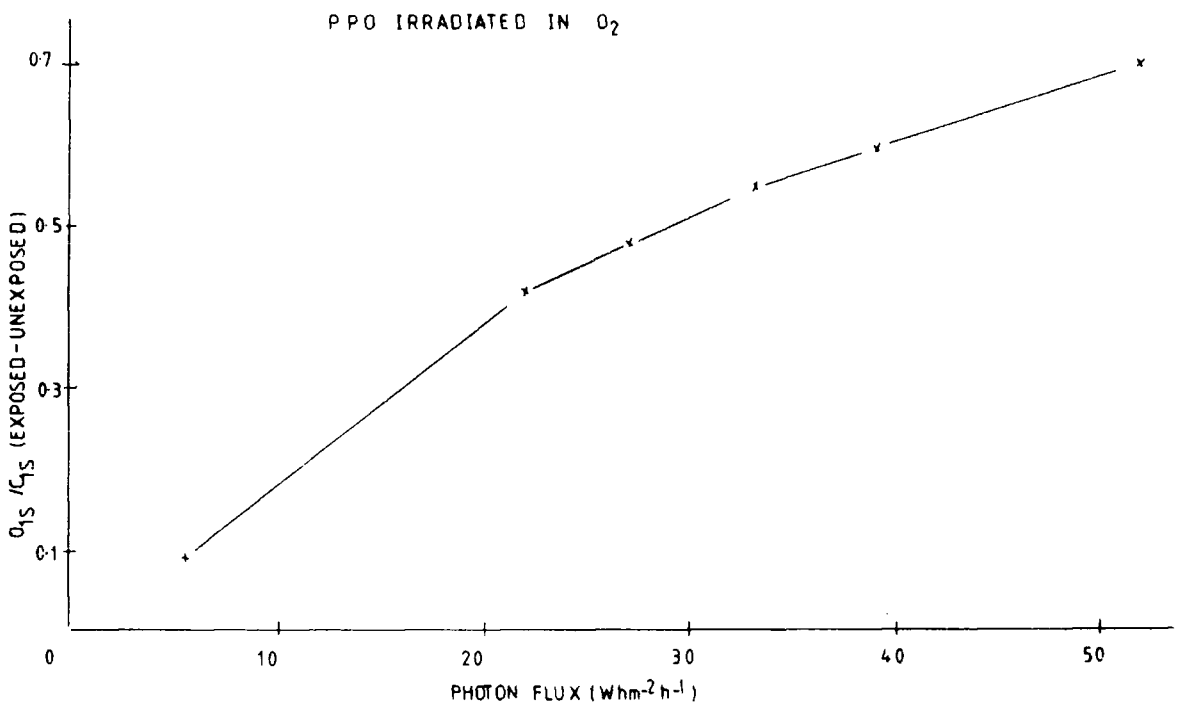

Figure 9.7 O_{1s}/C_{1s} intensity ratios for PPO films irradiated for 15 minutes as a function of photon flux.

The formation of hydroperoxides is believed to be an integral part of the photooxidation of PPO. In Chapter Four it was noted that in the surface regions it is not possible to delineate these features from the C_{1s} and O_{1s} core levels alone but their study may be facilitated by monitoring the S_{2p} core level after photooxidised films have been exposed to SO_2. From a knowledge of the appropriate instrumentally dependent sensitivity factors the level of C-OOH functionalities may be estimated. The relevant data for hydroperoxide levels as a function of irradiation time for PPO films exposed to a photon flux of 52.5 Whm^{-2}h^{-1} are displayed in Figure 9.8. It is clear that C-OOH

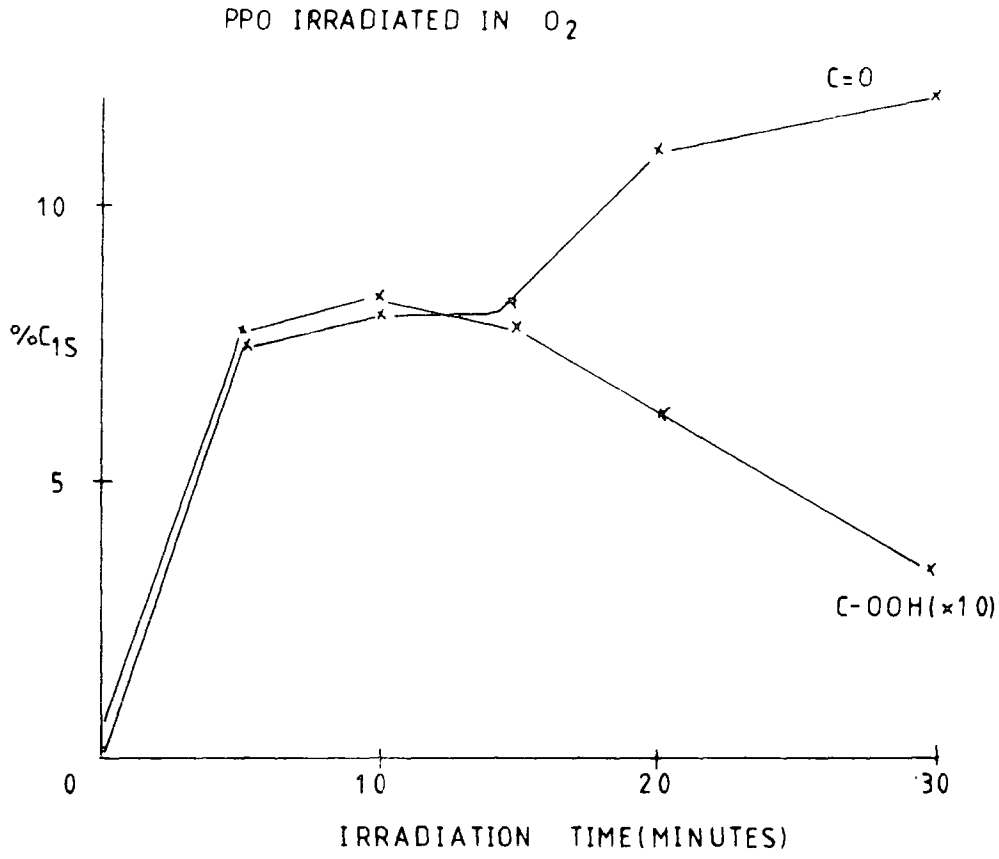

Figure 9.8 C-OOH formation in PPO films irradiated at 52.5 $Whm^{-2}h^{-1}$ for various periods of time.

formation is rapid and reaches a maximum after ∿10 minutes and these data confirm that hydroperoxides are involved in the surface photooxidation of PPO.

The results for photooxidation as a function of temperature (at high photon flux) for polycarbonate, polystyrene and polysulphone revealed that the effect of temperature is relatively small. This is also the case for PPO films irradiated at a photon flux of 27.4 $Whm^{-2}h^{-1}$ at 30, 50 and 70°C as is apparent from the data in Table 9.1 which again reveals a balance between photooxidation and desorption of low molecular weight species from the surface.

TABLE 9.1 Oxygen uptake for PPO films photooxidised as a function of temperature (Io=27.4 $Whm^{-2}h^{-1}$).

T(^{o}C)	Time	oxygen uptake	(O_{1s}/C_{1s} (exposed-unexposed))
30	0	0	
	5	0.18	
	10	0.32	
	15	0.44	
	20	0.55	
50	0	0	
	5	0.23	
	10	0.37	
	15	0.45	
	20	0.42	
70	0	0	
	5	0.20	
	10	0.37	
	15	0.45	
	20	0.48	

The changes in the surface chemistry of PPO films during prolonged natural weathering have been reported in the literature. The C_{1s} core levels in Figure 9.9 reveal the changes during exposure over 64 days in Dhahran, Saudi Arabia. As previously noted (cf. Chapters, Five, Seven and Eight) airborne particulates lead to a variable surface contamination as evidenced by the presence of an Si_{2p} core level in the ESCA spectra. Consequently due to contributions to the O_{1s} signal arising from the contamination no useful data can be obtained from the O_{1s}/C_{1s} intensity ratios. The C_{1s} levels show that extensive oxidative

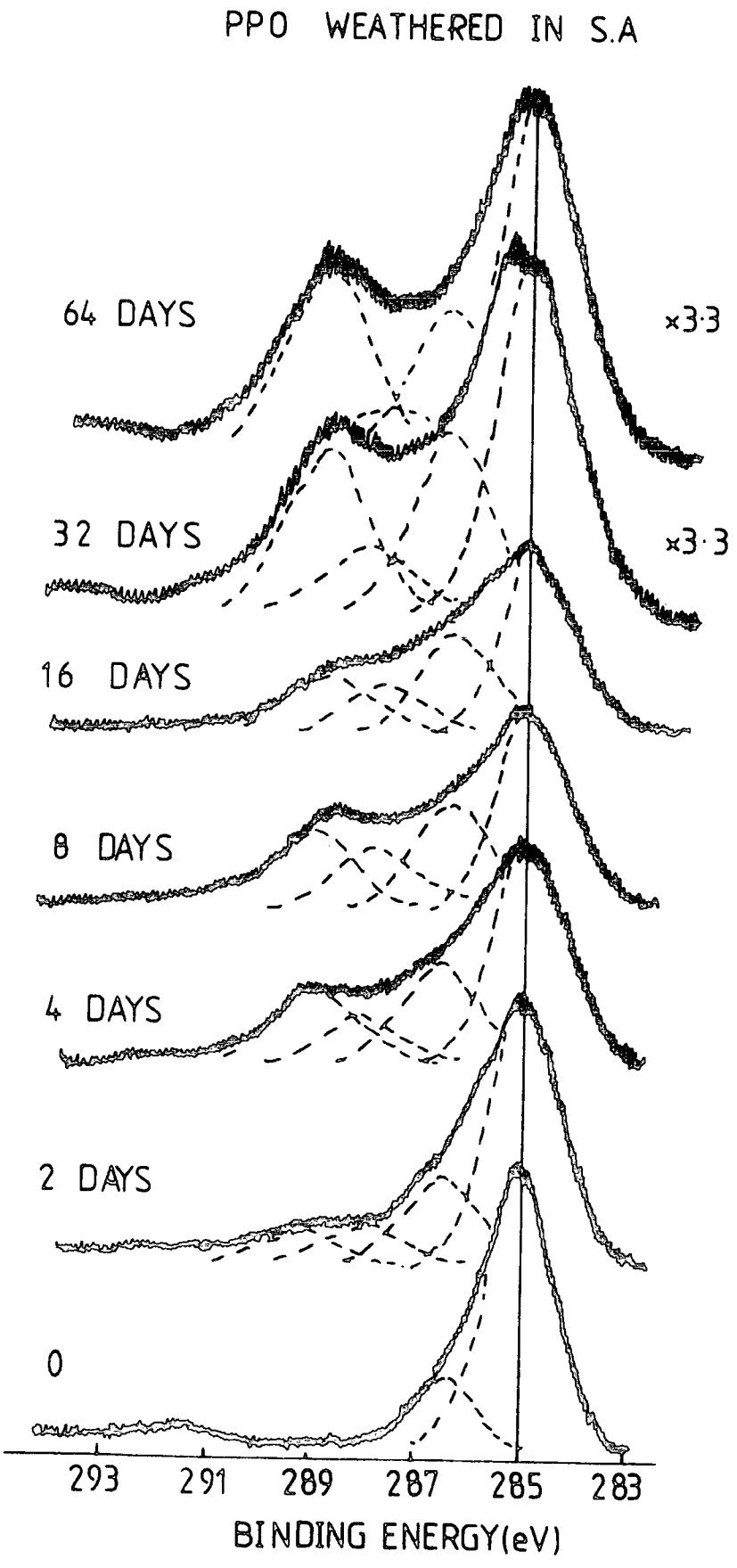

Figure 9.9 C_{1s} core levels for PPO films weathered in Saudi Arabia.

functionalisation has occurred and the nature of this is more apparent from the component analysis in Figure 9.10. It is clear that in comparison to the data for polystyrene, exposed over the same period, (cf. Chapter Seven) that PPO photo-oxidation in the natural environment is rapid. The distribution of components over the first eight days' exposure are similar to those for the model studies and the data indicates that both the methyl groups and the aromatic ring system are involved. Prolonged exposure reveals that ablation of the surface is occurring with concomitant continued photooxidation as shown by the fluctuations of the intensities of the various components.

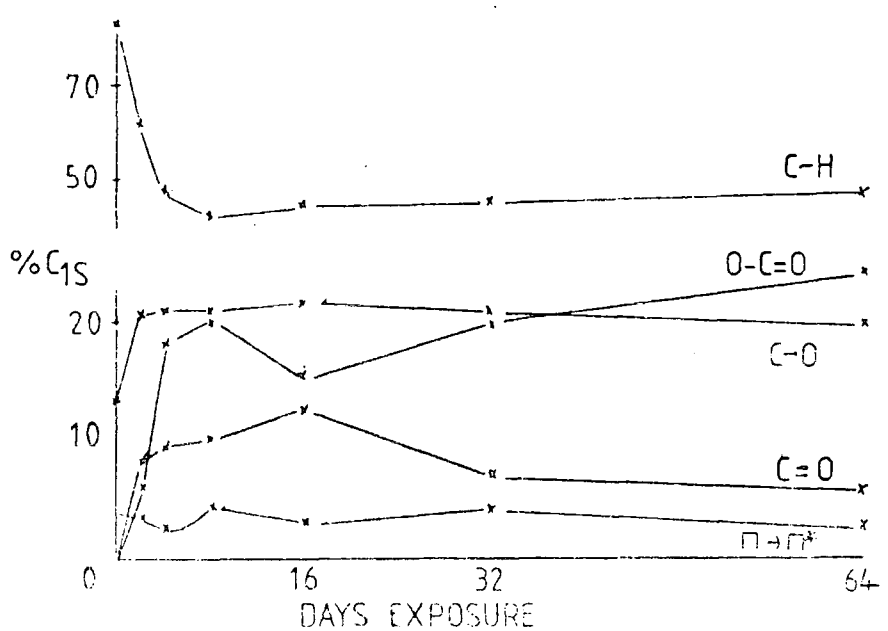

Figure 9.10 C_{1s} component analysis for the spectra in Figure 9.9

9.3.2 Phenoxy resin

From the studies of polycarbonate and polysulphone described in Chapters Four and Eight, extensive oxygen uptake is expected for films of phenoxy resin irradiated (λ>290nm) in an oxygen atmosphere at a photon flux of 5.7 $Whm^{-2}h^{-1}$ since this material is also a Bisphenol A polymer. The C_{1s} and O_{1s} core levels in Figure 9.11 show increasing complexity of the former and greater intensity of the latter as irradiation time increases indicative of a high degree of oxygen uptake. This is more apparent from the O_{1s}/C_{1s} intensity ratios displayed in Figure 9.12 where the percentage contribution to the C_{1s} level arising from oxidative functionalities are also included. Oxygen uptake is rapid with a steady state being reached after $\sim$4 hours' irradiation. In the initial stages of exposure the oxygen content in the surface decreases although the contribution of oxidative species increases. This suggests that a cross-linking mechanism is involved and this will be considered in greater detail further on.

The nature of the oxidised surface is revealed in Figure 9.13 where the various C_{1s} components are displayed as a function of irradiation time. Initially the C-H and C-O components decrease in intensity without the concomitant increases in C=O and O-C=O functionalities as observed in polycarbonate and polysulphone, i.e. an induction period is evident for these features. The carboxylate feature, however, on continued irradiation becomes a dominant feature of the surface and after 16 hours it contributes $\sim$30% to the total C_{1s} signal intensity. The extent of oxidation and the observed decrease in the $\Pi \rightarrow \Pi^*$ shake-up satellite suggest that photooxidation involves the

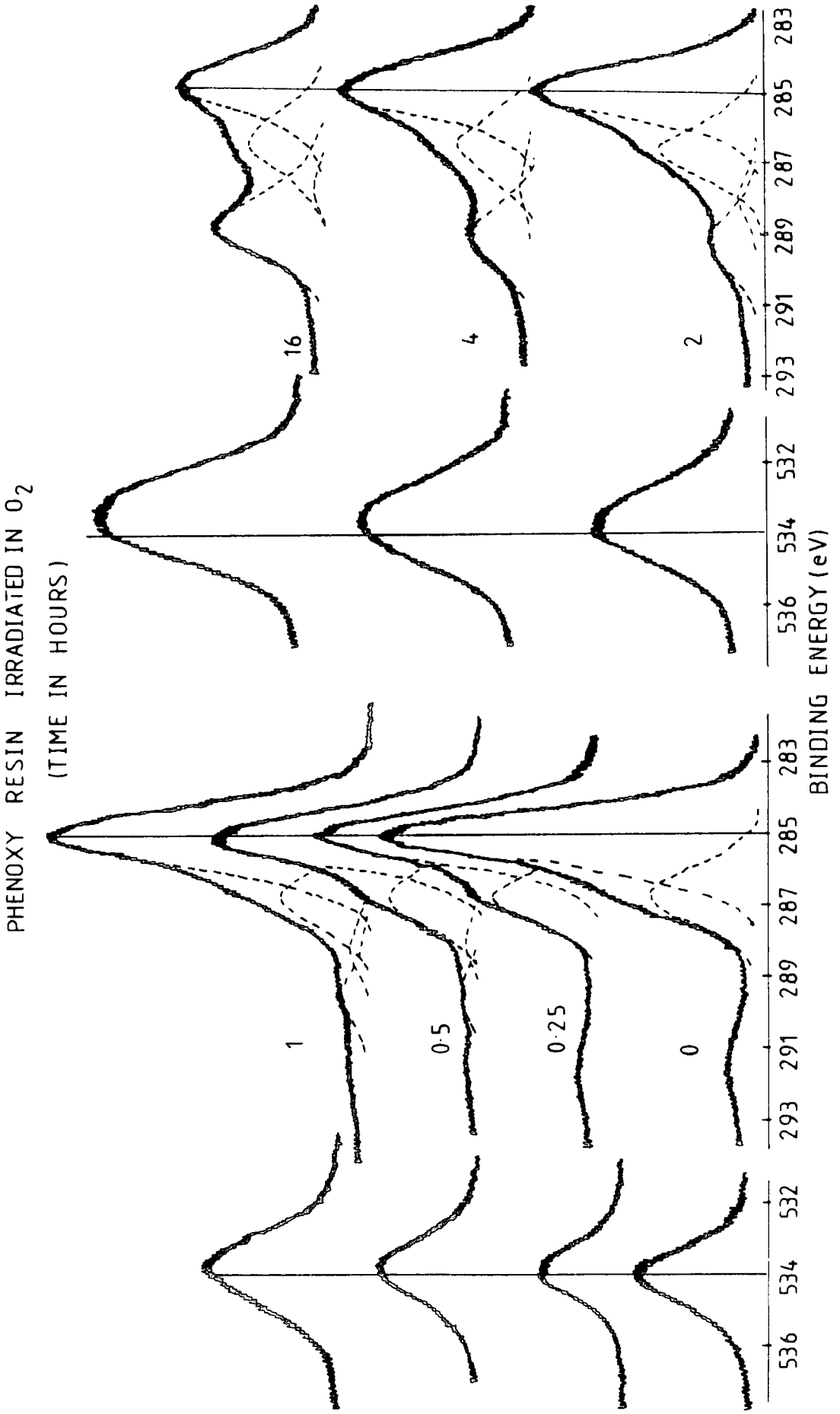

Figure 9.11 C_{1s} and O_{1s} core levels for phenoxy resin samples irradiated in oxygen (Io = 5.7 $Whm^{-2}h^{-1}$, λ>290nm)

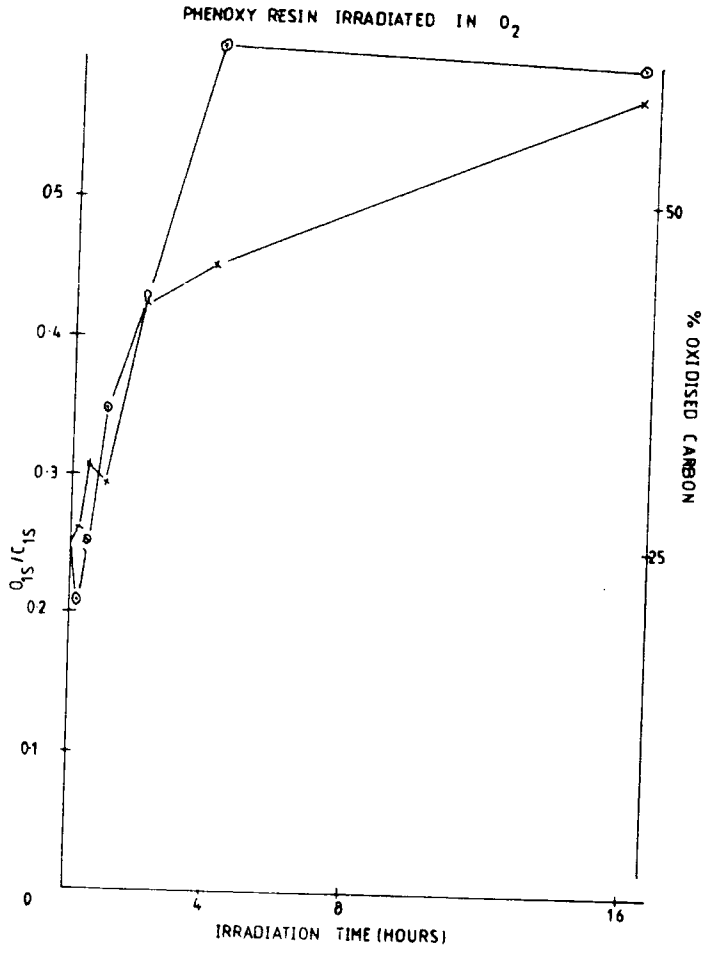

Figure 9.12 O_{1s}/C_{1s} intensity ratios and % oxidative functionalities for the spectra in Figure 9.11

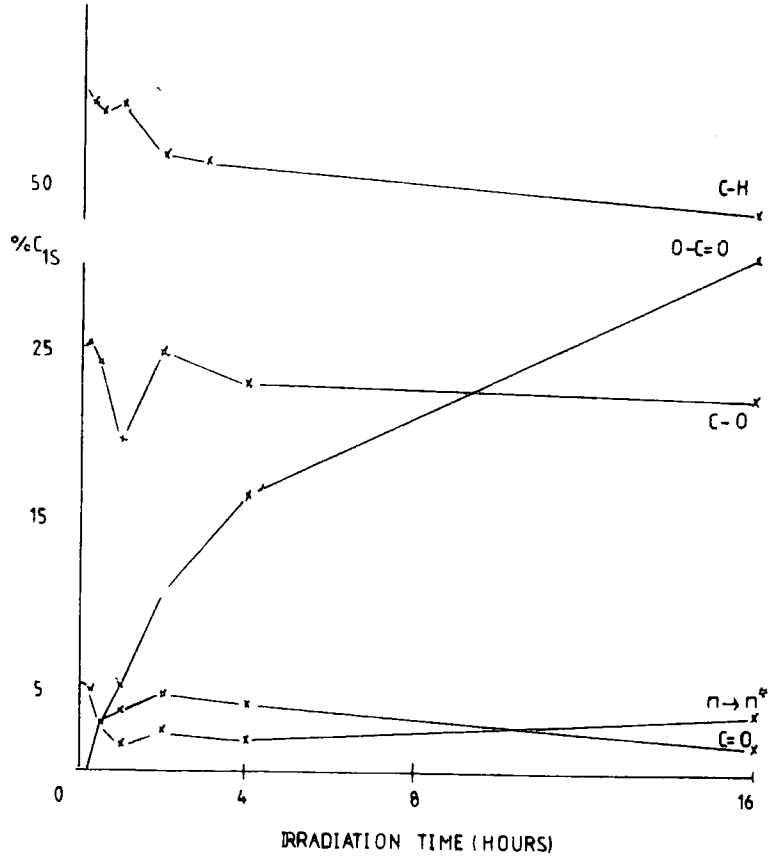

Figure 9.13 C_{1s} component analysis for the spectra in Figure 9.11

aromatic ring system as well as the dimethyl and hydroxy aliphatic ether portions of the polymer. As the $\Pi \rightarrow \Pi^*$ component moves to lower binding energy and fluctuates in intensity with increasing irradiation time, the formation of a low level of carbonate groups seems possible.

The initial decrease in the O_{1s}/C_{1s} intensity ratio, as noted earlier, is indicative of a crosslinking reaction in the surface. Bulk photooxidation studies of phenoxy resin revealed a rapid and simultaneous crosslinking reaction occurring with photooxidation. By replacing the hydroxy functionality of the aliphatic ether portion of the main chain with an ester (by reaction with acetyl chloride) it was found that the polymer did not give rise to gel formation when irradiated under identical conditions, indicating that the crosslinking was due to the hydroxy group. To investigate the role of this functionality in the surface phenoxy resin films were exposed to the vapour pressure of acetyl chloride before onset of irradiation. The C_{1s} and O_{1s} core levels in Figure 9.14 reveal the changes in the surface of phenoxy resin after such treatment. In the exposed sample a carboxylate peak at $\sim$289.2 eV is readily apparent and contributes $\sim$6% to the total C_{1s} intensity. The theoretical value should be $\sim$5% and this higher level may be attributable to Bisphenol A residues in the surface (cf. TFAA labelling in polycarbonate described in Chapter Five).

The O_{1s}/C_{1s} intensity ratios for the acetylated samples after irradiation over 60 minutes, as shown in Figure 9.15, reveal that the initial decrease in the oxygen level is not due to reactions involving the hydroxy functionality since the profiles are comparable. The higher oxygen content in the surface arises from contributions due to the ester group. As the

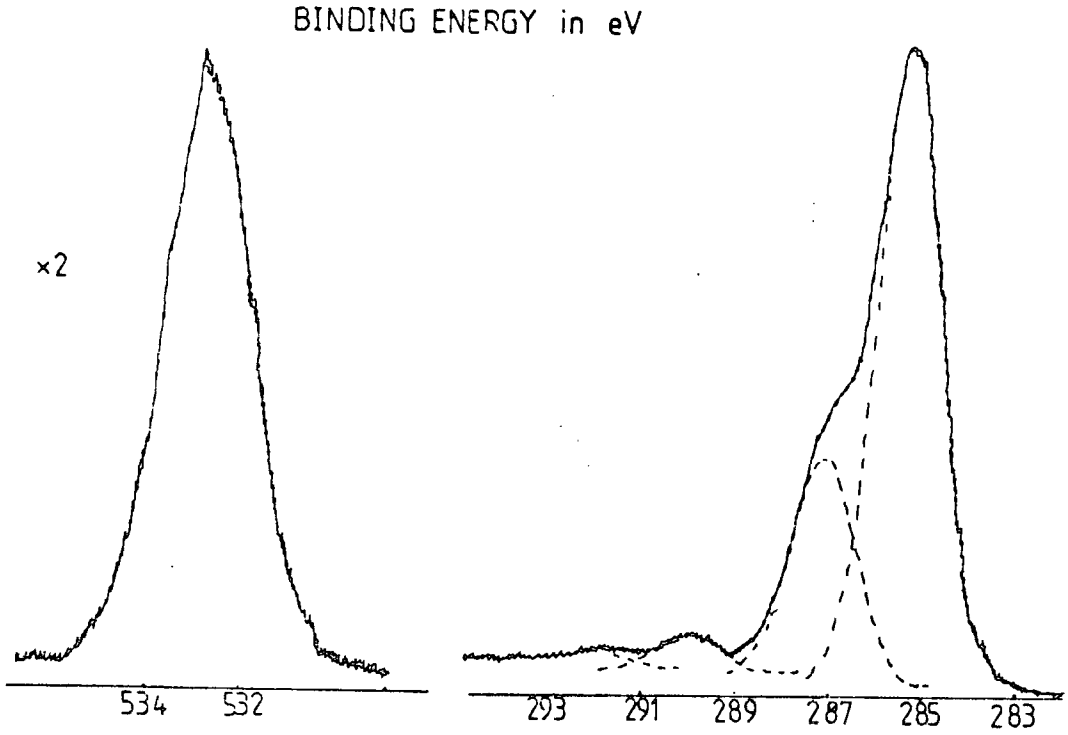

Figure 9.14 C_{1s} and O_{1s} core levels for acetylated phenoxy resin

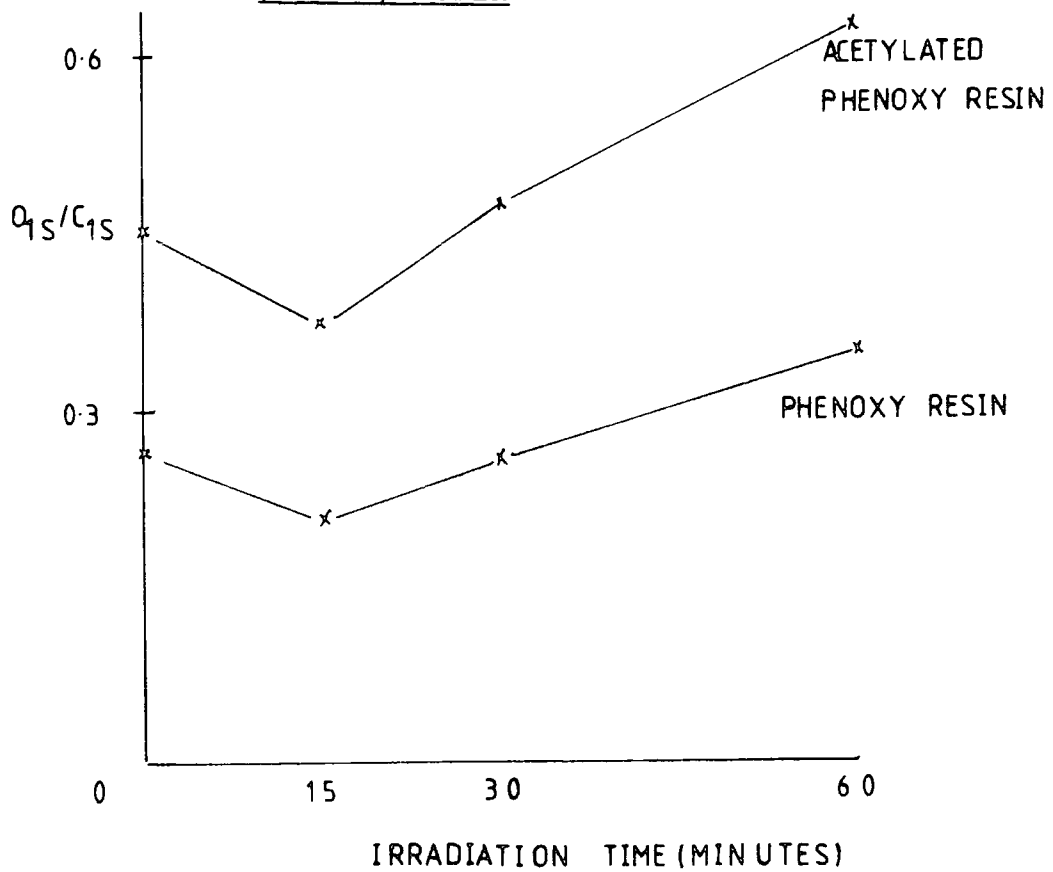

Figue 9.15 O_{1s}/C_{1s} intensity ratios for acetylated phenoxy resin irradiated in O_2. (For comparison the data for the unacetylated system are also included)

"crosslinking" reaction is not observed in neither polycarbonate nor polysulphone the process must still involve the aliphatic ether group.

It is of interest to compare the oxygen uptake in the surface of the three Bisphenol A based polymers studied and the relevant data are displayed in Figure 9.16. From these data the order of reactivity is polysulphone > polycarbonate > phenoxy resin which is in contrast with the bulk data. However, the simultaneous crosslinking reaction in phenoxy resin probably lowers the apparent oxygen uptake and as such the reactivity of this system is higher than polycarbonate. This is evidenced to some rextent from the high level of carboxylate features formed in phenoxy resin.

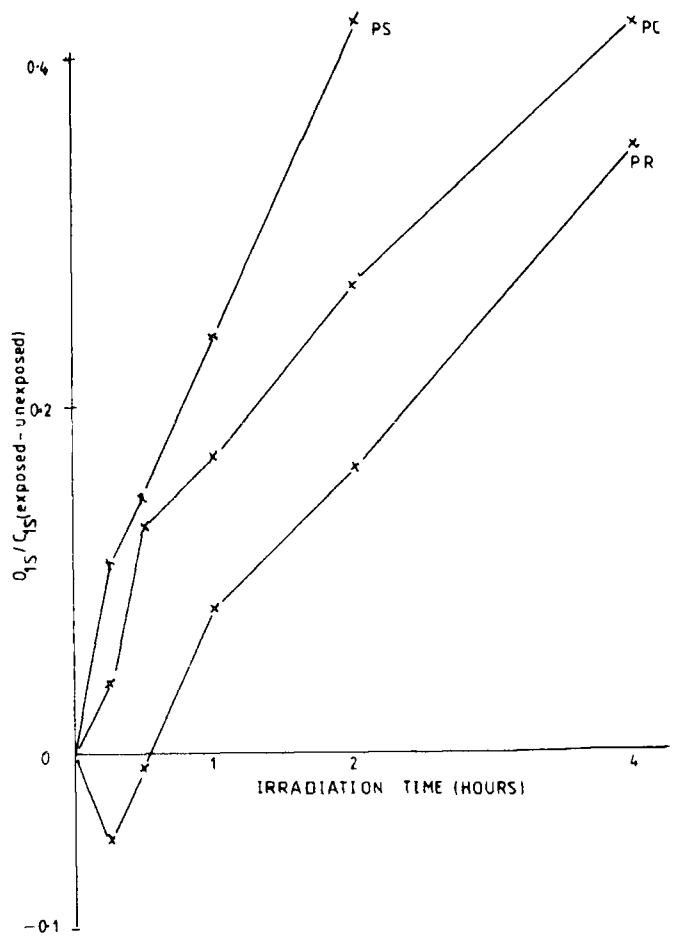

Figure 9.16 Comparison of oxygen uptake as a function of time for Bisphenol A based polymers irradiated at a photon flux of 5.7 $Whm^{-2}h^{-1}$.

9.3.3 Polyetherketone

The structure of this polymer is shown in Figure 9.1. It is apparent that it contains a benzophenone unit and consequently it is not unreasonable to expect that PEEK will be sensitive to uv radiation at wavelengths >290nm. This is also evident from the uv/visible absorption spectrum shown in Chapter One.

The C_{1s} and O_{1s} core levels in Figure 9.17 are for the unexposed material and after irradiation at a photon flux of 27.4 $Whm^{-2}h^{-1}$ in an oxygen atmosphere for various periods of time. From the increases in complexity of the C_{1s} level and increased O_{1s} signal intensities it is evident that extensive photooxidation has occurred. This is more clearly revealed from the data in Figure 9.18 where the relevant O_{1s}/C_{1s} intensity ratios and percentage contributions made by oxidative functionalities are displayed as functions of irradiation time.

The nature of the changes occurring in the surface are more apparent on consideration of the C_{1s} components and these data are displayed in Figure 9.19. The C-H component, as to be expected, decreases in intensity. There is an initial decrease in the intensity of the C-O functionality indicative that the ether linkages in the polymer are being cleaved. As in all the aromatic polymers with in-chain phenyl groups that have been studied, the rate of carboxylate formation is greater than that for carbonyl. The $\pi \rightarrow \pi^*$ component decreases in intensity and again as in the other aromatic polymers it would appear that a low level of carbonate functionalisation is present. The involvement of an oxidative process involving the phenyl group is readily apparent from these data.

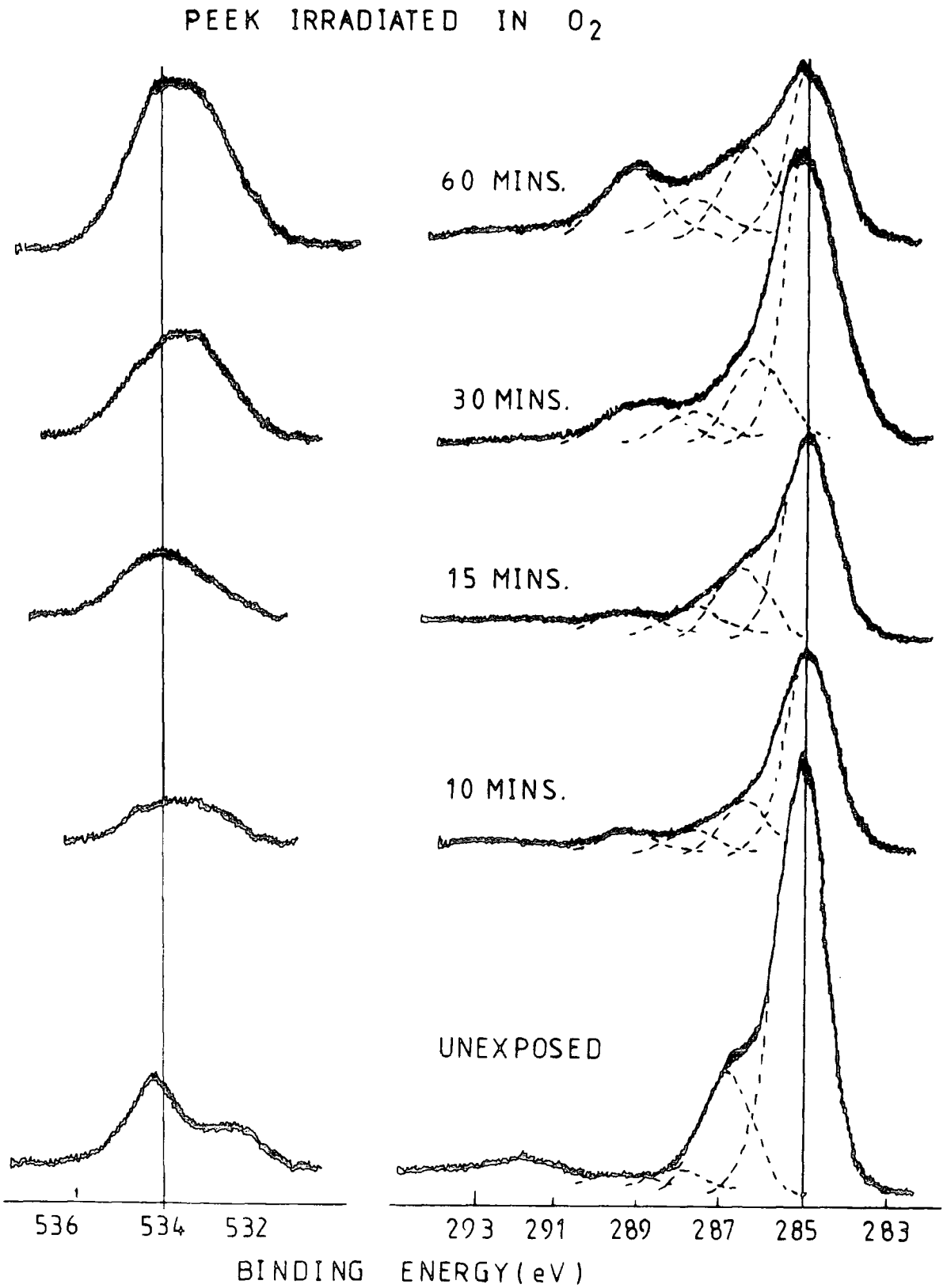

Figure 9.17 C_{1s} and O_{1s} core levels for PEEK before and after irradiation in O_2 at 27.4 $Whm^{-2}h^{-1}$.

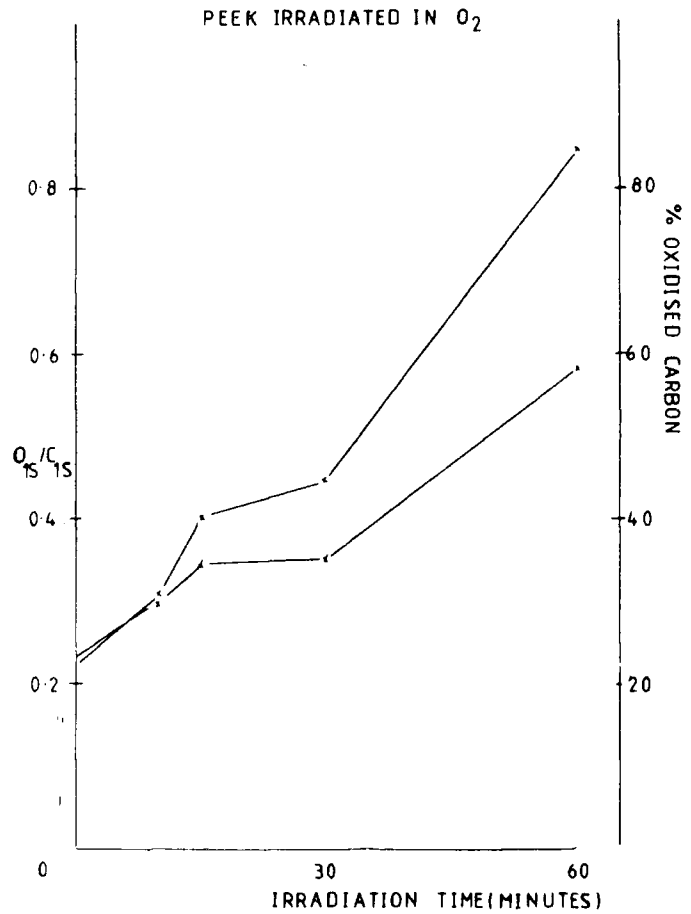

Figure 9.18 O_{1s}/C_{1s} intensity ratios and % oxidative functionalities for the spectra in Figure 9.17

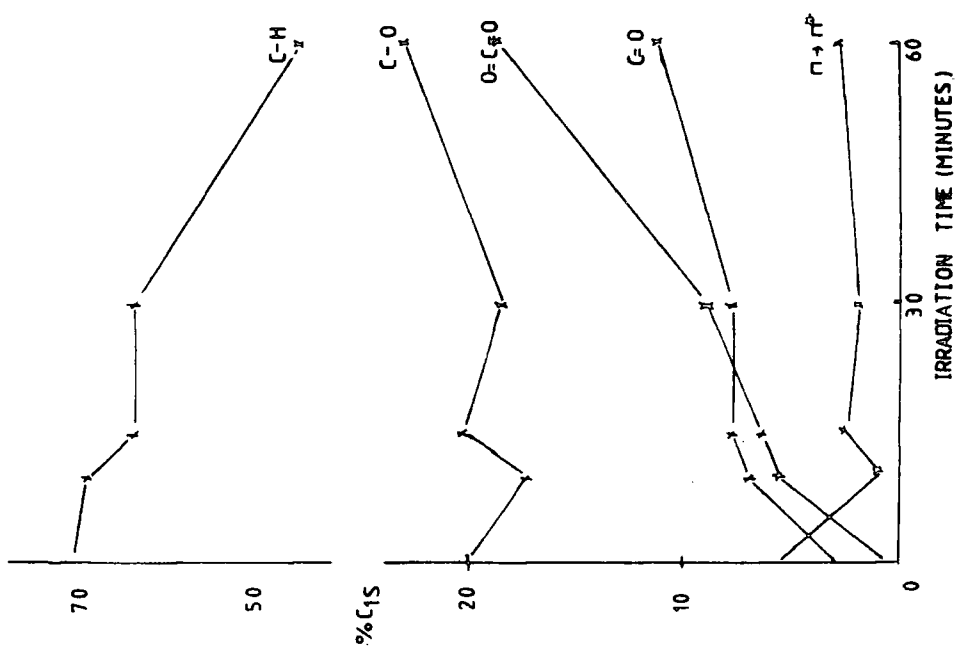

Figure 9.19 C_{1s} component analysis for the spectra in Figure 9.17

It is possible, therefore, from the results above, that an aromatic ketone of the type described by the repeat unit of PEEK can initiate phenyl ring oxidation.

9.4 Conclusions

The three aromatic polymers investigated in this chapter all show similar trends in surface chemistry during photo-oxidation as those discussed in previous chapters and consequently the general surface aspects of aromatic polymer photo-oxidation (λ>290nm) may be summarised as follows:

(1) Oxygen uptake in the surface is more extensive than in the bulk.

(2) When the partial pressure of oxygen at the gas/solid interface is high and the polymer contains 'in chain' phenyl groups then the rate of formation of carboxylate functionalities is $\geq$ than that for carbonyl groups.

(3) The oxidative mechanism involves oxidation of the aromatic rings as well as any aliphatic groups in the polymer.

(4) Low levels of carbonate groups are formed.

The exact nature of the mechanisms involved in the surface photooxidation of aromatic polymers is not clear from the ESCA data so far obtained but it is evident that the reactions involved in the surface are very extensive and may well influence the processes occurring in the bulk.

APPENDIX

Lectures and Seminars attended during the period 1979-1982

21 November 1979

Dr. J. Muller (University of Bergen),
"Photochemical Reactions of Ammonia".

28 November 1979

Dr. B. Cox (University of Stirling),
"Macrobicyclic Cryptate Complexes, Dynamics and Selectivity".

5 December 1979

Dr. G.C. Eastmond (University of Liverpool),
"Synthesis and Properties of some multicomponent Polymers".

12 December 1979

Dr. C.I. Ratcliffe (University of London),
"Rotor Motions in solids".

19 December 1979

Dr. K.E. Newman (University of Lausanne),
"High Pressure Multinuclear NMR in the elucidation of the Mechanisms of Fast, Simple Inorganic reactions".

6 February 1980

Dr. J.M.E. Quirke (University of Durham),
"Degradation of Chlorophyll-a in Sediments".

23 April 1980

Mr. B. Grieveson (University of Durham),
"Halogen Radio pharmaceuticals".

14 May 1980

Dr. R. Hutton (Water Associates, U.S.A.),

"Recent Developments in Multi-milligram and Multi-gram Scale Preparative High Performance Liquid Chromatography".

21 May 1980

Dr. T.W. Bentley (University of Swansea),

"Medium and Structural Effects in Solvolytic Reactions".

7 October 1980

Professor T. Tehlner (Notre-Dam University, U.S.A.),

"Metalloboranes Cages or Coordination Compounds?".

16 October 1980

Dr. D. Maas (Salford University)

"Reactions a Go-Go".

30 October 1980

Professor N. Grassie (Glasgow University),

"Inflammability Hazards in Commercial Polymers".

6 November 1980

Professor A.G. Sykes (Newcastle upon Tyne University),

"Metallo-proteins: An Inorganic Chemists' Approach".

12 November 1980

Dr. M. Gerloch (University of Cambridge),

"Magnetochemistry is about Chemistry".

13 November 1980

Professor N.N. Greenwood (Leeds University),

"Metalloborane Chemistry".

19 November 1980

Dr. T. Gilchrist (University of Liverpool),

"Nitroso-olefins as Synthetic intermediates".

4 December 1980

Reverend R. Lancaster,

"Fireworks".

18 December 1980

Dr. R. Evens (University of Brisbane, Australia),

"Some Recent Communications to the Editor of the Australian Journal of Failed Chemistry".

29 January 1981

Mr. H. Maclean (I.C.I. Ltd.),

"Managing in the Chemical Industry in the 1980s".

18 February 1981

Professor S. Kettle (University of East Anglia),

"Variations in the Molecular Dance at the Crystal Ball".

25 February 1981

Dr. K. Bowden (University of Essex),

"The Transmission of Polar Effects of Substituents".

17 March 1981

Professor W. Jencks (Brandeis University, Massachusetts),

"When is an Intermediate not an Intermediate?".

7 May 1981

Professor M. Gordon (Essex University),

"Do Scientists Have to Count?".

10 June 1981

Dr. J. Rose (I.C.I. Plastics),

"New Engineering Plastics".

21 September 1981

Dr. P. Plimmer (Dupont),

"From Conception to commercialisation of a Polymer".

14 October 1981

Professor E. Kluk (University of Kotowice),

"Some Aspects of the Study of Molecular Dynamics - Simple Molecular Liquids".

22 October 1981

Dr. P.J. Corrish (Dunlop Ltd.),

"What would life be like without Rubber".

6 November 1981

Dr. W. Moddeman (Monsanto Ltd., U.S.A.),

"High Energy Materials".

12 November 1981

Professor A.I. Scott (University of Edinburgh),

"An Organic Chemist's View of Life in the N.M.R. Tube".

26 November 1981

Dr. W.O. Ord (Northumbrian Water Authority),

"The Role of the Scientist in a Regional Water Authority".

2 December 1981

Dr. G. Beamson (University of Durham),

"Photoelectron Spectroscopy in a Strong Magnetic Field".

20 January 1982

Dr. M. Bryce (Universith of Durham),
"Organic Metals".

28 January 1982

Professor I. Fells (University of Newcastle upon Tyne),
"Balancing the Energy Equations".

3 February 1982

Dr. D. Parker (University of Durham),
"Modern Methods for the Determination of Enautiomeric Purity".

10 February 1982

Dr. D. Pethrick (University of Strathclyde),
"Conformational Dynamics of Small and Large Molecules".

17 February 1982

Professor D.T. Clark (University of Durham),
"Structure, Bonding, Reactivity and Synthesis of Surfaces as revealed by ESCA".

3 March 1982

Dr. P. Banfield (I.C.I. Organics Division),
"Computer Aided Synthesis Design: A view from Industry".

19 May 1982

Professor R.D. Chambers (University of Durham),
"Fluorocarbanions - some 'Alice in the Looking Glass' Chemistry

28 June 1982

Professor D.J. Burton (University of Iowa),
"Some Aspects of the Chemistry of Fluorinated Phosphonium Salts and Phosphonates".

Conferences Attended During the Period 1979-1982

Royal Institute of Chemistry/Chemical Society Annual Congress, April 1980, Durham.

Polymer Characterisation Symposium, July 1981, Durham.

NATO Advanced Study Institute Summer School on 'The Dynamic and Static Properties of Polymers in the Solid State", Strathclyde, 1981.

Graduate Symposium, Durham 1982, (Paper presented on the 'Natural and Artificial Weathering of Polystyrene').

REFERENCES

1. A.W. Hofmann,J.Chem.Soc., 13, 87 (1861).

2. S.T. Henderson, "Daylight and its Spectrum", Adam Hilger Ltd., Bristol (1977).

3. A. Davis, G.H.W. Deane, D. Gordon, G.V. Howell and K.J. Ledbury, J.Appl.Pol.Sci., 20, 1165 (1976).

4. J.G. Calvert and J.N. Pitts, "Photochemistry", John Wiley and Sons, Inc., New York (1966).

5. M.M. Jaffe and M. Orchin, "Theory and applications of ultraviolet spectroscopy", Wiley, New York (1962).

6. J.B. Birks, "Photophysics of Aromatic Molecules", Wiley, Interscience (1970).

7. B.R. Henry and M. Kasha, J.Chem. Phys., 47, 3319 (1967).

8. C.N. Banwell, "Fundamentals of Molecular Spectroscopy", 2nd edition, McGraw-Hill, London (1972).

9. A. Jablonski, Z.Physik., 94, 38 (1935).

10. B. Rånby and J.F. Rabek, "Photodegradation, Photooxidation and Photostabilization of Polymers", Wiley-Interscience, London (1975).

11. A.C. Somersall and J.E. Guillet, J. Macromol.Sci., Revs. Macromol.Chem., C(B), 135 (1975).

12. J.F. McKellar and N.S. Allen, "Photochemistry of Man-Made Polymers", Applied Science Publishers Ltd., London (1979

13. S.L. Fitton, R.N. Harward and G.R. Williamson, Brit.Polym.J., 2, 217 (1970).

14. R.B. Fox and R.F. Cozzens, "Encyclopaedia of Polymer Science and Technology", Wiley-Interscience, New York, 11, 760 (1971).

15. S.W. Beavan and D. Philips, Eur.Polym.J., 10, 593 (1974).

16. J.L. Bolland, Quart,Rev., 3, 1 (1949).

17. J.L. Bolland and H.R. Cooper, Proc.Roy.Soc., A225, 405 (1954)

18. J.L. Bolland and G. Gee, Trans.Faraday Soc., 42, 236 (1946) and 42, 244 (1946).

19. G. Herzberg, "Molecular spectra and molecular structure", Van Nostrand, New York (1950), p.560.

20. N. Uri in W.O. Lundberg, "Autoxidation and antioxidants", Interscience, New York (1962), p.65.

21. J.C.W. Chien, J.Amer.Chem.Soc., 89, 571 (1967).

22. J.C.W. Chien and C.R. Boss, J.Polym.Sci., A-1, 5, 3091 (1967)

23. S.W. Benson, J.Chem.Educ., 42, 502 (1965).

24. D.J. Carlsson and D.M. Wiles, Macromolecules, 2, 587, 597 (1969).

25. F.R. Mayo, J.Polym.Sci., B, 10, 921 (1972).

26. J.P. Luongo, J.Polym.Sci., 42, 139 (1960).

27. J.P. Luongo, J.Appl.Polym.Sci., 3, 303 (1960).

28. L.H. Lee, C.L. Stacy and R.G. Engel, J.Appl.Polym.Sci., 10, 1699, 1717 (1966).

29. L. Reich and S.S. Stivala, J.Appl.Polym.Sci., 12, 2033 (1968)

30. J.F. Rabek in "Comprehensive Chemical Kinetics", ed. by C.H. Bamford and C.F.H. Tipper, 14, 425 (1975), Elsevier Scientific Publishing Company, Amsterdam.

31. J.H. Adams and J.E. Goodrich, J.Polym.Sci., A1, 8, 1269 (1970

32. J.C.W. Chien, E.J. Vandenburg and H. Jabloner, J.Polym.Sci., A1, 6, 381 (1968).

33. M.M. Jaffe and M. Orchin, 'Theory and Applications of Ultraviolet Spectroscopy', Wiley, New York (1962)..

34. J.N. Murrel, 'The Theory of Electronic spectra of Organic Molecules', Methuen and Co. Ltd., London (1963).

35. N.J. Turro, 'Modern Molecular Photochemistry', The Benjamin/Cummings Publishing Co.Inc. (1978).

36. G. Geuskens in 'Comprehensive Chemical Kinetics', ed. by C.G. Bamford and C.F.H. Tipper, Elsevier Science Publishing Company, Amsterdam, 14, 333 (1975).

37. G.R. Cotten and W. Sacks, J.Polym.Sci., A-1, 1, 1345 (1963).

38. C. Kujirai, S. Hashiya, H. Furuno and N. Terada, J.Polym. Sci., A1, 6, 589 (1968).

39. J.A. Melchore, I and EC Prod.Res. and Dev., 1, 232 (1962).

40. A. Davis, G.H.W. Deane, D. Gordon, G.V. Howell and K.J. Ledbury, S.Appl.Pol.Sci., 20, 1165 (1976).

41. A. Davis, G.H.W. Deane and B.L. Diffey, Nature, 261, 169 (1976).

42. A. Davis, B.V. Howes, K.J. Ledbury and P.J. Pearce, Polym. Degrad. and Stab., 1, 121 (1979).

43. N.Z. Searle in 'Analytical Photochemistry and Photochemical Analysis', Ed. by J.M.F. Fitzgerald, Dekker (1971).

44. J.F. Rabek 'Experimental Methods in Polymer Chemistry', John Wiley and Sons (1980).

45. N.J. Harrick, 'Internal Reflectance Spectroscopy, Wiley-Interscience, New York (1967).

46. D.T. Clark, A. Dilks and H.R. Thomas, Chapter 4 in 'Developments in Polymer Degradation', Ed. N. Grassie Applied Science, London (1977).

47. D.T. Clark and A. Dilks, 101, in 'Characterization of Metal and Polymer Surfaces', Ed. L.H. Lee, Academic Press Inc. New York (1977).

48. D.T. Clark, A. Dilks and D. Shuttleworth, Chapter 9, in 'Polymer Surfaces', Eds. D.T. Clark and W.J. Feast, J. Wiley and Sons, London (1979).

49. J. Peeling and D.T. Clark, Polym.Degrad. and Stab., 3, 97 (1980-81).

50. J. Peeling and D.T. Clark, Polym.Degrad. and Stab., 3, 177 (1981).

51. J. Peeling and D.T. Clark, J.Appl.Polym.Sci., 11, 3761 (1980).

52. A. Dilks and D.T. Clark, J.Polym.Sci.,Polym.Chem.Edn., 19, 2847 (1981).

53. D.T. Clark in "Electron Emission Spectroscopy" edited by W. Dekyser and D. Reidel, D. Reidel Pub.Co., Dordrect, Holland, 373 (1973).

54. H. Hertz, Ann.Physik, 31, 983 (1887).

55. P. Leanard, Ann.Physik, 2, 359 (1900).

56. A. Einstein, Ann.Physik, 17, 132 (1905).

57. H. Robinson, Phil.Mag., 50, 241 (1925).

58. M. de Broglie, Compt.Rend., 172, 274 (1921).

59. J.A. van Akker and E.C. Watson, Phys.Rev., 37, 1631 (1931).

60. M. Ference, Jr., Phys.Rev., 51, 720 (1937).

61. R.J. Steinhardt, Jr., F.A.D. Granados and G.I. Post, Anal.Chem., 27, 1046 (1955).

62. K. Seigbahn and K. Edvarson, Nucl.Phys., 1, 137 (1956).

63. K. Seigbahn, C. Nordling, A. Fahiman, R. Nordberg, K. Hamrin, J. Hedman, G. Johansson, T. Berkmark, S.E. Karlsson, I. Lidgren and B. Lindberg, 'ESCA, Atomic, Molecular and Solid State Structure Studied by means of Electron Spectroscopy', Almquist and Wiksells, Uppsala (1967).

64. K. Seigbahn, C. Nordling, G. Johansson, J. Hedman, P.F. Heden, K. Hamrin, U. Gelius, T. Bergmark, L.D. Werme, R. Manne and Y. Baer, 'ESCA Applied to Free Molecules', North Holland Publishing Co. (1969).

65. A.D. Baker and C.R. Brundle, 'An Introduction to Electron Spectroscopy', in 'Electron Spectroscopy. Theory, Techniques and Applications', Vol.1, Eds. C.R. Brundle and A.D. Baker, Academic Press, London (1977).

66. T.N. Rhodin and J.W. Gadzuk, 'Electron Spectroscopy and Surface Chemical Bonding', in 'The Nature of the Surface Chemical Bond', Eds. T.N. Rhodin and G. Erti, 112, North Holland Publishing Co., Amsterdam (1979).

67. D.W. Turner, C. Baker, A.D. Baker and C.R. Brundle, 'Molecular Photoelectron Spectroscopy', J.Wiley and Sons Ltd. (1970).

68. ----------

69. U. Gelius, Phys.Scr., 9, 133 (1974).

70. D.T. Clark, 'Structure and Bonding in Polymers as Revealed by ESCA', in Electron Structure of Polymers and Molecular Crystals', Eds. J. Lodik and J.M.Andre, Plenum Press, New York (1975).

71. L.S. Cederbaum and W. Domcke, J.Elec.Spec.Rel.Phenom., 13, 161 (1978).

72. H.B. Culien, Handbook of Physics, Section 8, Chapter 2, McGraw-Hill (1967).

73. A. Rosen and I. Lindgen, Phys.Rev., 176, 114 (1968).

74. P.S. Bagus, Phys.Rev.A., 139, 619 (1965).

75. D.A. Shirley, Advances in Chem.Phys., 23, 85, Eds. I. Prigogini and S.A. Rice, J. Wiley and Sons Ltd., New York (1973).

76. U. Gelius and K. Seigbahn, Faraday Discuss,Chem.Soc., 54, 257 (1972).

77. L.C. Snyder, J.Chem.Phys., 55, 95 (1971).

78. D.B. Adams and D.T. Clark, Theoret.Chim.Act., 31, 171 (1973).

79. M.F. Guest, I.H. Hillier, V.R. Saunders and M.W.Wood, Proc.Roy.Soc., A333, 201 (1973).

80. D.T. Clark, I.W. Scanlan and J. Müller, Theoret.Chim.Act., 35, 341 (1974).

81. D.T. Clark and I.W. Scanlan, J.Chem.Soc.Farad.Trans., 11, 70, 1222 (1974).

82. H. Basch, J.Elec.Spec.Rel.Phenom., 5, 463 (1974).

83. T.A. Koopmans, Physica, 1, 104 (1933).

84. D.T. Clark in 'Advances in Polymer Science', Ed. H.J.Cantow, Springer Verlag, Berlin, 24, 125 (1977).

85. R. Manne and T. Åberg, Chem.Phys.Lett., 7, 282 (1970).

86. D.T. Clark, D.B. Adams, A. Dilks, J. Peeling and H.R. Thomas, J.Elec.Spec.Rel.Phenom., 8, 51 (1976).

87. D.T. Clark and A. Dilks, J.Polym.Sci.Polym.Chem. Edn., 14, 533 (1976).

88. D.T. Clark and A. Dilks, J.Polym.Sci.Polym.Chem.Edn., 15, 15 (1977).

89. A.E. Sandstrom in 'Handbook of Physics', Vol.XXX, 'X-rays', 164, Ed., S.F. Flugge, Springer-Verlag (1957).

90. K. Seigbahn, 'Alpha, Beta and Gamma Ray Spectroscopy', Chapter 3, Ed. K. Seigbahn, North Holland Publishing Co., Amsterdam (1965).

91. P. Auger, J.Phys.Radium, 6, 205 (1925).

92. P. Auger, Compt.Rend., 65, 180 (1925).

93. J.J. Lander, Phys.Rev., 91, 1382 (1953).

94. c.f. T.A. Carlson, 'Photoelectron and Auger Spectroscopy', Plenum Press, New York (1975).

95. D. Coster and R. de L. Kronig, Physica, 2, 13 (1935).

96. E.H.S. Burhop, 'The Auger Effect and other Radiationless Transitions', Cambridge University Press (1952).

97. O. Keski-Rahkonen and M.I. Krause, At.Data Nucl.Data Tables, 14, 139 (1974).

98. J.P. Coad, M. Gettings and J.G. Riviere, Faraday Discuss. Chem.Soc., 60, 269 (1975).

99. c.f. C.D. Wagner, Discuss,Faraday Soc., 60, 291 (1975).

100. S.P. Kowalczyk, F.R. McFeely, R.A. Pollak, L. Ley and D.A. Shirley, Phys.Rev., B8, 3583 (1973).

101. L. Ley, S.P. Kowalczyk, F.R. McFeely, R.A. Pollak and D.A. Shirley, Phys.Rev., B8, 2392 (1973).

102. S.P. Kowalczyk, L. Ley, F.R. McFeely, R.A. Pollak and D.A. Shirley, Phys.Rev., B8, 2387 (1973).

103. S.P. Kowalczyk, L. Ley, F.R. McFeely, R.A. Pollak and D.A. Shirley, B9, 381 (1974).

104. C.D. Wagner, Anal.Chem., 44, 1050 (1972).

105. C.D. Wagner and P. Bilden, Surface Sci., 35, 82 (1973).

106. C.D. Wagner, Faraday Discuss.Chem.Soc., 60, 291 (1975).

107. C.D. Wagner, W.M. Riggs, L.E. Davis, J.F. Moulder and G.E. Muilenberg, 'Handbook of X-ray Photoelectron Spectroscopy', Perkin Elmer Cooperation, Physical Electronic Division (1979).

108. C.D. Wagner, L.H. Gale and R.H. Raymond, Anal.Chem., 51, 466 (1979).

109. D.T. Clark, B.J. Cromarty and A. Dilks, J.Poly.Sci.Polym. Chem. Edn. 16, 3173 (1978).

110. D.T. Clark and A. Harrison, J.Polym.Sci.Chem.Edn., 19, 1945 (1981).

111. W.L. Jolly and D.N. Hendrickson, J.Amer.Chem.Soc., 92, 1863 (1970).

112. J.N. Murrell and B.J. Ralston, J.Chem.Soc., Faraday Trans., 11, 68, 1393 (1972).

113. M.E. Schwartz, Chem.Phys.Lett., 6, 631 (1970).

114. D.A. Shirley, Chem.Phys.Lett., 15, 325 (1972).

115. C.S. Fadley, 'Basic Concepts of X-ray Photoelectron Spectroscopy' in 'Electron Spectroscopy, Theory echniques and Applications', Vol.2, 1, Eds. C.R. Brundle and A.D. Baker, Academic Press (1978).

116. R.E. Watson and A.J. Freeman in 'Hyperfine Interactions', Eds. A.J. Freeman and R.B. Frankel, Academic Press, New York (1967).

117. C.S. Fadley, D.A. Shirley, A.J. Freeman, P.S. Bagus and J.V. Mallow, Phys.Rev.Lett., 23, 1397 (1969).

118. J.V. van Vleck, Phys.Rev.Lett., 45, 405 (1934).

119. C.S. Fadley in 'Electron Spectroscopy'. Ed. D.A. Shirley, 781, North Holland Publishing Co. (1972).

120. T. Novakov, ref. 26 of ref. 119.

121. G.M. Bancroft, I. Adams, H. Lampe and T.K. Sham, Chem.Phys.Lett., 32, 173 (1975).

122. R.P. Gupta and S.K. Sen, Phys.Rev.Lett., 28, 1311 (1972).

123. T. Novakov and J.M. Hollander, Bull.Amer.Phys.Soc., 14, 524 (1969).

124. T. Novakov and J.M. Hollander, Phys.Rev.Lett., 21, 1133 (1968).

125. G.K. Wertheim, 'Mössbauer Effect: Principles and Applications', Academic Press, New York (1964).

126. G. Johansson, J. Hedman, A. Berudtsson, M. Klasson, and R. Nilsson, J.Elect.Spect.and Rel.Phenom., 2, 295 (1973).

127. P. Ascerelli and G. Missoni, J.Elect.Spect. and Rel.Phenom., 5, 417 (1974).

128. J.F. McGlip and I.G. Main, J.Elect.Spect. and Rel.Phenom., 6, 397 (1975).

129. D.A. Huchital and R.T. McKeon, Appl.Phys.Lett., 20, 158 (1972)

130. J.S. Brinnen, Acc.Chem.Res., 9, 86 (1976).

131. D.T. Clark, H.R. Thomas and A. Dilks (unpublished data).

132. c.f. R.S. Swingle and W.M. Riggs, CRC Crit.Rev.Anal.Chem., 5, 267 (1975) CRC Press, Cleveland.

133. D.T. Clark, A. Dilks, D. Shuttleworth and H.R. Thomas, J.Polym.Sci.,Polym.Chem.Ed., 17, 627 (1979).

134. D.T. Clark, Physica Scripta, (Sweden), 16, 307 (1977).

135. J.H. Scofield, Lawrence Livermore Laboratory Report UCRL, 51326, Jan (1973).

136. J.H. Scofield, J.Elect.Spect.Rel.Phenom., 8, 129 (1976).

137. D.T. Clark and H.R. Thomas, J.Polym.Sci.,Polym.Chem.Ed., 15, 2843 (1977).

138. D.T. Clark and D. Shuttleworth, J.Polym.Sci.,Polym.Chem.Ed., 16, 1093 (1977).

139. D.R. Penn, J.Elect.Spect.Rel.Phenom., 9, 29 (1976).

140. D.T. Clark in 'Advances in Polymer Science', Springer-Verlag, 24. 125 (1977).

141. T. Novakov and J.M. Hollander, Phys.Rev.Lett., 21,1133 (1968).

142. L.G. Parrat, Rev.Mod.Phys., 31, 616 (1959).

143. c.f. N. Beatham and A.F. Orchard, J.Elect.Spect.Rel. Phenom., 9, 129 (1976).

144. A.F. Carley and R.M. Joyner, J.Elect.Spect.Rel.Phenom., 16, 1 (1979).

145. R.M. Eisenberg in 'Fundamentals of Modern Physics, Chapter 14, J. Wiley and Sons, New York (1981).

146. C.D. Wagner, J.Elect.Spect. and Rel.Phenom., 10, 305 (1977).

147. C.D. Wagner, L.H. Gale and R.H. Raymond, J.Vac.Sci.Tech., 15, 518 (1978).

148. B.L. Henke, Adv.X-ray Analysis, 13, 1 (1969).

149. C.D. Wagner, Faraday Discuss.Chem.Soc., 60, 306 (1975).

150. K. Yates, A. Barrie and F.J. Street, J.Phys., E6, 130 (1973).

151. K. Seigbahn, D. Hammond, H. Fellner-Feldegg and E.F. Barnett, Science, 176, 245 (1972).

152. E.M. Purcell, Phys.Rev., 54, 818 (1938).

153. J.C. Helmer and N.H. Weichert, Appl.Phys.Lett., 13, 268 (1968).

154. c.f. H. Seigbahn, L. Asplund, P. Kelfve and K. Seigbahn, J.Elect.Spect.Rel.Phenom., 7, 411 (1975) and references therein.

155. K. Seigbahn, J. Elect.Spect.Rel.Phenom., 5, 3 (1974).

156. c.f. ref. 145.

157. J.J. Huang, J.W. Rablais and F.O. Ellison, J.Elect.Spect. Rel.Phenom. 6, 85 (1975)

158. R.A. Davenport and A.J. Manuel, Polymer, 18, 557 (1977).

159. A. Gupta, A. Rembann and J. Moacanin, Macromolecules, 11, 1285 (1978).

160. A. Gupta, R. Liang, J. Moacanin, R. Goldbeck and D. Kliger, Macromolecules, 13, 262 (1980).

161. J.S. Humphrey, Jr. and R.S. Roller, Mol.Photochem., 3, 35 (1971).

162. A.D. Williams and P.J. Flory, J.Polym.Sci., A-Z, 6, 1945 (1968).

163. A. Prietzchk, Kolloid-Z, 8, 156 (1957).

164. M. Obi and H. Nakanisbi, Bull.Chem.Soc.Jpn., 44, 3419 (1971).

165. A.E. Tonelli, Macromolecules, 5, 558 (1972).

166. c.f. ref. 34.

167. J.A. Baltrop and J.D. Coyle, "Excited States in Chemistry", Wiley, London (1975).

168. M.J.S. Dewar and W. Thiel, J.Am.Chem.Soc., 99, 4899 (1977).

169. M.J.S. Dewar and W. Thiel, J.Am.Chem.Soc., 99, 4907 (1977).

170. W.S. Hehre, R.F. Stewart and J.A. Pople, J.Chem.Phys., 51, 2657 (1969).

171. R.W. Kiels, C.C. Lin and E.B. Wilson,Jr., J.Chem.Phys., 26, 1695 (1957).

172. V.R. Saunders and M.F. Guest, Atlas Computing Division, Rutherford Laboratory, Chilton, Didcot, Oxon, Oxll OQX.

173. E. Clementi and H. Popkie, J.Chem.Phys., 57, 4870 (1972).

174. J.E. Meeks, J.F. Arnett, D. Larson and S.P. McGlynn, Chem.Phys.Lett., 30, 190 (1975).

175. D. Turner, 'Molecular Photoelectron Spectroscopy', Wiley Interscience, Chichester (1970).

176. D.T. Clark, W.J. Feast, P.J. Tweedale and H.R. Thomas, J.Polym.Sci., Polym.Chem.Edn., 18, 1651 (1980).

177. D.T. Clark, B.J. Cromarty and A. Dilks, J.Polym.Sci., Polym.Chem.Ed., 16, 3173 (1978).

178. A. Factor and M.L. Chu, Polym.Degrad. and Stab. 2, 203 (1980)

179. J. Mitchell and L.R. Perkins, Appl.Polym.Sym., 4, 167 (1967).

180. D.T. Clark, M.M. Abu Shbak and W.J. Brennan, J.Elect.Spect. Rel.Phenom., in Press (1982).

181. A. Dilks, Ph.D. Thesis, Durham (1977).

182. R. Wilson, M.Sc. Thesis, Durham (1981).

183. J. Hammond, J. Hobluka, A. Durisin and R. Dickie, Abstract from Colloid and Interfacial Science Section, ACS Meeting (1978)

184. J.E. Moore, Am.Chem.Soc.Symp.Series, 151, 97 (1981).

185. P.A. Mullen and N.Z. Searle, J.Appl.Polym.Sci., 14 765 (1970).

186. c.f. ref. 110.

187. D.T. Clark, B.J. Cromarty and A. Dilks, J.Polym.Sci., Polym.Chem.Edn., 16, 3173 (1978).

188. Eds. B. Ranby and J.F. Rabek, 'Singlet Oxygen, Reactions with Organic Compounds and Polymers', John Wiley and Sons, New York (1978).

189. E. Wasserman, 'Singlet Oxygen', Academic Press Inc., New York (1979).

190. R.W. Murray in 'Polymer Stabilization' Chapter 5, ed. W.L. Hawkins, John Wiley and Sons, New York (1972).

191. A.R. Meetham, Quart.J.Roy.Meterol.Soc. 70, 20 (1944).

192. S.D. Razumovskii, A.A. Kefeli and G.E. Zaikov, Eur.Polym.J., 7, 275 (1971).

193. J. Peeling, D.T. Clark and M.S. Jazzar, unpublished data.

194. J. Peeling and M.S. Jazzar, Arab.J.Sci.Tech., in Press (1982).

195. A.M. Trozzolo and F.H. Winslow, Macromolecules, 1, 98 (1968).

196. J.W. Coomber and J.N. Pitts, Jr., Environ.Sci.Technol., 4, 506 (1970).

197. R.H. Kummler and M.H. Bortner, Amer.Chem.Soc.Div.Petrol. Che,.Prepr., 16, A44 (1971).

198. A. Dilks, J.Polym.Sci.Polym.Chem.Edn., 19, 1319 (1981).

199. E.A. Ogryzlo in 'Singlet Oxygen' Chapter 2, ed. E. Wasserman, Academic Press Inc., New York (1979).

200. J.A. Brysdon, 'Plastic Materials', Newnes-Butterworths, London (1975).

201. R.E. Huie and J.T. Herron, 'Progress in Reaction Kinetics', 8, 1 (1975).

202. J.R. MacCallum and C.T. Rankin, Makromol.Chem., 175, 2477 (1974)

203. M.L. Kaplan and A.M. Trozzolo, Chapter 11 of ref. 189.

204. J.F. Rabek and B. Ranby, J.Polym.Sci., Polym.Chem.Ed., 14, 1463 (1976) also c.f. ref. 198.

205. H.C. Ng and J.E. Guillet, Chapter 27 of ref. 188.

206. B. Rånby and J.F. Rabek, Chapter 21 of ref. 188.

207. N. Grassie and N.A. Weir, J.Appl.Polym.Sci., 9, 963 (1965) and J.Appl.Polym.Sci., 9, 975 (1965).

208. N. Grassie and N.A. Weir, J.Appl.Polym.Sci., 9, 987 (1965).

209. N. Grassie and N.A. Weir, J.Appl.Polym.Sci., 9, 999 (1965).

210. J.F. Rabek and B. Rånby, J.Polym.Sci.Polym.Chem.Edn., 12, 273 (1974).

211. G. Geuskens, D. Baeyens-Volant, G. Delannois, Q. Lu-Vinh, W. Piret and C. David, Eur.Polym.J., 14, 291 (1978).

212. N.A. Weir, Eur.Polym.J., 14, 9 (1978).

213. J.R. MacCallum and D.A. Ramsay, Eur.Polym.J., 13, 945 (1977).

214. V. Kovačević, M. Bravar and D. Hace, Bulletin De la Chimique Beograd, 14, 167 (1980).

215. L.A. Wall, M.R. Harvey and M. Tyron, J.Phys.Chem., 60, 1306, (1956).

216. L.A. Wall and M. Tyron, Nature, 178, 101 (1956).

217. L.A. Wall and D.W. Brown, J.Phys.Chem., 61, 129 (1956).

218. P.J. Burchill and G.A. George, J.Polym.Sci., Polym.Letts. Edn. 12, 497 (1974).

219. G.A. George and D.K.C. Hodgeman, J.Polym.Sci., Part C, 55, 195 (1976).

220. G.A. George and D.K.C. Hodgeman, Eur.Polym.J., 13, 63 (1977).

221. M. Tyron and L.A. Wall in 'Autoxidation and Antioxidants', Vol.II, 919, Interscience, New York (1961).

222. B.D. Gesner and P.G. Kelleher, J.Appl.Polym.Sci., 12, 1199 (1968).

223. B.D. Gesner and P.G. Kelleher, J.Appl.Polym.Sci., 13, 2183 (1969).

224. D. Shuttleworth, Ph.D. Thesis, Durham (1978).

225. A. Davis and D. Gardiner, Polym.Degrad. and Stab., 4, 159 (1982).

226. N.S. Allen and J.F. McKellar, J.Appl.Polym.Sci., 21, 1129 (1979).

227. P.G. Kelleher, L.B. Jassie and B.D. Gesner, J.Appl.Polym. Sci., 11, 137 (1967).

228. R.A. Jerussi, J.Polym.Sci., A-1, 9, 2009 (1971).

229. J. Tsuji and T. Seiki, Polymer J., 4, 589 (1973).

230. P.G. Kelleher and B.D. Gesner, J.Appl.Polym.Sci., 13, 9 (1969).

231. J. Peeling, unpublished data.